Civil Engineering Department

MECHANICAL BEHAVIOUR OF STRESS ABSORBING MEMBRANE INTERLAYERS

OGUNDIPE OLUMIDE MOSES

B.Eng., M.Eng.

Thesis Submitted to the University of Nottingham for the Degree of Doctor of Philosophy

OCTOBER 2011

TO ALMIGHTY GOD

ABSTRACT

This study assesses the contribution of some selected stress absorbing membrane interlayers (SAMIs) on overlaid pavement performance in delaying the offset of reflective cracking using laboratory and full scale testing. Materials characterization were carried to have knowledge of the properties of the SAMIs and overlay and some of the properties were required as input for the finite element modelling. The characterization tests include the particle size distribution, penetration and softening point tests, dynamic mechanical analysis, indirect tensile stiffness modulus test (ITSM), indirect tensile fatigue test (ITFT) and repeated load axial test (RLAT). The interface bond was investigated using the Leutner shear test and pull off test. The assessment of the contribution of selected SAMIs on overlaid pavement performance in delaying offset of reflective cracking was carried out using a wheel tracking test supported by finite element modelling, a large scale pavement test facility test and a thermal cycling test.

The Leutner shear test and pull-off test were used to examine the strength and stiffness of the overlay-SAMI interface. The interface strength/stiffness was determined because it is one of the factors that influence the crack resistance of SAMIs. The wheel tracking test was carried out to evaluate the effects of the thickness and stiffness of SAMI, thickness of overlay, SAMI composition, interface stiffness, load level and temperature on the performance of SAMIs under traffic loading. To study the performance of SAMIs under conditions close to the field, a large pavement test facility test was carried out. The finite element analysis of the wheel tracking test was carried out to evaluate the deflection, stress and strain distribution in a cracked pavement with and without SAMIs. The performance of SAMIs under thermal loading (temperature variation) was investigated using the thermal cycling test.

The study shows that SAMI composition, SAMI thickness and stiffness, overlay thickness, interface stiffness, temperature and load levels influence the performance of SAMIs under traffic loading. It also demonstrates that the main factor that influences the performance of SAMIs under thermal loading is the interface stiffness. Design guidelines for the successful use of SAMIs against reflective cracking were prepared and the OLCRACK software was used to demonstrate the benefits of SAMIs in an overlay over a cracked pavement.

ACKNOWLEDMENTS

I will like to give special thanks to my supervisors, Dr Nick Thom and Prof. Andy Collop for their advice, guidance and encouragement throughout the course of this study. I acknowledge Petroleum Technology Development Fund Nigeria that funded the study.

My sincere thanks go to Nottingham Transportation Engineering Centre for making laboratory facilities available for the study. Also, I will like to appreciate Shell Bitumen UK, Aggregates Industry UK, Nynas Bitumen UK and Colas UK for their generosity in making materials available for this study.

I am grateful to Dr James Grenfell for his help with instrumentation of specimens. The technical support from Barry Brodrick, Jon Watson, Michael Winfield, Richard Blakemore, Lawrence Pont, Nancy and others of Nottingham Transportation Engineering Centre laboratory is highly appreciated. Special thanks go to my employer, Ekiti-State University Nigeria (formerly University of Ado-Ekiti, Nigeria) for granting me leave to pursue this study. I am grateful to my colleagues in the research office for the thought-provoking discussions and the good time we had together during the course of this study.

I am grateful to my parents, Mr Hamzart Ogundipe and Mrs Omolade Ogundipe and my siblings for their encouragement and support. I owe a debt of gratitude to my wife, Folake and kids, Ayomide and Olamide for their support and understanding, when I could not be there because of the demand of the study.

DECLARATION

The work described in this thesis was carried out at the Nottingham Transportation Engineering Centre, Civil Engineering Department, University of Nottingham between September 2008 and September 2011. The thesis is my own work, except the work of other authors that has been referenced. No part of this thesis has been submitted for any degree at another University.

Ogundipe Olumide Moses

October 2011

LIST OF CONTENTS

LIST OF FIGURES

LIST OF TABLES

NOTATIONS

AC	Asphalt Concrete
CBGM	Cement Bound Granular Mixtures
CBM	Cement-Bound Material
CBR	California Bearing Ratio
CRL	Crack Relief Layer
DBM	Dense Bitumen Macadam
FWD	Falling Weight Deflectometer
HMA	Hot Mix Asphalt
HRA	Hot Rolled Asphalt
ISAC	Interlayer Stress Absorbing Composite
LVDT	Linear Variable Differential Transformer
LVDTs	Linear Variable Differential Transformers
MA	Marshall Asphalt
OGAC	Open Graded Asphalt Concrete
OGFL	Open Graded Friction Layer
PA	Porous Asphalt
PCC	Portland Cement Concrete
PCCP	Portland Cement Concrete Pavement
PFC	Porous Friction Course
PVC	Polyvinyl Chloride
SAF	Sand Anti-Fracture
SAMI	Stress Absorbing Membrane Interlayer
SAMIs	Stress Absorbing Membrane Interlayers
SBS	Styrene-Butadiene-Styrene
SMA	Stone Mastic Asphalt

MEPDG	Mechanistic-Empirical Pavement Design Guide
ACP	Asphalt Concrete Pavement
FEM	Finite Element Method
PTF	Pavement Test Facility
ESAL	Equivalent Standard Axle Load
LEFM	Linear Elastic Fracture Mechanics
AASHTO	American Association of State Highway and Transportation Officials

1 INTRODUCTION

1.0 Background

Pavement rehabilitation is rapidly becoming one of the most important issues facing many highway agencies in both developed and developing countries. This is because when road pavements (flexible, rigid and composite) reach critical condition, the need arises for them to be restored back to good condition. One form of deterioration in pavements is cracking, which can either be fatigue (wheel load) or thermal cracking. The method commonly used to rehabilitate deteriorated pavements is by overlaying with a new surfacing material. Cleveland et al. (2002) and Roberts et al. (1996) stated that for both flexible and composite pavements, a common technique used by many agencies for preventive maintenance and/or rehabilitation was simply to construct a thin HMA overlay, normally between 25.4 and 50.8 mm thick.

Overlaying cracked pavements prevents water from infiltrating through the cracks into the pavement structure, thus preventing the deterioration of the pavement structure and increasing its structural capacity. It reduces roughness, restores skid resistance, and improves the overall ride quality to the travelling public. However, repairing cracked roads by overlaying has been found to be a short term solution, because the cracks re-appear on the new surface after a short period of time. This phenomenon is referred to as reflective cracking. Reflective cracking is one of the more serious problems associated with the use of thin overlays (Cleveland et al, 2002; Dempsey, 2002; Engle, 2001; Bhosale and Mandal, 2008; and Khodaii et al, 2008).

Reflective cracking is often initiated at the bottom of the overlay material and grows until it appears at the surface. Also top-down cracking (cracks initiating at the surface and growing into the lower layers) occurs especially where there are large temperature variations in the pavement (thermal cracking). Once a reflective crack reaches the surface or when it reaches

the lower layer (when originating at the surface), it creates a path for the flow of surface water into the lower layers of the pavement. When left untreated, this situation will lead to deterioration of the pavement structure and a reduction in serviceability (Penman and Hook, 2008). This usually results in discomfort to road users and increased maintenance cost; in some cases the road may have to be rebuilt from the foundation (subgrade). Vervaecke et al. (2008) stated that cracks are rapidly reflected at the surface as a result of the combined effects of thermally induced stresses and traffic loading. The movement at the joints and cracks in the underlying pavement layer generates stresses. Temperature associated horizontal movement of the slab, concentrated in underlying joints and cracks in the existing pavement, leads to tensile stresses, and traffic load induced vertical movements produce shear and tensile stresses in the overlay. The stress concentration at the crack tip leads to initiation and propagation of a crack through the overlay to the surface.

A number of measures have been adopted by engineers with the aim of retarding reflective cracking in overlays and results achieved have been mixed. These measures include: thick overlay, overlay mixture modification, overlay reinforcement, stress or strain absorbing interlayer and reinforcing interlayer. Al-Qadi et al. (2008) stated that various interlayer materials namely: geosynthetics, geocomposites, steel reinforcement netting, and modified HMA, have been used as interlayer systems for the purpose of reducing reflective cracking, although their effectiveness is still not well quantified due to lack of understanding of the reflective cracking mechanism and because imperfect evaluation approaches are used. No current pavement rehabilitation techniques have been shown to solve completely the problem of reflective cracking. This has been attributed to the number of variables that are involved in reflective cracking (Bhosale and Mandal, 2008).

This research work aims to evaluate the contribution of some stress absorbing membrane interlayers (SAMIs) on overlaid pavement performance in delaying reflective cracking and the influence of certain variables such as temperature, overlay thickness, load levels, SAMI thickness on performance.

1.1 Pavement failure modes

Pavements are rehabilitated by overlaying with new surfacing material because of distresses in the existing pavement. Distress may occur in the pavement during construction and while in service. It may be due to the materials used for pavement construction, poor workmanship, environmental factors or the loading to which they are subjected. The two principal modes of failure in pavements are fatigue cracking and permanent deformation. Engineers seek to hold these forms of failure to acceptable limits within a pavement design life. Another mode of failure, which has not been given much attention and is not considered in most pavement design approaches, is reflective cracking. This form of failure occurs when pavements with critical level of serviceability are rehabilitated by overlaying. Reflective cracking is now a major concern to pavement engineers and attempts are being made to solve the problem.

1.1.1 Permanent deformation

Permanent deformation or rutting is the depression along the wheel path. This is caused by gradual build up of irrecoverable strains under repeated loading which develop into a measurable rut. These strains are due to the visco-elastic response of bituminous materials to dynamic loading. Figure 1.1 shows the visco-elastic response to millions of wheel loadings. Also, rutting may occur because of base, subbase or subgrade failure. It is usually measured with a profiler or straight edge.

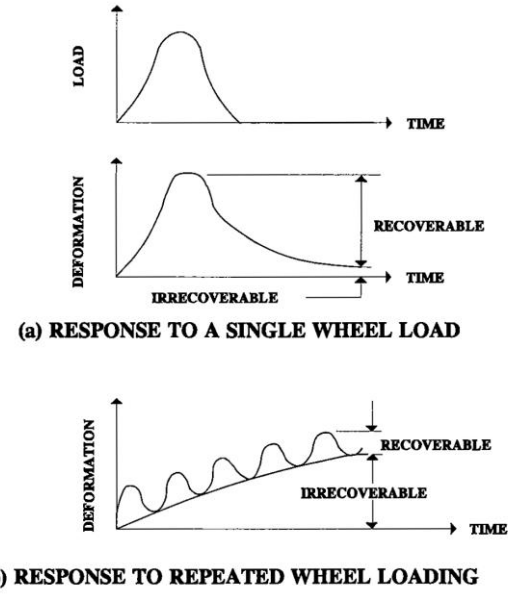

Figure 1.1: Visco-elastic response to millions of wheel loading (Read, 1996)

1.1.2 Fatigue cracking

Fatigue cracking can be defined as the phenomenon of fracture under repeated or fluctuating stress having a maximum value generally less than the tensile strength of the material (Rahman, 2004). Fatigue resistance of an asphalt mixture is the ability of the mixture to withstand repeated bending without fracture. Fatigue is one of the common forms of distress in asphalt pavements and manifests itself in the form of cracking under repeated traffic loading or a series of temperature fluctuations/variation in the pavement. The latter is referred to as thermal fatigue cracking. Fatigue cracking consists of two phases namely: crack initiation and crack propagation. Fatigue cracking initiates at the bottom of asphalt base and appears on the pavement surface as interconnected tracks of different forms and it may also start at the surface and grow downwards as is the case for thermal (fatigue) cracking. Some forms of fatigue cracking include longitudinal cracking, transverse cracking, and block cracking

Longitudinal cracking is a type of fatigue failure with cracks parallel to the centre line of the pavement. Transverse cracking has cracks perpendicular to the centreline of the pavements at

regular intervals. They are caused mostly by severe drops in temperature or by thermal fatigue resulting from repeated low and high temperature cycles. Block cracks are interconnected cracks that divide the pavement surface into approximately rectangular pieces.

1.2 Reflective cracking

This section looks at the definition of reflective cracking. Mallick and El-Korchi (2009) described reflective cracking as cracks in asphalt overlays caused by discontinuities in the pavement structure underneath. Cleveland et al (2002) defined it as the propagation of cracks from the movement of the underlying pavement or base course into and through the new overlay as a results of load-induced and/or temperature induced stresses.

Penman and Hook (2008) put it as the process by which an existing crack, joint or discontinuity propagates towards the surface through an overlying layer of asphalt concrete, with the rate of propagation varying significantly based on various environmental and trafficking factors. Debondt (1999) defined it as the propagation of cracks or joints from an old pavement into and through the overlay. Caltabiano (1990) described it as the propagation of a previously defined crack through subsequent layers of a pavement. Bennett (2003) put it as cracking in HMA overlays that reflects the crack or joint pattern in the underlying pavement. Shalaby and Frenchette (2000) defined it as the premature occurrence of cracks on overlays at positions and orientations that corresponds to locations of cracks in lower pavement layers.

In summary, reflective cracking can simply be defined as the propagation of existing cracks in an old pavement through the underside of the overlay to the surface. All these definitions imply that two processes are involved in the appearance of reflective cracks on the surface of the overlays, which are the crack initiation and crack propagation processes and they also

highlighted the two major causes of reflective cracking. Figure 1.2 shows a schematic of reflective cracking in HMA overlay on Portland cement concrete (PCC) slab or asphalt concrete (AC).

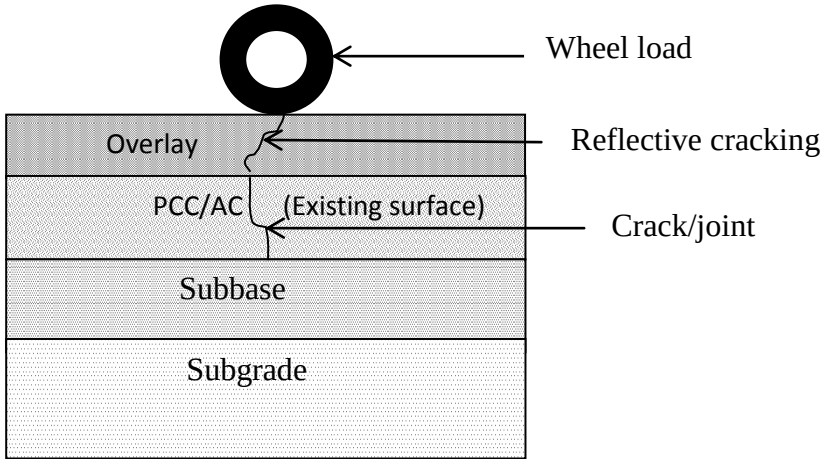

Figure 1.2: Schematic of reflective cracking in pavement

1.3 Causes and mechanism of reflective cracking

A number of factors have been identified as the causes of reflective cracking. Palacios et al (2008) reported that cracks propagate to new overlays due to vertical movement of the underlying pavement layer which may be due to traffic loading, frost heave and consolidation of the subgrade soils and/or the horizontal movement of the pavement upper layers due to temperature changes. Von Quintus et al (2007) reported three causes of reflective cracking, the major being horizontal movements from the expansion and contraction of the base pavement that is caused by temperature changes; the differential vertical deflections between the approach and departure slabs or across transverse cracks, which create shear stresses; and the curling of PCC slabs during colder temperature when the HMA overlay is stiff and brittle.

Abe et al (2000) stated that cracking was caused on the surface of the overlay at an early stage by the movement of the pavement and traffic load. Smith (1983) also mentioned the differential vertical movement at a crack or slab joint in the old pavement which induces a

vertical shear stress in the overlay, horizontal movement associated with temperature or moisture changes in the old pavement which induces tensile stress in the overlay or live load flexural stress in the overlay, which tends to concentrate directly over discontinuities. Based on the causes identified by researchers, there seems to be an agreement on the causes of reflective cracking. While it is common knowledge that factors such as subgrade conditions, pavement materials quality, workmanship etc affect the performance of a pavement; the principal factors responsible for reflective cracking are the action of traffic loading on an overlay on a cracked pavement and thermal stresses developed on the crack tip as a result of daily/seasonal temperature variation. These two factors have been investigated in this study.

It is important that the mechanisms of reflective cracking are well understood to be able to provide a solution to the problem. This is illustrated in Figures 1.3 and 1.4. Figure 1.3 (a and c) depicts a situation where the moving wheel on the edge of the pavement above the crack produces maximum shear stresses, A and C, respectively as shown in Figure 1.4, while in Figure 1.3(b), the wheel directly on the overlay above the cracked pavement generates flexural stresses producing maximum bending stress, B as indicated in Figure 1.4. Figure 1.3(d) expresses the tensile stresses developed in the overlay as a result of daily/seasonal temperature variation.

This illustration clearly indicates that there are three modes of reflective cracking. Molenaar (1993) established the three modes: mode I, mode II and mode III cracking. Mode I cracking occur due to tensile stresses caused by a drop in temperature or flexure under traffic loading. Mode II cracking is caused by the effects of shear stress induced by a loaded wheel crossing from one side of a transverse crack or joint to the other. Mode III referred to as the tearing mode is less common. This occurs in pavements when the wheel load travels along (parallel to) a crack. Figure 1.5 shows the three modes of cracking.

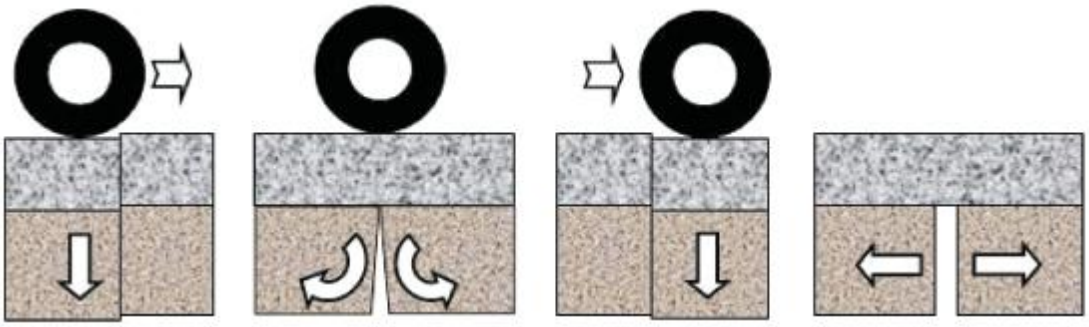

(a) (b) (c) (d)

Figure 1.3: Movements in pavement joints and cracks (Prieto et al, 2007)

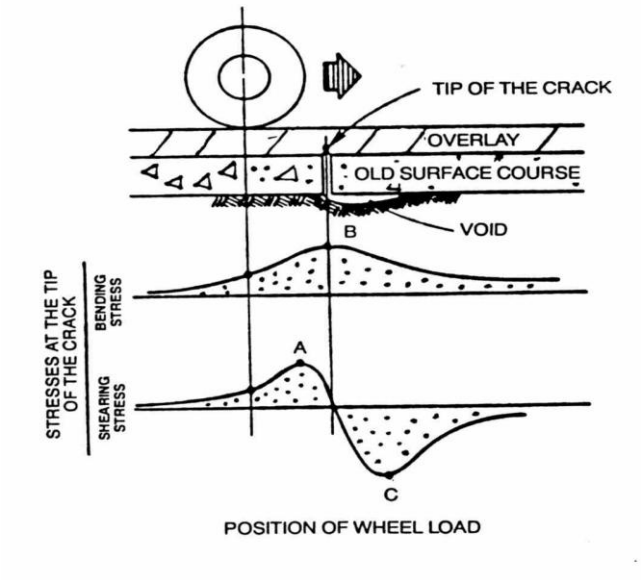

Figure 1.4: Stresses induced at crack tip by wheel load (Lytton, 1989)

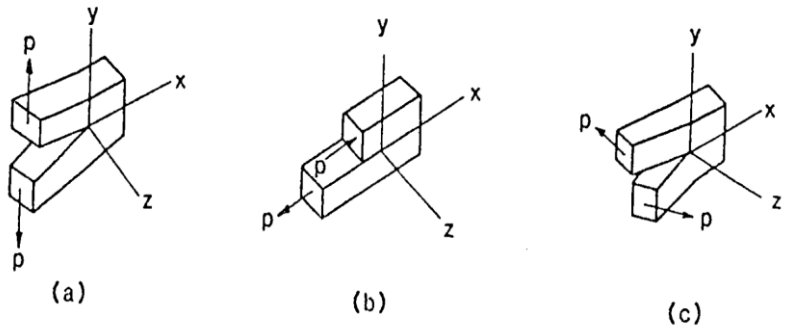

Figure 1.5: Modes of cracking (a) mode I (b) mode II and (c) mode III (Hughes, 1986)

1.4 Stress absorbing membrane interlayers (SAMIs)

These are interlayers designed to dissipate energy by deforming horizontally or vertically, therefore allowing the movement (vertical/horizontal) of the underlying pavement layers without causing large tensile stresses in the asphalt overlay. Barksdale (1991) defined a stress-relieving interlayer as a soft layer that is usually thin and is placed at or near the bottom of the overlay. He stated further that the purpose of the soft layer is to reduce the tensile stress in the overlay in the vicinity of the crack in the underlying old layer and hence "absorb" stress.

The application of stress-relieving systems at the interface between the overlay and the old pavement surface reduces the shear stiffness of the interface. Debondt (1999) proved using theoretical analysis that the reduction of shear stiffness allows slip of the interface, thereby isolating the overlay from the stress concentration of the crack tip.

Lytton (cited in Elseifi, 2003) summarised stress relief failure mode as follows:

- The crack starts to propagate (due to thermal and traffic loading) from its original position upwards until it reaches the stress-relieving layer. Due to its low stiffness, the interlayer will exhibit large deformations, which will be accompanied with a dissipation of energy. The crack propagation will stop for a while due to the lack of energy, and then propagate from the top of the interlayer upward to the surface bottom-up cracking).
- In the second failure mode, the crack starts to propagate from its original position upward until it reaches the stress-relieving layer. The crack then begins from the top of the overlay to the interlayer (top-down cracking).

1.5 Research Objectives

Most of the pavement projects around the world today are rehabilitations of existing road pavements (rigid and flexible). The common method adopted (overlaying) has been plagued with the problem of reflective cracking. Engineers have battled the problem for years introducing various measures, but the fight is far from being won. This study assesses the contribution of some stress absorbing membrane interlayers (SAMIs) on overlaid pavement performance in delaying the offset of reflective cracking.

The principal aim of this research was to examine the mechanical behaviour of stress absorbing membrane interlayers (SAMIs) placed over an existing cracked flexible pavement with a view to developing better understanding of their use to retard/reduce reflective cracking.

The specific objectives were to:

i. characterise the materials used in selected SAMI systems and an overlay material;
ii. develop laboratory tests to simulate reflective cracking due to traffic and thermal loadings;
iii. evaluate the effects of composition of the SAMI system (binder, glass fibre, aggregates) and thickness on resistance to reflective cracking;
iv. examine the interface bond between the SAMI systems and overlay;
v. investigate the performance of the SAMI systems in the Pavement Test Facility under more realistic traffic loading conditions;
vi. model the wheel tracking test to assess the crack resistance of SAMI systems;
vii. and produce a simplified design guide for effective use of SAMI systems against reflective cracking on an existing cracked flexible pavement.

1.6 Scope of research

This research involved three major activities. The first was the laboratory evaluation of the effects of traffic loading and thermal induced stresses on an overlay (with and without SAMIs) on cracked pavements. This involved characterization of the materials (overlay and SAMIs) for the research; determination of the bonding properties of the interface between the SAMI and the overlay; evaluation of the effect of traffic and thermal loads on reflecting cracking.

The second activity was a large scale test in the pavement test facility. This was carried out to reflect the condition that is obtainable in the field as nearly as possible. It involved construction of a flexible pavement section in the laboratory and dividing the pavement into sections with different sections having different SAMIs (and control sections) over a simulated cracked pavement and overlaying with new surfacing material. The performance of different sections was monitored and the data analysed.

The third activity was the theoretical investigation of the role of SAMIs in reducing/retarding reflective cracking. This was carried out with Abaqus finite element software to model the wheel tracking test. This gives a better understanding of the mechanical behaviour of the SAMIs and allows combinations that cannot be tested in the laboratory to be analysed. The proposed investigation for the research is shown in the flow chart in Figure 1.6.

1.7 Thesis structure

This thesis is divided into ten chapters. Chapter one gives the background of the study. The objectives and the scope of the study are highlighted in this chapter. The literature review on the laboratory and field/accelerated investigation of the use of interlayers against reflective cracking is reported in chapter two. Different interlayer materials and the methods of

assessment and specimen sizes were considered. Also, the interface bond between pavement layers with and without interlayer materials was reviewed.

The properties of the materials for the study are detailed in Chapter three. The properties examined include the aggregate particle size distribution, stiffness modulus, fatigue and permanent deformation. The Leutner shear test and the pull-off test carried out to examine the interface bond of the overlay-SAMIs interface are reported in chapter four.

Chapter five consists of the wheel tracking test procedure, specimen preparation and results. The chapter looks at the effect of factors such as SAMI thickness, overlay thickness, SAMI composition, temperature and load levels etc on the crack resistance potential of SAMIs. The modelling of the wheel tracking test using commercial finite element software Abaqus is reported in chapter six. The pavement test facility (PTF) carried out to simulate field conditions is discussed in chapter seven. The construction of the PTF pavement, instrumentation and results are reported.

Chapter eight discusses the thermal cycling test developed and carried out in the study to evaluate the crack resistance potential of the SAMIs against temperature variation. The design guide developed from the findings of the study for the effective use of SAMIs against reflective cracking under traffic and thermal loadings is reported in chapter nine.

Lastly, the conclusions from this study and recommendations for further study are given in chapter ten.

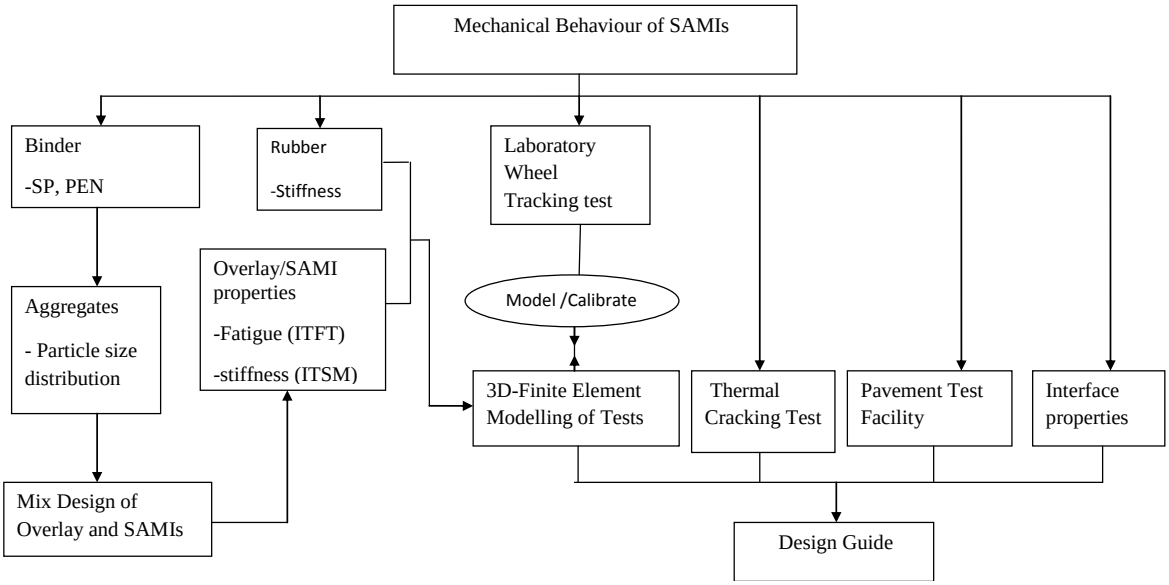

Figure 1.6: Proposed Research Plan

REFERENCES

Abe N., Maehara H., Maruyama T., and Ooba K. (2000): An Examination of Factor which affects Reflective Cracking. Proceedings of 4th International RILEM Conference, Ottawa, Canada. 464-474.

Al-Qadi I.L., Baek J., and Buttlar W.G. (2008): Development of Reflective Cracking Index to Determine the Effectiveness and Service Life of Strip Interlayer Systems. Proceedings of 6th International RILEM Conference, Chicago, U.S.A. 801-810.

Barksdale R.D. (1991): Fabrics in Asphalt Overlay and Pavement Maintenance. National Cooperative Highway Research Program Synthesis of Highway Practice 171. Transportation Research Board. Washington D.C.

Bennett (2003): Guidelines and Proceedings for Maintenance of Airport Pavements. Federal Aviation Administration, U.S. Department of Transportation. AC-150/5380-6A.

Bhosale S.S. and Mandal J.N. (2008): Open Graded Asphalt Concrete for Mitigation of Reflection Cracking on Asphalt Concrete Overlays. 12th International Conference of International Association for Computer Methods and Advances in Geomechanics (IACMAG), India. 4409-4416.

Caltabiano M.A (1990): Reflection Cracking in Asphalt Overlays. Thesis submitted to University of Nottingham for the degree of Master of Philosophy.

Cleveland G.S., Button J.W., and Lytton R.L. (2002): Geosynthetic in Flexible and Rigid Pavement Overlay. Texas Transport Institute, Texas A&M University System. Report 1777-1.

Debondt A.H. (1999): Anti Reflective Cracking Design of (Reinforced) Asphaltic overlays. PhD Thesis submitted to Delft University of Technology, Netherlands.

Dempsey B.J. (2002): Development and Performance of Interlayer Stress-Absorbing Composite in Asphalt Concrete Overlays. Transportation Research Record 1809. 175-183.

Elseifi M.A. (2003): Performance Quantification of Interlayer Systems in Flexible Pavements Using Finite Element Analysis, Instrument Response and Non Destructive Testing. PhD Thesis submitted to Virginia Polytechnic Institute and State University.

Engle E. (2001): Field Evaluation of Engineering Fabrics for Asphalt Concrete Resurfacing - Audubon County. Iowa Department of Transportation. Iowa, USA. Final Report 8-93 to 6-99.

Hughes D.A.B. (1986): Polymer Grid Reinforcement of Asphalt Pavements. Thesis submitted to University of Nottingham for the degree of Doctor of Philosophy.

Khodaii A., Fallah S. and Nejad F.M. (2008): Effects of geosynthetics on reduction of reflection cracking in asphalt overlay, Geotextile and Geomembrane, doi:10.1016/j.geotexmem.2008.05.007.

Lytton R.L. (1989): "Use of Geotextiles for Reinforcement and Strain Relief in Asphalt Concrete. Journal of Geotextiles and Geomembranes. 8(3) Pp 217-237

Mallick R.B. and El-Korchi T. (2009): Pavement Engineering: Principle and Practice. Taylor and Francis Group, USA.

Moleenar A.A.A. (1993): Evaluation of Pavement Structure with Emphasis on Reflective Cracking. Proceedings of 2nd International RILEM Conference, 21-48.

Palacios C., Chehab G.R., Chaignon F. and Thompson M. (2008): Evaluation of fibre reinforced bituminous interlayers for pavement preservation. Proceedings of 6th International RILEM Conference, Chicago, U.S.A. 721-729.

Penman J. and Hook K.D. (2008): The Use of Geogrids to Retard Reflective Cracking on Aiports, Runways, Taxiways and Aprons. Proceedings of 6th International RILEM Conference, Chicago, U.S.A. 713-720.

Prieto J.N., Gallego J. and Perez I. (2007): Application of the wheel reflective cracking test for assessing geosynthetics in anti-reflection pavement cracking systems, Geosynthetics International, 14(5) P 287-297.

Rahman M. (2004): Characterisation of Dry Process Crumb Rubber Modified Asphalt Mixtures. PhD Thesis submitted to University of Nottingham.

Read J.M. (1996): Fatigue Cracking of Bituminous Paving Mixtures. PhD Thesis submitted to University of Nottingham, Nottingham, UK.

Roberts, F.L.; Kandhal P.S.; Brown E.R.; Lee D.Y.; and Kennedy T.W. (1996): Hot Mix Asphalt Materials, Mixture Design and Construction. NAPA Research and Education Foundation, Lanham, Maryland.

Shalaby A. and Frechette L. (2000): Reflective cracking on C-SHRP Long Term Pavement Performance Sites. Proceedings of 4th International RILEM Conference, Ottawa, Canada. 241-250.

Smith (1983): Laboratory Testing of Fabric Interlayers for Asphalt Concrete Paving: Interim Report. Transportation Research Record 916. 6-17

Vervaecke F., Maeck J. and Vanelstraete A. (2008): On Site Validation and Long Performance of Anti-Cracking Interfaces. Proceedings of 6th International RILEM Conference, Chicago, U.S.A. 761-768.

Von Quintus H.L., Mallela J., Weiss W. and Shen S. (2007): Techniques for Mitigation of Reflective Cracking. Applied Research Associates, Champaign, IL, USA. Interim Report AAPTP 05-04.

2 LITERATURE REVIEW

2.0 Introduction

Researchers have carried out investigations into a number of methods of reducing/retarding reflective cracking, with their works achieving mixed results. The research works included both laboratory (small and large scale) and field investigations. Some of them are reviewed in this section. The literature review was necessary in this study to understand the factors that influence the performance of interlayers in general and SAMIs in particular. It is important to understand the benefits or otherwise of the test methods adopted. Also, this section examines design approaches or methods documented for cracked pavements incorporating interlayers.

2.1 The use of interlayers to reduce reflective cracking

Different interlayer materials have been used in pavement to delay reflective cracking. These are classified generally as stress relieving interlayers or stress absorbing membrane interlayers and reinforcing interlayers. This study looks at the former and has been defined in section 1.4. Stress relieving interlayers are usually made of bituminous mixtures, modified bitumen, glass fibres sandwiched with bitumen, and bitumen impregnated geotextiles (Woven and non-woven). Reinforcing interlayers are required to have higher stiffness than the surrounding layers (the overlay and existing pavement). This allows an overlay over a cracked pavement to support greater bending for a given strength of the asphalt concrete. A reinforcing system enables the transfer of tensile forces at the bottom of the overlay after the asphaltic mix has cracked at this location (Debondt, 1999). As observed by Asphalt Academy (2008), the primary effect of grid reinforcement is to hold the two sides of a developing crack together. This results in reduction of the stresses and strains at the tip of the crack. Types of reinforcing interlayer include polyester grid, glass fibre grid, steel mesh etc. Debondt (2000)

observed that the strength values range between 15 and 250kN/m and that the selection of the reinforcing products based on strength criterion is not possible, as the effect of reinforcement in tackling cracking depends on its stiffness and the resistance it can generate against pullout from the surrounding asphalt concrete.

2.1.1 Laboratory investigations

Different test configurations have been used to study the effectiveness of interlayer materials against reflective cracking. Some of these are discussed in this section.

Caltabiano (1990) carried out a series of beam tests to assess the performance of interlayers to delay the propagation of cracks through asphaltic concrete overlays. The beam testing used a servo-hydraulic device to apply simulated loading to the specimen (see Figure 2.1). The testing programme was split into three series A, B, and C with thicknesses of 100mm for A, 75mm for B and C and maximum applied traffic load pressure of 810kPa for A and B and 555kPa for C. The interlayers included polymer modified binder, geotextile interlayer, geogrid interlayer and a control (standard asphaltic concrete). In order to further ascertain the performance of the interlayers and overlay thicknesses, he also conducted tests on slabs with and without the interlayers. The slab test simulated traffic loading by passing a moving wheel of variable load and speed over a slab of asphaltic concrete compacted on a timber base. The test arrangement was similar to the beam test. He reported that although there was debonding between overlay and timber bases (old pavement), the polymer modified binder, geotextiles, and geogrid interlayers gave 2.5, 5.0 and 10 times increase in life, respectively. Also, he found that an increase in asphalt concrete thickness of 25% produced a corresponding increase in life for the control beam of 400%. He observed that increasing the load from 555kPa to 810kPa produced three-fold increase in life for geogrid or geotextiles interlayer compared to control, while no increase was produced for specimen with polymer modified binder.

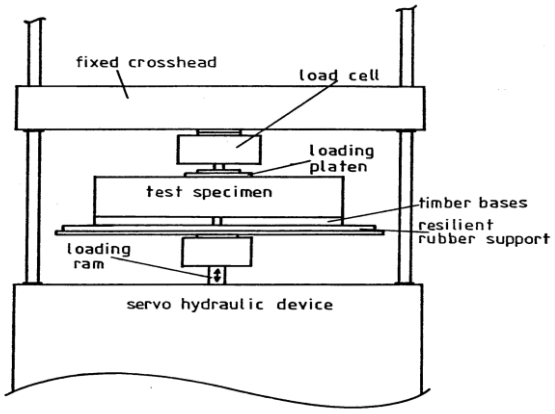

Figure 2.1: Beam testing arrangement (Caltabiano, 1990)

Sanders et al (1999) carried out laboratory tests to evaluate the effect of grids and fabrics on crack and rut control. He made use of beams similar to those used by Caltabiano, but the beam was placed on a 13 mm rubber foundation. The laboratory work included beam testing (on elastic foundation), large scale cyclic shear box testing and wheel loading in a pavement test facility. The beams, of dimension 400 mm in length, 200 mm width and 120 mm height, were reinforced at 30 mm from the bottom of the beam. They reported that the beam test results showed changes of behaviour which depend on reinforcement type. The beams reinforced with glass grids and control samples had similar shapes, as did the plots of composite-reinforced and steel and polypropylene grid-reinforced beams. It was stated that the difference in performance of the grids was due largely to the level of stress generated in the asphalt-reinforcement bond. They pointed out that the pavement test results showed clear differences in the performance of reinforced and unreinforced sections, both in cracking and rutting. They concluded that the reinforced pavements withstood approximately twice the number of wheel loads before the development of active surface cracking.

Krevtov and Gorelysheva (2000) examined the influence of thin interrupting layers on the development of reflected cracks. They used a different approach from Caltabiano and

Sanders. This involved pressing the specimens between two parallel plates of diameter equal to that of the specimen with continuous distributed load, P, applied at two air temperatures, +20^{o}C and 0^{o}C. They based their analysis on the relative shear viscosities of the specimen, because the elastic moduli did not differ much from each other and did not deviate from the norm. They concluded that specimens without a thin layer demonstrated high rates of forming reflected cracks, while specimens with a thin layer gave mixed results at both +20^{o}C and 0^{o}C. Their conclusion was based on the opinion that upper course material shear viscosity, related to elastic modulus of the pavement courses, is the parameter most completely determining the processes of both creep and stress relaxation and consequently the capability to slow down development of cracks in pavement upper courses. It has to be stated that their approach is not commonly used because it did not simulate the field situation (shear, flexural and tensile stresses in pavement).

Nataraj and Vander Meer (2000) studied the use of a crack relief layer (CRL) in airport pavements for rehabilitation of existing pavements and for construction of new ones using triaxial tests. In their study, 6 cylindrical specimens of field mix CRL with height 200mm and a diameter of 100mm were subjected to cyclic vertical stress (dynamic) due to traffic loading at temperatures of 50^{o}C and 60^{o}C. They observed that CRL specimens showed a large initial permanent vertical strain. After the initial phase the further development of permanent deformation in the CRL specimen was limited. They concluded that the CRL would perform well under heavy aircraft load without traffic densification or rutting and would play a significant part as a structural layer in the total pavement. Although, the present study does not focus on permanent deformation, their test demonstrated that when a CRL or SAMI is used in pavement rehabilitation or construction, it does not give permanent deformation concerns. They concluded from their field trial that a CRL with at least 20% air voids can effectively be used for airport pavements as a means of prevention of reflection of cracks and

as structural layer. Blankenship et al (2004) reported the use of an interlayer of asphalt rich, highly polymer modified binder and fine aggregate hot mix to retard reflective cracking. They used flexural beam fatigue tests. Their results showed that specimens with reflective crack relief interlayers had a minimum of 100,000 cycles at 2000 micro strain before failure, while unmodified asphalt typically failed at 2000 cycles. A high quality polymer modified asphalt such as PG76-28 withstood three times as many cycles as the unmodified asphalt, but still failed at 6000 cycles at 2000 micro strain.

Cleveland et al (2002) evaluated geosynthetics placed under or within a hot mix asphalt (HMA) overlay to reduce the severity or delay the appearance of reflection cracks using the Texas Transport Institute (TTI) overlay tester (see Figure 2.2). The overlay tester evaluates the relative ability of a HMA beam (3"(76.2mm) × 6"(152.4mm) ×20"(508mm)) with and without geosynthetics to resist thermal cracking. The geosynthetics used in the research were Bitutex composite, Pave-Dry 381, PetroGrid 4582, Ha Telit C40/17, Glass Grid 8501 and Star Grid G+PF. In the study, six beams were reinforced with geosynthetic materials, with the seventh unreinforced representing the "control" beam. The beams were prepared by compaction of a 1-inch (25.4mm) HMA "level up" course and cured in the mould for a minimum of 24 hours at room temperature. A geosynthetic material was applied to the level up course using AC-20 binder. After the material was allowed to set overnight and obtain full adhesion with the level-up course, the final overlay course of HMA was compacted in two 1" (25.4mm) layers. The beams were tested to failure in the overlay tester. They stated the geosynthetic materials consistently increased the number of cycles to failure in the laboratory test. The ranking of the relative effectiveness of each geosynthetic product in reducing reflective cracking in HMA overlays as tested in the laboratory is shown in Table 2.1

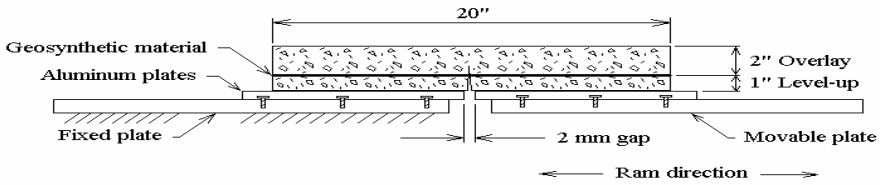

Figure 2.2: Schematic of TTI overlay tester (Cleveland et al, 2002)

Table 2.1: Ranking of the geosynthetic products (Cleveland et al 2002)

Product tested	Relative effectiveness (1= best; 8 = worst)
StarGrid GP+F	1
GlassGrid 8501	2
PaveDry 381	3
Bitutex Composite	4
PetroGrid 4582	5
Control (with tack)	6
HaTelix C40/17	7
Control (with no tack)	8

Farshad (2005) found that paving fabric effectiveness is related to joint or crack movement in the underlying pavement, crack width, overlay thickness, subgrade conditions, climate and traffic volume. He reported that nonwoven geotextile interlayer systems (paving fabrics) used in conjunction with asphalt overlays, typically 1.5-2.5 inches (38.1-63.5mm) may be used to absorb the stresses normally transferred from cracks in an old pavement into the overlay, thus retarding reflective cracking. He stated that the interlayer enhanced performance through two mechanisms, which are by stress relieving and water proofing. Prieto et al (2007) carried out research at the Road Laboratory of the Technical University Madrid in Spain to gather insight into the reflective cracking phenomenon, the evolution and configuration of the cracks and bonding conditions between materials. Rather than examining each parameter responsible for reflective cracking separately as Caltabiano, Sanders et al, Krevtov and Gorelysheva etc did,

they developed laboratory equipment capable of simultaneously applying the flexural, tensile and shear stresses involved in the process of reflective cracking in the overlays and geotextile-based anti-reflective system. The potential benefit of using three different geotextile inclusions was studied. They carried out the study with a test temperature of 5±1^{o}C; maximum deflection of 0.45 mm; crack opening velocity of 0.6mm/hr and the response variable was the time to achieve relative vertical movement between edges greater than 0.2mm. The specimens which comprised 10mm base and 50mm asphalt have width and height of 75mm and 60mm, respectively. The results indicated that the crack reflection strength values for specimens with geotextile were greater than those without. They reported that specimens without geotextile did not debond, thus the cracks reflected in a vertical direction, while those with geotextile experienced debonding making the cracks form at the side of the specimen. This highlighted that the introduction of interlayer materials may cause debonding at the interface. A schematic of their test equipment is shown in Figure 2.3.

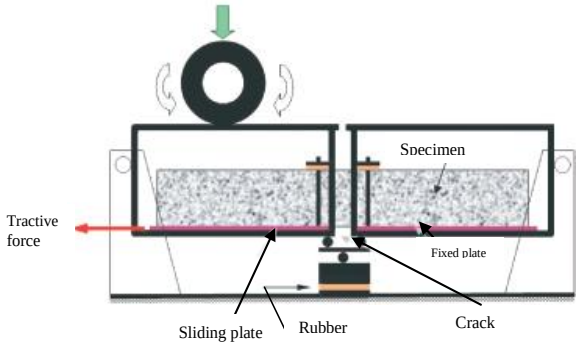

Figure 2.3: A schematic of wheel reflective cracking equipment (Prieto et al, 2007)

Zielinski (2008) evaluated the influence of geosynthetics on interlayer bonding and fatigue life of beams reinforced with geosynthetic. The overlay mix was asphaltic concrete with gradation 0/12, 8mm and 0/16mm and stone mastic asphalt (SMA). The geosynthetics were polyester nonwoven, polyester geocomposite, composite: glass grid with polyester nonwoven and control (specimens without geosynthetics). The bitumens used were pure bitumen D-70,

two ordinary bitumen emulsions: K1:65 and K1:70 and bitumen emulsion K-1-65MP modified with polymer. Fatigue tests were performed on 3-point bending beam samples, under constant load frequency and the number of cycles leading to fatigue and initial strain under bending of beams were measured. He concluded that application of non-wovens in asphalt layers had no influence on fatigue characteristics, because of the low stiffness modulus. He stated further that the effectiveness of application of geocomposites increased at the higher temperature (e.g. +18^{o}C), while at the temperature of -2^{o}C, the effect of geosynthetics application gave a weaker influence on fatigue properties. He also found that the interlayer bonding achieved by spreading bitumen has a strong influence on fatigue properties of a layer, but did not consider the effect of the bond on the potential of the geosynthetic to retard reflective cracking.

Bhosale and Mandal (2008) carried out a laboratory study on open graded asphalt concrete (OGAC) as a crack relief layer using an asphalt concrete slab fatigue testing equipment. Like Prieto et al, they evaluated both the effects of traffic load and temperature variation simultaneously. In the research, they investigated conventional dense bitumen macadam (DBM) and the OGAC overlay under simulated thermal and traffic loads with 5mm differential deflection. They performed the experimental work in a strain-controlled environment with an average room temperature of 29^{o}C. A gap of 5mm was maintained between two pavement plates, representing the initial existing crack width in the old distressed pavement. Simulation of daily and seasonal thermal contraction and expansion cycles was achieved by cyclically opening and closing the initial existing crack by 1.83mm at a strain rate of 4.547mm/min. In mixed mode of displacement, vertical compressive load, generating a contact pressure of 478.7 kPa for a standard axle load of 80 kN was applied using a pneumatic jack through a 15 mm thick pressure plate which simulated the highway truck dual tire assembly. The vertical load with a load pulse of 1 second and a rest period of 4

seconds, simulating a vehicle speed of 1 mile/h (1.6 km/h), was applied simultaneously with simulated thermal load cycles of opening mode of displacement. They concluded that the conventional overlay of DBM showed a faster rate of decay with the number of simulated thermal load cycles than the OGAC overlay.

Khodaii et al (2008) conducted an experimental program to determine the effect of geosynthetic reinforcement on mitigating reflection cracking in asphalt overlays. The study consisted of the following components representing a layered pavement structure: asphalt overlay 380mm × 150mm × 75mm, which was reinforced at the base and at one-third depth from the bottom and unreinforced, a block of asphalt or concrete simulating a discontinuous existing pavement (depth, 100mm) and a resilient subgrade modelled with neoprene rubber with an elastic modulus of 11000 kN/m^2. Simulated repeated loading was applied to the specimens using a hydraulic dynamic loading frame, which applied cyclic square loads to the top centre of the beam through a circular loading plate (112mm diameter) with a frequency of 10Hz simulating high speed traffic. A maximum load of 6.79kN creating $690kN/m^2$ was applied at 20^oC and 60^oC. Their test set up was as shown in Figure 2.4. Their results showed that geogrid inclusion in the asphalt sample improved overlay performance. Specimens with embedded geogrids outperformed non-reinforced samples both in terms of resistance to cracking as well as rutting. They stated that placing the geogrid at 1/3 height in the overlay was most effective, although it required the contractors to place the overlay in two layers, resulting in extra costs. Also, the effectiveness of the geogrid for overlay reinforcing with increasing crack/joint from 10-20 mm was not decreased, but at high temperature the effectiveness of the geogrid in overlay reinforcing in proportion to low temperature was reduced.

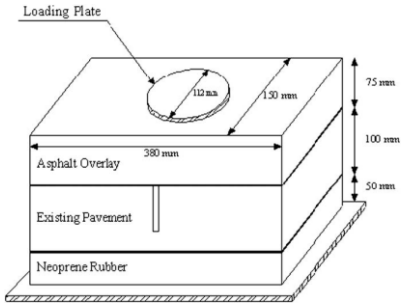

Figure 2.4: Test set-up (Khodaii et al, 2008)

In summary, it is clear from the literature that crack resistance of interlayers has been principally investigated using beam tests (three-point or four point bending) and repeated load from traffic has been mostly simulated in the laboratory using hydraulic loading machines capable of applying dynamic loads. The crack resistance of interlayers against reflective cracking has been investigated either by simulating the simultaneous effect of both temperature variation and traffic loading in a test or by studying the effect of each independently. While both processes may occur in practice simultaneously, studying the effect of each independently will allow better understanding of the mechanisms involved. Therefore, in this study each parameter has been studied independently. The present study is meant to simulate the field situation as closely as possible, therefore a wheel tracking device has been chosen to study the effect of traffic loading, while a thermal cycling device capable of opening and closing a joint/crack in a specimen at chosen rates has been used to study the effect of temperature variation.

Also this review has shown that the effectiveness of various interlayers depends on a number of factors such as crack movement, crack width, subgrade condition, climate, traffic volume, temperature etc. Furthermore, it was documented that the introduction of interlayers in a pavement may result in the debonding of the interlayer-overlay interface. Some of these

conditions have been investigated in this study in order to understand their influence on crack resistance.

Other methods of delaying reflective cracking include thick overlay, modification of overlay mixtures, crack control methodologies, and crack and seat/rubblization. The Defence Estates design options for minimization of reflective cracking in the medium term and long term is shown in Table 2.2. Also, the Highways Agency recommended the use of a minimum of 180mm asphalt overlay to jointed concrete, 150 mm for cracked and seated concrete and 180mm for composite pavement when cement bound granular mixture (CBGM) is pre-cracked (DMRB, 2006).

Thick overlay

The theory is that the thicker the overlay, the less the strain concentration around crack region. Also, when crack is intiated at the bottom of the overlay, it has to travel a longer distance to reach the surface. Mukhtar and Dempsey (1996) stated that thick overlays constructed with a high quality dense graded asphalt mix and low viscosity asphalt considerably delays reflective cracking. However, they noted they are usually the most expensive alternative.

Modification of overlay mixtures

This method is used to improve the fracture resistance of the overlay. The resistance of asphalt to cracking depends mainly on the binder content and its elastic characteristics, although the coefficient of expansion of the aggregate also contributes to the performance (Ellis et al, 2002). Thus, overlay modification is achieved majorly by modifying the binder. The use of modified binder improves the asphalt (overlay) ability to absorb stresses generated at cracks, its self healing properties and its resistance to ageing, which causes the asphalt to become brittle with time. A number modify asphalt mixes are described below:

Rubber asphalt: Addition of rubber particles to asphalt makes it more flexible, enabling it to withstand higher strains without breaking. The asphalt becomes softer and more elastic.

Polymer modified asphalt: Admixing styrene-butadiene-styrene (SBS), ethylene-vinyl-acetate (EVA) or styrene-butadiene-rubber (SBR) polymers to bitumen produces binders which are less temperature susceptible and which have higher viscosity at ambient temperature than unmodified bitumen (Von Quintus et al, 2007; Ellis et al, 2002). The improved properties of the binder increase the resistance of the modified asphalt mixes to cracking.

Sulphur asphalt: This is the modification of HMA by adding sulphur. This process increases the stability and stiffness of HMA at high temperatures and at the same time maintains the low (viscous) property of the asphalt. Admixing sulphur with HMA makes it soft at low temperatures and hard at high temperatures, thus the HMA has less cracking at low temperature as well as less rutting at high temperatures (Von Quintus et al, 2007).

Air-blown asphalt: This involves improving temperature susceptibility of waxy and low viscosity asphalt by oxidation (air blowing).

Carbon black: This is the addition of carbon black to HMA to increase its tensile strength.

Crack control methodologies

These are methods used to improve the load transfer across a crack. They include sawing and sealing of joints, re-strengthening of cracked pavement, heater scarification and pre-overlay repair.

Sawing and sealing of joints in HMA overlay: This involves sawing straight clean joints in the overlay on top of a joint, the HMA overlay directly above the joint in the existing

pavement. It has the advantage that the controlled saw cut can be more effectively sealed than a self-propagating zigzag reflection crack.

Re-strengthening, treatment or modification of cracked pavement before overlaying: In this case, the cracked pavement is strengthened to have a better pavement surface condition before overlaying

Heater scarification: This involves scarifying the cracked pavement surface to a depth of approximately 0.75in (9mm), so that the upper portion of any crack can be removed with any crack sealant and the lower portion of the crack sealed by the heating process. The remixed and re-compacted layer would then serve as a uniform un-cracked layer above the crack tip. As a consequence, the reflection cracking of the overlay should be significantly slowed down (Von Quintus et al, 2007).

Pre-overlay repair: This means injecting cement grout under PCC slab to fill any voids. This produces a good result when used in conjunction with other methods to prevent reflective cracking.

Crack and seat/Rubblization

PCC slab are broken into small sections (2ft to 6 ft fragments) and properly seated using a roller before the overlay is laid. This method is recommended for jointed reinforced concrete pavement. Potter et al (2000) demonstrated the potential of crack and seat technique to inhibit reflective cracking in the maintenance of a jointed unreinforced concrete pavement. Mukhtar and Dempsey (1996) stated that the cracking and seating operation reduces the structural integrity of the existing pavement and it requires a much thicker overlay. The thick overlay not only increases the cost but also creates problems of clearance and shoulder edge drop off.

Table 2.2: Design options for the minimisation of reflective cracking in the medium and long term (Defence Estates, 2005)

Severity Level	Medium term	Long term
Low	80mm Marshall Asphalt (MA) overlay	150mm MA overlay or 80mm MA asphalt + Porous Friction Course (PFC)
Medium	150mm MA overlay	220mm MA overlay or 150mm MA overlay + PFC
High	220mm MA overlay	300mm MA overlay or 220mm MA overlay + PFC or Crack and seat and overlay (MA/PFC)
Very high	Crack and seat and overlay or Geogrid +Overlay (MA/PFC)	Crack and seat and overlay (MA/PFC)

2.1.2 Field Investigations/ Accelerated pavement testing

Although laboratory tests have been used successfully to investigate the crack resistance of interlayer materials, it is essential that field investigations or accelerated (large scale) testing are carried for the results obtained from laboratory tests to be applicable in the field. This is because the field conditions cannot be completely simulated in the laboratory. Large scale testing has been carried out in different ways. Sanders (2001) highlighted four different approaches: building a pavement and monitoring under real traffic; building trial sections as part of a new road or as part of a maintenance treatment and monitoring performance under real traffic; building trial sections in the field and monitoring performance under accelerated traffic; and building trial sections in the laboratory for use with accelerated loading. The last two options have usually been embraced because they save time as results can be quickly obtained and prevent wastage of resources (money, manpower, etc) in case trials do not work. This section looks at some studies that had been carried out in this regard.

Allison (1989) evaluated the ability of rubber-asphalt binder stress absorbing membrane interlayer (SAMI) to delay or prevent reflective alligator cracking in the field under real traffic. In the study, rubber asphalt was placed as SAMI on two sections of SR-12 near

Morton, Washington in the US. The rubber asphalt consisted of AR-4000W asphalt and reclaimed rubber grade G274. In the field study, the existing roadway constructed in 1967 & 1968 consisted of 0.25ft (76.2mm) of asphalt concrete pavement (ACP) over 0.92ft (280.4mm) of untreated gravel and had severe alligator cracking. Also a 400 ft control section (without SAMI) was constructed. He reported that alligator cracking reflected in neither the SAMI section nor the adjacent control section after 10 years. His conclusion was that either the overlay was sufficient to mask the benefits of the interlayer or that the interlayer provided no benefits. His test further buttresses the fact that the performance of interlayers in reducing reflective cracking have been mixed.

Furthermore, Krevtov and Gorelysheva (2000) reported the use of organomineral mix (VOMS) as a thin interrupting layer on a rigid base course. They stated that inspection of the sections built with the mineral showed that VOMS slowed down development of reflected cracks in pavements. Also, Storsteen and Rumpca (2000) evaluated the ability of geosynthetics (LinqTac-711N and Strata Grid-200's) to ease distress and reflective cracking in asphalt overlays of jointed concrete pavements under real traffic. In their study, a test section of 2.2 km (1.4 miles) located at MRM 14 in the southbound lane of an Interstate was divided into twelve segments. Each segment had 10 joints. Each set of joints either contained geosynthetic Strata Grid-200 or LinqTac-711N, no fabric, maximum or minimum rehabilitation, and a sawed or unsawed joint. They defined maximum rehabilitation as cutting and removing four-foot sections to the base aggregate and minimum rehabilitation as brushing off and repairing small holes. Their results like those of Allison showed that LinqTac-711N and Strata Grid-200's were not effective in reducing/retarding reflective cracking. Rather, they recommended that the minimum rehabilitation including restoring load transfer where necessary and repairing spalled areas on Portland cement concrete pavement (PCCP) joints be carried out prior to completing asphalt concrete overlays. The failure of the

geosynthetic in this case might be due to a number of factors like the workmanship, the properties of the geosynthetics, condition of the existing pavement etc. All these should be considered before selecting an interlayer for maintenance work.

Engle (2001) investigated the effectiveness of two engineering fabrics: PavePrep and Proguard, to reduce reflective cracking on County F16, Audubon County, Iowa US. The existing hot mix asphalt (HMA) pavement was 22ft (6.71m) wide and was built in 1957. The original structure was a 6"(0.15m) HMA pavement placed over a granular surfaced roadway built in 1937. It was resurfaced in 1970 with a 3" (0.076m) asphalt overlay. He reported there was at least one slurry levelling course and at least one seal coat prior to his project. The existing pavement exhibited transverse cracking at approximately 40ft (12.19m) spacing, some quarter point cracking and some alligator cracking. A seal coat was placed in 1958 to alleviate surface ravelling in the experimental pavement. The field study consisted of a 3"(0.076m) thick HMA overlay with PavePrep, Proguard and a “control” with no geosynthetic. The data indicated a statistically significant decrease in reflective crack formulation in the Proguard fabric sections compared to the control. There was little evidence of a similar effect for the PavePrep fabric section compared to the control. However, the rate of cracking for both fabrics and the control tended to be similar after three years. Thus, he concluded that the benefit of using a fabric did not outweigh the costs of up to $4200.00 per mile. His conclusion was in line with Allison and Storsteen and Rumpca.

Ellis et al (2002) studied the performance of techniques to minimise reflection cracking for maintenance of UK military airfields. The techniques studied were: application of airfield friction course directly onto a jointed pavement before overlaying with Marshall asphalt, Stress Absorbing Membrane Interlayer (SAMI), SBS modified Marshall asphalt, fibreglass reinforcing grid and crack and seat. He found that the application of airfield friction course directly onto the jointed concrete pavement before overlaying with Marshall asphalt reduced

the occurrence of reflection cracking after nine years in service. Also, they reported that a SAMI and SBS modified Marshall asphalt wearing course overlay applied to a cracked flexible composite pavement reduced the amount of reflection cracking by about 80 per cent and the severity of cracks compared to an equivalent control area after nine years in service. They stated that the use of fibre glass reinforcing grid demonstrated the importance of installing it on an asphalt regulating layer and not directly on a milled surface under an asphalt overlay. They submitted that fewer reflection cracks occurred in test sections incorporating a polyester grid or fibreglass grid under 100mm of Marshall asphalt overlay, yet an associated control had cracked extensively. Again, Dempsey (2002) developed and evaluated the use of interlayer stress absorbing composite (ISAC) to alleviate the problem of reflective cracking in asphalt pavements. The ISAC consisted of a low-stiffness geotextile as the bottom layer, a viscoelastic membrane layer as the core, and a very high stiffness geotextile for the upper layer. In his study, a laboratory pavement section with an AC overlay placed on a jointed Portland cement concrete slab was constructed and tested in an environmental section. The thermal strain was simulated using a mechanical device, opening and closing the joint at extremely low rate. The temperature of the chamber was maintained at -1.1^{o}C. His results showed that the laboratory AC overlay section without ISAC (control) cracked and separated completely within seven cycles of joint movement. The AC overlay performed exceedingly well when it was treated with the ISAC system and tested under the same conditions as the control pavement. He reported that the overlay remained intact, when the slab movement increased progressively, and the crack appeared only when the slab movement had increased to 5.08mm and over and the ISAC geotextile had been subjected to 158 cycles.

Elseifi (2003) evaluated the potential of a specially designed geocomposite membrane to delay the reflection of cracks in flexible pavement systems using a 2D finite element model

and falling weight deflectometer (FWD). The geocomposite membrane was made of a 2mm thick low modulus polyvinyl chloride (PVC) backed on both sides with polyester nonwoven geotextile. The test section consisted of 150mm of 21B (base stone) aggregate layer (Virgiana Department of Transpotation specifications), 75mm of cement-treated drainage layer, a geocomposite membrane sandwiched between two lifts of base mix and a surface mix, SM-9.5D (asphalt concrete with 9.5 mm nominal maximum aggregate size), and the surface mix was an open-graded friction layer (OGFL). His FWD results showed that the area with geocomposite membrane had greater deflection than the area without geocomposite membrane. He concluded that the layer deflection should be anticipated and considered when geocomposite membrane is used to retard reflective cracking. He stated that large deflection implied that a pavement with a strain energy absorber (geocomposite membrane) would be less resistant to fatigue than a pavement without it, thus the overlay mixtures and thickness should be well designed to avoid premature failure of the pavement through a fatigue related mechanism. The test demonstrated the importance of having an overlay mixture with good properties and that caution should be taken in the design of the overlay mixture and thickness.

Vespa (2005) evaluated the use of interlayer stress absorbing composite (ISAC) and three other products namely: PavePrep, Roadtac and Sand Anti-Fracture (SAF). The ISAC considered in the study was a three-layer system. The top layer was a high strength woven geotextile. The middle layer was a modified rubberized asphalt layer to absorb the strain energy and bond the two geotextiles together. The bottom layer was a low strength geotextile. His distress survey showed that the formation of reflective cracks and the subsequent deterioration of the cracks were delayed at ISAC treated joints and cracks. He reported that the ISAC areas consistently outperformed PavePrep and Roadtac. When compared to SAF, ISAC delayed reflective cracks by about two years. The test showed that interlayers were able to reduce reflective cracking, one interlayer performing better than the other. Antunes et

al (2008) carried out eight years' performance monitoring of anti-reflective cracking solutions. The anti-reflective solutions considered in the study were SAMI with modified binder, cold asphalt concrete overlay, bitumen-impregnated geotextile and steel mesh with slurry. Also, two sections were constructed of asphalt concrete without anti-reflective cracking solution (reference). The monitoring activities comprised visual assessment of the pavement surface, rut depth measurement and falling weight deflectometer (FWD) test. They monitored the performance of the test sections between 1998 and 2005 and found that the section where cracking and rutting were developing fastest was the one with the cold asphalt overlay, and the sections with better performance were the ones with bitumen-impregnated geotextile and steel mesh reinforcements. They observed from the cores from the test sections that cracks originated at the surface and there was debonding at the geotextile and steel mesh interfaces. They stated that lack of bond was reflected in the FWD test results, since only the debonded sections presented an increase in the deflections between 2001 and 2005. Their study showed that top-down cracking may occur in the rehabilitated pavements with SAMIs.

Farshad (2005) reported that the field performance of paving fabric interlayer has generally been successful, but that there were cases where their use gave little or no improvement. He stated that they have been most effective when used for load-related fatigue distress, while they have not performed well when used to delay or retard thermal cracking. Vervaecke et al (2008) studied the long term performance of anti-cracking interfaces. In one of their experimental roads (Sint-Pieters-Leeuw), the bituminous overlay consisted of 5cm thick stone mastic asphalt (SMA), and four different anti-cracking interfaces were applied on the concrete slabs: a SAMI, a non-woven impregnated with elastomeric binder, a glass fibre grid, steel reinforcing nettings and a reference section without interface system. They divided the anti-cracking interfaces into two classes based on their performances. The first class was

formed by the SAMI and non-woven, both of which gave a considerable delay in crack initiation; the second class which performed noticeably better than the first class consisted of the grid and steel reinforcing netting. They reported that almost no cracks were visible with second class interlayers eight years after rehabilitation. While their tests showed that the reinforcing interlayers performed better than the stress absorbing ones, the cost analysis was not reported. It is generally known that the reinforcing interlayers are more expensive than stress relieving ones.

Also, Palacios et al (2008) evaluated the use of fibre reinforced asphalt treatment as a stress absorbing membrane interlayer (SAMI) to mitigate reflective cracking. Their study involved field evaluation and comparison of overlays with interlayers and those without an interlayer (control) on pavement test sections at the Pennsylvania Transportation Institute (PTI) test track. The evaluation comprised observation of construction process, accelerated trafficking, periodic distress and image surveys, in addition to non-destructive and destructive structural evaluation. The control section consisted of 2" (50.8mm) hot mix asphalt (HMA) overlay on top of an existing asphalt pavement, while the experimental section additionally contained the SAMI between the old and the new HMA overlay. Both sections were made to experience controlled bus traffic and 1 million loading cycles using the Mobile Model Load Simulator 1/3scale (MMLS3). They concluded the use of fibre-reinforced interlayer gave partial improvement in reflective cracking resistance. The examination of the field cores showed no reflected cracks were observed in the cores from the SAMI section, however an existing crack was observed propagating towards the surface of the new layer in the control section.

In summary, field/accelerated trafficking evaluation of interlayer materials to retard reflective cracking clearly indicates that results have been mixed. While some researchers have reported that the introduction of interlayer materials retards the appearance of cracks in the overlay, some have reported that they were not effective and some investigations were

inconclusive. It is intended to bridge this gap in knowledge by studying the effectiveness of some selected stress absorbing membrane interlayers in retarding reflective cracking in a pavement test facility. The pavement facility is a large scale wheel tracking test (laboratory based) at the University of Nottingham capable of applying a load of up to 12kN at room temperature. The test is reported in chapter seven. The test was chosen because the facility is readily available for the study and past studies reviewed in this section have shown that accelerated pavement testing with trial sections in the laboratory has been used successfully to evaluate the performance of interlayer materials.

2.2 Pavement design methods

The objective of pavement design is to produce an engineering structure that will distribute traffic loads efficiently whilst minimising the whole life cost of the pavement (Read and Whiteoak, 2003). The two common methods of pavement design are the empirical and analytical approaches. The analytical approaches can further be classified into mechanistic-empirical and mechanistic approaches. The empirical method is based on experience accumulated in practice and from specially constructed test sections. The empirical design methods are limited by the lack of capability to accommodate different conditions, such as temperatures, material properties, subgrade conditions, speed of traffic and other conditions that were not considered when they were developed. The mechanistic-empirical approach involves the relation of theory (calculated strains, stress and deflection) to observed performance under various conditions of traffic loading and environmental factors, while the mechanistic method employs the theoretical analysis of the mechanical properties of the materials and is able to accommodate any design situation.

2.2.1 Empirical design approach

In this method, the design traffic is estimated for new roads by a traffic study and for maintenance schemes or realignment by carrying out a 12, 16 or 24 hours traffic count, which is converted to an average annual daily flow (AADT) and design value read from charts. Also, the California bearing ratio (CBR) of the subgrade is assessed by test and the thickness of the sub-base and if necessary capping is also obtained from charts. The design traffic is used to calculate the total thickness of the layers above the subbase for different pavement types: flexible, flexible composite, rigid and rigid-composite. Examples of empirical design methods include the Asphalt Institute method developed in 1982, and the AASHTO Interim Design Method first developed in 1972 and subsequently updated in 1983 and 1993.

2.2.2 Analytical design approach

The philosophy of analytical design is that a pavement should be treated in the same way as other civil engineering structures (DMRB, 2006). The procedures involved in the analytical design approach are as follows:

a) Estimate the traffic loading in terms of an equivalent number of standard axle loads.
b) Consider the available and permitted pavement materials.
c) Estimate the size of the components (in situ dimensions and long-term performance of each individual layer of the pavement).
d) Carry out structural analysis to determine the stresses, strains and deflections at critical points in the structure (using a simplified multi-layer elastic model of the pavement structure).
e) Compare the critical stresses, strains and deflections in the pavement with maximum allowable values to check if the design is satisfactory.

f) Repeat steps c, d and e until a satisfactory pavement design is achieved.

g) Consider the economic feasibility (the whole life value) of the design

A number of computer programs have been developed which are capable of calculating stresses, strains and deflections for various pavement configurations. Some of them are as follows:

- Bitumen Stress Analysis in Road (BISAR) developed by Shell.
- CIRCLY developed in Australia as an integral component of the Austroads pavement Design Guide.
- KENLAYER developed at University of Kentucky.
- Design Manual for Roads and Bridges, Volume 7, (HD 24, 25 and 26) developed in the United Kingdom by the Highways Agency.

Also, designers have adapted some of these into design models (software) for overlay designs. Some of these include:

- EVERPAVE (Washington State Department of Transportation (WSDOT) mechanistic-empirical overlay design based on multilayered elastic analysis program;
- WESLEA (Waterways Engineering Station Elastic Layer Analysis Pavement Suite)
- AASHTO (DARwin) based on the AASHTO guide for design of pavement structures;
- M-E pavement design guide;
- Asphalt Institute (MS -17) equivalent thickness method.

Although some of these methods have been used to design pavements against reflective cracking, it has to be stated that these methods do not account directly for reflective cracking. Different models have been generated for design of overlays incorporating reinforcing or

stress relieving interlayers against reflective cracking. Some of them are highlighted in section 2.2.3

2.2.3 Design of overlays with interlayers

A number of design methods have been used for the design of overlays incorporating reinforcing or stress relieving interlayers. Sanders (2001) observed that although several design approaches exist, assessment of the accuracy and applicability of the methods is not straight-forward. He noted this was because the comparison of predicted behaviour and subsequent performance was not often done. Hughes (1986) modified an analytical design procedure for flexible pavements designed at the University of Nottingham by Brown and Brunton (1984) to include the benefits of using polymer grid reinforcement at various positions in the pavement. He concluded the programme was able to demonstrate the benefits of polymer grids in pavements including increase in design life of pavements susceptible to fatigue permanent deformation and reflective cracking. Hughes considered the benefit of reinforcing interlayer inclusion in an overlay over a cracked pavement by introducing a life increase factor of 3. This is based on the results of his laboratory study. His approach is limited because it does not consider the factors that are responsible for the increase in life. Also, his choice of increase in life of a factor of three was based on laboratory work, which may be totally different from what will happen in the field.

Also, Sousa et al (2001) developed a mechanistic overlay design method for reflective cracking. Their model was based on the finite element method (FEM) used to determine the stresses and strains in a hot mix asphalt overlay above a crack. They calibrated the FEM-modelled crack movements using field measurements with a crack activity meter and a falling weight deflectometer (FWD) conducted in Portugal, Arizona and California. They carried out laboratory testing that simulated the observed field crack movement and measured stresses and strains on test specimens similar to the actual field mixes to generate data for the

model. They converted the mathematical statistical model into a practical pavement design method for reflective cracking by calculating the estimated traffic until reflective cracking for a given layer thickness and layer modulus and then comparing the actual and observed number of truck loadings and percent cracking. The researchers stated that the models were generated for dense-graded hot mix asphalt and gap-graded asphalt rubber (wet process- 80% asphalt and 20% ground tyre rubber), but that other HMA mixes used for overlay may be calibrated and used through the proposed method. Their approach is noteworthy in that it considers some of the factors that are responsible for reflective cracking on overlay over an existing pavement. The shortcoming of their design is that the model was developed for a particular region and mixtures. As they stated, while it is possible to use the moduli and fatigue characteristic of other mixtures, it must be assumed that the temperature adjustment factor or the aging adjustment factor will be identical to that of dense-graded hot mix asphalt (HMA-DG) and gap-graded asphalt rubber (AR-HMA-GG) used to generate the models.

Elseifi and Al-Qadi (2003) developed an overlay design procedure to predict the service life of rehabilitated flexible pavement structures against reflective cracking. They used linear elastic fracture mechanics (LEFM) principles to derive a simple equation based on three-dimensional (3D) finite element (FE) models that can be used to predict the number of cycles to failure against reflective cracking for rehabilitated flexible pavements. Their model considered both the crack initiation and propagation stages. The crack initiation stage was described using a traditional fatigue law (see equation 2.1) and the crack propagation stage was described using the Paris' law (see equation 2.2). They used the commercial software ABAQUS 5.8-1 to indirectly calculate the stress intensity factor using the path independent integral, called J-integral (plain strain) (see equation 2.3).They established three levels of overlay fracture characteristics by relating the first fracture parameter (n) of the material to its

creep properties (see equation 2.4) and the second fracture parameter (*A*) was determined by means of the volumetric and modulus of the mix (see equation 2.5). They developed a regression model to predict the number of cycles in ESALs as a function of the significant variables. The developed design equation (see equation 2.6) was based on the results of all the considered cases in their study. Although, Elseifi's approach is thorough in considering crack initiation and crack propagation through overlay on a crack pavement, it does not consider the introduction of a stress relieving or reinforcing interlayer to retard or delay reflective cracking.

$$N = 4.856\ 10^{-16}\varepsilon_{zx}^{-4.73} \quad \ldots\ldots\ldots\ldots\ldots\ldots\ldots\ldots\ldots\ldots\ldots\ldots\ (2.1)$$

Where,

N = number of cycles before crack initiation

εzx = shear strains 0.4 inch (10 mm) above the existing crack

$$\frac{dc}{dN} = A(\Delta K)^n \quad \ldots\ldots\ldots\ldots\ldots\ldots\ldots\ldots\ldots\ldots\ldots\ldots\ldots\ldots\ (2.2)$$

Where, *C* = crack length

N = number of loading cycles

A and *n* = fracture parameters of the material

ΔK = stress intensity factor amplitude.

$$J = \frac{1-v^2}{E}(K^2) \quad \ldots\ldots\ldots\ldots\ldots\ldots\ldots\ldots\ldots\ldots\ldots\ldots\ldots\ldots\ldots\ (2.3)$$

Where,

J = J integral

V = Poisson's ration

E = elastic modulus

K = stress intensity factor

$$n = \frac{2}{m} \quad \text{..... (2.4)}$$

Where, *m* = slope of the log creep compliance versus log time curve

$$\text{Log A} = -2.605104 + 0.184408\text{AV} - 4.704209 \log \text{AC} - 0.00000066\text{E} \quad \text{..... (2.5)}$$

Where

AV = air-voids (%)

AC = asphalt content (%)

E = resilient modulus of the mixture (in psi).

$$Log\ W_{t80} = (255H_{overlay} + 2.08E_{overlay} + 45.3H_{HMA} + 8.73E_{HMA} + 1.34H_{base} + 6.93E_{base} + 1.49E_{subgrade}) \quad \text{..... (2.6)}$$

Where,

Wt80 = total number of 80-kN single-axle load applications

$H_{overlay}$ = thickness of HMA overlay (mm)

$E_{overlay}$ = resilient modulus of HMA overlay (MPa)

H_{HMA} = thickness of existing HMA layer (mm)

E_{HMA} = resilient modulus of existing HMA layer (MPa)

H_{base} = thickness of base layer (mm)

E_{base} = resilient modulus of base layer (MPa)

$E_{subgrade}$ = resilient modulus of subgrade (MPa)

The new AASHTO Mechanistic-Empirical Pavement Design Guide (MEPDG) for HMA overlays of existing HMA surfaced pavements considers distresses developing in the overlay as well as the continuation of damage in the existing pavement structure. However, it was stated that the reflective cracking models incorporated in the MEPDG were based strictly on empirical observations and were not a result of rigorous mechanistic-empirical analysis (Hajj et al, 2008). The proposed MEPDG overlay design procedure allows engineers to consider two types of reflective cracks: reflective cracks that exist on the surface prior to overlay placement; and those that develop in the existing surface after overlay placement. The percentage of reflective cracks through the overlay is predicted as a function of time using a sigmoidal function (see equation 2.7). The *a* and *b* fitting parameters are functions of the HMA overlay thickness and are hard coded in the MEPDG software. The designer cannot directly alter these parameters as inputs, but can change them in the software. They recommended that an agency use historical data to develop a local reflection cracking model. Also, the MEPDG approach assumes based on empirical considerations that a properly installed fabric is equivalent to 2 inches (50.8 mm) of HMA overlay. Lastly, they recommended a minimum of 2 inches (50.8 mm) for the HMA overlay thickness (*hac*) of flexible pavements. As mentioned earlier, the consideration of reflective cracking in the new AASHTO Mechanistic-Empirical Pavement Design Guide (MEPDG) was based on empirical observation. This makes it difficult to accommodate other factors/conditions that were not considered in the empirical observation.

$$RC = \frac{100}{1+e^{a+bt}} \quad \text{..... (2.7)}$$

Where:

RC = the percent cracks reflected

T = the time in years

a = 3.5 + 0.7 × h_{ac}

b = - 0.688584 – 3.37302 × $(h_{ac})^{-0.915469}$

h_{ac} = HMA overlay thickness in inches

Also, OLCRACK, a design program that allows the design of reinforced overlay against top-down and bottom-up cracking was designed at University of Nottingham by Thom (2000). The program (in an Excel spreadsheet) estimates the rate of crack propagation using the relationship between tensile strain in the crack zone and material (fatigue) coefficients (see equation 2.8). The approach is similar to the Paris law described in equation 2.2, except that the stress intensity factor is replaced by the strain in the cracked zone. The software is in two parts - the first one considers two layers of asphalt over the existing pavement, while the second considers one layer of asphalt with reinforcement over existing pavement. OLCRACK is considered the best out of all the methods highlighted in this section because it considers many of the factors that play a part in crack initiation and propagation. It takes into account the debonding (slip) at interfaces. It also introduces the crack stitching effect which reduces the stresses and strains within the crack region. Again, it considers the stiffness and fatigue characteristics of the overlay and the interlayer, the crack width factor, crack spacing and crack shear modulus. Sanders (2001) used OLCRACK in his study to demonstrate the savings in asphalt thickness in overlay incorporating reinforcing grids.

$$\frac{dc}{dN} = A(\varepsilon)^n \quad \text{..... (2.8)}$$

Where,

$\frac{dc}{dN}$ = crack growth rate

A, n = Fatigue parameters

ε = strain in the crack region

It has been shown in this section that a lot of methods are available for the design of overlay. The shortcomings of some of the methods have been mentioned. These include application of laboratory results without calibration in the field, consideration of reflective cracking based on empirical observations, and non consideration of reinforcing or stress relieving interlayer in the design. It is intended in this study to use analytical design method for the design of overlay incorporating SAMIs. This will be achieved by using software "OLCRACK" developed at University of Nottingham by Nick Thom (Thom, 2000). The choice of OLCRACK is informed by its unique ability to consider most of the factors responsible for crack initiation and propagation through overlay over a cracked pavement.

2.3 Interface properties in pavement

A number of researchers have investigated the bond between layers of pavement with and without interlayers using different approaches. Some of them are reviewed in this section. This was done to understand the importance of bond between pavement layers in pavements with and without interlayers.

Hughes (1986) developed a shear box to study the strength of various interface conditions. He noted that there were some limitations with its use. The test specimens were constructed in two lifts. Normal and shear forces were applied using hydraulic actuators and monitored using load cells. The normal load was held approximately constant and the shearing force was supplied at a constant rate of strain (5mm/min). He examined five interface conditions namely: chip seal only; chip seal and grid; grid only; no treatment; and no interface (specimen compacted in one lift). He observed that both chip seal only and grid and chip seal interfaces had a reduction in shear strength of approximately 20% when compared to the no treatment condition. He observed that the chip seal rich in bitumen combined with the slow rate of loading in the test (5 mm/min) created a viscous failure along the predetermined

failure plane. The grid only condition reduced the shear strength of the interface by 10% compared to the untreated surface. He concluded that the reduction in shear strength should not be a problem in general practice, since rates of loading are significantly higher under traffic loading and viscous failure of the chip seal would be unlikely. Also, Caltabiano (1990) used the same shear box developed by Hughes to determine the interface shear strength for materials used to prevent reflection cracking employing a vibrating hammer instead of static pressure adopted by Hughes. He stated that the greatest reduction in shear strength was recorded for a geotextile interlayer (30% of control) placed with a bituminous seal in accordance with the manufacturer's recommendations. He observed that the geogrid interlayer with chip seal and the timber/emery paper interlayer showed a reduction of approximately 20% in shear strength from the control sample, which agreed with earlier findings of Hughes. Also, he concluded like Hughes that reduction in shear strength of the order of 20-30% obtained for laboratory testing should not cause any problems with overlay slippage for in-situ conditions, as field loading rates are significantly higher than the shearing rate used during testing. Sanders (2001) showed in his research on interface bonding in pavements with a reinforced interlayer using the same shear box as Hughes and Caltabiano that failure occurred on the interface between the reinforcement and the lower layer of asphalt. He concluded that the bonds between freshly-applied asphalt and the reinforcement were better than the bonds between the reinforcement and the 'older' pavement. The shear box apparatus used by Hughes, Caltabiano and Sanders has the advantage that large specimen can be tested, allowing a representative sample of an interlayer to be examined. While it has been used successfully to study interface properties of pavement, it has a number of limitations. These include non-uniform stress distribution at the interface and stress concentration at the front and rear edges of the specimen causing failure along the shear plane, without the full shear strength of the interface being mobilized. This underestimates the shear strength of the

interface. However, their tests showed that the introduction of interlayers in cracked pavement gave a reduction in shear strength of the interface of the order of 10-30% of specimens without interlayer.

Tschegg et al (1995) used a different approach from Caltabiano, Hughes and Sanders. He developed a wedge splitting test to characterize the fracture mechanical behaviour of layer bonding. The test involved introducing a rectangular groove into the specimen and placing a starter notch in the interface at the bottom of the groove, from where a crack started to grow into the interface during loading. Their results indicated that the specimens with an interface had less specific fracture energy than the ones without an interface, indicating a decrease in the interface stiffness. Although, the wedge splitting test is able to determine the maximum strength of interlayer bond, the fracture properties of an interlayer and differentiate between brittle and ductile behaviour, the loading method is not the type dominant in the field (an overlay over a cracked pavement). Therefore the method is considered inappropriate for the present study. Raab and Partl (2004) reported on research carried out by Swiss Federal Road Authority to determine the interface properties of a 30-year old concrete pavement of a motorway test section rehabilitated with an asphalt surface layer using three different intermediate bituminous layers: glass fibre mesh reinforced, steel wire grid reinforced and unreinforced. In the first system, before the application of the glass fibre mesh, as a first step, they sprayed a hot tack coat on the concrete pavement and the stone mastic asphalt was built (thickness 4 cm). The second system consisted of a steel wire grid reinforcement and slurry generally used for cold micro surfacing. In this case the steel wire grid was directly applied on the concrete pavement and slurry (thickness 0.5 to 1cm) was applied onto the steel wire grid and after the breaking of the emulsion the surfacing was finished with the application of a stone mastic layer (thickness 4.5cm). For the bituminous interlayer without reinforcement a hot tack coat was applied and spread with gravel, which was compacted afterwards. After

sucking off the surplus gravel, a 4 cm asphalt concrete surface was applied. They examined the interlayer adhesion with the Layer-Parallel Direct Shear Device (LPDS) and the modified pull-off device according to the Swiss standard. For the pull off test, they reported that the specimens with still wire reinforcement were broken; hence the test could not be conducted, indicating insufficient bond. Their results showed the importance of interlayer shear performance, because the pavement with no reinforcement had the highest shear and pull-off force. The pavement with steel wire had less shear force than the one with glass fibre, while the maximum pull-off force for glass fibre was considerably less than that of the pavement with no reinforcement. They concluded that when using stress absorbing intermediate bituminous layers, it is important to choose appropriate and sufficiently established systems and construction techniques in order to minimize negative effects on adhesion. In the context of the present study, the test modes (shear and tension) used by Raab and Partl are very important because the an overlay over a cracked pavement is subjected to shear and tensile stresses as the wheel approaches the edge of the crack and tensile stresses when the wheel is directly over the crack. Therefore the two modes are considered in the present study.

Investigations have also been carried out to evaluate the effects of the interface conditions such as the type and amount of tack coat, construction practice etc on the bond strength of the interface. Some of them are highlighted here. Collop et al (2003) used the Leutner shear test to assess the bond condition between surfacing and binder course materials and binder course and base materials without any interlayer. They investigated the bond at the upper two interfaces in a typical flexible or semi-rigid pavement structure. The cores 150 mm in diameter were conditioned in a temperature-controlled cabinet at 20^{o}C and tested at 20^{o}C using a standard test loading rate (50mm/min), and the shear force and shear displacement were measured. They observed that for HRA/20DBM, SMA/20DBM and 20DBM/28DBM interfaces, in the cases where a standard tack coat application was used, the interface shear

strengths approached those obtained from tests directly through each of the materials comprising the upper layer. For the HRA/20DBM and SMA/20DBM combinations, where no tack coat was used the interface shear strength was reduced, but not greatly. However, for the 'very dirty' condition extra tack coat did not compensate, and the interface shear strengths were significantly reduced. The results for the 20DBM/28DBM combinations show significantly higher levels of variability (in terms of shear strength) compared with the results for the surfacing/binder course interfaces. They reported that it was likely due to the fact that significantly larger aggregates were involved compared with the surfacing/binder course combinations. In the 20DBM/CBM combination, it proved impossible to achieve a good bond, reflecting common experience on site. They stated that zero penetration of stones from the DBM into the CBM (that is, reduced aggregate interlock) may be the main reason. Their tests clearly showed that a number of factors influence the bond achieved at the interface. These factors include the interface condition, the amount of tack coat and materials in contact, with the principal factors that reduce the interface bond significantly being the interface condition and materials in contact. This implies that when an interlayer is used in pavement, it is very important to take into consideration the type of overlay or maximum nominal aggregates in the overlay and the interlayer as this may have influence on the interface properties.

Kruntcheva et al (2006) investigated the factors affecting bond development between pavement layers using the Nottingham shear box. Their main set of test cases included a constant base material (20 mm DBM) and two distinct surfacing materials: 10 mm stone mastic asphalt (SMA); and porous asphalt (PA) with 15% voids. For these materials, they examined four different interface conditions: normal tack coat K1-40 application at 0.33 L/m^2 within the limits recommended by the British Standards Institute; excess tack coat rate (1.0 L/m^2); dirty interface (a clay-water slurry was placed on the interface); and no tack coat.

They observed like Collop et al (2003) that the interface bond depends on the materials in contact, but not the amount of the applied tack coat. Also, contrary to the finding of Collop et al, they found that the interface condition did not have significant effect on the interface bond. It was pointed out, that using materials that require more compaction time will ensure good bond at interface.

Tashman et al (2008) investigated the influence of several construction practices on the bond strength at the interface between existing HMA surface and a newly constructed 50mm HMA overlay (Superpave 12.5 mm nominal maximum aggregate). The factors studied included the following: surface treatment (milled versus non-milled); Curing time (broken versus unbroken); approximate target residual binder (0.00, 0.08, 0.22 and 0.32 L/m$^{2)}$; and equipment tracking (wheel path (WP) versus middle of lane (ML)). They performed three tests namely Florida Department of Transportation, FDOT shear test, the torque bond test, and the University of Texas El Paso, UTEP pull-off test. In the FDOT test, the field core was conditioned at a temperature of 25^{o}C for 2hr before the test. The laboratory torque bond test was conducted at 20^{o}C. They observed that the results from the UTEP pull-off test were generally different from the other two tests. Overall, milling provided a significantly better bond at the interface between the existing surface and the new overlay. For milled sections, the absence of tack coat did not significantly affect the bond strength at the interface. This was not true for the non-milled sections, where their results showed the absence of tack coat severely decreased the bond strength (there was no bond at all). They reported curing time had minimal effect on the bond strength at the interface and the residual rates in the range of 0.08–0.32 L/m^2 did not generally affect the bond strength at the interface which agreed with the findings of Kruntcheva et al (2006). Also the equipment tracking did not occur to the extent expected during the experiment; hence its effect on the bond strength was insignificant. Their tests showed that the interface condition play a great role in the quality of adhesion

achieved at the interface. This means that it is important that when SAMIs are to be introduced, the existing pavement surface must be free of dirt, dust, water and other things that may have negative impact on adhesion.

In summary, researchers have used different methods to determine the interface properties. It is important to consider the stresses that are dominant in the field before choosing any of the methods to assess the interface properties. In the present study as highlighted in section 1.3, tensile and shear stresses are generated when an overlay is placed on a cracked pavement Therefore, the interface properties between the SAMIs and the overlay have been studied using Leutner shear test and pull-off test at different temperatures. The Leutner shear test measures the bond strength of the interface between the layers in shear mode, while the pull-off test measures the tensile strength of the interface in tension mode.

As documented in the literature a number of factors affect interface bond. These include construction practice, the materials in contact, amount of tack coat, interface condition etc. While some authors stated that the interface bond was influenced by the amount of tack coat and interface condition, others suggested that the interface bond was influenced principally by the materials in contact. In this study, the overlay material is 10 mm asphalt concrete with 40/60 penetration bitumen. This has been used with the SAMIs to produce specimens and examine the interface bond. The findings from literature reported in this section showed that it is important that the interface properties be examined when a different overlay material is to be used. The review showed that introducing interlayer materials of different types into a pavement affects the interface shear performance.

REFERENCES

Allison R.E. (1989): Rubber Asphalt Binder "Stress Absorbing Membrane Interlayers Washington State Department of Transportation.

Antunes M.L., Fontul S. and Pinelo A.M (2008): Anti-Reflective Cracking Solutions for Asphalt Overlays: 8 Years Performance Monitoring. Proceedings of 6th International RILEM Conference, Chicago, U.S.A. 791-798.

Asphalt Academy (2008): Technical Guideline: Asphalt Reinforcement for Road Construction. TG3, First edition, Pretoria.

Bhosale S.S. and Mandal J.N. (2008): Open Graded Asphalt Concrete for Mitigation of Reflection Cracking on Asphalt Concrete Overlays. 12th International Conference of International Association for Computer Methods and Advances in Geomechanics (IACMAG), India. 4409-4416.

Blankenship P, Iker N. and Drbohlav J. (2004): Interlayer and Design Consideration to Retard Reflective Cracking. Pavement Design and Accelerated Testing. Transportation Research Board, No 1896.

Brown S.F and Brunton J.M (1984): The Analytical Design of Bituminous Pavements. University of Nottingham.

Caltabiano M.A (1990): Reflection Cracking in Asphalt Overlays. Thesis submitted to University of Nottingham for the degree of Master of Philosophy.

Cleveland G.S., Button J.W., and Lytton R.L. (2002): Geosynthetic in Flexible and Rigid Pavement Overlay. Texas Transport Institute, Texas A&M University System. Report 1777-1,

Collop A.C. Thom N.H. and Sangiorgi C. (2003): Assessment of Bond using the Leutner Shear Test. Proceedings of the Institution of Civil Engineers. Transport 156. 211-217.

Debondt A. (2000): Effect of Reinforcement Properties. Proceedings of 4th International RILEM Conference. Canada. 13-22.

Debondt A.H. (1999): Anti Reflective Cracking Design of (Reinforced) Asphaltic overlays. PhD Thesis submitted to Delft University of Technology, Netherlands.

Defence Estates (2005): Reflection Cracking on Airfield Pavements- A Design Guide for Assessment, Treatment, Selection and Future Minimization. Design and Maintenance Guide 33, Defence Estates, Ministry of Defence.

Dempsey B.J. (2002): Development and Performance of Interlayer Stress-Absorbing Composite in Asphalt Concrete Overlays. Transportation Research Record 1809. 175-183.

DMRB (2006): Design Manual for Roads and Bridges. Pavement Design and Maintenance. Volume 7, Highways Agency, The Scottish Office Development Department, The Welsh Office and The Department of the Environment for Northern Ireland.

Ellis S.J., Langdale P.C. and Cook J. (2002): Performance of Techniques to minimize Reflection Cracking and Associated Developments in Pavement Investigation for

Maintenance of UK Military Airfields. Federal Aviation Administration Airport Technology Transfer Conference.

Elseifi M.A. (2003): Performance Quantification of Interlayer Systems in Flexible Pavements Using Finite Element Analysis, Instrument Response and Non Destructive Testing. PhD Thesis submitted to Virginia Polytechnic Institute and State University.

Elseifi, M., and Al-Qadi, I. (2003): A Simplified Overlay Design Model against Reflective Cracking Utilizing Service Life Prediction. Paper No. 03-3285 presented at the TRB 82nd Annual Meeting, Washington, D.C.

Engle E. (2001): Field Evaluation of Engineering Fabrics for Asphalt Concrete Resurfacing - Audubon County. Iowa Department of Transportation. Iowa, USA. Final Report 8-93 to 6-99.

Farshad Amini (2005): Potential Applications of Paving Fabrics to Reduce Reflective Cracking. Jackson State University, Mississippi.

Hajj E.Y., Sebaaly P.E. and Loria L. (2008): Reflective Cracking of Flexible Pavements Phase II: Review of Analysis Models and Evaluation of Test, Nevada Department of Transportation, Research report No 13JF-1.

Hughes D.A.B. (1986): Polymer Grid Reinforcement of Asphalt Pavements. Thesis submitted to University of Nottingham for the degree of Doctor of Philosophy.

Khodaii A., Fallah S. and Nejad F.M. (2008): Effects of Geosynthetics on Reduction of Reflection Cracking in Asphalt Overlay, Geotextile and Geomembrane, doi:10.1016/j.geotexmem.2008.05.007.

Kretov V.A. and Gorelysheva L.A. (2000): Influence of Thin Interrupting layer to Development of Reflected Cracks. Proceedings of 4th International RILEM Conference. Canada. 291-295.

Kruntcheva M.R., Collop A.C. and Thom N.H. (2006): Properties of Asphalt Concrete Layer Interfaces. American Society of Civil Engineers. Journal of Materials in Civil Engineering. 467-471.

Mukhtar M.T. and Dempsey B.J. (1996): Interlayer Stress Absorbing Composite (ISAC) for Mitigating Reflection Cracking in Asphalt Concrete Overlays. Project IHR-533, Illinois Cooperative Highway Research Program.

Nataraj A.R. and Vander Meer A. (2000): Use of Asphalt Crack Relief Layer in Airport Pavements. Proceedings of 4th International RILEM Conference. Canada, 307-317.

Palacios C., Chehab G.R., Chaignon F. and Thompson M. (2008): Evaluation of Fibre Reinforced Bituminous Interlayers for Pavement Preservation. Proceedings of 6th International RILEM Conference, Chicago, U.S.A. 721-729.

Potter J.F., Dudgeon R. and Langdale P.C. (2000): Implementation of Crack and Seat for Concrete Pavement Maintenance. Proceedings of 4th International RILEM Conference. Canada. 367-377.

Prieto J.N., Gallego J. and Perez I. (2007): Application of the Wheel Reflective Cracking Test for Assessing Geosynthetics in Anti-reflection Pavement Cracking Systems, Geosynthetics International, 14(5), 287-297.

Raab C. and Partl M.N. (2004): Interlayer Performance: Experience with Different Pavement Structures. 3rd Eurasphalt & Eurobitume Congress, Vienna. 535-545.

Read J. and Whiteoak D. (2003): The Shell Bitumen Handbook. Fifth Edition, Thomas Telford Publishing, London, UK.

Sanders P.J. (2001): Reinforced Asphalt Overlays for Pavements. PhD Thesis submitted to University of Nottingham, Nottingham, United Kingdom.

Sanders P.J., Brown S.F., and Thom N.H (1999): Reinforced Asphalt for Crack and Rut Control. 7th Conference on Asphalt Pavements for Southern Africa.

Sousa, J., Pais, J., Saim, R., Way, G., and Stubstad, R. (2001). "Development of a Mechanistic Overlay Design Method Based on Reflective Cracking Concepts," Final Report for Rubber Pavements Association, Consulpav International.

Storsteen M. and Rumpca H. (2000): Evaluation of Geosynthetics in Asphalt Overlays of Jointed Concrete Pavements. South Dakoda Department of Transportation. SD95-23-X.

Tashman M., Nam K., Papagiannakis T., Willoughby K., Pierce L., and Baker T. (2008): Evaluation of Construction Practices that Influence the Bond Strength at the Interface between Pavement Layers. ASCE, Journal of Performance of Constructed Facilities, 154-161.

Thom N.H. (2000): A Simplified Computer Model for Grid Reinforced Asphalt Overlays. Proceedings of 4th International RILEM Conference on Reflective Cracking in Pavements, Otawa, Ontario, Canada, 37-46.

Tschegg E.K, Kroyer G., Tan D. and Stanzl-Tschegg S.E. (1995): Investigation of Bonding between Asphalt Layers on Road Construction. ASCE, Journal of Transportation Engineering. 309-316.

Vervaecke F., Maeck J. and Vanelstraete A. (2008): On Site Validation and Long Performance of Anti-Cracking Interfaces. Proceedings of 6th International RILEM Conference, Chicago, U.S.A. 761-768.

Vespa J.W. (2005): An Evaluation of Interlayer Stress Absorbing Composite (ISAC) Reflective Crack Relief System. Illinois Department of Transportation, Physical Research No. 150.

Von Quintus H.L., Mallela J., Weiss W. and Shen S. (2007): Techniques for Mitigation of Reflective Cracking. Applied Research Associates, Champaign, IL, USA. Interim Report AAPTP 05-04.

Zielinski P. (2008): Fatigue Investigations of Asphalt Concrete Beams Reinforced with Geosynthetic Interlayers. Proceedings of 6th International RILEM Conference, Chicago, U.S.A,751-760.

3 MATERIAL PROPERTIES

3.0 Introduction

The materials used for this study were aggregates, binder-penetration grade bitumen, polymer modified bitumen, and bitumen emulsion, glass fibre, forming different bituminous mixtures and rubber mat. The mechanical properties were determined using standard tests such as particle size distribution, penetration and softening point tests, dynamic mechanical analysis (DMA), indirect tensile stiffness modulus test (ITSM), indirect tensile fatigue test (ITFT) and repeated load axial test (RLAT).

The tests were carried out because knowledge of the materials properties would be expected to help in predicting their performance. Also some of the results were required for the modelling of the wheel tracking test. The tests were carried out in accordance with British standards.

3.1 Aggregate particle size distribution

The aggregates for this study were as follows:

- 6mm and 10mm single sized aggregate sourced from Bardon quarry, Leiscester, UK
- Dust sourced from Bardon aggregates, Leiscester, UK
- Sand from Hints quarry, Tamworth, Staffordshire, UK.
- Filler from Torr Works, Somerset, UK
- 0/4 Crushed rock fill graded aggregates sourced from Carnsew quarry, UK
- Fine sand from Binnegar quarry, UK. and

- Limestone filler from Francis flower, Somerset, UK.

The particle size distribution is a fundamental property which governs how an aggregate will perform (Hunter, 2000). The particle properties and size distribution play major roles in determining the strength of the material as a whole (Thom, 2008). The aggregate gradings were carried out in accordance with BS EN 933-1:1997 (BSI, 1997). The particle size distributions were as shown in Table 3.1 and Figure 3.1.

Table 3.1: Grading of aggregates

Sieve size (mm)	10mm	6mm	Dust	Hint Sand	Torr Filler	0/4 CRF	Binnegar sand	Limestone filler
	% Passing							
16	100	100	100	100	100	100	100	100
14	100	100	100	100	100	100	100	100
10	91.08	100	100	100	100	100	100	100
8	50.74	99.07	100	100	100	100	100	100
6.3	13.03	88.66	99.66	100	100	100	100	100
4	2.71	14.64	92.76	100	100	100	100	100
2.8	2.27	8.23	85.64	96.54	100	-	-	-
2	1.98	2.66	70.89	95.08	100	76	99.0	100
1	1.64	1.6	48.93	92.45	100	51.0	97.0	100
0.5	1.35	1.38	33.54	85.34	100	33.0	92.0	100
0.315	-	-	-	-	-	25.0	75.0	100
0.25	1.18	1.25	22.73	27.11	100	21.0	61.0	100
0.125	1.06	1.06	15.44	2.23	100	12.0	20.0	100
0.08	-	-	-	-	-	6.5	5.5	87.0
0.063	0.96	1.03	11.28	0.53	94.29	6.0	5.0	85.0

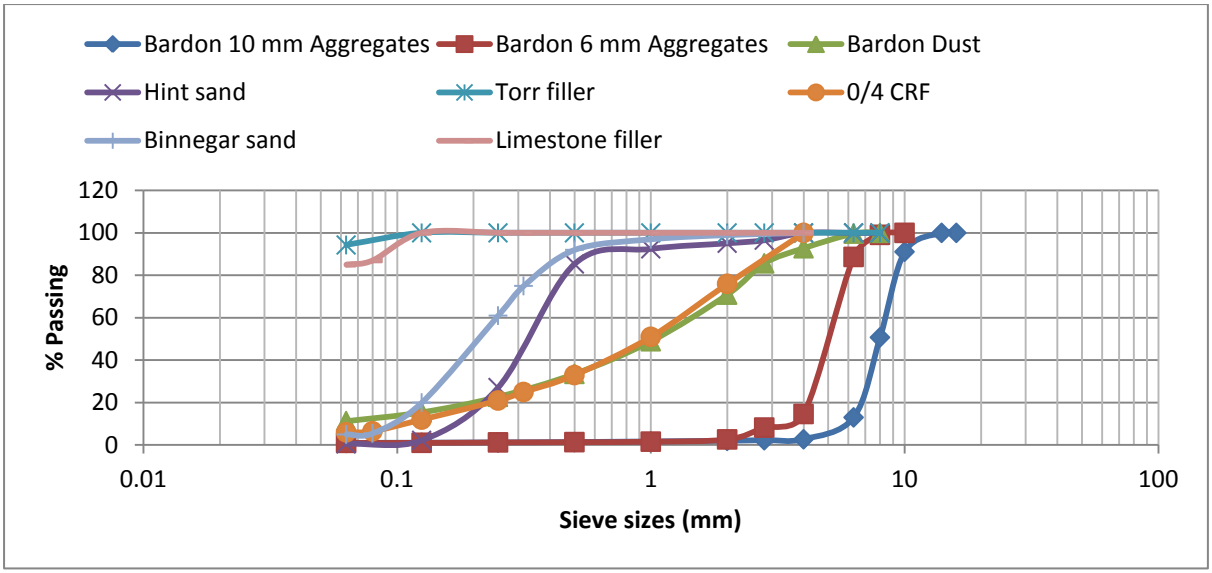

Figure 3.1: Particle size distribution of the aggregates

3.2 Binder characterization

The binders for the research were as follows:

- 10/20, 40/60 and 160/220 penetration grade bitumen from Shell bitumen
- Ordinary bitumen emulsion and polymer modified bitumen emulsion
- Polymer (styrene-butadiene-styrene (SBS)) modified binder

Penetration test: The penetration test is a measure of the consistency of the bitumen expressed as the distance in tenths of a millimetre (decimilimeter) that a standard needle is allowed to penetrate vertically into a sample of the bitumen, under a specified load and loading time, at a fixed temperature of 25^{o}C (Airey, 1997). The penetration test can be considered as an indirect measurement of the viscosity of the bitumen at 25^{o}C (Liao, 2007). The penetration test was carried out in accordance with BS EN 1426:2007 (BSI, 2007a).

Softening point: Softening point is the temperature at which material under standardized test conditions attains a specific consistency. The Ring and Ball method is an empirical test used to determine the consistency of bitumen by measuring the equiviscous temperature at which

the consistency of the bitumen is between solid and liquid behaviour (Airey, 1997). The procedure of the test is specified in BS EN 1427:2007 (BSI, 2007b).

Viscosity: The measure of bitumen resistance to flow defines its viscosity, η. This property determines how the bitumen behaves at a given temperature and over a range of temperatures, thus it is the ratio of applied shear stress to the rate of shear strain. The rotational viscometers are normally used to determine, and in some cases specify the viscosity of bitumens at application temperatures (Read and Whiteoak, 2003). The rotational viscometers allow the testing of a wide range of bitumen over a wide range of temperatures. The test procedure for the penetration grade and polymer modified bitumen is specified in BS EN 13302:2003 (BSI, 2003a), while the test procedure for bitumen emulsion is specified in BS EN 14896:2006 (BSI, 2006a). The penetration and softening point results are shown in Table 3.2, while the viscosity results are shown in Table 3.3.

Table 3.2: Softening point and penetration results

Binder Grade(Bitumen)	Penetration (dmm)	Softening point (^{o}C)
40/60 Bitumen	49.0	51.2
160/220 Bitumen	190.3	39.8
10/20 Bitumen	14.0	73.0
Polymer modified bitumen	60.0	52.2

Table 3.3: Viscosity test results

Penetration grade bitumen/ Polymer modified bitumen	Viscosity (Pa.s) @ 140^{o}C	Viscosity (Pa.s) @ 160^{o}C	Viscosity (Pa.s) @ 180^{o}C
40/60 Bitumen	0.17	0.36	0.08
160/220 Bitumen	0.13	0.08	0.04
10/20 Bitumen	1.61	0.53	0.23
Polymer modified bitumen	0.46	0.22	0.12
Bitumen emulsion	Viscosity (Pa.s) @ 25^{o}C	Viscosity (Pa.s) @ 30^{o}C	Viscosity (Pa.s) @ 40^{o}C
Ordinary bitumen emulsion	0.700	0.580	0.390
polymer modified bitumen emulsions	0.184	0.194	0.180

3.2.1 Bitumen rheology

The dynamic mechanical analysis (DMA) was performed in a Bohlin Model DSR50 in accordance with BS EN 14770:2005 (BSI, 2005a) and the test conditions were as follows:

Mode of loading: controlled strain

Temperatures: 0, 10, 20, 30, 40, 50, 60, 70, and 80^{o}C.

Frequencies: 0.1, 0.158, 0.251, 0.398, 0.631, 1, 1.58, 2.51, 3.98, 6.31, 10 Hz

The test parameters were as shown in Table 3.4. The DMA results were presented as master curves of complex modulus and phase angle at a reference temperature of 25^{o}C as shown in Figures 3.2 and 3.3 respectively. The complex modulus curves give an indication of the binder stiffness. Figure 3.2 shows the 40/60 bitumen has greater stiffness than polymer modified bitumen, while polymer modified bitumen has greater stiffness than 160/ 220 bitumen. This stiffness property of the binders is confirmed by the phase angle master curves, which show that the phase angle of polymer modified binder is greater than that of 40/60 bitumen at a given frequency. Also, the phase angle of 160/220 bitumen at a given frequency is greater than that of polymer modified binder.

Table 3.4: Test parameters for DMA

Parameters	40/60 bitumen		160/220 bitumen		Coflex N	
Temperature (^{o}C)	0-40	40-80	0-40	40-80	0-40	40-80
Plate diameter (mm)	8	25	8	25	8	25
Gap width (mm)	2000	1000	2000	1000	2000	1000
Strain	0.2	0.5	5	10	1.5	0.5

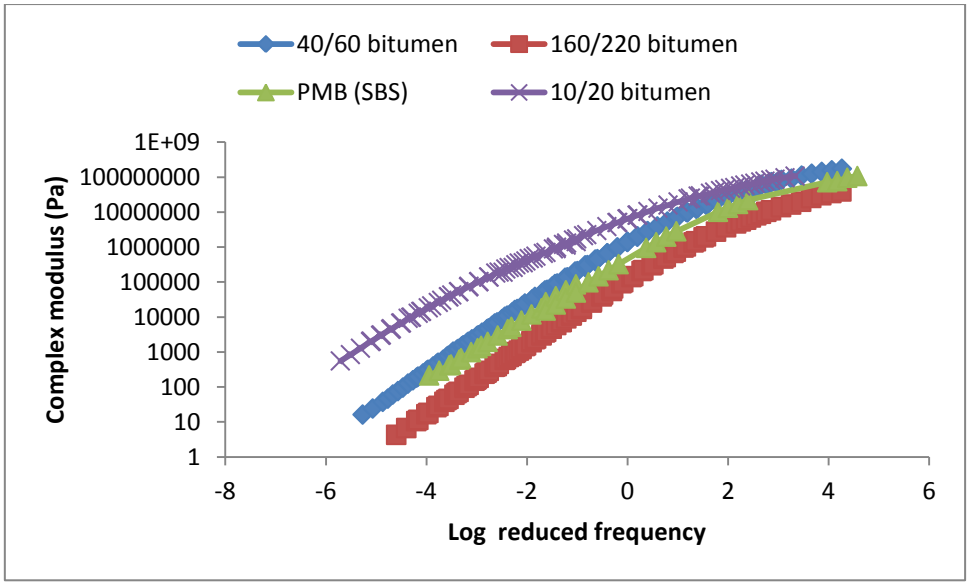

Figure 3.2: Complex modulus master curves at reference temperature of 25°C

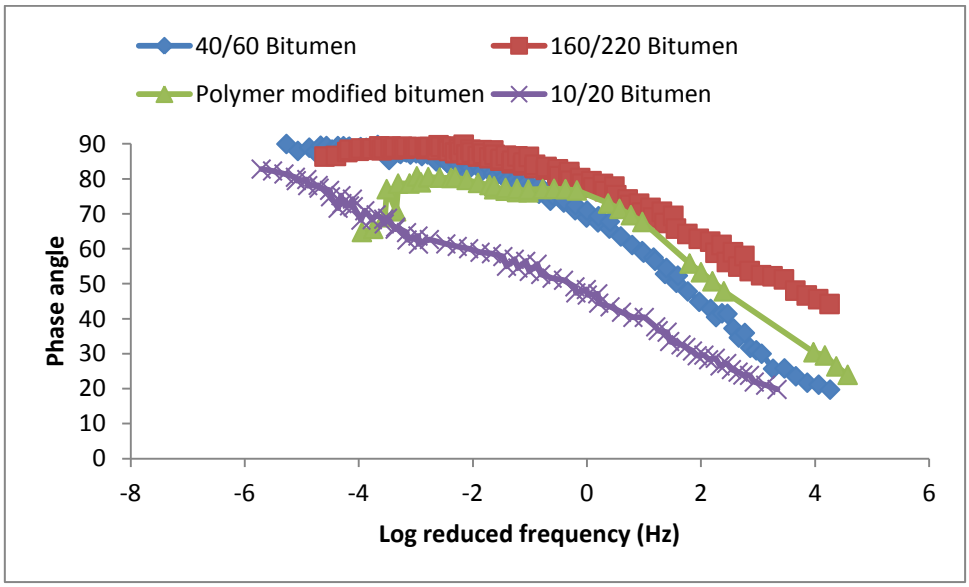

Figure 3.3: Phase angle master curves at reference temperature of 25°C

3.3 Rubber stiffness

The rubber mat was used in the wheel tracking test to simulate an elastic foundation and induce bending stress. The stiffness of the rubber mat was determined by conducting a compression test using the MAND axial testing machine. The stress rate was 100 N/s and the

diameter of load bearing plates (top and bottom) (mm) was 150 mm. Figure 3.4 shows the load-displacement curve. The rubber stiffness was calculated as follows:

Rubber stiffness, k = $\frac{PL}{\delta A}$ ……..3.1

Where, P = load; L = the rubber thickness, δ = displacement and A = area of the rubber.

Where $\frac{P}{\delta}$ is the slope of the load-displacement curve. The rubber stiffness was calculated as 6.45MPa.

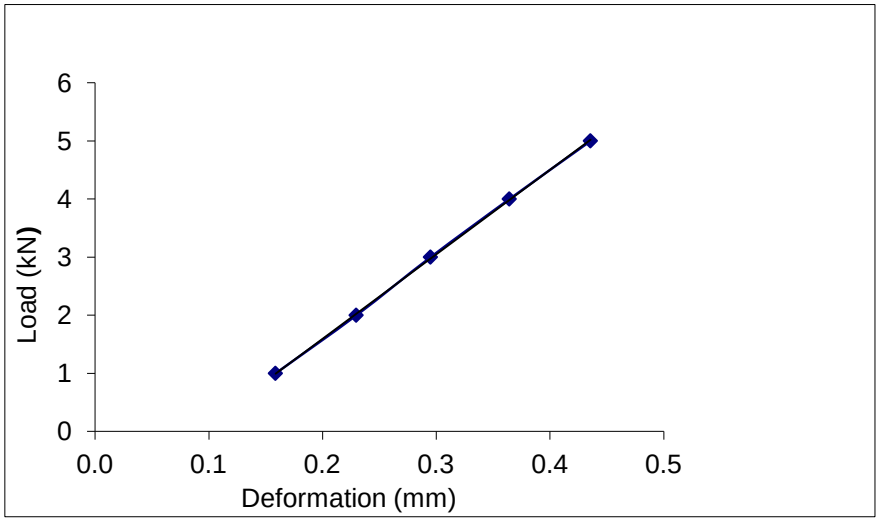

Figure 3.4: Load-displacement curve for the rubber mat

3.4 Bituminous mixtures

The bituminous mixtures for the research were prepared in accordance with the British standards. The particle size distribution for the blend of aggregates for the mixtures is shown in Figure 3.5.

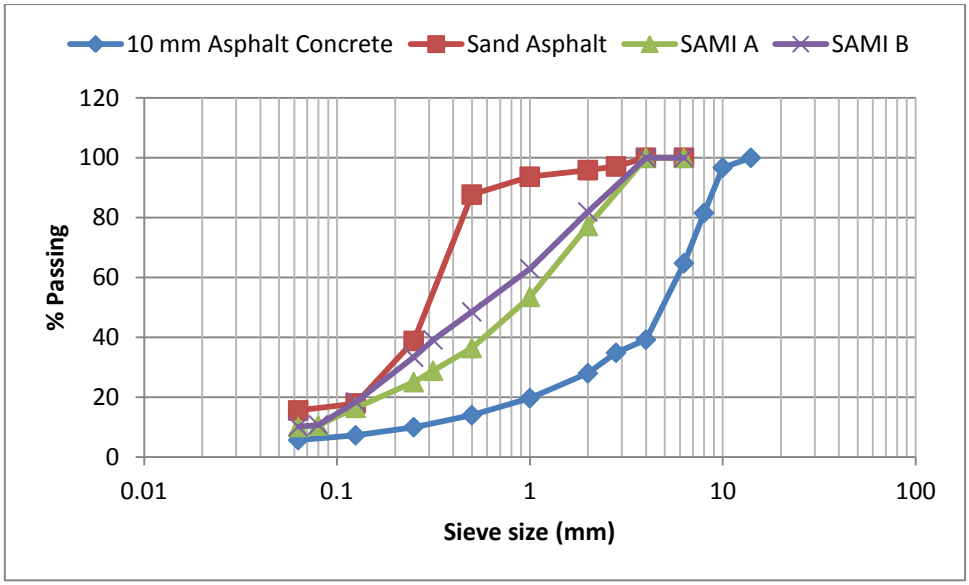

Figure 3.5: Particle size distribution for the blend of aggregates for overlay and SAMIs

3.4.1 Overlay and base mixtures

A 10 mm Asphalt concrete in accordance with BS EN 13108-1:2006 (BSI, 2006b) was chosen as the overlay and the base (simulating existing pavement) mix. The mixture composition was as shown in Table 3.5. The same mixture was used for the base layer but the 40/60 penetration grade bitumen was replaced with 10/20 penetration grade bitumen. The mixture was first selected in accordance with BS 4897-1:2005 (BSI 2005b) before it was withdrawn and replaced with the current standard for asphalt concrete.

Table 3.5: Mix design for 10 mm asphalt concrete

Sample type	**Percent by composition of aggregate**
10mm aggregate	37%
6 mm aggregate	26%
Dust	36%
Filler	1%
Binder type	[a]40/60 bitumen, [b]10/20 bitumen
Binder content	5.3% by mass of total mix
Target air void	5%

[a]Overlay [b]Base layer (existing pavement)

3.4.2 Sand asphalt

A surface course mixture in accordance with BS EN 13108-4:2006 (BSI, 2006c) was chosen as one of the SAMIs. The mixture composition was as shown in Table 3.6. Also, the mixture was first selected in accordance with BS 594-1:2005 (BSI, 2005c) before it was withdrawn and replaced with the current standard.

Table 3.6: Mix design for sand asphalt

Sample type	**% by composition of aggregate**
Sand	84%
Filler	16%
Binder type	160/220 bitumen
Binder content	10.3% by mass of total mix
Target air void	5%

3.4.3 Proprietary SAMIs A and B

Two blends of proprietary SAMI mixtures A and B were studied in this work. The mix compositions were as shown in Table 3.7.

Table 3.7: Mix design for proprietary SAMIs A and B mixtures

Sample type	**% by composition of aggregate**	**% by composition of aggregate**
	SAMI A	**SAMI B**
Carsew 0/4 CRF	95%	74.5%
Binegar fine sand	-	20%
Filler	5%	5.5%
Binder type	Polymer modified binder	Polymer modified binder
Binder content	9 % by mass of total mix	9.1 % by mass of total mix
Target air void	2%	2%

3.4.4 Proprietary SAMIs C and D

Proprietary SAMIs C and D were produced by sandwiching glass fibres chopped to 60 mm at a rate of 120 g/m^2 between two layers of bitumen emulsion spread at a rate of 0.9L/m^2. A

layer of 6 mm aggregates spread at a rate of 8 kg/m^2 was then compacted on the sandwiched glass fibres.

Proprietary SAMI C was produced using ordinary bitumen emulsion while proprietary SAMI D was produced with polymer modified bitumen emulsion.

3.5 Bituminous mixtures properties

3.5.1 Sample preparation

The aggregates and binder were batched as indicated in the mix designs and heated in the oven at 160^{o}C, 185^{o}C, 140^{o}C and 180^{o}C for 10 mm asphalt concrete (40/60 bitumen), 10 mm asphalt concrete (10/20 bitumen), sand asphalt and proprietary SAMIs A and B, respectively. The heated aggregates and binder were mixed in accordance with BS EN 12697-35:2004 (BSI, 2004a).

The mixtures were compacted with a roller compactor in accordance with BS EN 12697-33:2003 (BSI, 2003b) at a temperature of 150^{o}C, 180^{o}C, 130^{o}C and 154^{o}C for 10 mm asphalt concrete (40/60 bitumen), 10 mm asphalt concrete (10/20 bitumen), sand asphalt and proprietary SAMIs A and B mixtures, respectively. Five cores of diameter 100 mm and thickness 40 mm were cut from each slab for the tests.

3.5.2 Maximum density and air voids

The maximum density for the samples was determined in accordance with BS EN 12697-5: 2002 (BSI, 2002), while the air voids were determined in accordance with BS EN 12697-8:2003 (BSI, 2003c). The maximum density was carried out to know the mass of materials to be used in the production of specimens for this study. Table 3.8 shows the maximum density for 10 mm asphalt concrete, sand asphalt and proprietary SAMIs A and B. The air voids results are presented in Table 3.9.

Table 3.8: Maximum density of mixtures

Mixture types	Maximum density (kg/m^3)
10 mm AC	2559
Sand asphalt	2276
Saflex AF (Mix A)	2312
Saflex AF (Mix B)	2307

Table 3.9: Air voids of mixtures

Mixtures	10 mm AC	Sand asphalt	SAMI A	SAMI B
Air void (%)	5.6	6.7	2.6	1.9
	5.5	6.7	2.6	2.2
	5.7	6.6	2.0	2.4
	5.2	5.8	1.5	2.0
	4.7	6.5	2.4	2.3
	5.4	6.5	2.5	1.9
	5.2	6.0	2.3	2.0
	6.0	6.4	1.8	2.0
	4.3	6.1	2.0	2.0
	5.4	6.0	2.5	2.0
	4.8	6.8	2.7	2.2
	4.8	6.6	2.7	1.8
Mean	5.2	6.4	2.3	2.1

3.5.3 Indirect tensile stiffness modulus test (ITSM)

The ITSM test described in accordance with BS EN 12697-26:2004; DD 213: 1993 (BSI, 2004b; BSI, 1993) is one of the most commonly used tests for asphalt because it is relatively simple to perform and non-destructive in nature. In the ITSM a load pulse is applied to the vertical diameter of the specimen positioned centrally between the upper and the lower platens and the resultant peak transient deformation along the horizontal diameter is measured. The method uses cylindrical specimens cored from the field or slabs in the laboratory.

This is usually 150mm or 100mm in diameter and has thickness between 30 and 80mm. Input parameters include target horizontal deformation, load rise time, Poisson's ratio, test

temperature, specimen thickness and diameter. The test configuration for the ITSM in the Nottingham asphalt tester (NAT) is shown in Figure 3.6.

For this study, the test conditions were as follows:

Sample diameter: 100 mm

Sample thickness: 40 ± 4mm

Target rise time: 124 ± 4 ms

Mean horizontal deformation: 5 ± 2 μm

The stiffness of the mixtures at 20^{o}C is shown in Table 3.10. The stiffness results at 10^{o}C and 30^{o}C are shown in Tables 3.11 and 3.12, respectively. The mean values of the tests are shown in Table 3.13. The results show that the stiffness of the mixtures decreased with increasing temperature. Also, all the SAMI mixtures have lower stiffness than the overlay mixture (10 mm asphalt concrete with 40/60 penetration grade bitumen). The sand asphalt with very low stiffness was chosen to evaluate an extreme case, different from the two proprietary SAMIs A and B.

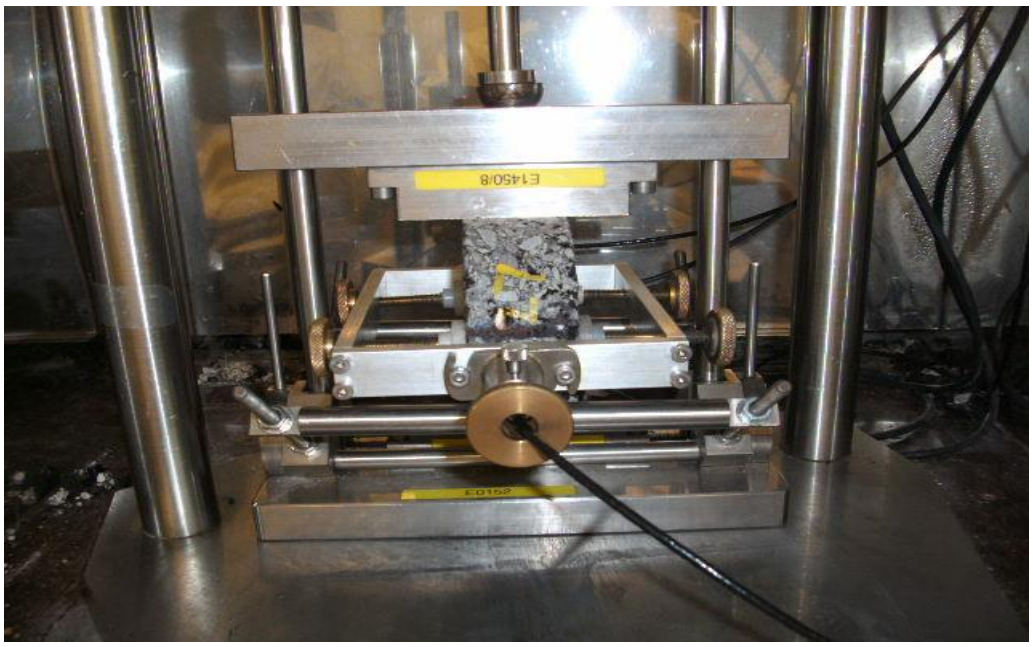

Figure 3.6: Test configuration for ITSM in NAT

Table 3.10: Stiffness of mixtures at 20°C

Mixture type	Stiffness (MPa) at 20°C											
10 mm AC (40/60)	3504	3658	3667	3934	3644	4040	3566	3568	4271	4207	4280	4449
10 mm AC (10/20)	9351	9726	9652	8247	9057	9395	10612	9454	9524	9743	10297	10029
Sand asphalt	220	198	222	236	191	185	195	213	203	235	183	225
SAMI A	2588	2746	2843	2951	2747	2723	2724	2697	2889	2381	2675	2739
SAMI B	2773	2479	2298	2364	2280	2335	2497	2447	2332	2521	2508	2490

Table 3.11: Stiffness of mixtures at 10°C

Mixture type	Stiffness (MPa) at 10°C				
10 mm AC (40/60)	10435	10271	9492	10158	9819
10 mm AC (10/20)	16043	16254	14663	15462	14755
Sand asphalt	521	596	673	614	772
SAMI A	7449	9623	7776	8936	8932
SAMI B	8262	8614	7989	6393	6563

Table 3.12: Stiffness of mixtures at 30°C

Mixture type	Stiffness (MPa) at 30°C				
10 mm AC (40/60)	1072	1100	1041	1206	1073
10 mm AC (10/20)	5116	5030	5411	4666	4816
SAMI A	604	637	552	727	658
SAMI B	662	545	444	472	427

Table 3.13: Average stiffness of asphalt concrete and SAMIs

Asphalt Concrete/SAMIs	**Stiffness (MPa)**		
	Temperature		
	10°C	**20°C**	**30°C**
AC10 (40/60)	10035	3899	1098
AC10 (15)	15435	9591	5008
Sand asphalt	635	209	118
SAMI A	8548	2725	636
SAMI B	7564	2444	510

3.5.4 Indirect tensile fatigue test (ITFT)

The test involves applying a repeated diametrical line loading along the vertical diameter of the cylindrical specimen. This produces an indirect tensile stress on the horizontal diameter. The magnitudes of the stresses vary along the diameter but are at the maximum at the centre of the specimen. The ITFT has proved to be a quick and reliable procedure with potential use in practice (Hunter, 2000).

This is due to its simplicity relative to other methods, its use of cylindrical specimens, which can be easily manufactured in the laboratory or cored from the pavement in the field. The test is described in BS EN 12697-24:2004; DD ABF: 1993 (BSI, 2004c; BSD 1993). The result is expressed as a relationship between tensile microstrain and the number of cycles to failure. The test configuration for the ITFT in the Nottingham asphalt tester (NAT) is shown in Figure 3.7.

For this study, the test conditions were as follows:

Target rise time of 124 ± 4 ms; stress level from 225-600kPa and temperature of 20^{o}C.

Figure 3.8 shows the fatigue lines for the overlay mixture (10 mm AC (40/60)), base mixture (10 mm AC (10/20)), sand asphalt, proprietary SAMI A and proprietary SAMI B. The empirical relationship used for regression analysis is as shown in equation 3.1 (Pell, 1973). Table 3.14 shows the material constants and the R-square of the regression analysis of the fatigue lines. Read (1996) stated that fatigue failure normally occurs at 30 to 200 microstrain. The fatigue life of the mixtures was compared at 200 microstrain (see Table 3.15). It can be seen that proprietary SAMI B has twice the fatigue life of proprietary SAMI A. This was due to the 20 percent of sand in the SAMI B mixture. Dukatz (1989) reported that the aggregate shape, morphology, gradation and strength have a major effect on fatigue.

$$N_f = k_1 (\varepsilon_i)^{k_2} \quad \text{..... (3.1)}$$

Where:

N_f is the number of load applications to failure

ε_i is the initial strain and

k_1, and k_2 are the material coefficients

Figure 3.7: Test configuration for ITFT in NAT

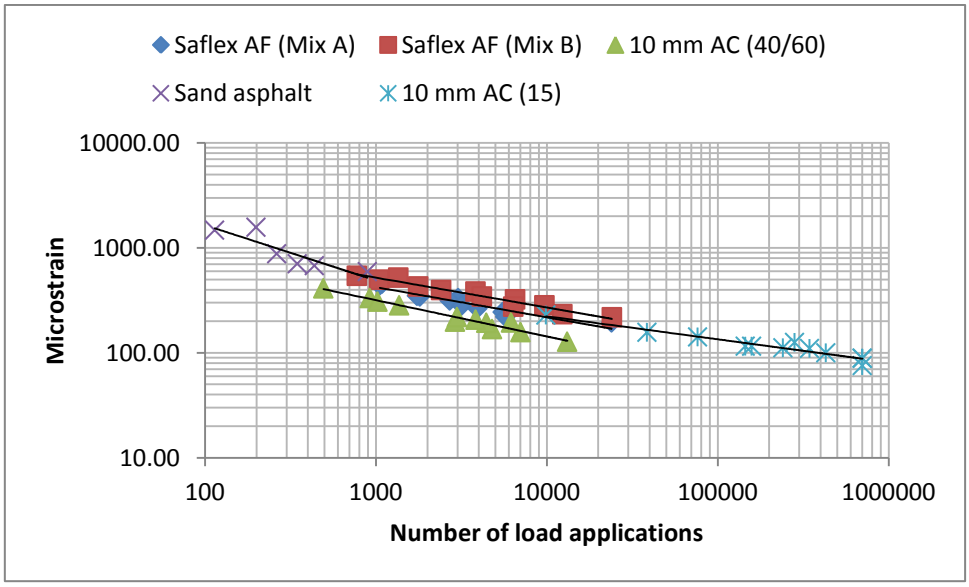

Figure 3.8: Fatigue lines for the bituminous mixtures

Table 3.14: Material constants and the R-square of fatigue regression analysis

Mixture	K_1	K_2	R-square
10 AC (40/60)	1E+10	-2.798	0.9662
10 AC (10/20)	1E+14	-4.260	0.9314
Sand asphalt	8E+06	-1.498	0.7898
SAMI A	2E+11	-3.115	0.8937
SAMI B	2E+12	-3.377	0.9589

Table 3.15: Fatigue life of mixtures at 200 microstrain

Materials	Fatigue life at 200 microstrain
10 mm AC (40/60)	3645
10 mm AC (10/20)	15762
Sand asphalt	2859
Saflex AF A	13593
Saflex AF B	33920

3.5.5 Repeated load axial test (RLAT)

The test was developed in the University of Nottingham to measure the permanent deformation of bituminous mixtures. The test configuration is as shown in Figure 3.9. The input parameters are the temperature, stress and number of load pulses, the thickness and diameter of the cylindrical specimen. The test sample is usually a core of 40 mm thickness and either 100 or 150 mm in diameter.

In the RLAT, the specimens are conditioned to ensure that the loading plates are properly seated on the specimen before testing commences. The conditioning is achieved by applying a static stress of 10 kPa on the specimen for ten (10) minutes. Then a 100kPa axial stress is applied in 1 second square wave pulses with 1 second rest periods. The test is repeated for 1800 load cycles at 30 or 40^{o}C lasting a period of 1800 seconds. The test is stopped, if the deformation of the specimen is more than 8 mm before reaching the specified number of pulses.

The deformation is monitored by a pair of linear variable differential transformers (LVDTs) mounted on the upper loading plate. The permanent axial deformation is recorded after every

10^{th} load application until the test is completed or stopped. The permanent axial strain is calculated as in equation 3.2. The test method is described in DD 226: 1996 (BSI, 1996). The results of the permanent strain in this study are shown in Figure 3.10. The results show that the accumulated strain increased rapidly at the start (primary stage) and with an almost linear relationship in log-log space towards the end defining the secondary stage of deformation. It shows that the 10 mm asphaltic concrete with 10/20 penetration grade bitumen has the lowest axial strain, while the sand asphalt has the highest axial strain. The permanent strains at 1800 cycles are shown in Table 3.16. It can be seen in Table 3.16 that proprietary SAMI A has a better resistance to permanent deformation than SAMI B.

$$\varepsilon_P\ (n,T) = \Delta h/ho \ \ldots\ldots\ldots\ldots\ldots\ldots\ldots\ldots\ldots\ldots\ldots\ldots\ldots\ldots\ldots\ldots\ldots\ldots\ldots.. \ (3.2)$$

Where,

$\varepsilon P\ (n,T)$ = Permanent axial strain after n load applications at temperature, T.

h_o = Original distance between loading surfaces (specimen thickness)

Δh = Change in distance between specimen loading surfaces (measures axial permanent deformation).

Figure 3.9: Test configuration for RLAT in NAT

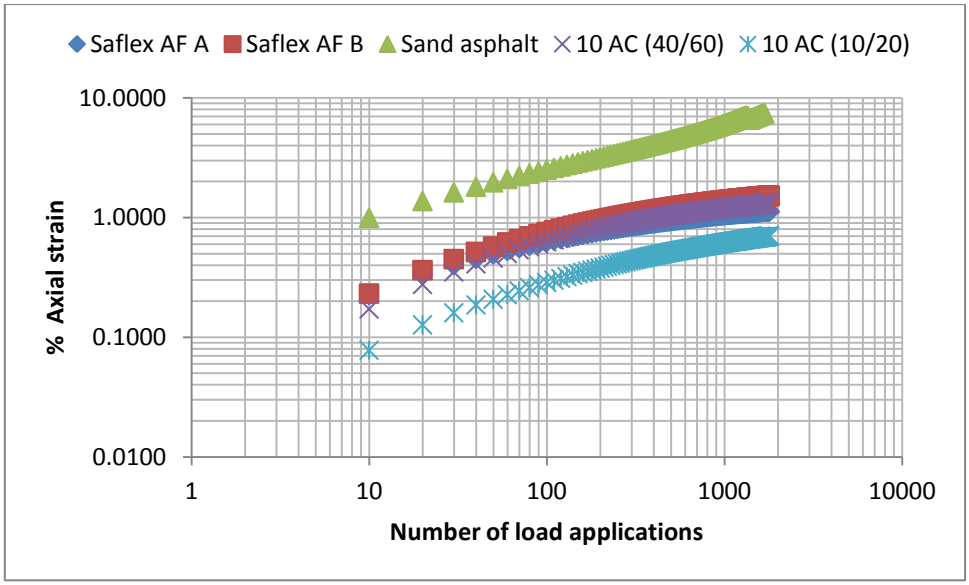

Figure 3.10: Permanent deformation results

Table 3.16: Permanent strain at 1800 load applications

Materials	Permanent strain (%)
10 mm AC (40/60)	1.3070
10 mm AC (10/20)	0.7060
Saflex AF A	1.1274
Saflex AF B	1.5204
Sand asphalt	7.4828

3.6 Conclusion

The properties of the materials reported in this section were determined in order to give better understanding of the materials that are used in this research. Also, some of the properties are required as input for the finite element modelling of the wheel tracking test to understand the stress-strain distribution and deflections in an overlay with and without SAMIs on a cracked pavement.

REFERENCES

Airey G. (1997): Rheological Characteristics of Polymer Modified and Aged Bitumens. PhD Thesis submitted to University of Nottingham.

BSD (2003): Method for Determination of the Fatigue Characteristics of Bituminous Mixtures using Indirect Tensile Fatigue. British Standard Draft, London, UK (DD ABF: 1993)

BSI (1993): Method for Determination of the Indirect Tensile Stiffness Modulus of Bituminous Mixture. British Standard Institution, London, UK (DD 213:1993).

BSI (1996): Method for Determining Resistance to Permanent Deformation of Bituminous Mixtures Subject to Unconfined Dynamic Loading. British Standard Institution, London, UK (DD 226:1996).

BSI (1997): Tests for Geometrical Properties of Aggregates- Determination of Particle Size Distribution (Sieving Method). British Standard Institution, London, UK (BS EN 933-1:1997).

BSI (2002): Bituminous Mixtures Test Methods for Hot Mix Asphalt- Determination of the Maximum Density. British Standard Institution, London, UK (BS EN 12697-5:2002).

BSI (2003a): Methods of Test for Petroleum and its Product: Bitumen and Bituminous Binders– Determination of Viscosity of Bitumen using a Rotating Spindle Apparatus. British Standard Institution, London, UK (BS EN 13302:2003; BS 2000-505:2003).

BSI (2003b): Bituminous Mixtures-Test Method for Hot Mix Asphalt: Specimen Prepared by Roller Compactor. British Standard Institution, London, UK (BS EN 12697-33:2003).

BSI (2003c): Bituminous Mixtures Test Methods for Hot Mix Asphalt- Determination of Void Characteristics of Bituminous Specimens. British Standard Institution, London, UK (BS EN 12697-8:2003).

BSI (2004a): Bituminous Mixtures-Test Method for Hot Mix Asphalt: Laboratory Mixing. British Standard Institution, London, UK (BS EN 12697-35:2004).

BSI (2004b): Bituminous Mixtures-Test Method for Hot Mix Asphalt: Stiffness. British Standard Institution, London, UK (BS EN 12697-26:2004).

BSI (2004c): Bituminous Mixtures-Test Method for Hot Mix Asphalt: Resistance to Fatigue. British Standard Institution, London, UK (BS EN 12697-24:2004).

BSI (2005a): Methods of Test for Petroleum and its Products. Bitumen and Bituminous Binders-Determination of Complex Shear Modulus and Phase Angle (Dynamic Shear Rheometer). British Standard Institution, London, UK (BS 2000-536:2005; BS EN 14770:2005).

BSI (2005b): Coated Macadam (Asphalt Concrete) for Roads and other Paved Areas-Specification for Constituent Materials and for Mixtures. British Standard Institution, London, UK (BS 4987-1:2005).

BSI (2005c): Hot Rolled Asphalt for Roads and other Paved Areas- Specification for Constituent Materials and Asphalt Mixtures (BS 594-1:2005).

BSI (2006a): Bitumen and Bituminous Binders- Dynamic Viscosity of Bituminous Emulsions, Cut-back and Fluxed Bituminous Binders (Rotating Spindle Viscometer Method) (BS EN 14896:2006; BS 2000-546:2006).

BSI (2006b): Bituminous Mixtures- Material Specifications: Asphalt Concrete. British Standard Institution, London, UK (BS EN 13108-1:2006).

BSI (2006c): Bituminous Mixtures- Material Specifications: Hot Rolled Asphalt. British Standard Institution, London, UK (BS EN 13108-4:2006).

BSI (2007a): Bitumen and Bituminous Binders- Determination of Needle Penetration. British Standard Institution, London, UK (BS EN 1426:2007; BS 2000-49:2007).

BSI (2007b): Bitumen and Bituminous Binders- Determination of the Softening Point (Ring and Ball Method). British Standard Institution, London, UK (BS EN 1427:2007; BS 2000-58:2007).

Dukatz, E.L. (1989): Aggregates Properties Related to Pavement Performance. Association of Asphalt Paving Technologists (AAPT), Vol. 58, 492-502.

Hunter R.N. (2000): Asphalts in Road Construction. First edition, Thomas Telford Publishing, London.

Liao M. (2007): Small and Large Strain Rheological and Fatigue Characterisation of Bitumen-Filler Mastics. PhD Thesis submitted to University of Nottingham.

Pell, P. S. (1973): Characterisation of Fatigue Behaviour. Symposium on Structural Design of Asphalt Concrete Pavements to Prevent Fatigue Cracking. Nottingham.

Read J. and Whiteoak D. (2003): The Shell Bitumen Handbook. Fifth Edition, Thomas Telford Publishing, London, UK.

Read J.M. (1996): Fatigue Cracking of Bituminous Paving Mixtures. PhD Thesis submitted to University of Nottingham, Nottingham, UK.

Thom N. (2008): Principles of Pavement Engineering. Thomas Telford Publishing, London, UK.

4 INTERFACE BOND

4.0 Introduction

Road pavement structures are made up of several layers and each layer contributes to pavement performance. The strength of the pavement depends on the strength and stiffness of each individual layer and the bond between the layers. This is because the state of adhesion at the interfaces between different layers seriously influences stress and strain distribution among the pavement layers, and thus, affects the performance of the pavement (Mohammad et al, 2005). If the bond at an interface is inadequate, the strains throughout the pavement may increase (under trafficking) and its life may consequently be reduced (Collop et al, 2003). Some state agencies, such as Wisconsin Department of Transportation (WisDOT) have experienced pavement failures that have been attributed to poor bonding at the interlayer (Mehta and Siraj, 2007).

However, the situation is different in rehabilitated pavements having interlayers and overlay, where the properties of the interface influence the crack resistance of the interlayer. Debondt (1999) observed that the presence of layer interfaces is certainly not a disadvantage. The interfaces close to the surfacing layer are the most critical as observed by Mehta and Siraj (2007) and Sanders (2001). The introduction of interlayer materials which have different properties from other typical pavement interfaces may affect the interface bond. Other factors that affect the interface bond include segregation, low compaction of lower base layer, poor or excessive tack coat, contamination of lower layer due to the presence of dust or spillage of oil or fuel from construction traffic, cold joints and poor foundation condition (Khweir and Fordyce, 2003). However, in this study attention is focused on the effects of SAMIs and temperature on the overlay-SAMI interface bond.

The common method of assessing pavement interface bond is by a direct shear test, which measures the interface strength in shear mode. Sanders (2001), Caltabiano (1990) and Hughes (1986) used a shear box apparatus to assess the interface properties of reinforced overlay. Other methods include the pull off test (tension mode), torque bond test (torsional shear), and wedge splitting test. Also, Hakim et al. (1999) used a falling weight deflectometer to examine the interface bond. The cases where these methods have been used to determine interface bond have been reported in section 2.3. The test modes most important to the present study are the shear and tension modes.

Debondt (1999) carried out theoretical analysis of the overlay-interlayer interface and found that the tensile stresses which occur along the interface is influenced by degree of subgrade support, overlay thickness and the amount of load transfer across the crack/joint. He stressed that the presence of tensile stresses demonstrates the importance of testing the interface properties in tension. In this study, the interface bond between overlay and SAMI was investigated using the Leutner shear test and pull-off test. This was done to assess the effect of the interface bond on the performance of the SAMIs against reflective cracking. The cross-section of the system examined for both Leutner shear test is shown in Figure 4.1 while that of the pull-off test is shown in Figure 4.2. The thickness of proprietary SAMIs A and B and sand asphalt for both tests were 20mm, while the thickness of proprietary SAMIs C and D was about 7 mm.

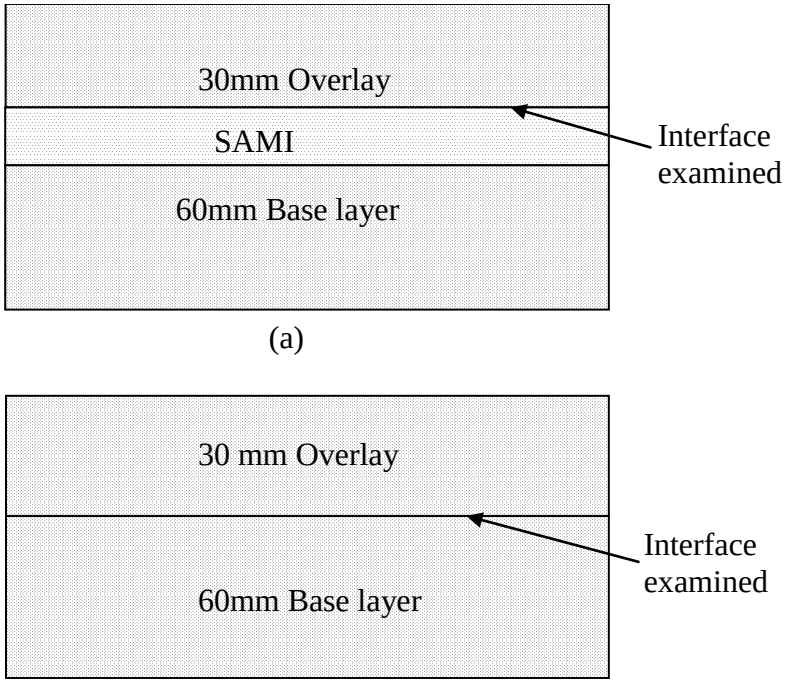

Figure 4.1: Cross-section of the system examined using Leutner shear test (a) with SAMI (b) without SAMI

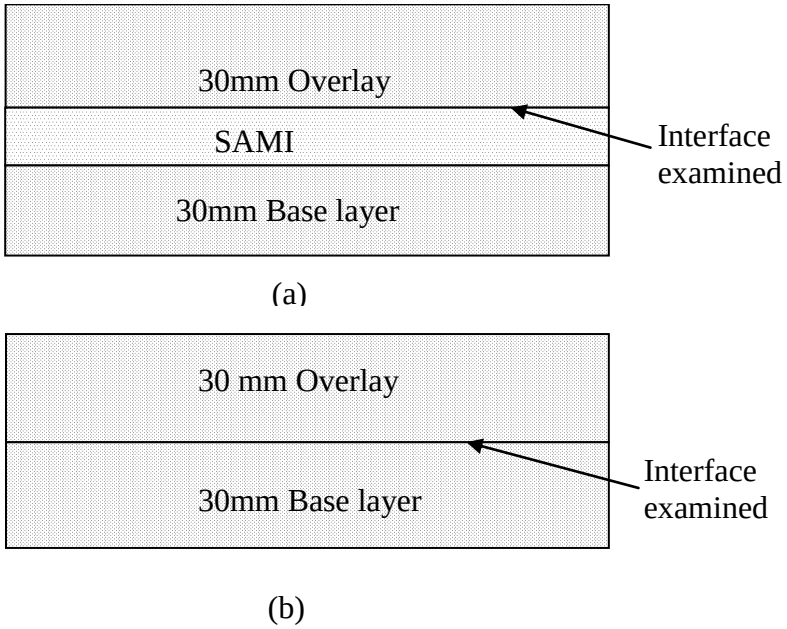

Figure 4.2: Cross-section of the system examined using Pull-off test (a) with SAMI (b) without SAMI

4.1 Leutner shear test

The Leutner test was developed in Germany in the late 1970s as a simple means of undertaking a direct shear test on the bond between two asphalt layers. The test applies a constant shear displacement rate across the interface under investigation and the resulting shear force is monitored. The test is normally carried out on 150 mm diameter cores comprising at least two layers and the standard loading (displacement) rate and temperature are 50 mm/min and 20^{o}C, respectively. The Leutner shear test is different from the direct shear box test because normal force is not applied. The shear test apparatus for this study was a modified Leutner shear apparatus which introduced a 5 mm gap into the shear plane to avoid misalignment between the interface to be examined and the shear plane of the Leutner load frame. The peak shear stress, displacement at peak shear stress and shear stiffness modulus are determined during the test

The peak shear stress is the maximum value of shear stress, determined as the maximum force divided the initial cross sectional area of the specimen when tested. Displacement at peak shear stress is the displacement at the maximum value of shear stress of a specimen when tested and the shear stiffness modulus is the peak shear stress divided by the displacement at the peak shear stress of a specimen when tested. A schematic of the Leutner frame cross section and the Leutner shear test apparatus in an Instron hydraulic machine are shown in Figures 4.3 and 4.4 respectively.

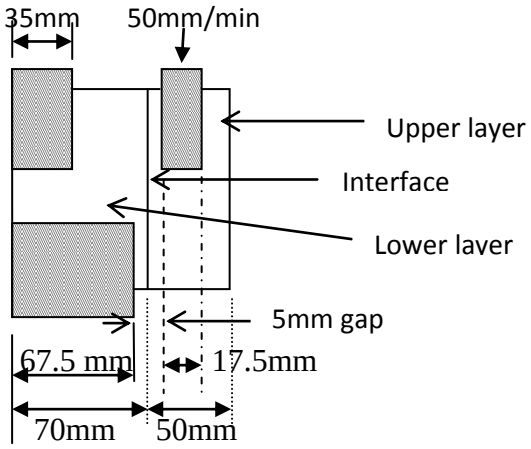

Figure 4.3: Schematic of the shear test equipment

Figure 4.4: Leutner shear test equipment

4.2 Specimen preparation

The test specimens were prepared in three layers, the top layer (overlay) was a 10 mm asphaltic concrete with 40/60 penetration grade bitumen (see Table 3.5), the middle layer was the SAMI and the base layer was also a 10mm asphaltic concrete with 10/20 penetration grade bitumen (see Table 3.5). The control specimens were prepared in two layers (top and base) without a SAMI. The base layer for each specimen was 60 mm thick, the top layer (overlay) was 30 mm thick and the middle layer (where present) was 20 mm thick for proprietary SAMIs A and B (see Table 3.7) and sand asphalt (see Table 3.6), while

proprietary SAMIs C and D defined in section 3.4.4 were about 7mm thick. The mix compositions for the asphalt concrete and SAMIs were detailed in chapter 3.

For the base layer, the aggregates and binder were batched and heated in the oven at 185^{o}C. The heated aggregates and binder were mixed and compacted in a mould 305 mm × 305 mm × 130 mm with roller compactor at 180^{o}C to a thickness of 60 mm. For the middle layer, the sand asphalt and SAMIs A and B aggregates and binder were batched and heated at 140^{o}C and 180^{o}C, respectively. The heated aggregates and binder were mixed and compacted on the base layer at temperatures of 130^{o}C and 150^{o}C, respectively to a thickness of 20 mm. Proprietary SAMIs C and D were prepared by sandwiching 60 mm glass fibre strands between layers of bitumen emulsion and 6 mm aggregates were compacted on them. The bitumen emulsion for proprietary SAMI C was ordinary bitumen emulsion while that of proprietary SAMI D was polymer modified emulsion.

The top layer (overlay) aggregates were batched and heated at 160^{o}C and the heated aggregates and binder were mixed and compacted to achieve a thickness of 30mm at 150^{o}C. Two cores of diameter 150mm and depth 110 mm were cut from each slab. All the mixtures were mixed in accordance with BSI, (2004) and compacted in accordance with BSI (2003). Typical 150 mm cores are shown in Figure 4.5.

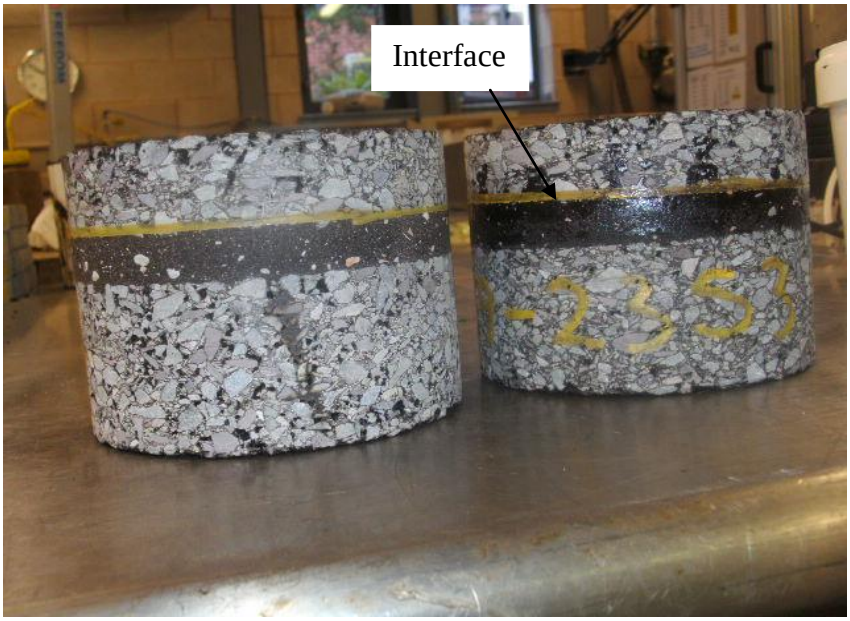

Figure 4.5: Typical 150 mm cores

4.3 Test procedure

The specimens were placed in a temperature control conditioning cabinet at the test temperature for a minimum of 5 hours. The specimen was fitted in the Leutner test frame and the interface to be evaluated was aligned between the upper and the lower shear ring. The Leutner shear frame was fixed into Instron hydraulic machine with a temperature control cabinet. The load (shear displacement) was applied at the rate of 50mm/min and the resulting load was recorded to the nearest 0.1kN and the displacement to the nearest 0.1mm. The test was stopped when the interface failed. The shear stress-shear displacement graphs were produced and the peak shear stress, displacement at peak shear stress and shear stiffness modulus were determined. The peak displacement was adjusted with a correction factor to account for displacement when the load starts to build up. The correction factor was determined as the ratio of the slope and the intercept of the linear part of the shear stress-displacement curve. The tests were carried out at 10^{o}C, 20^{o}C and 30^{o}C. The test procedure is described in Highways Agency (2008). The shear stress was calculated as shown in equation 4.1.

$$\tau = \frac{F}{\pi r^2} \quad \text{..... 4.1}$$

Where:

τ = shear stress in (MPa)

F = shear force (load) (in kN)

r = initial radius of specimen (in mm)

4.4 Results and analysis of Leutner shear test

The results of the Leutner shear test are presented as graphs of the shear stress versus displacement. A typical graph of shear stress versus displacement is shown in Figure 4.6. All the other graphs are shown in Appendix A. These show that the shear stress increased with increasing shear displacement until the peak shear stress was attained (defining the shear strength of the interface). After the peak shear stress, the interface started failing and the shear stress decayed rapidly to zero as the sample split into two. Tables 4.1, 4.2 and 4.3 show the results of the Leutner shear tests at 10^{o}C, 20^{o}C and 30^{o}C respectively. Figures 4.7, 4.8, and 4.9 show the peak shear stress versus peak shear displacement of the interfaces tested at 10^{o}C, 20^{o}C and 30^{o}C, respectively.

It can be seen from Figure 4.7 that the overlay-SAMI A interface had the highest shear strength of all the interfaces tested at 10^{o}C. It was followed closely by the overlay-SAMI B interface. The shear strengths of these two interfaces were greater than that of the control (AC10 (40/60)-AC10 (10/20)) indicating that they were well bonded to the overlay. Also, the overlay-SAMI C interface has higher shear strength than overlay-SAMI D interface, while their shear strengths were lower than that of overlay-sand asphalt. This implied the overlay-sand asphalt interface had stronger bond than the overlay-SAMI C and the overlay-SAMI D

interfaces. Figure 4.8 indicates that the overlay-SAMI B interface had greater shear strength than overlay-SAMI A interface at 20^{o}C. Also, both overlay-SAMI A and overlay-SAMI B interfaces have higher shear strength than the control (AC10 (40/60)-AC10 (10/20)), but the control had higher shear strength than other interfaces. Again, the overlay-SAMI C interface had greater shear strength than SAMI D interface, but their shear strengths were less than that of the sand asphalt.

Figure 4.9 indicates that the interface bond at 30^{o}C followed the same trend as interfaces tested at 20^{o}C, but with less shear strength at the interfaces. Although as presented in Figures 4.7, 4.8 and 4.9 both overlay-SAMI A and overlay-SAMI B interfaces have higher shear strength than the control specimens, their shear stiffnesses were lower, because the control specimens have lower displacement rate. Figure 4.10 shows that the interfaces with SAMIs have lower shear stiffness than the control interface and the interface stiffness decreased with increasing temperature. In general, it can be concluded that the introduction of stress absorbing membrane interlayers in a pavement influences the interface bond. A typical failed interface after the test is shown in Figure 4.11. Also, comparing the interface shear strength of the overlay-SAMI interface with Highways Agency's recommendation for good performance (1MPa), it can be seen that at 10^{o}C and 20^{o}C, all the interfaces examined have greater interface shear strength except the overlay-proprietary SAMI C and overlay-proprietary SAMI D interfaces, while at 30^{o}C, all the interfaces have lower interface strength.

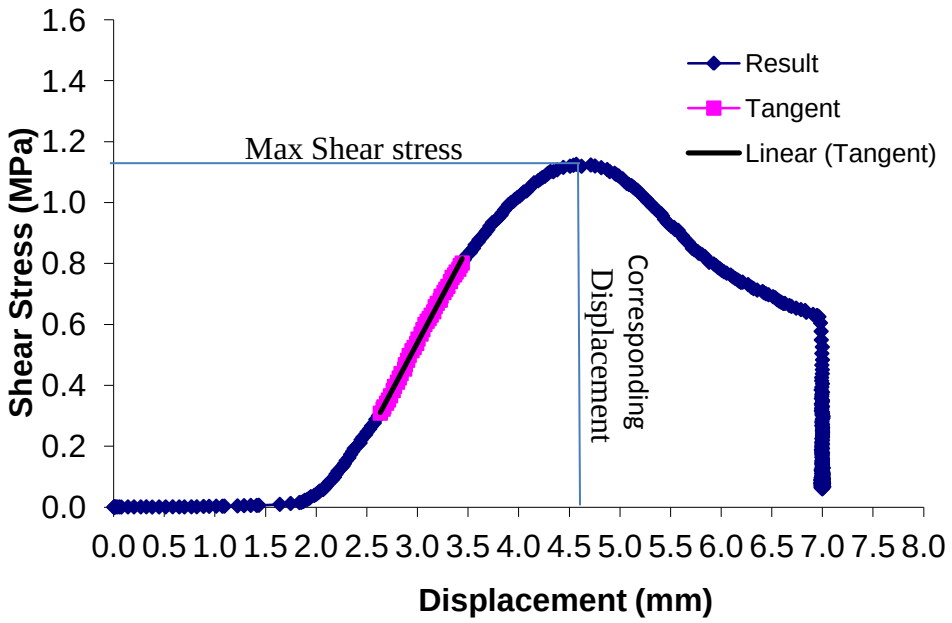

Figure 4.6: A typical shear stress versus displacement graph

Table 4.1: Leutner shear test results at 10°C

Interface	Average Peak shear force(kN)	Average peak displacement (mm)	Average Peak shear stress (MPa)	Shear stiffness modulus (MPa/mm)	Shear stiffness modulus as % of control
10AC(40/60)-SAMI A	86.5	2.57	4.96	2.23	69.91
10AC(40/60)-SAMI B	83.8	3.07	4.81	1.56	48.90
10AC(40/60)-Sand asphalt	27.25	2.05	1.56	0.76	23.82
10AC(40/60)-SAMI C	14.5	0.85	0.83	0.98	30.72
10AC(40/60)-SAMI D	11.7	1.38	0.68	0.53	16.61
Control 10AC(40/60)-10AC(10/20)	38.25	0.74	2.20	3.19	100

Table 4.2: Leutner shear test results at 20°C

Interface	Average Peak shear force(kN)	Average peak displacement (mm)	Average Peak shear stress (MPa)	Shear stiffness modulus (MPa/mm)	Shear stiffness modulus as % of control
10AC(40/60)-SAMI A	40.15	3.16	2.31	0.75	57.69
10AC(40/60)-SAMI B	45.45	3.24	2.61	0.81	62.31
10AC(40/60)-Sand asphalt	19.1	2.37	1.10	0.46	35.38
10AC(40/60)-SAMI C	6.6	1.71	0.38	0.22	16.92
10AC(40/60)-SAMI D	4.75	1.41	0.27	0.20	15.30
Control 10AC(40/60)-10AC(10/20)	26.35	1.17	1.51	1.30	100

Table 4.3: Leutner shear test results at 30°C

Interface	Average Peak shear force(kN)	Average peak displacement (mm)	Average Peak shear stress (MPa)	Shear stiffness modulus (MPa/mm)	Shear stiffness modulus as % of control
10AC(40/60)-SAMI A	15.85	4.41	0.91	0.21	42.86
10AC(40/60)-SAMI B	16.15	4.19	0.93	0.23	46.94
10AC(40/60)-Sand asphalt	6.05	2.97	0.35	0.12	24.49
10AC(40/60)-SAMI C	2.05	1.26	0.12	0.11	24.45
10AC(40/60)-SAMI D	2.10	1.98	0.12	0.08	16.32
Control 10AC(40/60)-10AC(10/20)	14.10	1.69	0.81	0.49	100

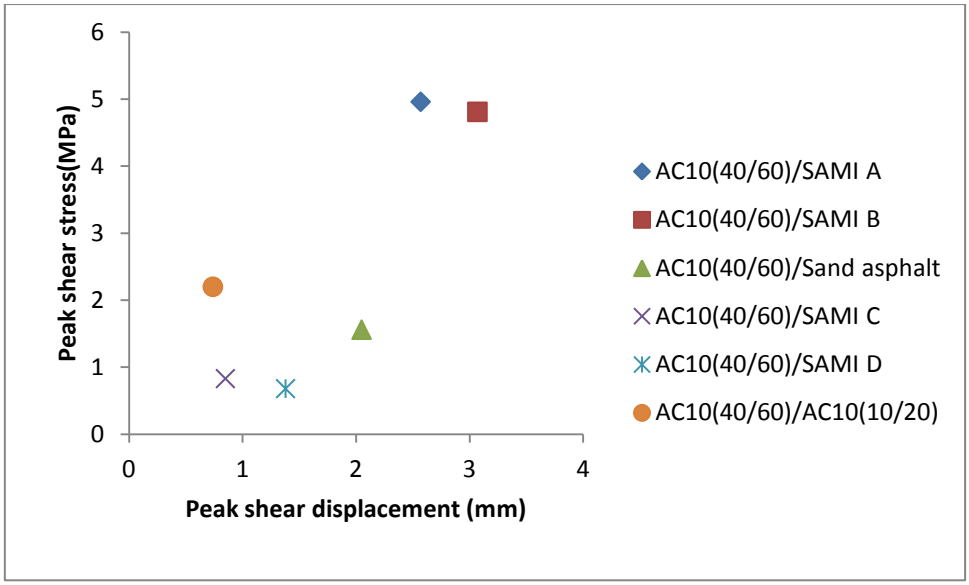

Figure 4.7: Peak shear stress versus peak shear displacement at 10°C

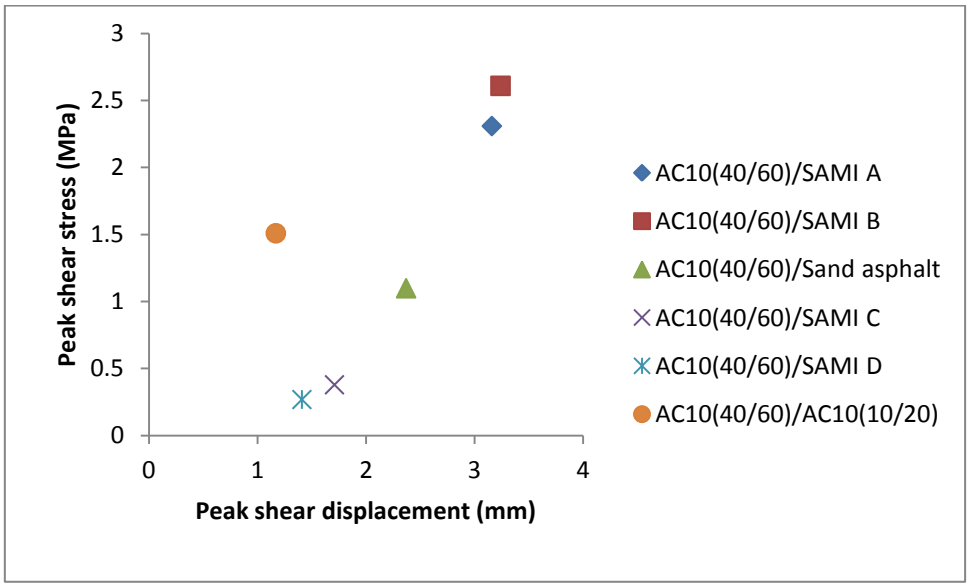

Figure 4.8: Peak shear stress versus peak shear displacement at 20°C

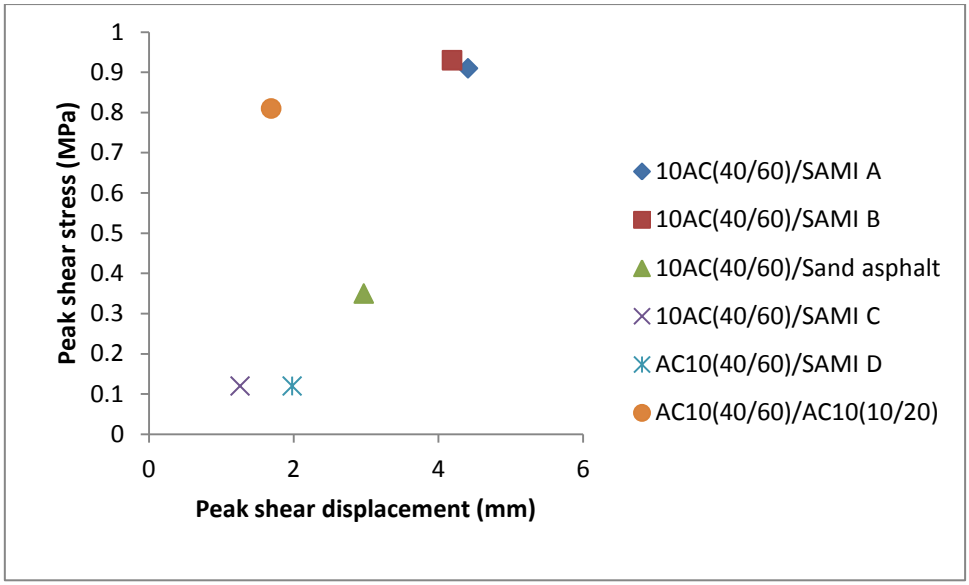

Figure 4.9: Peak shear stress versus peak shear displacement at 30°C

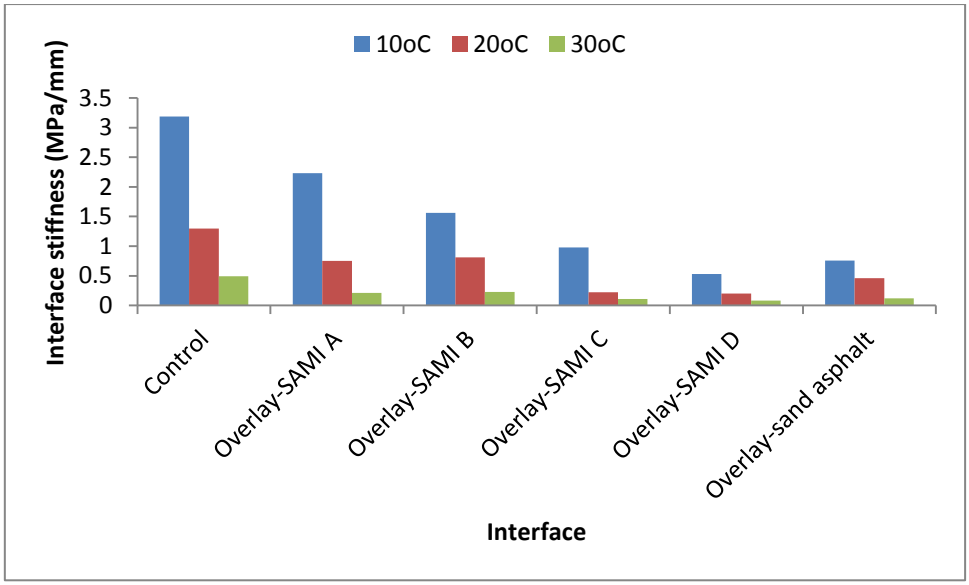

Figure 4.10: Shear stiffness of the interface

Figure 4.11: A typical failed interface after test

4.5 Summary

- The Leutner shear test showed that the shear strength of the interface between the SAMIs and the overlay increases with decreasing temperature
- The overlay-SAMI A and overlay-SAMI B interfaces have greater shear strength but lower shear stiffness than the control specimens.
- Overlay-sand asphalt, overlay-SAMI C and overlay-SAMI D interfaces have lower shear strength than the control specimens.
- The Overlay-SAMI C interface has greater shear strength than the overlay-SAMI D interface.
- Overlay-SAMI C and overlay-SAMI D interfaces have the weakest bond. This is thought to be due to the aggregate being compacted onto the sandwiched fibre which did not bond well with the overlay.
- The shear stiffnesses of all the interfaces with SAMI are lower than the control interface.
- The effect of the interface stiffness on the performance of the SAMIs is considered in chapters five and eight.

4.6 Pull-off test

The pull off test was developed at the University of Texas at El Paso (UTEP) (Tashman et al. 2008). The test measures the tensile strength of the interface. The pull-off test is usually considered because the surfacing layer of a road pavement is not only effective in shear but also in tension mode under trafficking, as the moving traffic exerts normal pressure on the interface. Debondt (1999) observed that due to the action of wheel loads at locations next to discontinuities (cracks/joints) in the existing pavement structure, quite large tensile stresses perpendicular to the plane of the interface were found to occur. In this study, the tensile strength of the overlay-SAMI interface was examined using the pull-off apparatus shown in Figure 4.12.

Figure 4.12: Pull-off test set up

4.7 Sample preparation

The test specimen for the pull-off test was a 3-layer asphaltic slab of dimension 305 mm × 305 mm × 80 mm. The base layer was 30 mm thick 10 mm asphaltic concrete with 10/20 bitumen (see Table 3.5), the middle layer was SAMI (20 mm thick proprietary SAMIs A and

B (see Table 3.7) and sand asphalt (see Table 3.6) and about 7 mm proprietary SAMIs C and D (see section 3.4.4)) and the top layer (overlay) was 30 mm thick 10 mm asphaltic concrete with 40/60 bitumen. The control specimen was manufactured in two layers without a SAMI, the base layer was 30 mm thick 10 mm asphaltic concrete with 10/20 bitumen and the top layer (overlay) was 30 mm thick 10 mm asphaltic concrete with 40/60 bitumen.

The mixtures were prepared for each of the layers as discussed in section 4.2. The top layer of the slab was isolated by cutting down to the top of the middle layer (SAMI) without damage to the SAMI. The plan for the cut was as shown in Figure 4.13. The cutting was done such that there were two isolated areas of 100 mm × 100 mm at the top layer. A steel plate of dimension 100 mm × 100 mm × 10 mm was glued to each of the areas with epoxy glue.

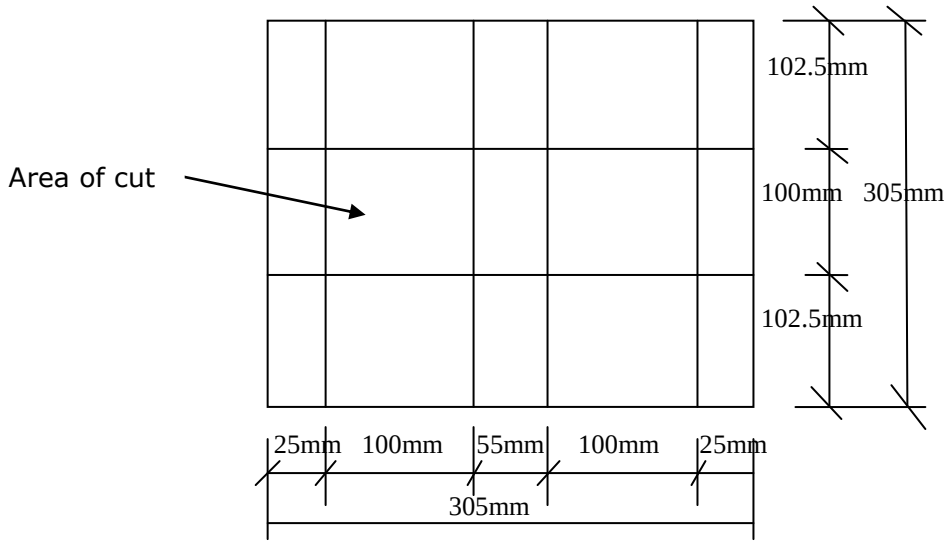

Figure 4.13: Plan of cuts for the 305 mm × 305 mm slab

4.8 Test procedure

The test was carried out in a tensile pull-off apparatus (Instron hydraulic machine). The sample for the test was placed in a temperature conditioning cabinet at test temperature for a minimum of 5 hours. The specimen was attached to the Instron hydraulic machine using a hook on the steel plate. It was loaded at a rate of 20 mm/min until the interface bond failed.

The maximum load required to pull-off the top layer from the interlayer was recorded and the tensile strength of the interface was calculated. Slower loading rate was applied to prevent premature failure of the interface.

4.9 Results and analysis of pull-off test

It can be seen from Tables 4.4, 4.5 and 4.6 that the overlay-SAMI A and overlay-SAMI B interface did not fail at 10^{o}C, 20^{o}C and 30^{o}C. The values are recorded with a greater than (>) sign because they are the maximum values to failure of the steel plate at the glue interface. This indicated they were well bonded and had stronger bond than the control (AC10 (40/60)/AC10 (10/20)), thus, confirming the results of the shear test. Also, as shown in table 4.4, the control (AC10 (40/60)/AC10 (10/20)) interface did not fail at 10^{o}C.

Figure 4.14 shows that at 10^{o}C, the overlay-sand asphalt interface has a greater tensile strength than the overlay-SAMI C or overlay-SAMI D interfaces, which had the same strength. Also, this was in agreement with the shear test results. The Figure shows that the overlay-SAMI C interface had slightly better interface tensile bond than the overlay-SAMI D interface at 20^{o}C and 30^{o}C, respectively, but both interfaces had lower tensile strengths than the overlay-sand asphalt interface. The control (AC10 (40/60)/AC10 (10/20)) had the highest tensile strength and better tensile bond than the other three interfaces.

Figure 4.14 indicates that the tensile strength of all the interfaces tested decreased with increasing temperature, indicating stronger bond at lower temperature than higher temperature as observed in the Leutner shear test. A typical failed interface is shown in Figure 4.15.

Table 4.4: Pull off test results at 10°C

Interface	Peak Tensile force (kN)	Mean Peak Tensile force (kN)	Peak Tensile Stress (MPa)	Mean Peak Tensile Stress (MPa)
AC10 (40/60)/SAMI C	5.27	4.48	0.53	0.45
	3.69		0.37	
AC10 (40/60)/SAMI D	5.30	4.64	0.49	0.45
	3.98		0.40	
AC10 (40/60)/SAMI A)	>14.74	>15.30	>1.47	>1.53
	>15.85		>1.59	
AC10 (40/60)/SAMI B)	>11.44	>12.56	>1.10	>1.21
	>13.67		>1.31	
AC10 (40/60)/Sand asphalt	14.91	12.98	1.49	1.31
	11.04		1.13	
AC10 (40/60)/AC10(10/20)	>10.02	>10.09	>1.00	>1.00
	>10.16		>1.00	

Table 4.5: Pull off test results at 20°C

Interface	Peak Tensile force (kN)	Mean Peak Tensile force (kN)	Peak Tensile Stress (MPa)	Mean Peak Tensile Stress (MPa)
AC10 (40/60)/SAMI C	2.17	1.79	0.22	0.18
	1.4		0.14	
AC10 (40/60)/SAMI D	2.36	1.66	0.24	0.17
	0.96		0.10	
AC10 (40/60)/SAMI A)	>9.05	>10.30	>0.90	>1.03
	>11.56		>1.16	
AC10 (40/60)/SAMI B)	>11.48	>11.58	>1.15	>1.15
	>11.67		>1.16	
AC10 (40/60)/Sand asphalt	6.40	6.06	0.63	0.60
	5.72		0.58	
AC10 (40/60)/AC10(10/20)	7.00	7.04	0.69	0.69
	7.08		0.69	

Table 4.6: Pull off test results at 30°C

Interface	Peak Tensile force (kN)	Mean Peak Tensile force (kN)	Peak Tensile Stress (MPa)	Mean Peak Tensile Stress (MPa)
AC10 (40/60)/SAMI C	1.39	1.2	0.14	0.12
	1.01		0.10	
AC10 (40/60)/SAMI D	0.98	1.08	0.10	0.11
	1.17		0.12	
AC10 (40/60)/SAMI A)	>6.53	>6.07	>0.64	>0.59
	>5.60		>0.55	
AC10 (40/60)/SAMI B)	>5.52	>5.51	>0.54	>0.54
	>5.49		>0.54	
AC10 (40/60)/Sand asphalt	2.86	2.89	0.29	0.29
	2.92		0.29	
AC10 (40/60)/AC10(10/20)	3.68	3.62	0.36	0.36
	3.55		0.36	

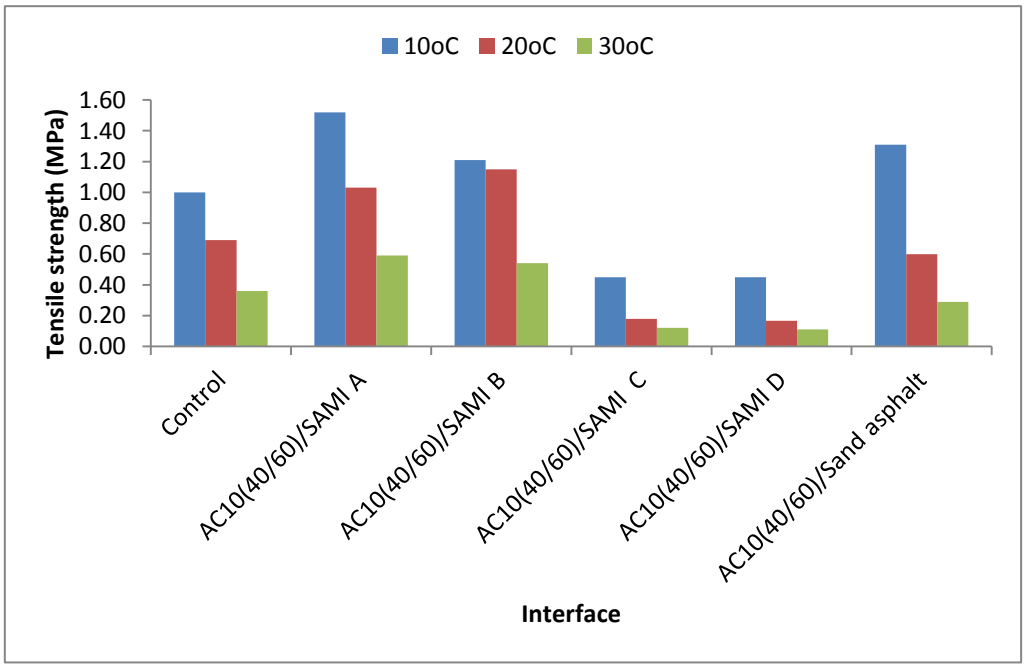

Figure 4.14: Pull of test results at 10°C, 20°C, 30°C

Figure 4.15: A typical failed interface after test

4.10 Summary

- The overlay-SAMI A and overlay SAMI B interfaces had greater tensile strengths than the control and overlay-sand asphalt, overlay-SAMI C and overlay-SAMI D interfaces at 10^{o}C, 20^{o}C and 30^{o}C.
- The overlay-sand asphalt, overlay-SAMI C and overlay-SAMI D interfaces had weaker tensile strength than the control at 10^{o}C, 20^{o}C and 30^{o}C.
- The overlay-SAMI C interface had a slight stronger bond than the overlay-SAMI D interface at 20^{o}C and 30^{o}C, while they have the same strength at 10^{o}C.
- The pull-off test like the Leutner shear test shows the strength of the interface is affected by the introduction of SAMIs.

REFERENCES

BSI (2003): Bituminous Mixtures-Test Method for Hot Mix Asphalt: Specimen Prepared by Roller Compactor. British Standard Institution, London, UK (BS EN 12697-33:2003).

BSI (2004): Bituminous Mixtures-Test Method for Hot Mix Asphalt: Laboratory Mixing. British Standard Institution, London, UK (BS EN 12697-35:2004).

Caltabiano M.A (1990): Reflection Cracking in Asphalt Overlays. Thesis submitted to University of Nottingham for the degree of Master of Philosophy.

Collop A.C. Thom N.H. and Sangiorgi C. (2003): Assessment of Bond using the Leutner Shear Test. Proceedings of the Institution of Civil Engineers. Transport 156. 211-217.

Debondt A.H. (1999): Anti Reflective Cracking Design of (Reinforced) Asphaltic overlays. PhD Thesis submitted to Delft University of Technology, Netherlands.

Hakim B., Cheung L.W., and Armitage R.J. (1999): Use of FWD Data for Prediction of Bonding between Pavement Layers. International Journal of Pavement Engineering, 1:1, 49-59.

Highways Agency (2008): Manual of Contract Documents for Highway Works: Specification for Highway Works. Volume 1, Series 900.

Hughes D.A.B. (1986): Polymer Grid Reinforcement of Asphalt Pavements. Thesis submitted to University of Nottingham for the degree of Doctor of Philosophy.

Khweir K. and Fordyce D. (2003): Influence of Layer Bonding on the Prediction of Pavement Life. Proceedings of the Institution of Civil Engineers. Transport 156. 73-83.

Mehta Y. and Siraj N. (2007): Effect of Stiffness Ratio on Slippage Cracking Due to Interlayer Bonding in Hot Mix Asphalt Pavement. Proceedings of the Mid-Continent Transportation Research Symposium, Ames, Iowa, USA.

Mohammad L.N, Wu Z., and Raqib M.A. (2005): Investigation of the Behaviour of Asphalt Tack Coat Interface Layer, Louisiana Transportation Research Center, Baton Rouge. LTRC Project No. 00-2B.

Sanders P.J. (2001): Reinforced Asphalt Overlays for Pavements. PhD Thesis submitted to University of Nottingham, Nottingham, United Kingdom.

Tashman M., Nam K., Papagiannakis T., Willoughby K., Pierce L., and Baker T. (2008): Evaluation of Construction Practices that Influence the Bond Strength at the Interface between Pavement Layers. ASCE, Journal of Performance of Constructed Facilities. Pp.154-161.

5 WHEEL TRACKING TEST

5.0 Introduction

Pavements that exhibit cracking (fatigue or thermal cracking), are normally rehabilitated by overlaying with new surfacing mixture. Experience has shown that the cracks are reflected onto the new surface after a period of service, a phenomenon known as reflective cracking. The two principal causes of reflective cracking highlighted are the effects of traffic loading and daily or seasonal temperature variation. Although field testing is the best way to assess the resistance of interlayer materials against reflective cracking, the use of small scale laboratory tests allows different factors and conditions to be investigated in a short period of time and gives room for better planning and utilization of highway budgets.

A number of test configurations have been used to study the effectiveness of interlayer materials against reflective cracking, among which are 4-point bending, 3-point bending, slab testing, etc. Most of the tests have been found suitable except the slab testing facility in which there can be difficulty in manufacturing the specimens and results can be masked by permanent deformation (Sanders, 2001).

It was intended that the current test should simulate field conditions as closely as possible, while being able to study different factors that affect crack initiation and propagation. Therefore, the use of small laboratory wheel tracking facilities was seen as the best option. The test was designed to study the effect of traffic loading on crack propagation in overlays with and without SAMIs. Trial tests were carried out and the equipment was found to function well and was able to evaluate SAMIs crack resistance potential. The test is capable of generating the maximum shear stress and the maximum bending stress that occur when a moving wheel is either slightly offset from or directly over a crack. This produces mode I and mode II cracking.

The test reported here was carried out in a wheel tracking machine located in a temperature controlled room, which allows the effect of temperature on SAMI performance to be studied. The wheel tracker consists of a reciprocating table which moves forwards and backwards with a frequency of 0.8Hz under the loaded wheel with a travel length of 225 mm. The solid tyre fitted to the wheel has an outside diameter of 200 mm and width of 50 mm. The test replicates what happens when a cracked pavement overlaid with and without interlayers (SAMIs) is trafficked. The schematic of the test is shown Figure 5.1.

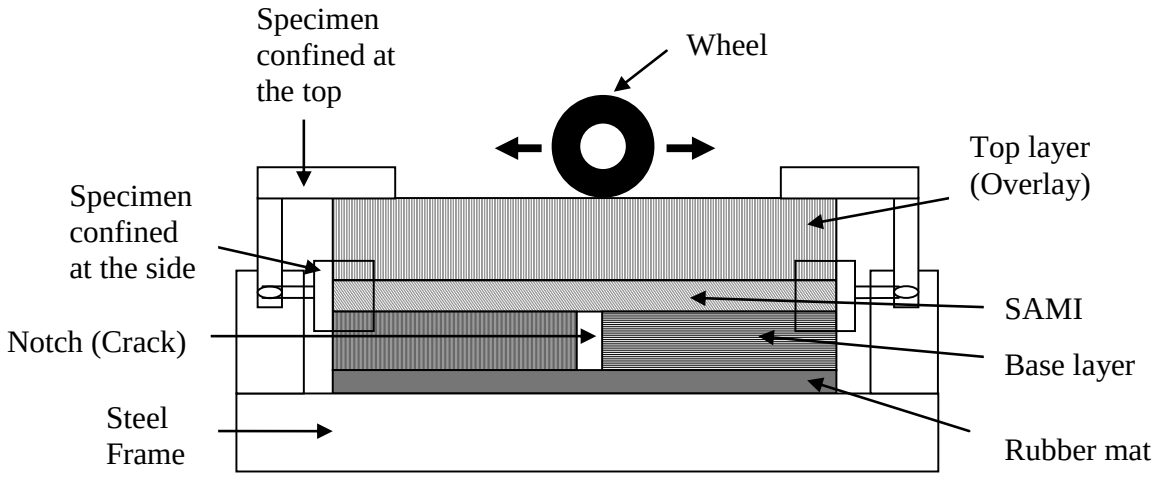

Figure 5.1: Schematic of the wheel tracking test

5.1 Materials

The materials for the specimens are as follows.

The base layer: The base layer simulates the old pavement. This was made of 10 mm asphaltic concrete with 10/20 penetration grade bitumen. The mix composition is as shown in Table 5.1.

The top layer: The top layer simulates the overlay. Also, this was made of 10 mm asphaltic concrete with 40/60 penetration grade bitumen. The mix composition is as shown in Table 5.1

The middle layer: The middle layer (where present) is the stress absorbing membrane interlayer (SAMI). The stress absorbing membrane interlayers (SAMIs) in this research included 4 proprietary mixtures and conventional sand asphalt with 160/220 penetration grade bitumen as shown in Table 5.2. The proprietary mixtures were named proprietary SAMI A (see Table 5.3), proprietary SAMI B (see Table 5.4) and proprietary SAMIs C and D.

Proprietary SAMI C is prepared by sandwiching chopped glass fibre at 120g/m^2 between layers of ordinary bitumen emulsion at 0.9L/m^2 and 6 mm aggregates spread and compacted on them at the rate of 8 kg/m^2. Proprietary SAMI D is prepared by sandwiching chopped glass fibre at 120g/m^2 between layers of polymer modified bitumen emulsion at 0.9L/m^2 and 6 mm aggregates spread and compacted on them at the rate of 8 kg/m^2. The indirect tensile stiffness moduli of the mixtures are shown in Table 5.5. The test procedure is described in section 3.5.3.

Table 5.1: Mix composition for 10 mm asphalt concrete

Sample type	**Percent by composition of aggregate**
10mm aggregate	37%
6 mm aggregate	26%
Dust	36%
Filler	1%
Binder type	10/20[1], 40/60[2] bitumen
Binder content	5.3% by mass of total mix
Target air void	5%

[1] Base layer [2] Top layer

Table 5.2: Mix composition for sand asphalt

Sample type	**% by composition of aggregate**
Sand	84%
Filler	16%
Binder type	160/220 bitumen
Binder content	10.3% by mass of total mix
Target air void	5%

Table 5.3: Mix composition for Proprietary SAMI A

Sample type	**% by composition of aggregate**
Carsew 0/4 CRF	95%
Filler	5%
Binder type	Polymer modified binder
	9% by mass of total mix
Target air void	2%

Table 5.4: Mix composition for Proprietary SAMI B

Sample type	**% by composition of aggregate**
Carsew 0/4 CRF	74.5%
Binegar fine sand	20%
Filler	5.5%
Binder type	Polymer modified binder
Binder content	9.1 % by mass of total mix
Target air void	2%

Table 5.5: Indirect tensile stiffness moduli

Asphalt concrete (AC)/SAMIs	Stiffness (MPa)		
	Temperature		
	10°C	20°C	30°C
AC (40/60)	10035	3899	1098
AC (10/20)	15435	9591	5008
Sand asphalt	635	209	118
Proprietary SAMI A	8548	2725	636
Proprietary SAMI B	7564	2444	510

5.2 Sample preparation

The test specimens were made up of 3-layer beams of length 404 mm and width 50 mm. The bottom (base) layer was a 30 mm thick 10 mm asphaltic concrete with 10/20 penetration grade bitumen, the middle layer (where present) was SAMI (10mm, 20mm and 30 mm thicknesses used) and the top layer (overlay) was a 10mm asphaltic concrete with 40/60 penetration grade bitumen, of thickness up to 80 mm (thickness of each specimen varies with the SAMIs and overlay thicknesses). The control specimens were prepared in two layers without SAMI (the base and top layers).

The beams were obtained by manufacturing a slab of dimension 500mm × 500 mm (see Figure 5.2). Also, the slab thickness varies depending on the overlay and SAMI thicknesses. For the base layer, the aggregates and binder were batched as shown in Table 5.1, heated at 185^{o}C and compacted in a mould of dimension 500 mm × 500 mm × 205 mm with a roller compactor at a temperature of 180^{o}C to a thickness of 30 mm.

The aggregates and binders for sand asphalt were heated at 140^{o}C and compacted at 130^{o}C, while the aggregates and binder for proprietary SAMIs A and B were batched and heated at a temperature of 180^{o}C, and compacted on the bottom layer at a temperature of 150^{o}C. The Proprietary SAMIs C and D were prepared by sandwiching 60 mm glass fibre strands between layers of bitumen emulsion and 6 mm aggregates compacted on them. The top layer aggregates were batched and heated at 160^{o}C and compacted to the required thickness at 150^{o}C. All the mixtures were mixed in accordance with BSI, (2004) and compacted in accordance with BSI (2003).

Ten beams of length 404 mm and width 50 mm were cut from each slab and a 10mm notch in width was sawn at the centre of the beam through the 30 mm bottom layer to simulate the crack. A typical beam with 10 mm notch at the base layer is shown in Figure 5.3. Strain gauges were glued to beam, with one placed at 4mm above the crack top, the second was placed 20 mm from the bottom of the overlay (which is equivalent to 30 mm, 40 mm and 50mm from the bottom of the overlay for control specimens with 10 mm, 20 mm and 30 mm SAMIs) and the third was placed 40mm from the bottom of the overlay. The strain gauge placed 40 mm from the bottom of the overlay was discontinued later in the study. Two aluminium brackets were glued to each side of the split base as LVDT measurement points. A typical beam with strain gauges and aluminium brackets (LVDT measurement points) is shown in Figure 5.4.

Figure 5.2: A typical 500 mm by 500 mm slab

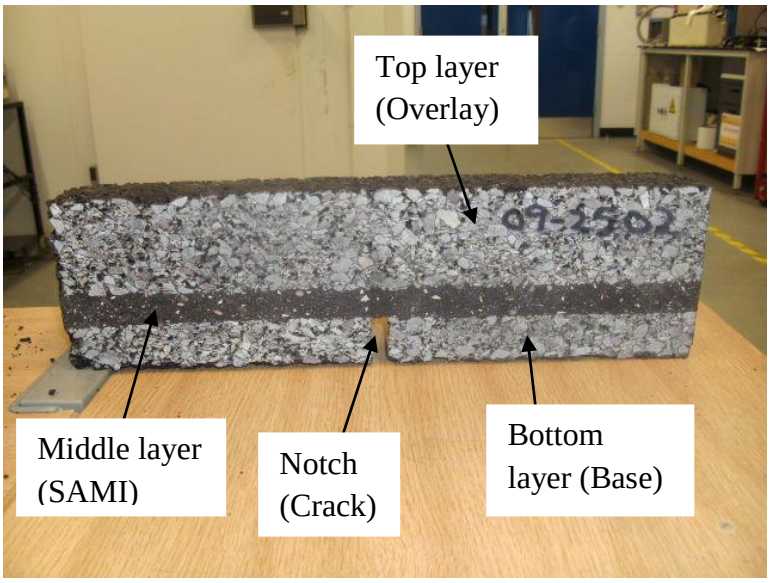

Figure 5.3: A typical beam with notch for wheel tracking test

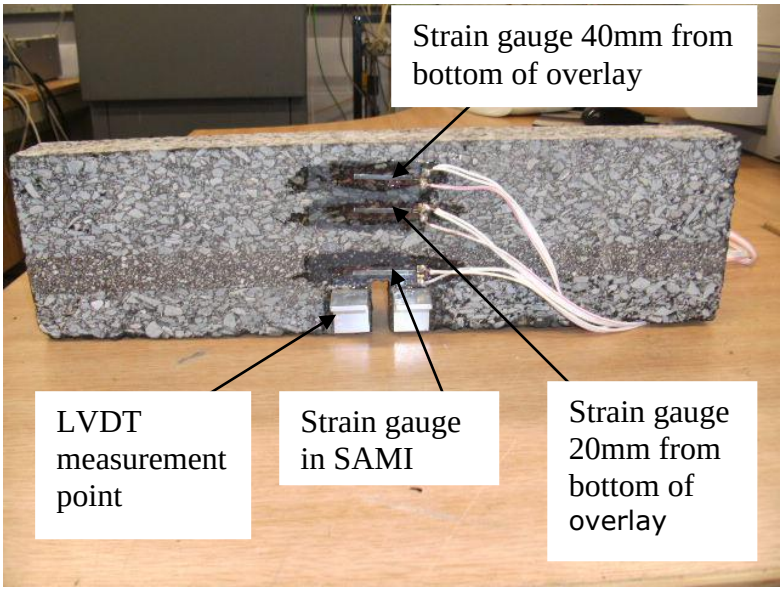

Figure 5.4: A typical beam with strain gauges and LVDT measurement points

5.3 Test procedure

The test was carried out by placing a 10 mm thick rubber mat on the base of a steel mould on a reciprocating table. The beams with the strain gauges were placed in the conditioning cabinet at test temperature for a minimum of five hours. The top and the middle layer (where present) above the simulated crack were painted white to allow monitoring of crack growth during the test. The beams were placed centrally on the 10 mm rubber mat such that the wheel loaded them symmetrically as the reciprocating table moved forward and backward. The beams were clamped at the top and at the sides of both ends to simulate pavement continuity. The linear variable differential transformers (LVDTs) and the strain gauges were connected to the data acquisition system. The tyre was released on the beams and loaded. The numbers of wheel cycles for crack growth from the crack tip to the top of the SAMI and top layer (overlay) were recorded. The strain gauges and LVDT readings were acquired using a data logger. The wheel tracker with the sample in place is shown in Figure 5.5. The test was carried out at 10^{o}C, 20^{o}C and 30^{o}C. The test plan is shown in Table 5.6.

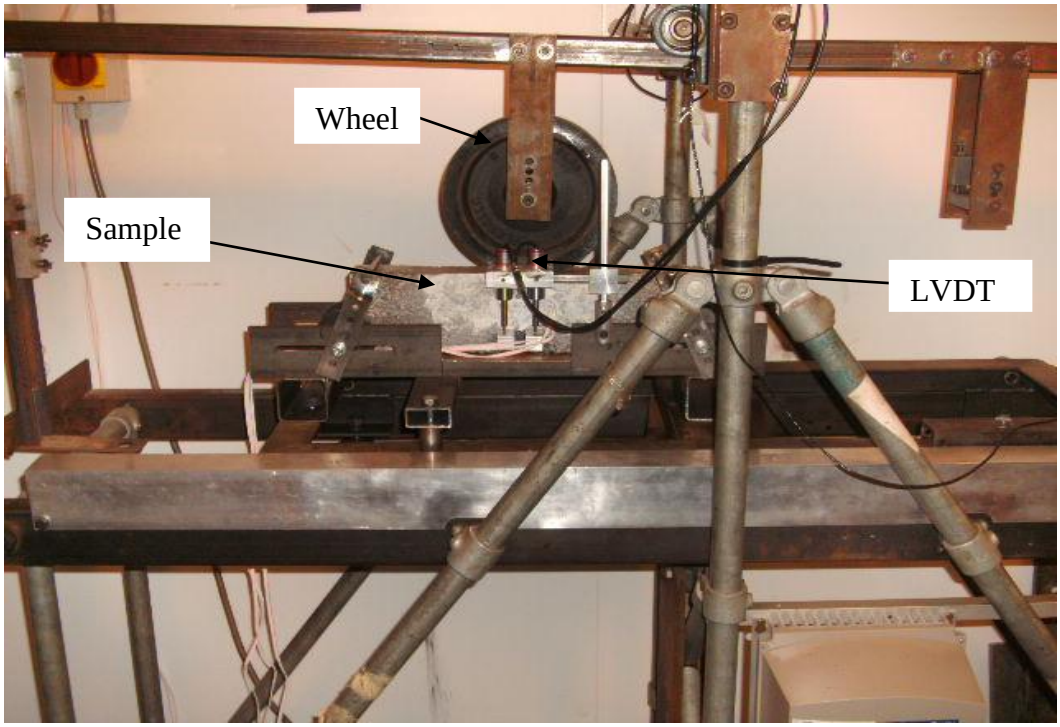

Figure 5.5: Wheel tracking machine with sample

Table 5.6: Test plan

Load		2.4kN									1.35kN		
Temperature (°C)		10			20			30			30		
Base thickness (mm)	Overlay thickness (mm)	SAMIs thickness (mm)											
		10	20	30	10	20	30	10	20	30	10	20	30
30	40	×	√	√	×	√	√	×	√	√	×	√	√
30	60	√	√	×	√	√	×	√	√	×	√	√	×

5.4 Test Results

The results from the wheel tracking test were processed. Firstly, the number of wheel cycles for crack propagation to the top of the SAMI was recorded for specimens with SAMIs. Also, the number of wheel cycles for crack propagation to failure (crack appearing at the top of the overlay) was recorded for specimens with SAMIs (test specimens) and without SAMIs (control specimens). The number of wheel cycles to failure as a ratio of control was obtained by dividing the number of wheel cycles to failure for the test specimens by the number of

wheel cycles to failure for the control specimens. This allows the comparison of the test specimens and the control specimens.

The vertical displacements of the specimens during test were obtained with linear variable differential transformers (LVDTs). The calibrated LVDT readings from the two measurement points on the specimens were logged in volts during tests. The readings were converted from volts to millimetres. The average of the readings for each LVDT was determined over 20 wheel cycles. The calculated average from the LVDT over 20 cycles was subtracted from each reading over the same cycles. The difference of the values was determined and the relative displacement was obtained as the average of the difference between the maximum and minimum relative displacements. The absolute displacement was determined as the point where the relative displacement equals zero, that is, when the load is at the centre of the beam directly above the crack. A typical LVDTs analysis is shown in Figure 5.6. As seen in Figure 5.6, there is relative movement of the split base as the moving wheel is offset from the crack, while the relative movement is zero when the moving wheel is directly over the crack.

The readings from the strain gauges placed at 4 mm above the crack top and at 20 mm from the bottom of the overlay for test specimens and at equivalent points for control specimens were logged. These were used to determine the initial strain under loading responsible for crack initiation. The value was calculated from readings logged in the first cycle. The average of the two trough readings (when the wheel load was at the edge of the beam) was subtracted from the average of the crest readings (when the wheel was at the centre) as shown in Figure 5.7. Two replicates were tested in each case and the results presented are the average of the readings.

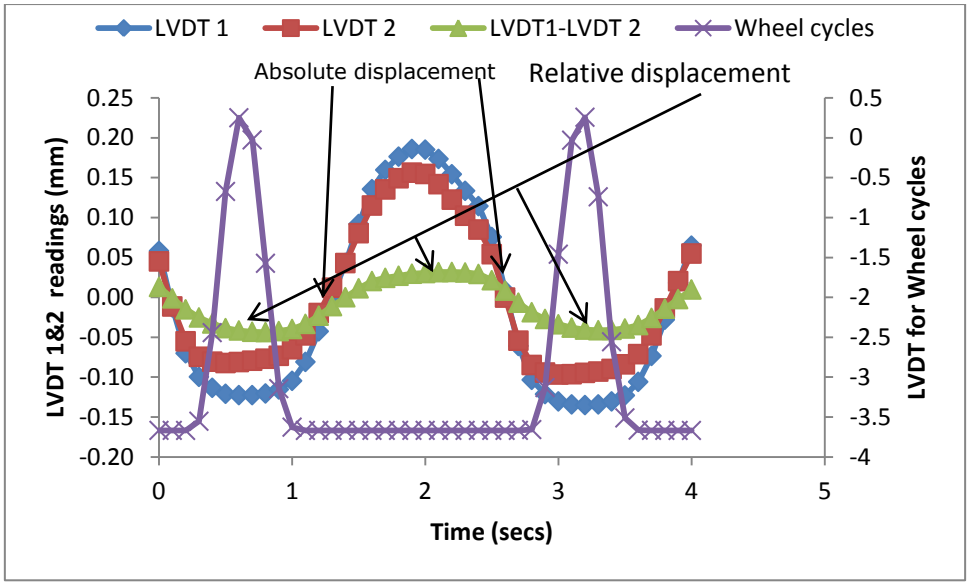

Figure 5.6: A typical LVDTs analysis

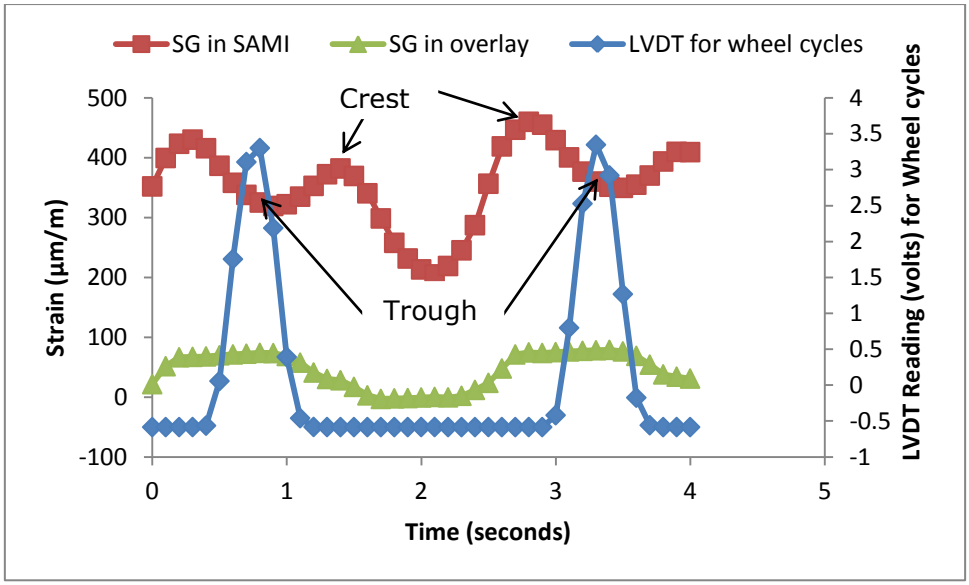

Figure 5.7: A typical strain readings analysis

5.4.1 Number of wheel cycles

The specimen names and references used for the presentation of results are shown in Table 5.7. The results for the number of wheel cycles to the top of the SAMI and the overlay (failure) at 10°C, 20°C and 30°C with 2.4 kN (1.1MPa) load applied are shown in Tables 5.8,

5.9 and 5.10 respectively. Table 5.11 shows the same results at 30^{o}C with 1.35 kN (0.6MPa) load applied.

Figure 5.8 shows that the SAMIs except Proprietary SAMI C and D were not able to retard reflective cracking with 2.4 kN (1.1 MPa) load applied at 10^{o}C, while 30 mm thick Proprietary SAMI A with 40 mm overlay matched the life of the control specimen. The inability of the SAMIs to retard reflective cracking at 10^{o}C is probably due to the high stiffness of the SAMIs (see Table 5.5), which restricts the SAMIs' flexibility and therefore hinders their ability to absorb strain concentration around the crack top. Also, the strong adhesion between the SAMIs and the overlay (see Figure 4.7) makes the beam act more like a unit, therefore it was not able to isolate the overlay from the strain concentration at the tip of the crack. In his study Debondt (1999) computed the tensile stresses at the bottom of an asphaltic overlay in relation to shear stiffness of the interface between overlay and the old surface. He observed that an optimum interface stiffness exists. Lower (too soft interlayer) and greater (too stiff) stiffnesses compared to the optimum lead to increased tensile stresses at the bottom of the overlay. This emphasizes the importance of the interface stiffness and the interlayer properties on their ability to retard reflective cracking.

Figure 5.9 indicates that when the test was carried out at a temperature of 20^{o}C under a 2.4 kN (1.1 MPa) load, the SAMIs except 30 mm thick sand asphalt with 40 mm overlay (SA30O40) and 20 mm thick sand asphalt with 60 mm overlay (SA20O60) have good resistance to reflective cracking. In general they have a life between 1.10 to 5.50 times that of the control specimens. For both SA30O40 and SA20O60, their ineffectiveness is thought to be due to the extreme low stiffness and thickness of the SAMI leading to more bending of the overlay. As explained earlier, very low stiffness of the SAMIs leads to increased tensile stresses. The optimum interface stiffness between the overlay and SAMIs seems to be achieved at 20^{o}C. It can be seen in Figure 5.10 that at 30^{o}C with a load of 2.4 kN (1.1MPa),

all the specimens with SAMIs outperformed those without, except the test specimens with sand asphalt as SAMI. The results as presented in Figure 5.11 show that at 30^{o}C and under a reduced load of 1.35 kN (0.6MPa), all the specimens with SAMIs outperformed those without, except for the 20 mm thick sand asphalt with 40 mm overlay (SA20O40) with a life 0.95 times the control and 30 mm thick sand asphalt with 40 mm overlay (SA30O40) with a life 0.93 times of control. The low stiffness of the SAMI at 30^{o}C allows the deformation of this layer vertically and horizontally in response to the shear and tensile stresses generated by the wheel load. Also, this is aided by the slip between the overlay and the SAMI as a result of the low shear strength/stiffness of the interface (see Figures 4.9 and 4.10). It was found that the specimens were susceptible to permanent deformation at 30^{o}C, especially the specimens with 40 mm overlay.

In general, it was found from the test that the SAMIs except the sand asphalt provide some gains in terms of life of the overlay compared to the control specimens. At 10^{o}C with the samples having high interface strength/stiffness and the SAMI stiffness very high, the SAMIs were ineffective, while at 20^{o}C and 30^{o}C with lower adhesion between the overlay and SAMI and lower SAMI stiffness, they were able to retard reflective cracking. This indicates that the stiffness of the overlay and SAMI interface and the SAMI stiffness have great effect on the performance of the SAMI. Again, it shows that the stiffness of the SAMI or its flexibility has an effect on the performance of the SAMIs against reflective cracking.

Table 5.7: Specimen names and references

Specimen name	Specimen reference
47 mm Overlay (Control)	O47
Proprietary SAMI C with 40 mm Overlay	PCO40
Proprietary SAMI D with 40 mm Overlay	PDO40
60 mm Overlay (Control)	O60
20 mm thick sand asphalt with 40 mm overlay	SA20O40
20 mm thick Proprietary SAMI A with 40 mm overlay	PA20O40
20 mm thick Proprietary SAMI B with 40 mm overlay	PB20O40
Proprietary SAMI C with 60 mm Overlay	PCO60
Proprietary SAMI D with 60 mm Overlay	PDO60
70 mm Overlay (Control)	O70
30 mm thick sand asphalt with 40 mm overlay	SA30O40
30 mm thick Proprietary SAMI A with 40 mm overlay	PA30O40
30 mm thick Proprietary SAMI B with 40 mm overlay	PB30O40
10 mm thick sand asphalt with 60 mm overlay	SA10O60
10 mm thick Proprietary SAMI A with 60 mm overlay	PA10O60
10 mm thick Proprietary SAMI B with 60 mm overlay	PB10O60
80 mm Overlay (Control)	O80
20 mm thick sand asphalt with 60 mm overlay	SA20O60
20 mm thick Proprietary SAMI A with 60 mm overlay	PA20O60
20 mm thick Proprietary SAMI B with 60 mm overlay	PB20O60

Table 5.8: Number of wheel cycles at 10^{o}C with 2.4 kN (1.1MPa) load applied

Specimen reference	Cycles to crack at top of SAMI	Cycles to failure	Cycles to failure as ratio of control
O47	-	223	1
PCO40	1606	2970	13.32
PDO40	715	1431	6.41
O60	-	5557	1
SA20O40	994	1569	0.28
PA20O40	1612	2349	0.42
PB20O40	1002	1862	0.34
PCO60	5051	6723	1.21
PDO60	3501	4537	0.82
O70	-	14503	1
SA30O40	6890	9223	0.64
PA30O40	10526	15192	1.05
PB30O40	6334	9970	0.69
SA10O60	3448	5915	0.41
PA10O60	4302	9350	0.64
PB10O60	2709	5003	0.34
O80	-	110038	1
SA20O60	11944	16293	0.15
PA20O60	22480	27425	0.25
PB20O60	9191	12718	0.12

Table 5.9: Number of wheel cycles at 20°C with 2.4 kN (1.1MPa) load applied

Specimen reference	Cycles to crack at top of SAMI	Cycles to failure	Cycles to failure as ratio of control
O47	-	68	1
PCO40	139	294	4.32
PDO40	128	257	3.78
O60	-	404	1
SA20O40	560	698	1.73
PA20O40	1051	1871	4.64
PB20O40	727	906	2.25
PCO60	1443	2221	5.50
PDO60	847	1472	3.65
O70	-	2421	1
SA30O40	478	924	0.38
PA30O40	2625	4486	1.85
PB30O40	2464	4548	1.88
SA10O60	2245	3304	1.36
PA10O60	1992	3362	1.39
PB10O60	1899	3446	1.42
O80	-	5645	1
SA20O60	2559	3062	0.54
PA20O60	5495	6396	1.13
PB20O60	5102	6224	1.10

Table 5.10: Number of wheel cycles at 30°C with 2.4 kN (1.1MPa) load applied

Specimen reference	Cycles to crack at top of SAMI	Cycles to failure	Cycles to failure as ratio of control
O47	-	50	1
PCO40	84	132	2.63
PDO40	68	117	2.34
O60	-	132	-
SA20O40	47	132	1
PA20O40	97	296	2.24
PB20O40	125	349	2.64
PCO60	176	340	2.58
PDO60	153	263	1.99
O70	-	693	1
SA30O40	81	147	0.21
PA30O40	324	548	0.79
PB30O40	747	1052	1.52
SA10O60	40	136	0.20
PA10O60	313	777	1.12
PB10O60	316	817	1.18
O80	-	851	-
SA20O60	243	491	0.58
PA20O60	563	1209	1.42
PB20O60	381	660	0.77

Table 5.11: Number of wheel cycles at 30°C with 1.35 kN (0.6MPa) load applied

Specimen reference	Cycles to crack at top of SAMI	Cycles to failure	Cycles to failure as ratio of control
O47	-	126	1
PCO40	282	507	4.02
PDO40	256	514	4.08
O60	-	736	1
SA20O40	322	699	0.95
PA20O40	2011	2968	4.03
PB20O40	764	1162	1.58
PCO60	583	953	1.29
PDO60	298	681	0.93
O70	-	1311	-
SA30O40	767	1214	0.93
PA30O40	1041	2543	1.94
PB30O40	1852	2983	2.28
SA10O60	1618	3136	2.39
PA10O60	2665	4241	3.24
PB10O60	2374	4309	3.29
O80	-	1621	1
SA20O60	943	1821	1.12
PA20O60	3918	5074	3.13
PB20O60	1749	2832	1.75

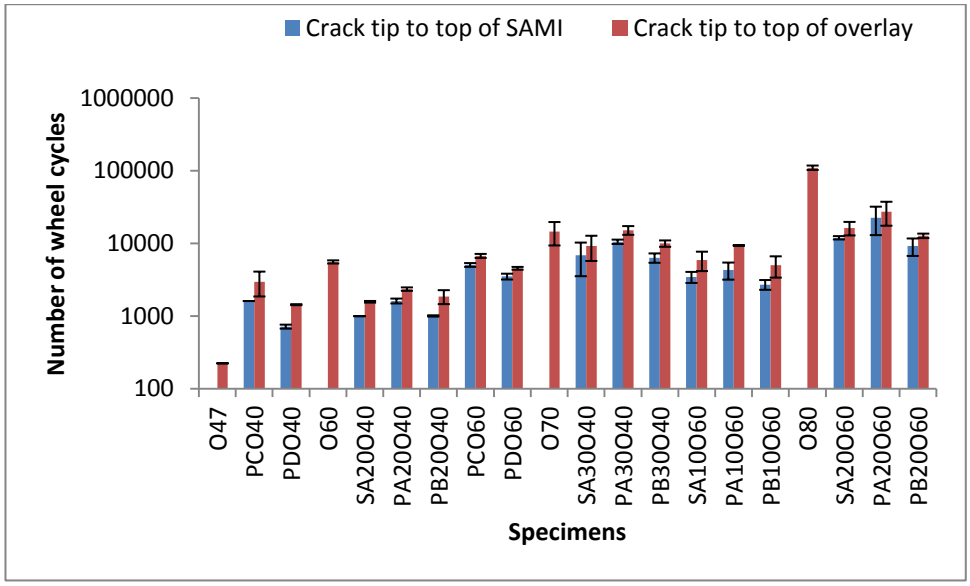

Figure 5.8: Number of wheel cycles to the top of SAMI and overlay at 10°C with 2.4kN load applied

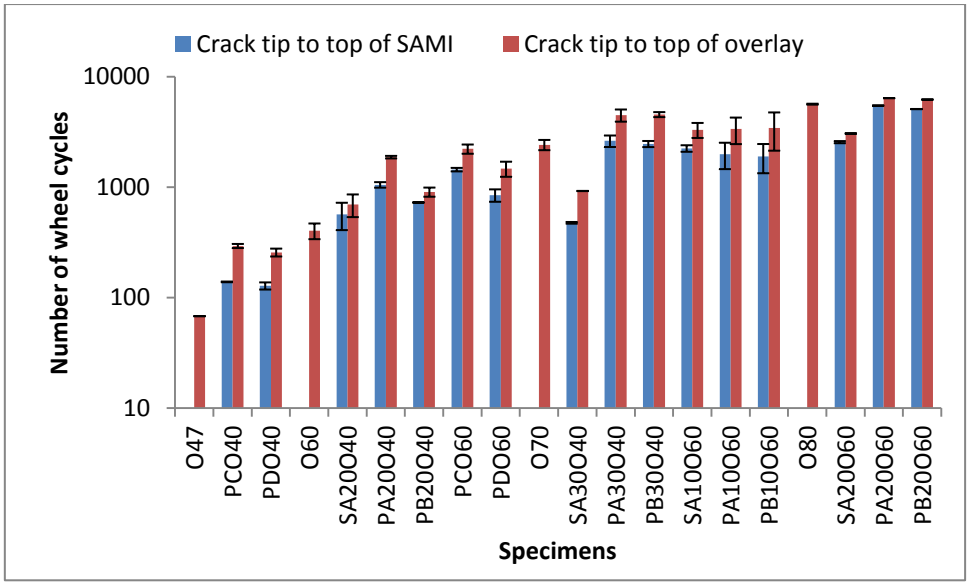

Figure 5.9: Number of wheel cycles to the top of SAMI and overlay at 20°C with 2.4kN load applied

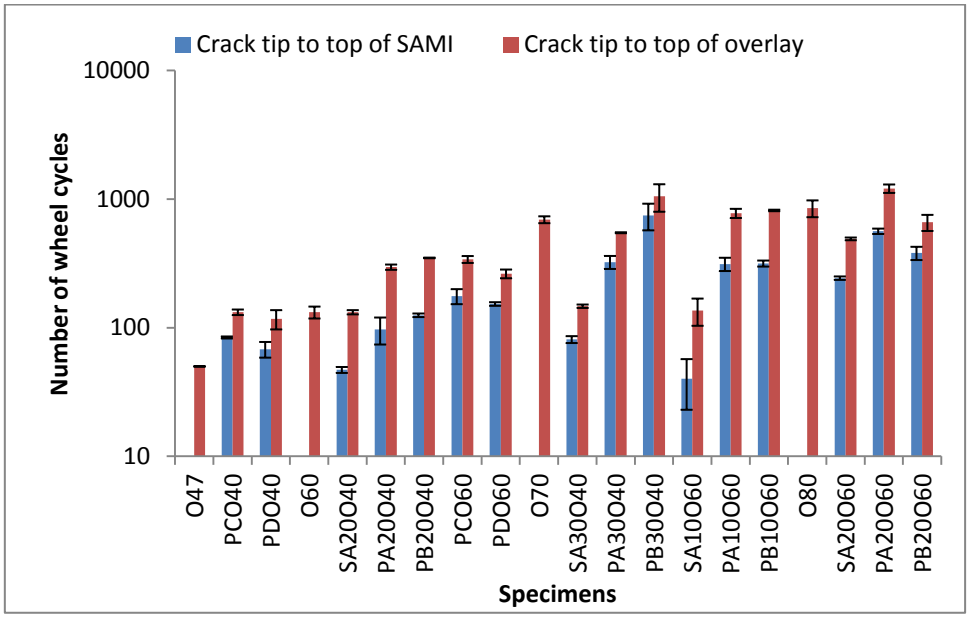

Figure 5.10: Number of wheel cycles to the top of SAMI and overlay at 30°C with 2.4kN load applied

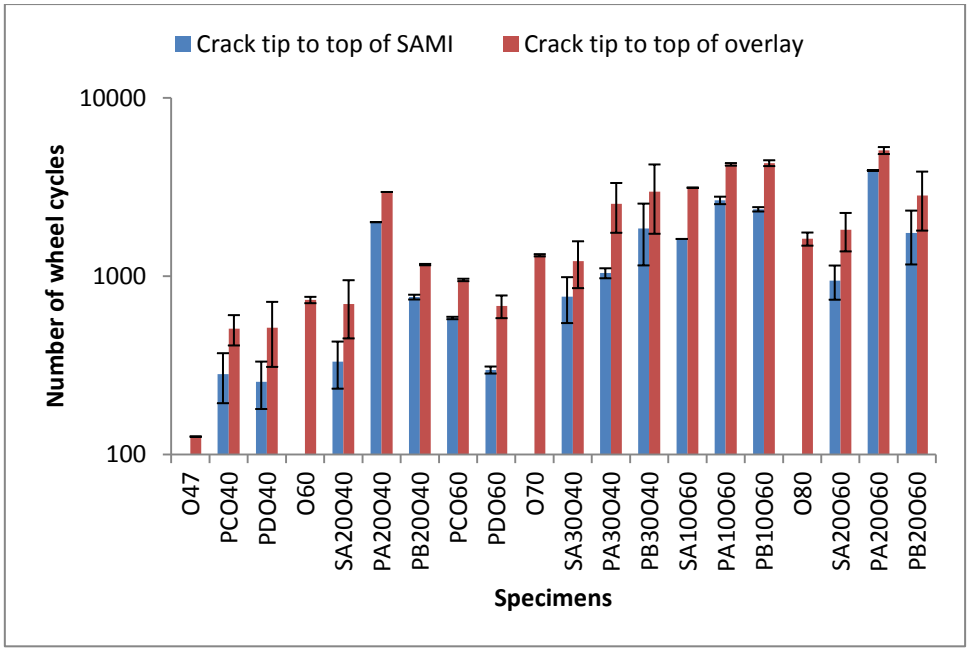

Figure 5.11: Number of wheel cycles to the top of SAMI and overlay at 30°C with 1.35kN load applied

5.4.2 Effect of SAMI thickness

In the study, the effect of the thickness of SAMIs against reflective cracking was investigated using SAMIs (sand asphalt, proprietary SAMIs A and B) of thicknesses 10 mm, 20mm and 30 mm. The results of two different SAMI thicknesses with the same overlay thickness were normalized against their respective control specimens and compared. The specimen references are shown in Table 5.12. Only the results of the tests carried out at 20°C and 30°C were considered because as explained in section 5.4.1, the SAMIs were found to be ineffective against crack propagation at 10°C.

At 20°C and 2.4 kN (1.1MPa) load as shown in Figures 5.12 and 5.13 the SAMIs' (sand asphalt, proprietary SAMIs A and B) resistance against reflective cracking was more pronounced when the thicknesses were 20 mm than 30 mm with 40 mm overlay, and at 10 mm than 20 mm with both having 60 mm overlay, respectively. This indicates that using a lower SAMI thickness provided a better resistance against reflective cracking. This is

probably because of the low stiffness of the SAMIs, so increasing the SAMI thickness tends to increase the flexure of the overlay causing rapid propagation of crack.

Figures 5.14 and 5.15 show that at 30^{o}C and 2.4 kN (1.1MPa) load, the results were mixed with the SAMIs being more effective when a thickness of 20mm was used than 30 mm with both having 40 mm overlay (Figure 5.12), while 20mm thick SAMIs were more effective than 10 mm with both having 60 mm overlay, except in the case of proprietary SAMI B. The reason for the mixed result is probably due to the combined action of high load magnitude and temperature. As shown in Figures 5.16 and 5.17, the test carried out at 30^{o}C under a reduced load of 1.35kN (0.6MPa) to remove the effect of high load showed that the SAMIs were more effective when lower thickness was used. Elseifi (2003) observed in his study that the use of a soft interlayer against reflective cracking results in more vertical and horizontal deformations. In the same vein, the finding was in line with that of Molenaar et al (1986), who identified important factors that affect SAMI performance including stiffness of the SAMI, which is affected by its modulus and thickness.

Table 5.12: Specimen names and references

Specimen name	**Specimen reference**
Sand asphalt with 40 mm overlay	SAO40
Proprietary SAMI A with 40 mm overlay	PAO40
Proprietary SAMI B with 40 mm overlay	PB040
Sand asphalt with 60 mm overlay	SAO60
Proprietary SAMI A with 60 mm overlay	PAO60
Proprietary SAMI B with 60 mm overlay	PBO60

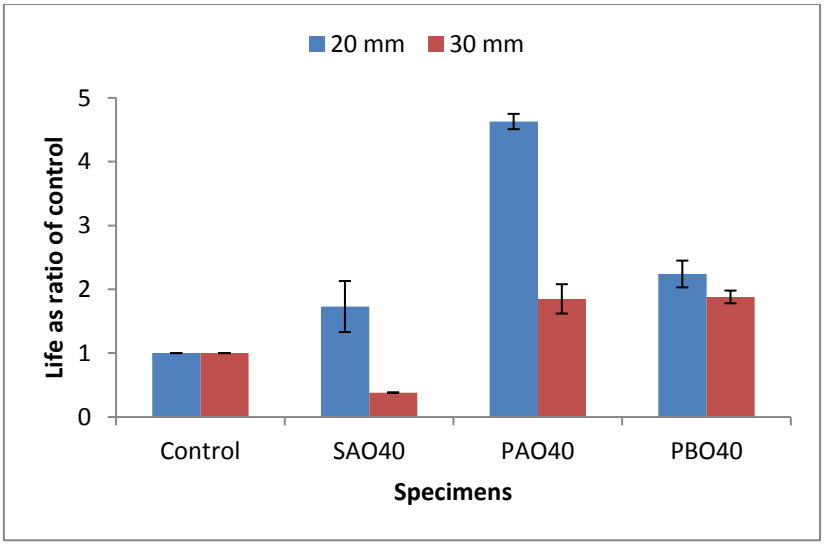

Figure 5.12: Number of wheel cycles to failure as ratio of control with 20 mm and 30 mm SAMIs and 40 mm overlay at 20°C and 2.4kN (1.1MPa)

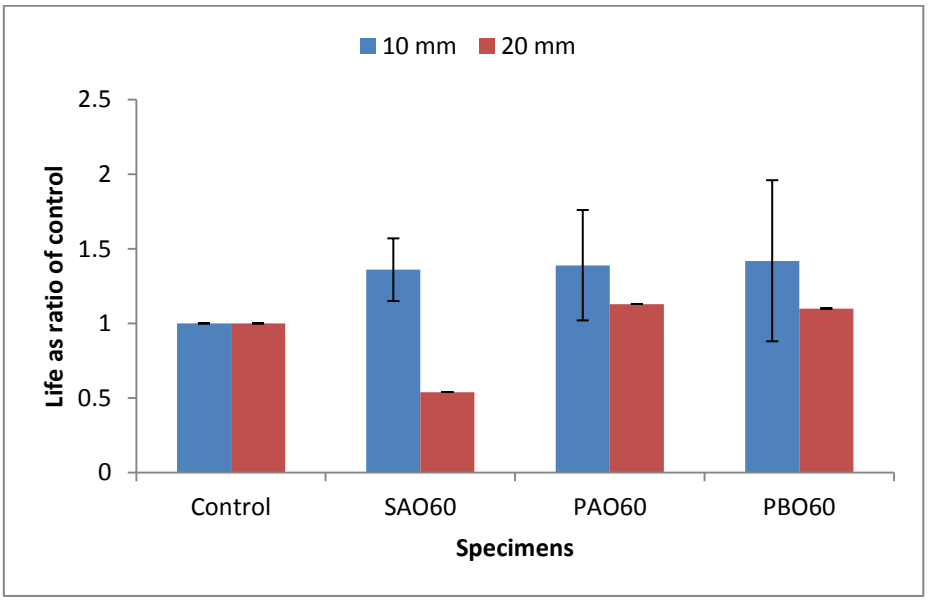

Figure 5.13: Number of wheel cycles to failure as ratio of control with 10 mm and 20 mm SAMIs and 60 mm overlay at 20°C and 2.4kN (1.1MPa)

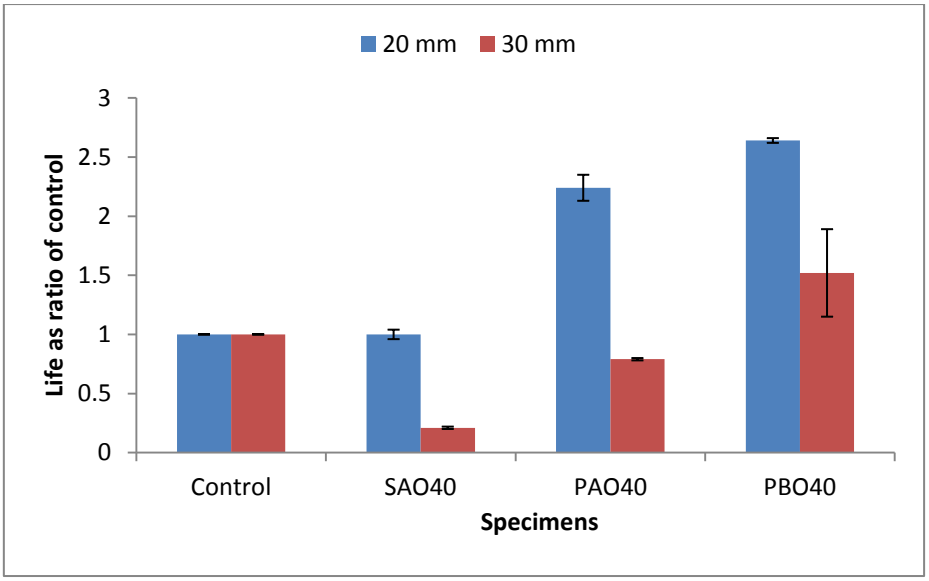

Figure 5.14: Number of wheel cycles to failure as ratio of control with 20 mm and 30 mm SAMIs and 40 mm overlay at 30°C and 2.4kN (1.1MPa)

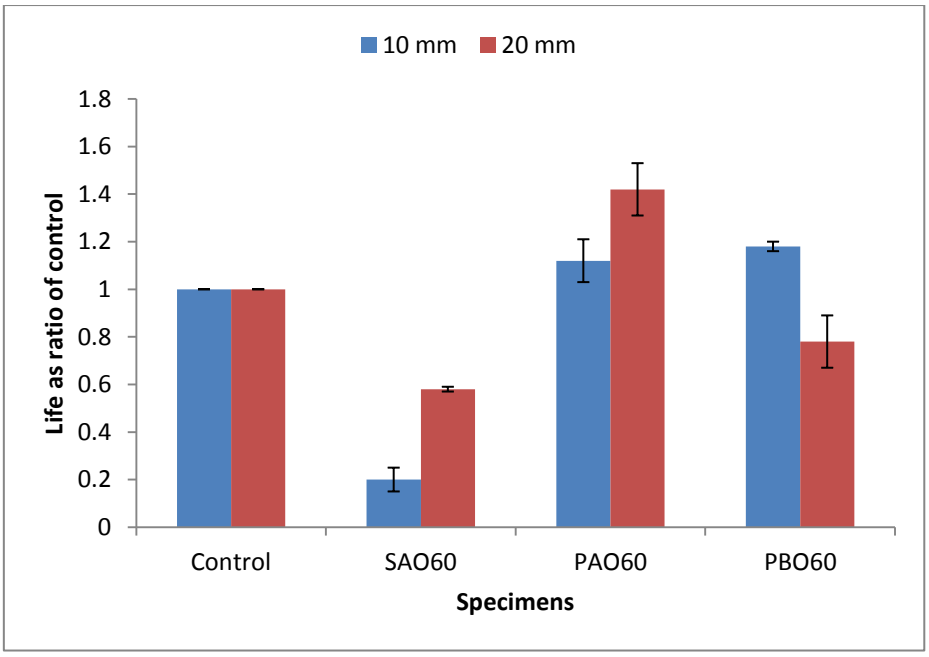

Figure 5.15: Number of wheel cycles to failure as ratio of control with 10 mm and 20 mm SAMIs and 60 mm overlay at 30°C and 2.4kN (1.1MPa)

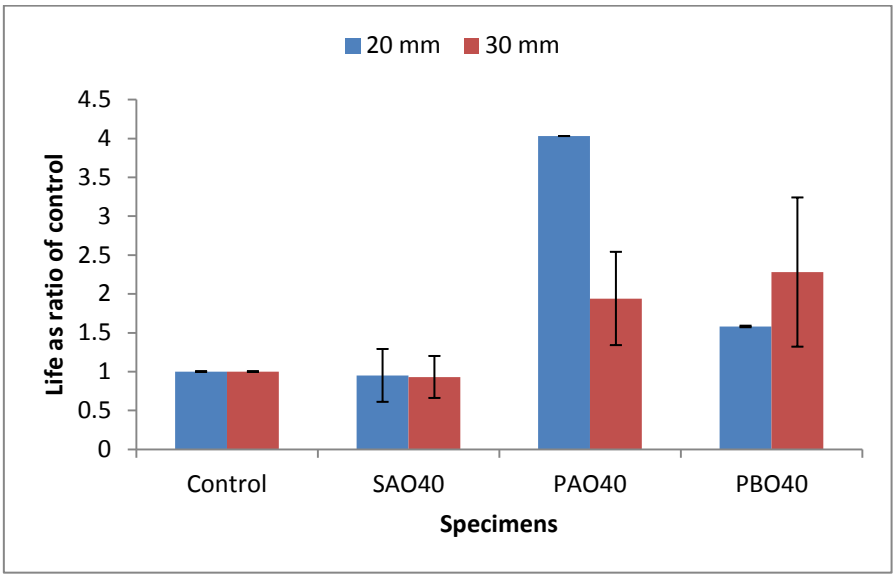

Figure 5.16: Number of wheel cycles to failure as ratio of control with 20 mm and 30 mm SAMIs and 40 mm overlay at 30°C and 1.35kN (0.6MPa)

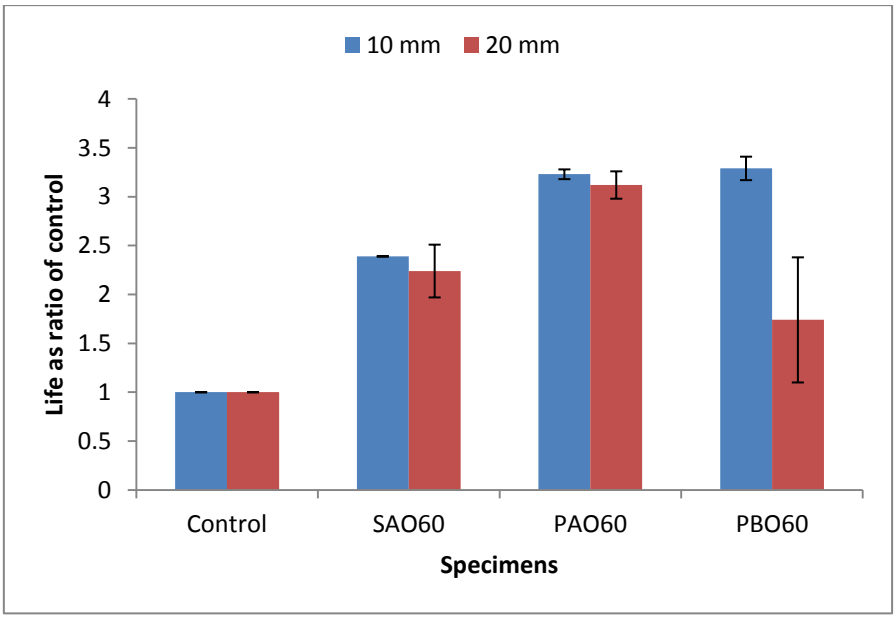

Figure 5.17: Number of wheel cycles to failure as ratio of control with 10 mm and 20 mm SAMIs and 60 mm overlay at 30°C and 1.35kN (0.6MPa)

5.4.3 Effect of load levels

The effect of load levels on the resistance of SAMIs against reflective cracking was investigated using two load levels 2.4kN (1.1MPa) and 1.35kN (0.6MPa) at 30°C. The former

is representative of tyre pressures on airfields and the latter representative of tyre pressures on highways. The numbers of wheel cycles to failure for the test specimens were normalized using their respective control specimens. The results as shown in Figure 5.18 indicate that the resistance of the SAMIs against reflective cracking was more pronounced in specimens tested under a load of 1.35kN (0.6MPa) than 2.4kN (1.1MPa).

This happens probably because the traffic loads on an overlay over a cracked pavement generate the critical stress concentration at the tip of the crack. As the load on the overlay increases, the stress concentration increases due to the low stiffness of the SAMI causing rapid propagation of the crack. Figure 5.18 shows that the SAMIs are more suited for highways than airfield pavements because of the low SAMI stiffness. For airfield pavements with higher load magnitude, a reinforcing interlayer (not investigated in this study) which allows the overlay to support larger bending of the pavement for a given asphalt strength may be more suitable.

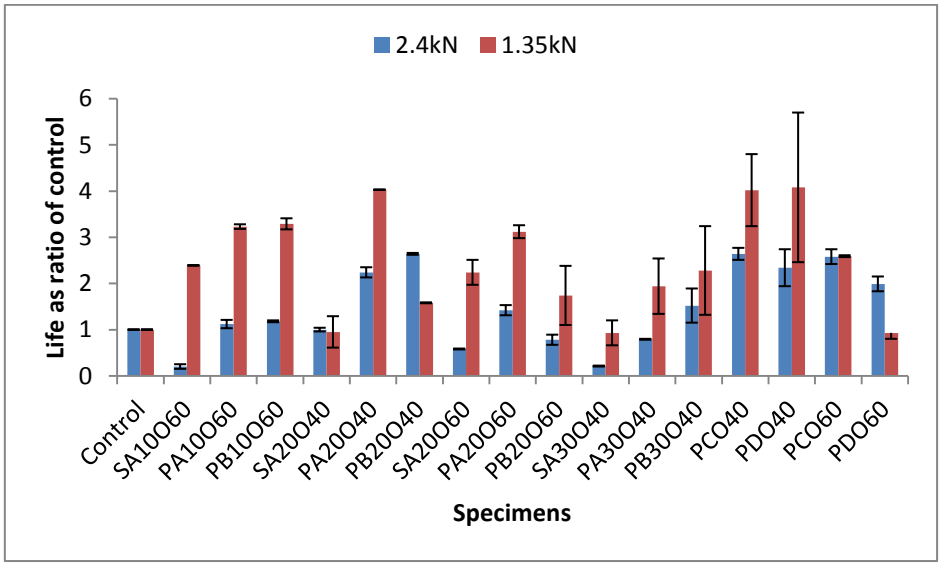

Figure 5.18: The number of wheel cycles to failure as ratio of control with 2.4kN and 1.35kN loads applied at 30°C

5.4.4 Effect of temperature

One of the factors that affect the rate of crack propagation is the environmental condition. Temperature is one of the environmental conditions that play a part in crack propagation. In this study, the influence of temperature on resistance of SAMIs against reflective cracking was investigated by carrying out tests at three different temperatures (10^{o}C, 20^{o}C and 30^{o}C) with a 2.4kN (1.1MPa) load applied. The results presented in Figures 5.19 show that although the SAMIs were ineffective at 10^{o}C, the life of the test specimens decreased as temperature increases. This is possibly because of the effect of temperature on overlay and SAMI stiffnesses and the interface stiffness. As shown in Table 5.5, the stiffness of the overlay and SAMIs increases with decreasing temperature.

In order to further understand the effect of temperature on the performance of SAMIs, the number of cycles to failure of the test specimens at 20^{o}C and 30^{o}C were normalized by their respective control specimens (see Figure 5.20). It can be seen from the graph that the SAMIs performed better at 20^{o}C, except for proprietary SAMIs C and D that were produced with bitumen emulsion. Although in this case, the SAMIs performed worse at 30^{o}C than 20^{o}C, probably because at 30^{o}C the overlay becomes susceptible to permanent deformation. Barksdale (1991) noted that as the interlayer becomes softer, and its shear strength lowers, it becomes more effective in delaying reflective cracking. For the specimens with proprietary SAMI C, the crack resistance increases with decreasing temperature, while proprietary SAMI D was more effective at 20^{o}C. This was the case probably because the bitumen emulsion used in proprietary SAMI C was more viscous than the one used in proprietary SAMI D, therefore allowing its flexibility to be mobilized at lower temperature.

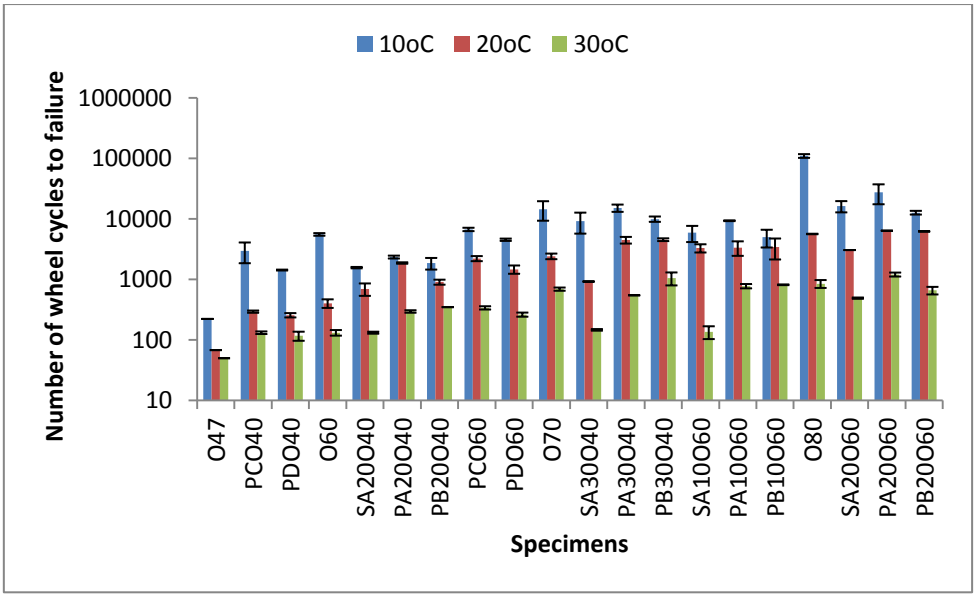

Figure 5.19: Number of wheel cycles to failure at 10°C, 20°C and 30°C under a load of 2.4kN (1.1MPa)

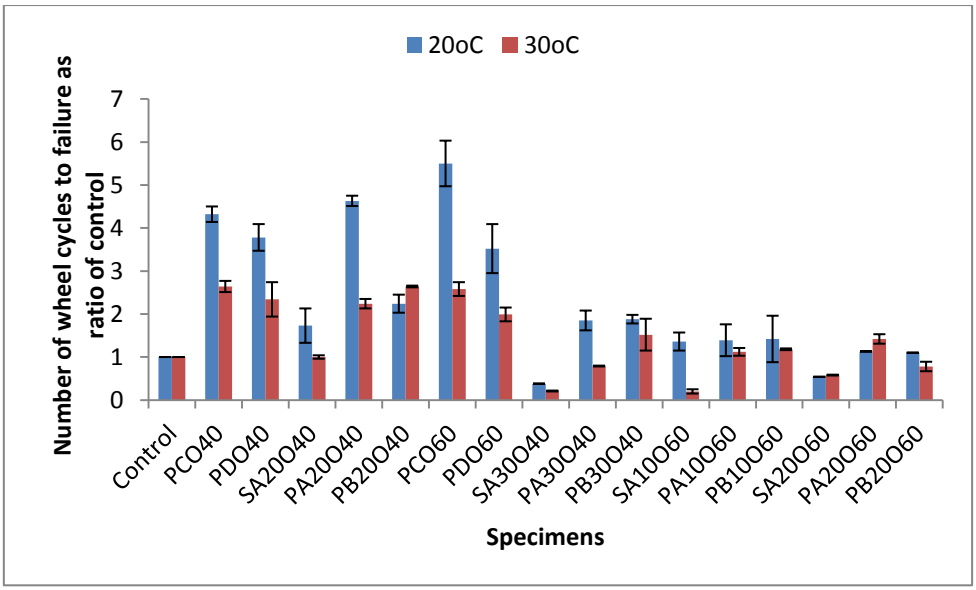

Figure 5.20: The number of wheel cycles to failure as ratio of control with 2.4kN load applied at 20°C and 30°C

5.4.5 Effect of overlay thickness

The thickness of the overlay is another factor considered in this study. The rule of thumb is that the thicker the overlay the more the life of the pavement. This is because an increase in overlay thickness results in less tensile stresses at the bottom of the overlay and when the

crack is initiated, it has to grow through more depth of the overlay before appearing at the surface. However life gained as a result of the increase in overlay depth may be small compared to the cost incurred, thus raising question about its cost effectiveness. Therefore, there is need to always use the most appropriate thickness that will be cost effective.

In this study to assess the influence of overlay thickness on performance of SAMIs, two different overlay thicknesses of 40 mm and 60 mm were used. To ensure the thickness of the SAMIs does not influence the results, SAMIs (sand asphalt, proprietary SAMIs A and B) with the same thickness of 20 mm and proprietary SAMIs C and D were compared. The results were normalized by dividing the number of cycles to failure of the test specimens by the number of wheel cycles to failure for control specimens of equivalent overall thickness. Therefore, for the test specimens with 20 mm SAMIs and 40 mm overlay, the control specimen thickness was 60 mm, while for the specimens with 20 mm SAMIs and 60 mm overlays, the control specimen thickness was 80 mm. The specimen references for presentation of the results are shown in Table 5.13.

The results shown in Figures 5.21 and 5.22 indicate that after normalizing with their respective control specimens, using 60 mm thick overlay on the 20 mm SAMIs was less effective than with a 40 mm thick overlay. Although Barksdale (1991) stated that a stress-relieving layer is not a substitute for the AC overlay's load-carrying capacity and that design thickness of the AC overlay should not be reduced even when a stress relieving layer is used in an attempt to delay reflective cracking, it was found in this study that an optimum overlay thickness at which the SAMI's incorporation in a cracked pavement gives good results and the best economical value exists. Molenaar et al (1986) found that when SAMIs are used against reflective cracking, a thin overlay would have a longer life than a thick overlay. The results of the test at 30^{o}C and 1.35 kN load (see Figure 5.23) shows that the 20 mm thick sand asphalt and proprietary SAMI B with 60 mm overlay were more effective than when the

overlay thickness is 40 mm. This reason for the mixed result in this case is probably because of high temperature and lower load magnitude, which results in deformation of the test specimens, a situation that is more pronounced in specimens with 40 mm overlay. Figures 5.24, 5.26 and 5.27 indicate that for proprietary SAMIs C and D, the use of 40 mm overlay was more effective than 60 mm overlay. However, in Figure 5.25 the reverse was the case, the test specimens with 60 mm overlay were more effective than the ones with 40 mm overlay.

Table 5.13: Specimen names and references

Specimen name	Specimen reference
20 mm thick Sand asphalt	SA20
20 mm thick proprietary SAMI A	PA20
20 mm thick proprietary SAMI B	PB20
Proprietary SAMI C	PC
Proprietary SAMI D	PD

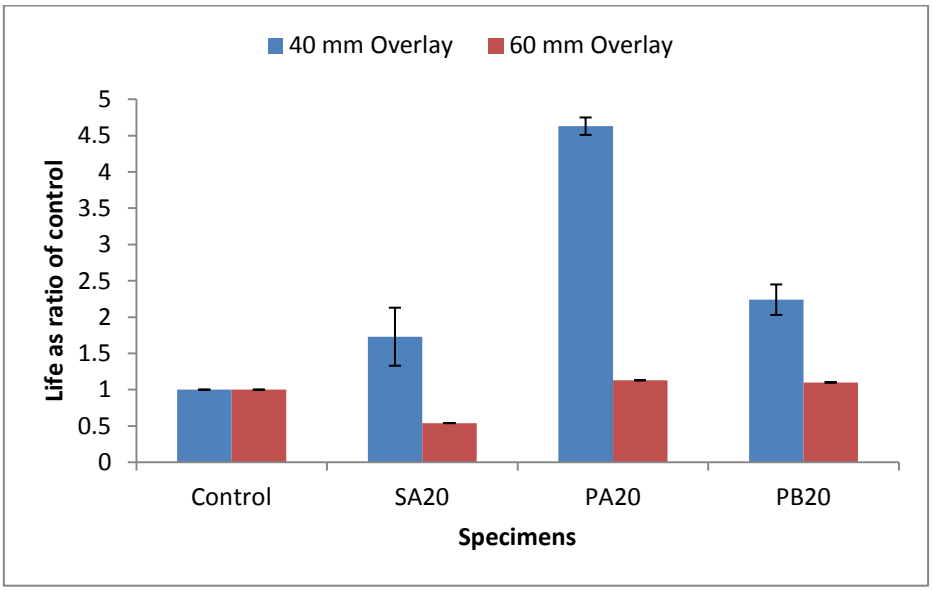

Figure 5.21: The number of wheel cycles to failure as ratio of control for specimens with 20mm SAMI and 40 mm and 60 mm overlay and 2.4kN load applied at 20°C

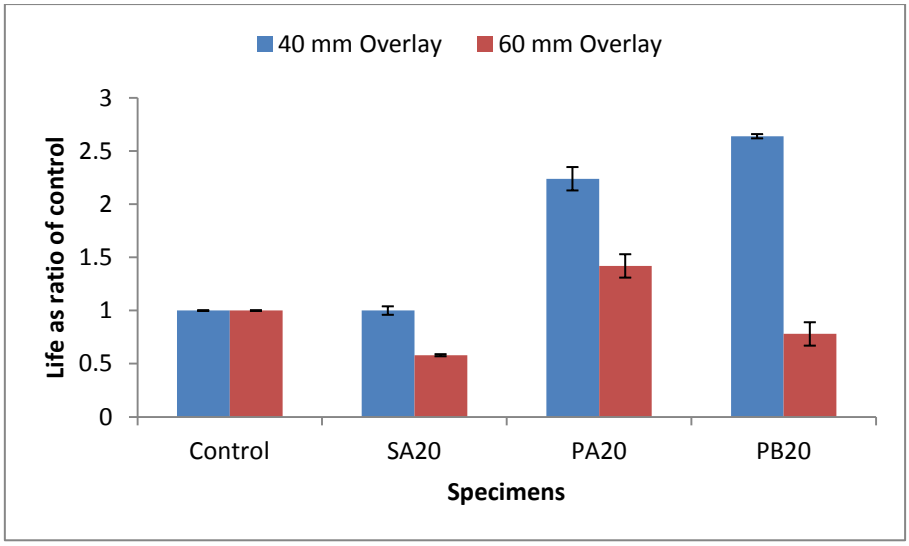

Figure 5.22: The number of wheel cycles to failure as ratio of control for specimens with 20mm SAMI and 40 mm and 60 mm overlay and 2.4kN load applied at 30°C

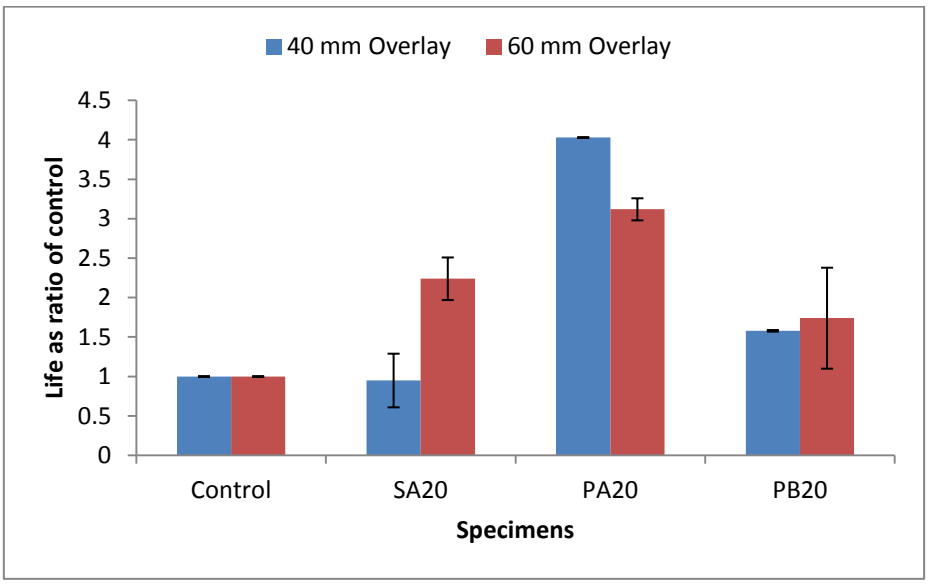

Figure 5.23: The number of wheel cycles to failure as ratio of control for specimens with 20mm SAMI and 40 mm and 60 mm overlay and 1.35kN load applied at 30°C

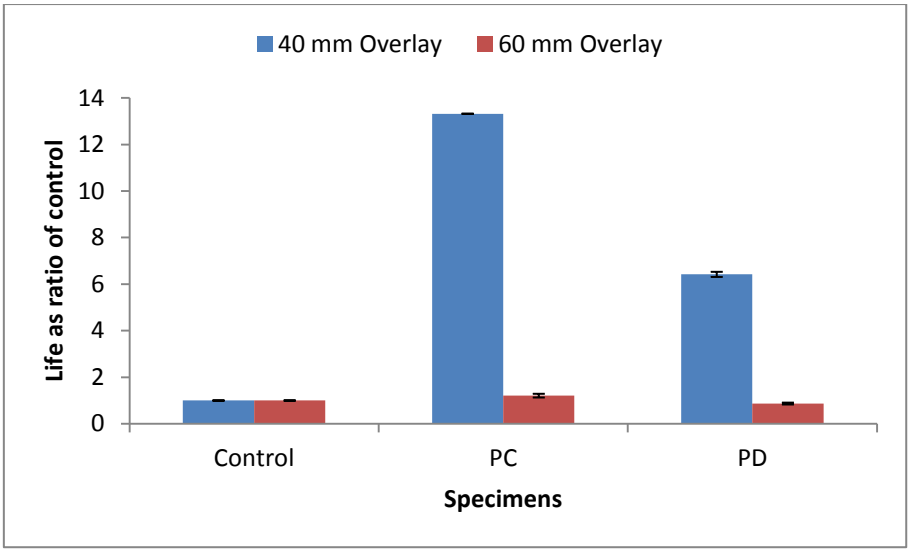

Figure 5.24: The number of wheel cycles to failure as ratio of control for specimens with SAMIs C and D and 40 mm and 60 mm overlay and 2.4kN load applied at 10°C

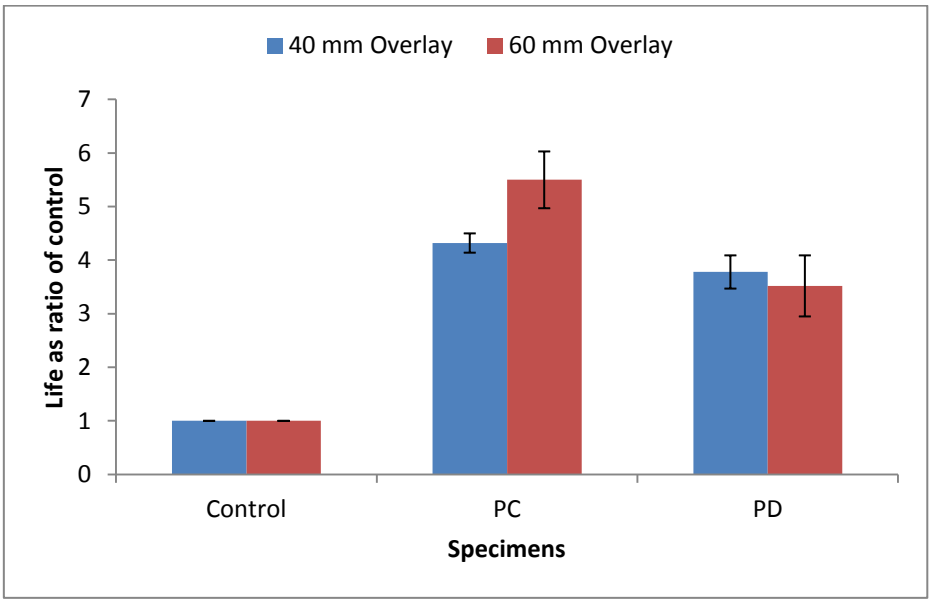

Figure 5.25: The number of wheel cycles to failure as ratio of control for specimens with SAMIs C and D and 40 mm and 60 mm overlay and 2.4kN load applied at 20°C

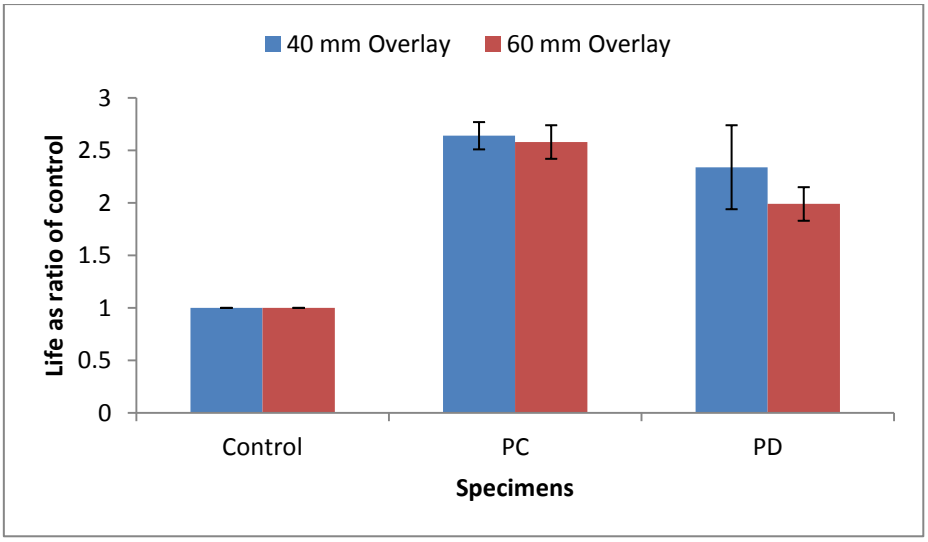

Figure 5.26: The number of wheel cycles to failure as ratio of control for specimens with SAMIs C and D and 40 mm and 60 mm overlay and 2.4kNload applied at 30°C

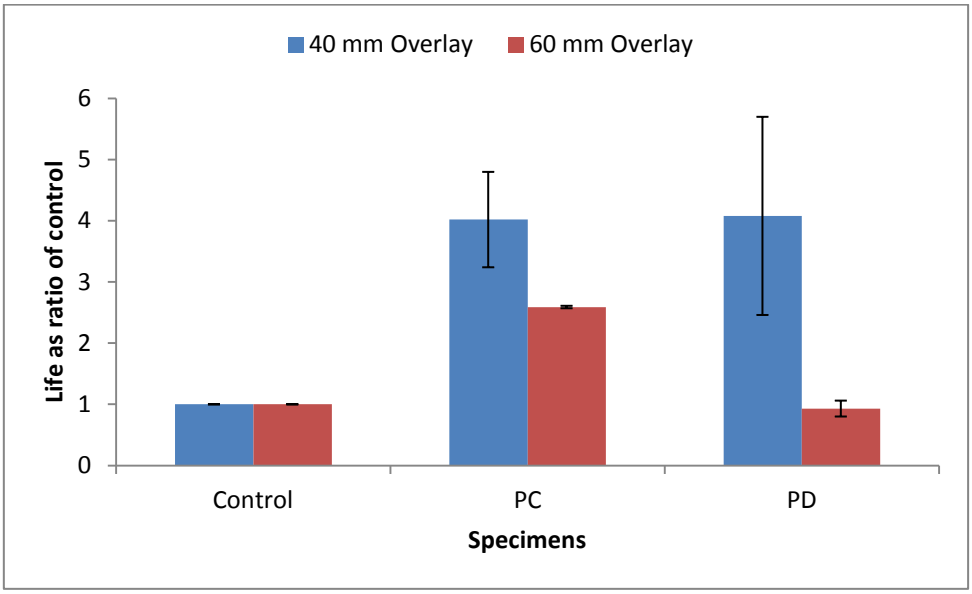

Figure 5.27: The number of wheel cycles to failure as ratio of control for specimens with SAMIs C and D and 40 mm and 60 mm overlay and 1.35kN load applied at 30°C

5.4.6 Displacement

As stated in section 5.4, the vertical movement of the sample during the test was measured using linear variable differential transformers (LVDTs). The results are presented here. Figures 5.28, 5.29, and 5.30 show the graphs of displacement versus number of wheel cycles at 10°C, 20°C and 30°C, respectively with 2.4kN load applied for proprietary SAMIs C and D

with 40 and 60 mm overlay and control (no SAMI) with 60 mm overlay, while Figure 5.31 was for a load of 1.35kN at 30^{o}C for the specimens with proprietary SAMIs C and D with 40 and 60 mm overlay and control (no SAMI) with 60 mm overlay. Figures 5.32, 5.33, and 5.34 show graphs of displacement versus number of wheel cycles at 10^{o}C, 20^{o}C and 30^{o}C, respectively with 2.4kN load applied for 20 mm thick SAMIs with 40 mm overlay and control (no SAMI) with 60 mm overlay, while Figure 5.35 was for the same specimens with a load of 1.35kN at 30^{o}C.

Also, Figures 5.36, 5.37, and 5.38 show the graphs of displacement versus number of wheel cycles at 10^{o}C, 20^{o}C and 30^{o}C, respectively with 2.4kN load applied for 30 mm thick SAMIs with 40 mm overlay and control (no SAMI) with 70 mm overlay, while Figure 5.39 was for the same specimens with a load of 1.35kN at 30^{o}C. The graphs of displacement versus number of wheel cycles at 10^{o}C, 20^{o}C and 30^{o}C with 2.4kN load applied were shown in Figures 5.40, 5.41 and 5.42, respectively for specimens having 10 mm thick SAMIs and 60 mm overlay and control (no SAMI) with 70 mm overlay, while Figure 5.43 was for the same specimens with a load of 1.35kN at 30^{o}C.

Figures 5.44, 5.45, and 5.46 are the graphs of displacement versus number of wheel cycles at 10^{o}C, 20^{o}C and 30^{o}C, respectively with 2.4kN load applied for 20 mm thick SAMIs with 60mm overlay and control (no SAMI) with 80 mm overlay, while Figure 5.47 was for a load of 1.35kN at 30^{o}C. The graphs show that the relative displacement of the split base increases as the test progresses due to crack propagation. It can be seen from the graphs that in most cases, the control specimens had lower displacement than the specimens with SAMIs. Although, Sanders (2001) stated that prediction of crack growth using deflection data would be difficult and inaccurate, the general trend in these graphs shows that the more the vertical movement of the test specimens the less the life. This will perhaps explain why most of the specimens with sand asphalt were not effective in retarding crack growth.

The initial absolute and relative displacements of the specimens are shown in Figures 5.48 and 5.49, respectively. Both graphs show that the vertical movement of the specimens increases with temperature. Also, although the low vertical movement of the specimens at 10^{o}C does imply increased life, the specimens with SAMIs except the ones with proprietary SAMIs C and D were ineffective at 10^{o}C. Furthermore, Figures 5.48 and 5.49 indicate that the control specimens have lower displacement than their equivalent test specimens with SAMIs. This means that introduction of soft interlayer materials in a pavement is accompanied by more vertical movement of the pavement structure. As observed by Debondt (1999), the larger flexural (bending) deformations/deflections caused by the introduction of interlayer materials do not necessarily imply that the tensile stress in the overlay increases.

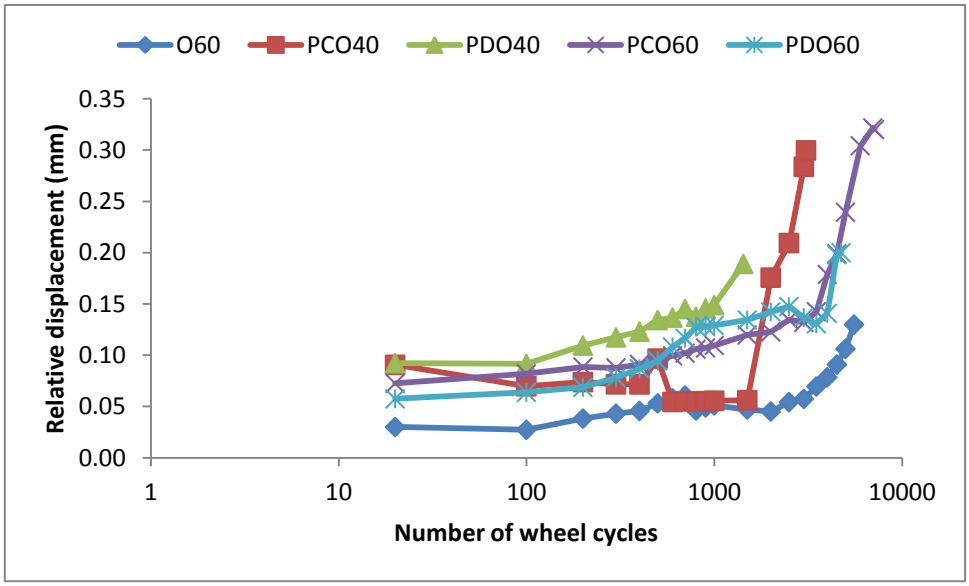

Figure 5.28: Displacement versus number of wheel cycles at 10^{o}C with 2.4kN (1.1MPa) load applied for specimens with proprietary SAMIs C and D

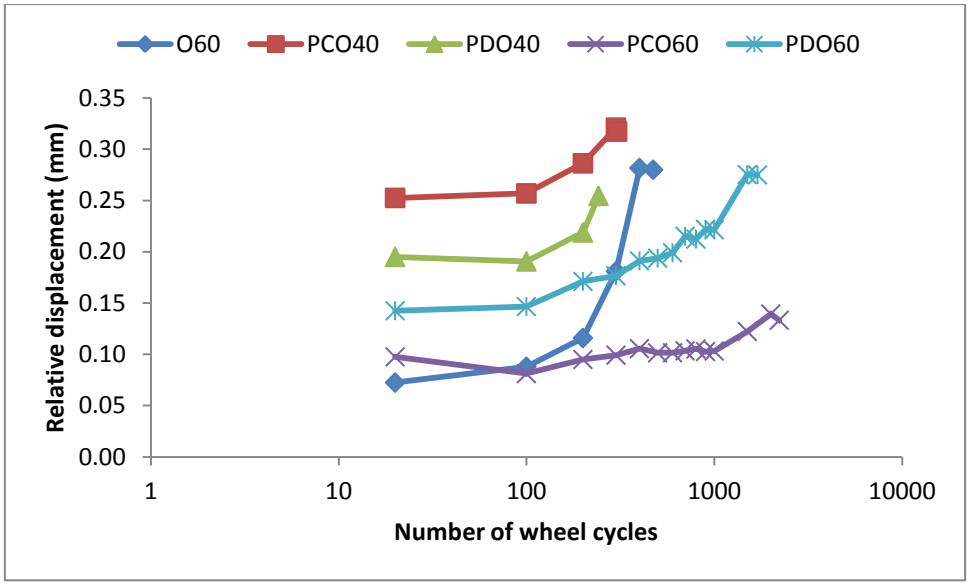

Figure 5.29: Displacement versus number of wheel cycles at 20°C with 2.4kN (1.1MPa) load applied for specimens with proprietary SAMIs C and D

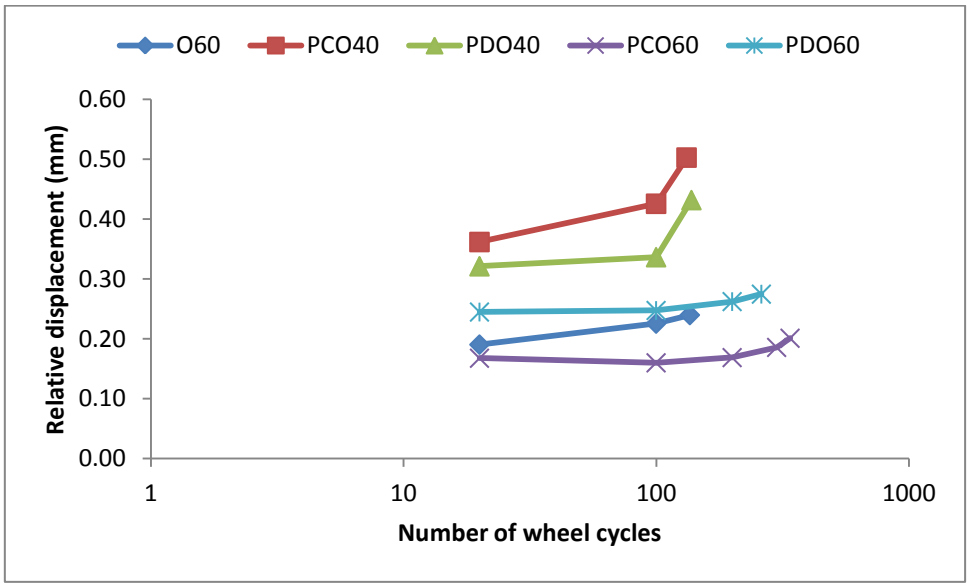

Figure 5.30: Displacement versus number of wheel cycles at 30°C with 2.4kN (1.1MPa) load applied for specimens with proprietary SAMIs C and D

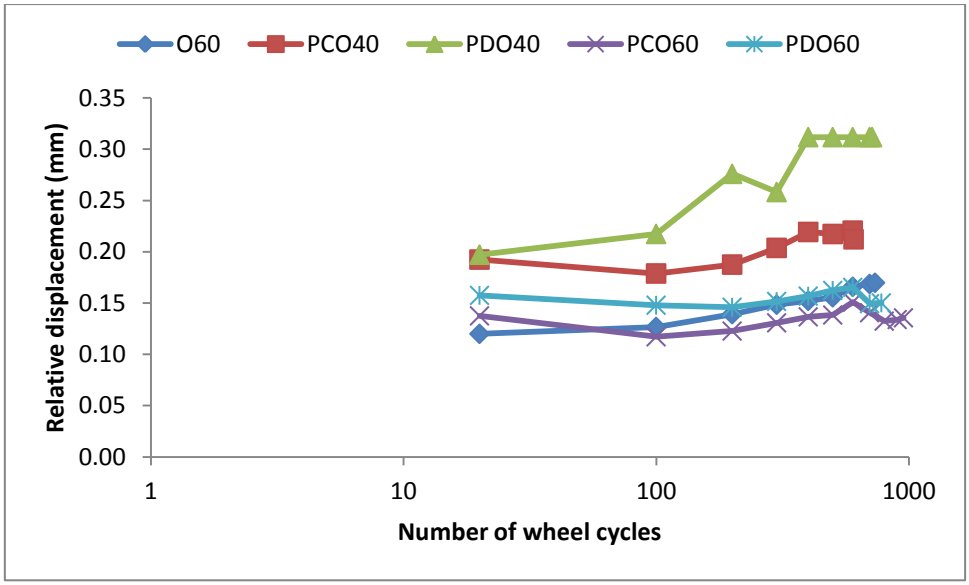

Figure 5.31: Displacement versus number of wheel cycles at 30°C with 1.35kN (0.6MPa) load applied for specimens with proprietary SAMIs C and D

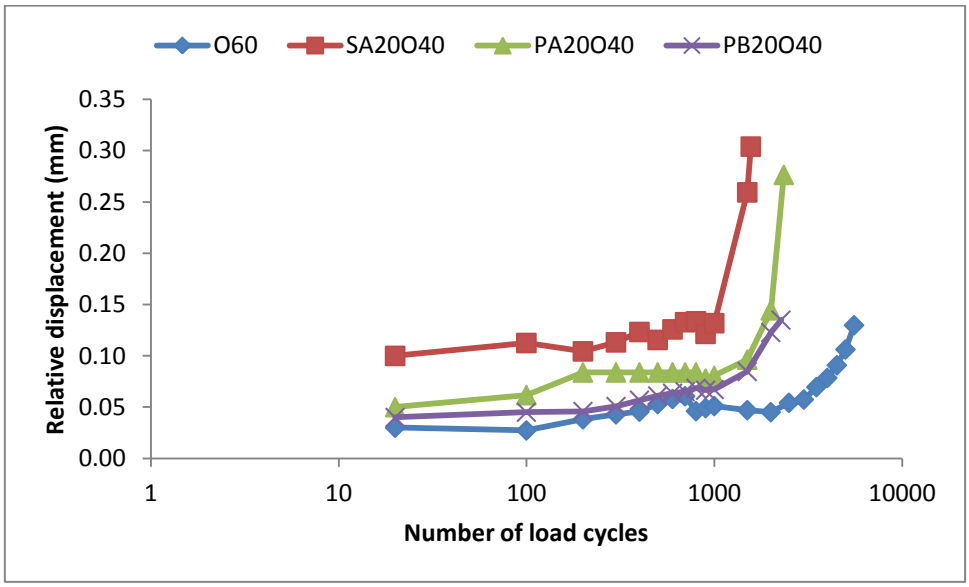

Figure 5.32: Displacement versus number of wheel cycles at 10°C with 2.4kN (1.1MPa) load applied for specimens with 20 mm SAMI and 40 mm overlay

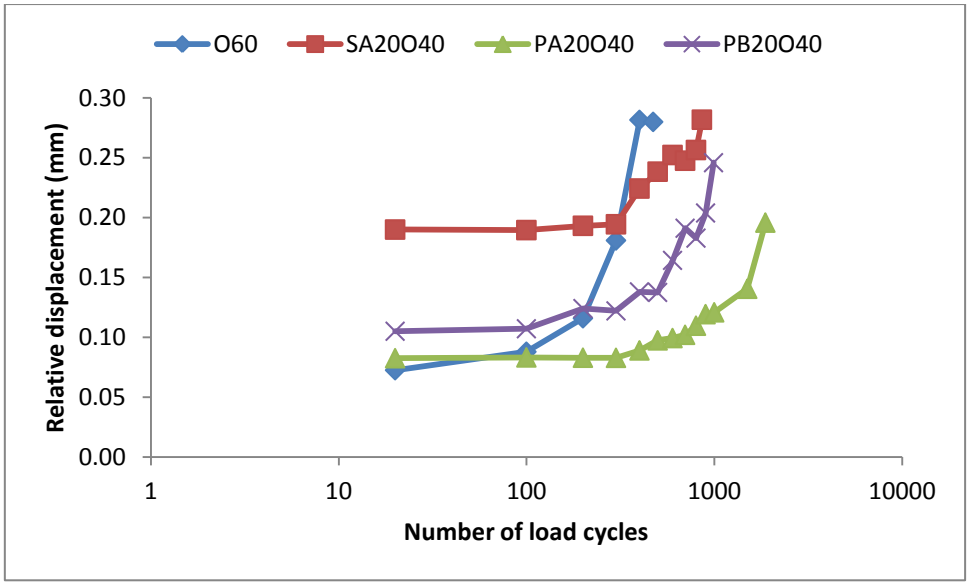

Figure 5.33: Displacement versus number of wheel cycles at 20°C with 2.4kN (1.1MPa) load applied for specimens with 20 mm SAMI and 40 mm overlay

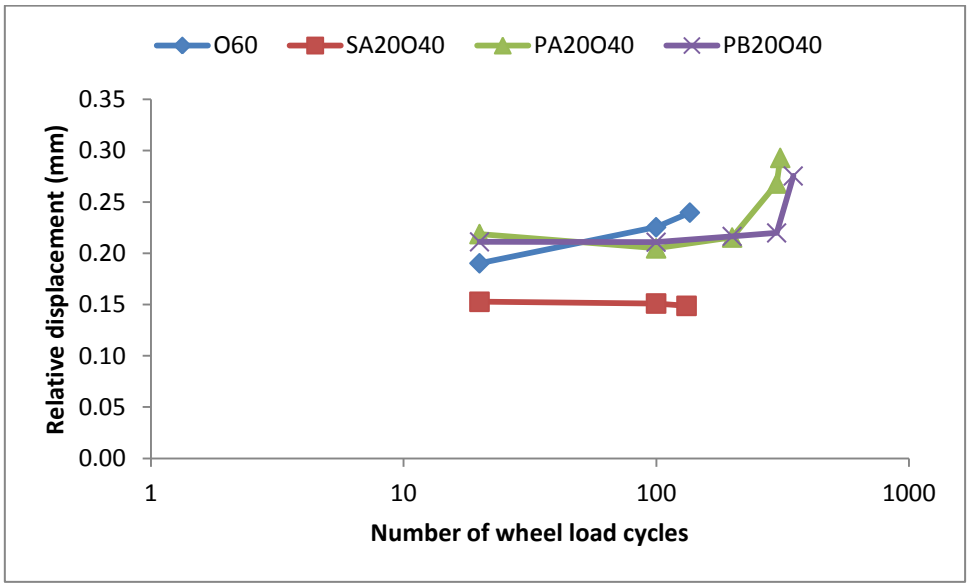

Figure 5.34: Displacement versus number of wheel cycles at 30°C with 2.4kN (1.1MPa) load applied for specimens with 20 mm SAMI and 40 mm overlay

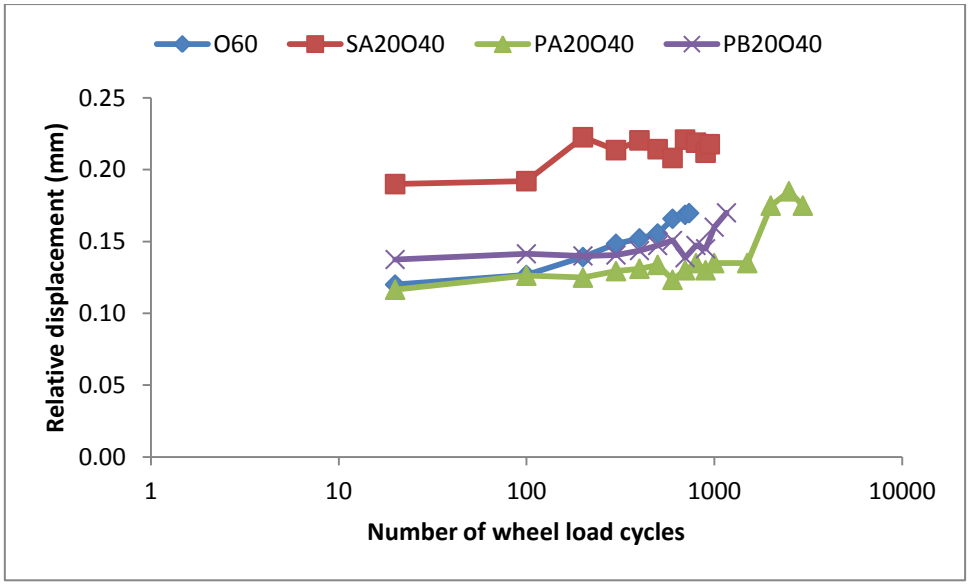

Figure 5.35: Displacement versus number of wheel cycles at 30°C with 1.35kN (0.6MPa) load applied for specimens with 20 mm SAMI and 40 mm overlay

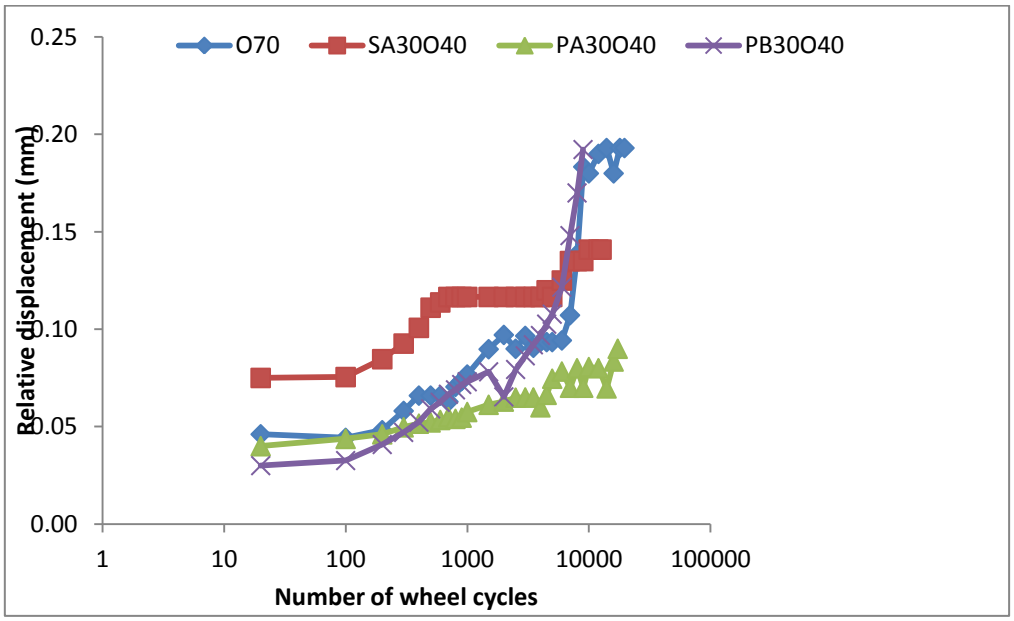

Figure 5.36: Displacement versus number of wheel cycles at 10°C with 2.4kN (1.1MPa) load applied for specimens with 30 mm SAMI and 40 mm overlay

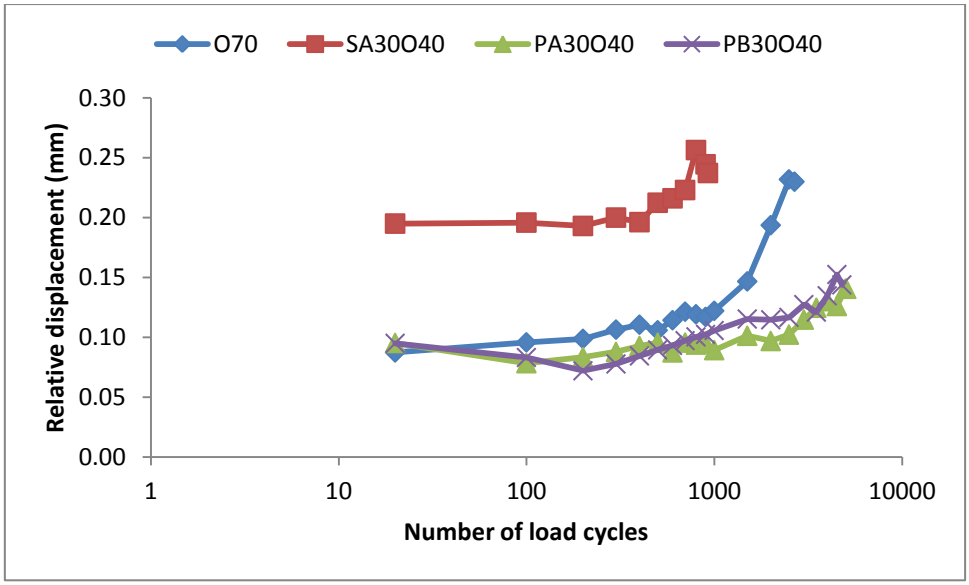

Figure 5.37: Displacement versus number of wheel cycles at 20°C with 2.4kN (1.1MPa) load applied for specimens with 30 mm SAMI and 40 mm overlay

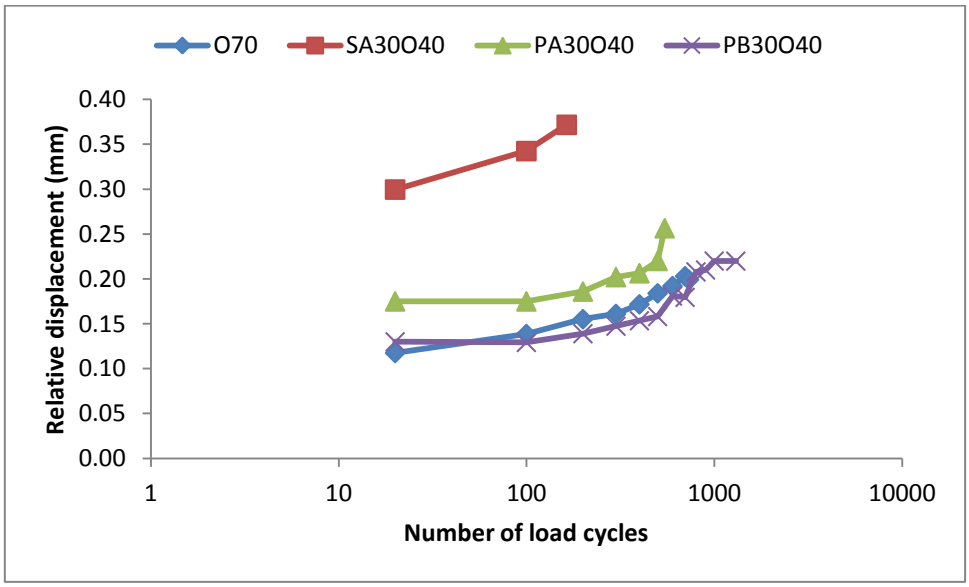

Figure 5.38: Displacement versus number of wheel cycles at 30°C with 2.4kN (1.1MPa) load applied for specimens with 30 mm SAMI and 40 mm overlay

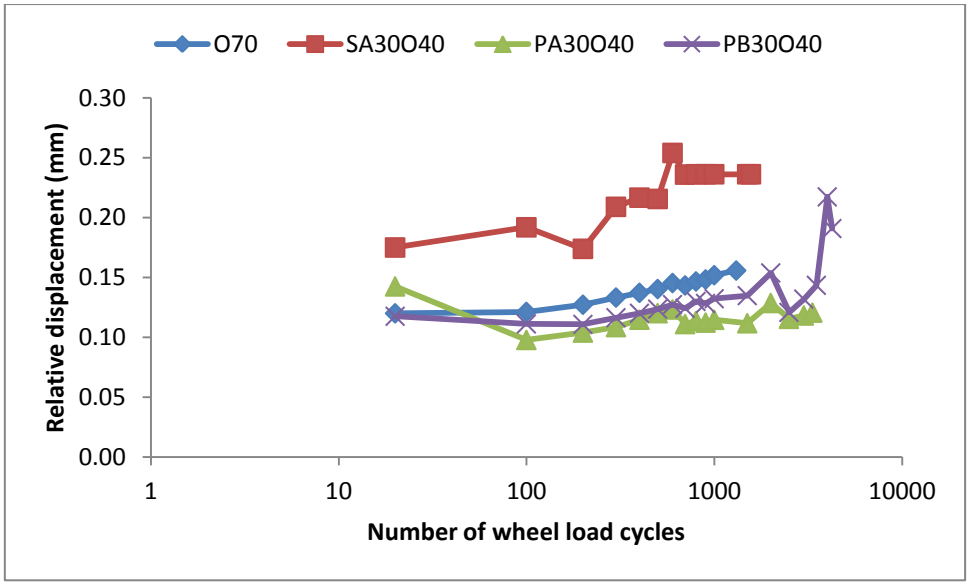

Figure 5.39: Displacement versus number of wheel cycles at 30°C with 1.35MPa (0.6MPa) load applied for specimens with 30 mm SAMI and 40 mm overlay

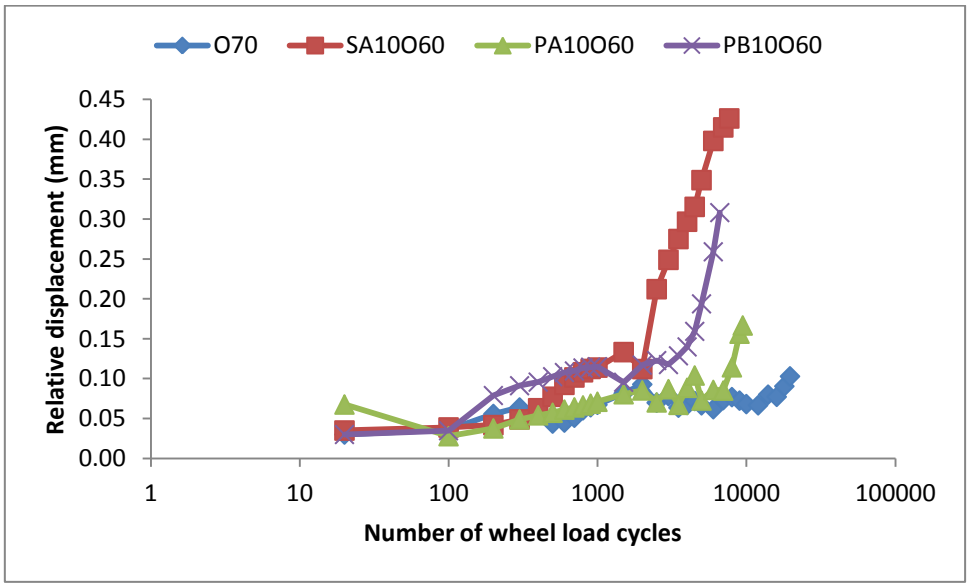

Figure 5.40: Displacement versus number of wheel cycles at 10°C with 2.4kN (1.1MPa) load applied for specimens with 10 mm SAMI and 60 mm overlay

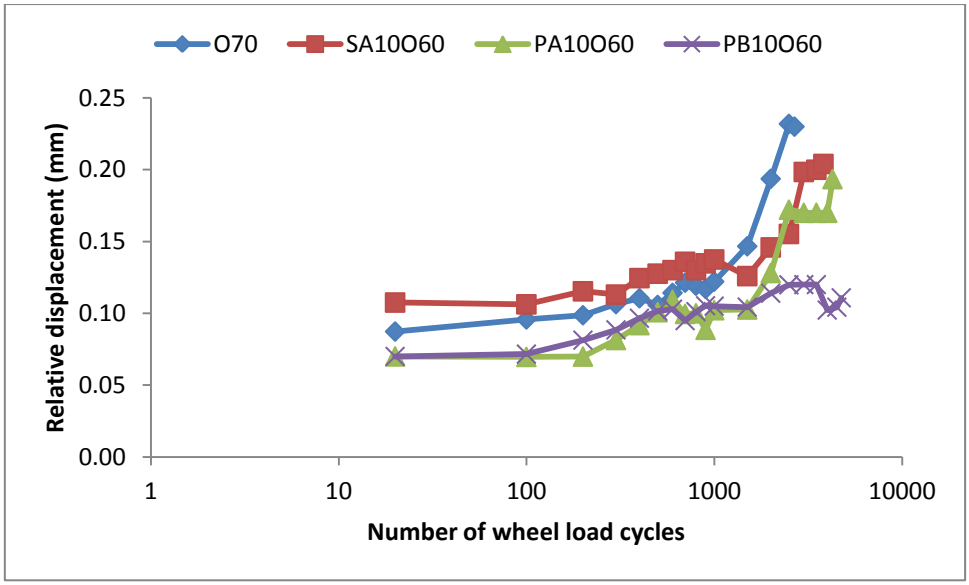

Figure 5.41: Displacement versus number of wheel cycles at 20°C with 2.4kN (1.1MPa) load applied for specimens with 10 mm SAMI and 60 mm overlay

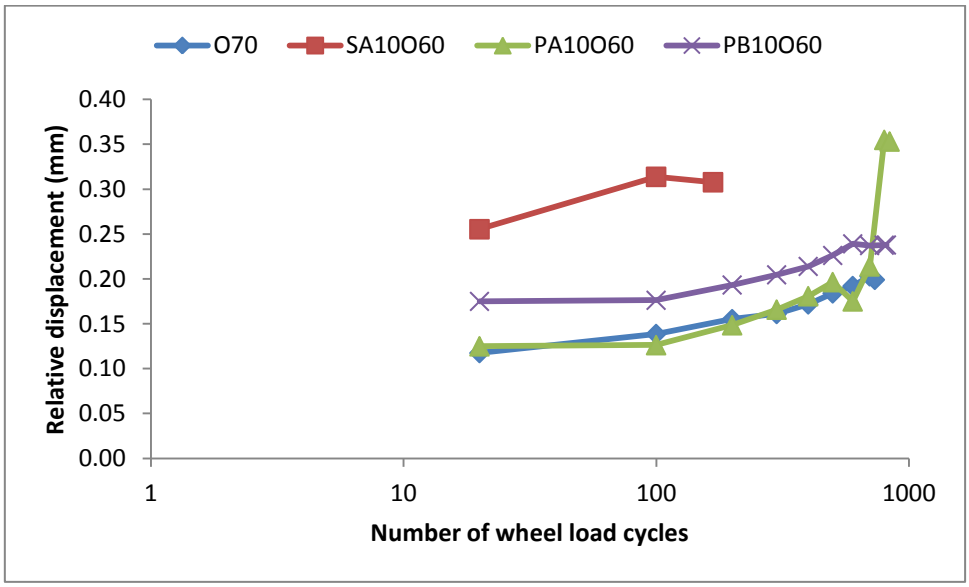

Figure 5.42: Displacement versus number of wheel cycles at 30°C with 2.4kN (1.1MPa) load applied for specimens with 10 mm SAMI and 60 mm overlay

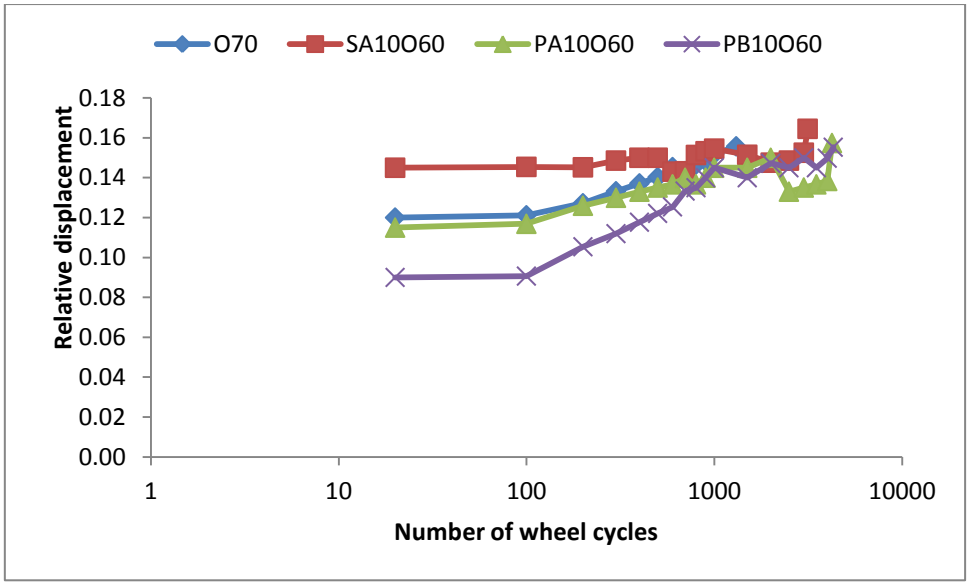

Figure 5.43: Displacement versus number of wheel cycles at 30°C with 1.35kN (0.6MPa) load applied for specimens with 10 mm SAMI and 60 mm overlay

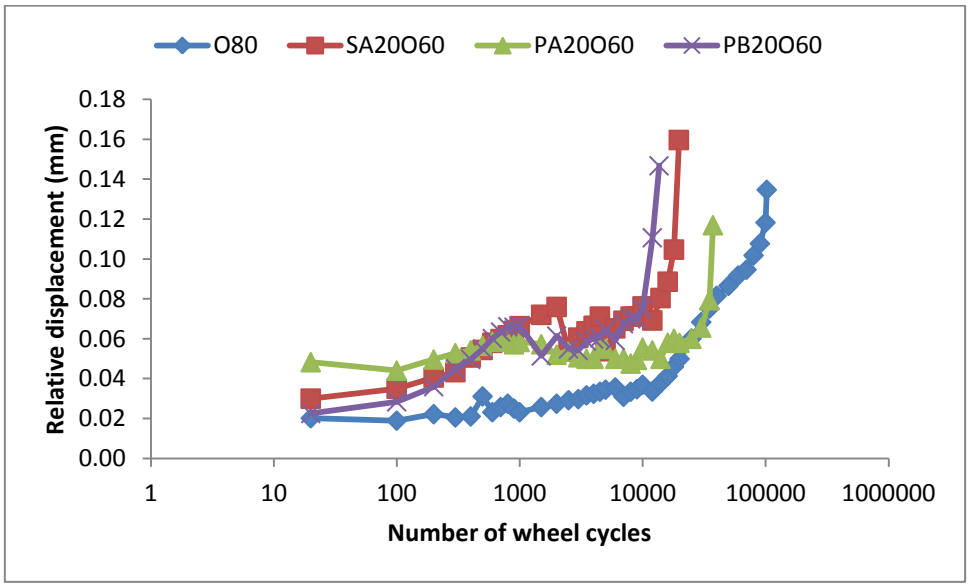

Figure 5.44: Displacement versus number of wheel cycles at 10°C with 2.4kN (1.1MPa) load applied for specimens with 20 mm SAMI and 60 mm overlay

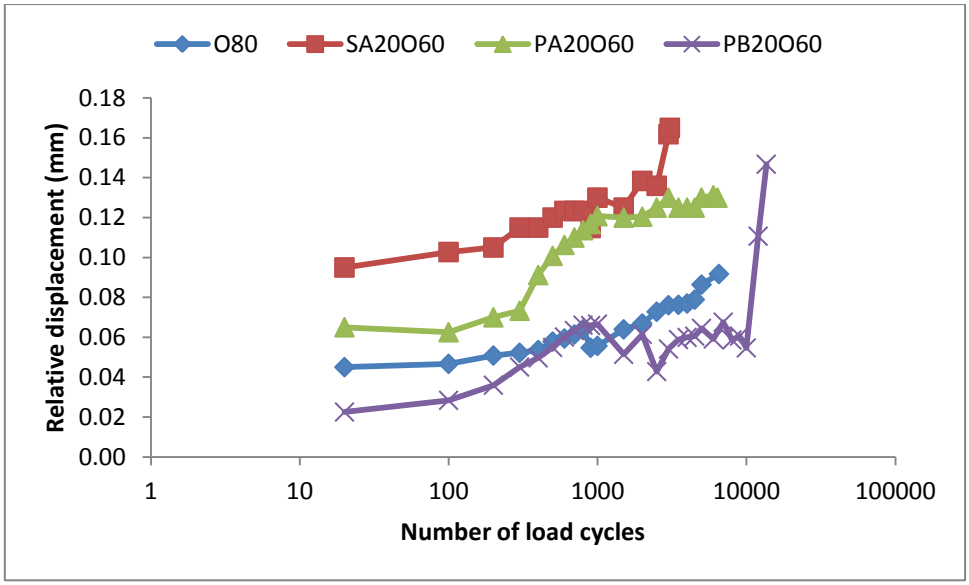

Figure 5.45: Displacement versus number of wheel cycles at 20°C with 2.4kN (1.1MPa) load applied for specimens with 20 mm SAMI and 60 mm overlay

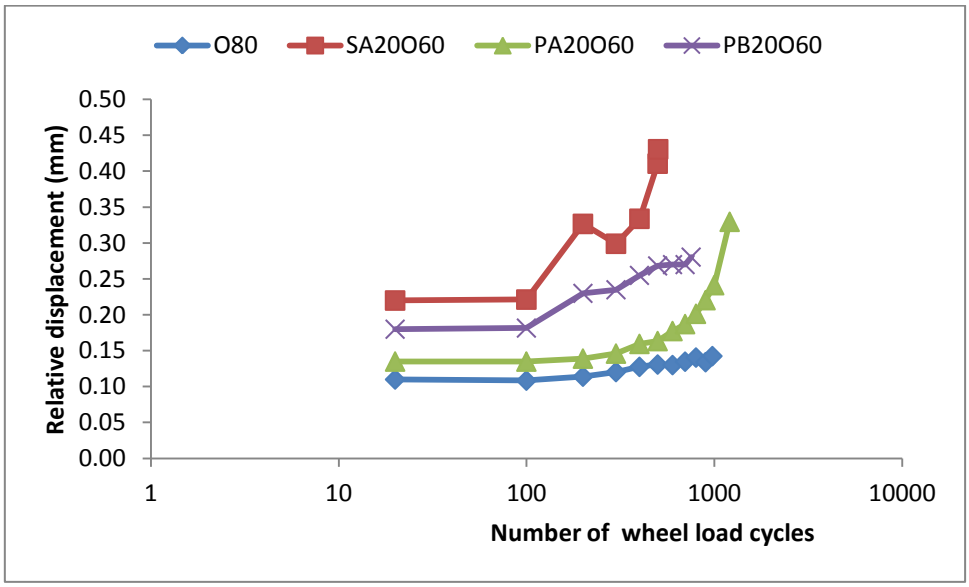

Figure 5.46: Displacement versus number of wheel cycles at 30°C with 2.4kN (1.1MPa) load applied for specimens with 20 mm SAMI and 60 mm overlay

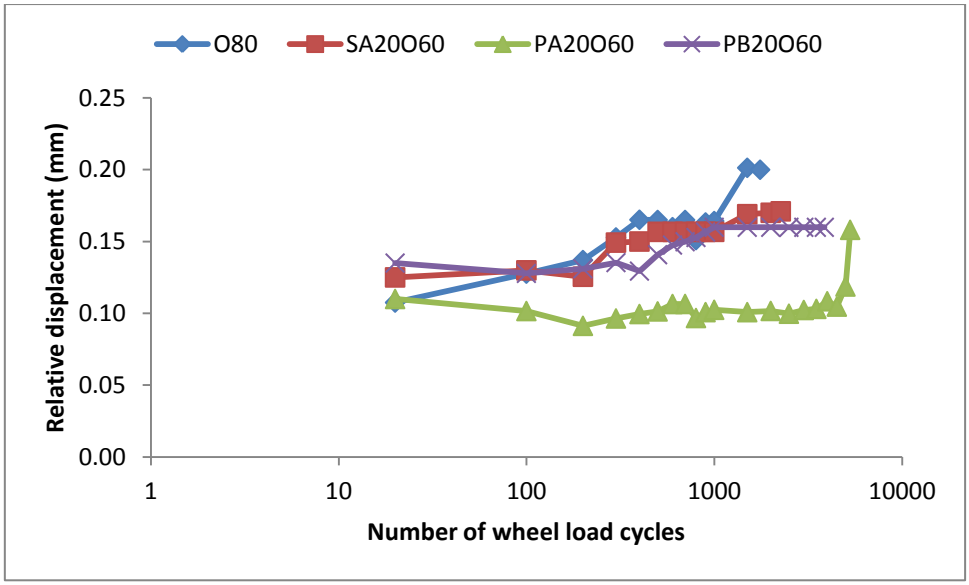

Figure 5.47: Displacement versus number of wheel cycles at 30°C with 1.35kN (0.6MPa) load applied for specimens with 20 mm SAMI and 60 mm overlay

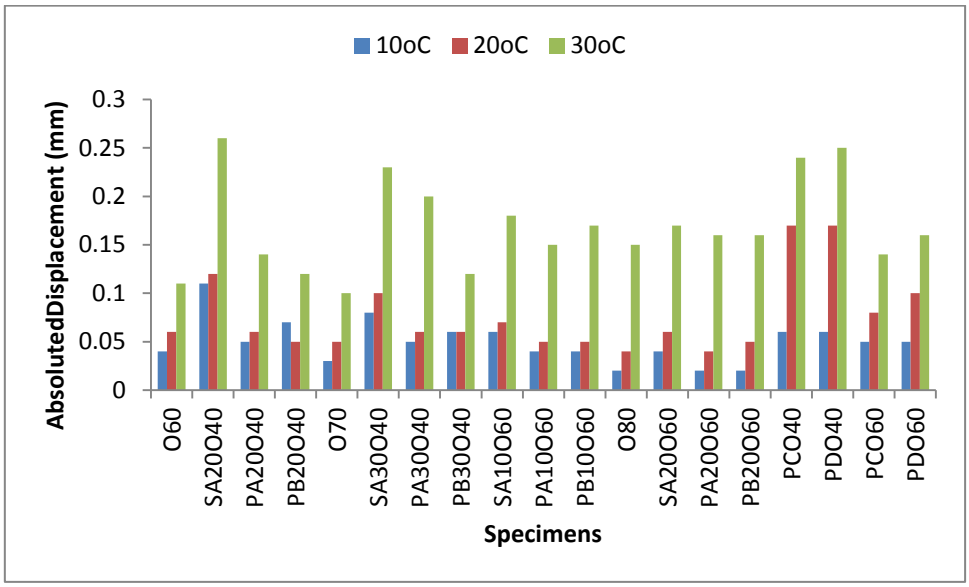

Figure 5.48: Initial absolute displacement of the specimens under 2.4kN load at 10°C, 20°C and 30°C

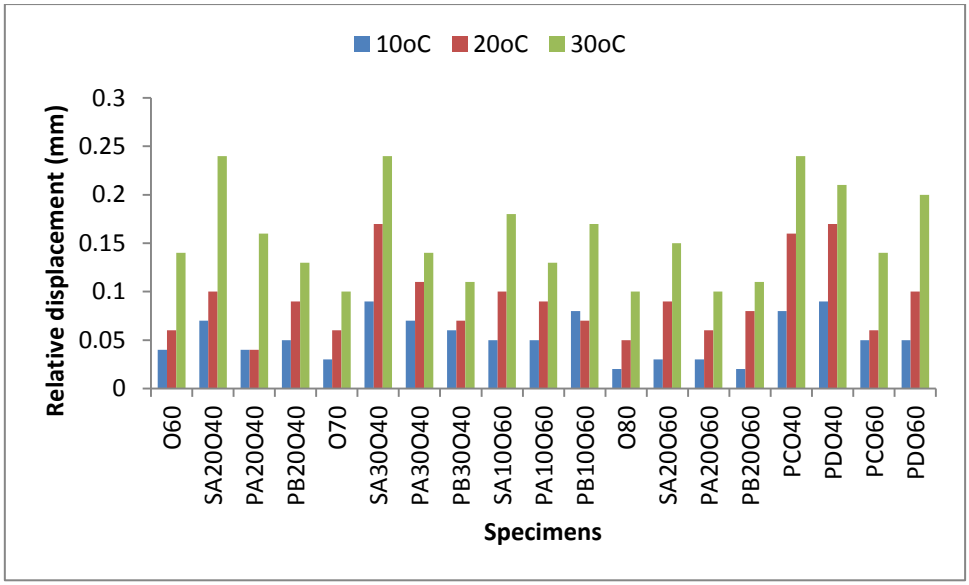

Figure 5.49: Initial relative displacement of the specimens under 2.4kN load at 10°C, 20°C and 30°C

5.5 Strain

The initial strain at 4mm above the crack top is shown in Figure 5.50, while the initial strain at 20 mm from the bottom of the overlay and equivalent positions in their respective control specimens is shown in Figure 5.51. For the control specimens with 60 mm overlay (O60) and 80 mm overlay (O80), the depth from the bottom of the overlay was 40 mm while for control specimens with 70 mm overlay (O70), the depth was 30 mm from the bottom. Figure 5.50 shows that there is greater strain concentration at 4mm above the crack top for the specimens with SAMIs than those without SAMI (control). However, Figure 5.51 shows that at 20 mm from the bottom of the overlay less strain is measured in the specimens with SAMIs than those without SAMI (control) with the exception of the specimens with sand asphalt. This shows the potential of SAMIs to isolate the overlay from stress concentration around the crack region. It can be seen from both figures that the strain in the specimens increases with temperature. Also, the specimens with less strain concentration give better performance than those with higher strain concentration.

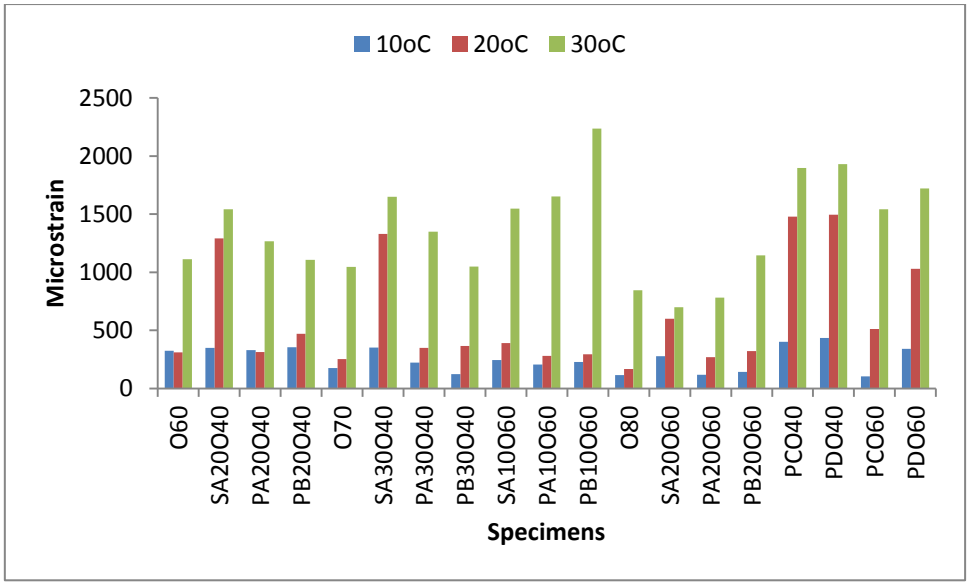

Figure 5.50: Strain at 4 mm above the crack top under 2.4kN (1.1MPa) load at 10°C, 20°C and 30°C

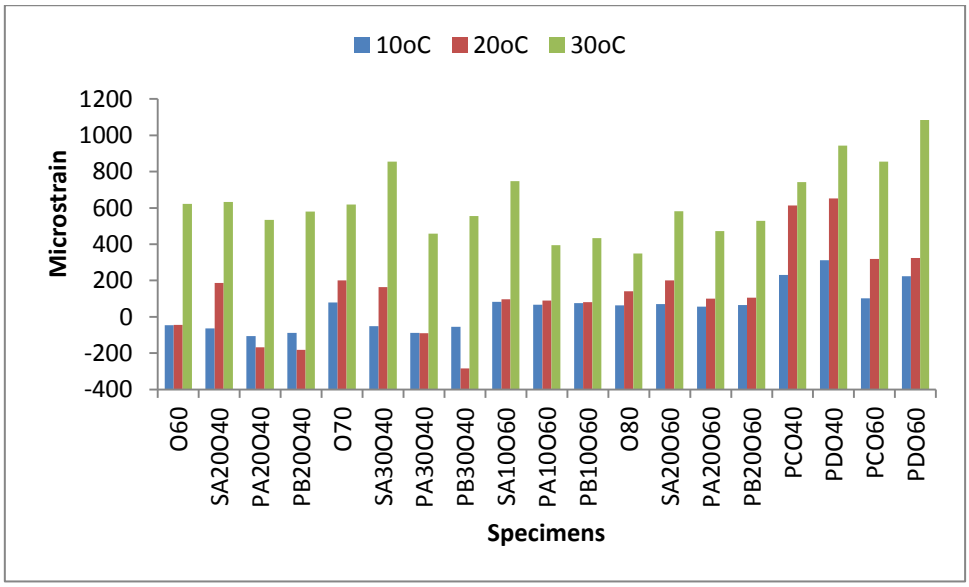

Figure 5.51: Strain at 20 mm from bottom of overlay and equivalent depth in control specimens under 2.4kN (1.1MPa) load at 10°C, 20°C and 30°C

5.6 Conclusion

The following conclusions were drawn from this study:

- The test was capable of simulating the situation of overlay over cracked pavement in the field.

- The SAMIs (proprietary SAMIs A, B, C and D) were able to retard reflective cracking at 20^{o}C and 30^{o}C, while only proprietary SAMIs C and D were able to retard reflective cracking at 10^{o}C.
- It was discovered that the performance of proprietary SAMIs A and B was mixed. Generally proprietary SAMI A performed better when the thickness was 20 mm while proprietary SAMI B performed better when the thickness was 30 mm. This was due to the composition of the mixtures.
- The study also showed that specimens with proprietary SAMIs C performed better than the ones with proprietary SAMI D. This was the case probably because the bitumen emulsion in proprietary SAMI C is more viscous, thereby allowing more flexibility of the interlayer.
- It was found that sand asphalt was mostly ineffective in retarding crack growth, a situation that was probably due to the very low stiffness of the SAMI and its fatigue resistance. This further demonstrates that an optimum stiffness at which the SAMIs are effective exists. Having too soft or too stiff (hard) an interlayer will yield undesired results.
- The test results showed that SAMI thickness (sand asphalt, proprietary SAMIs A and B) has an effect on performance. They were found to be more effective when lower thickness was used. This is possibly due to increased flexure caused by increasing the thickness of the soft interlayer.
- It can also be seen that the resistance of the SAMIs against reflective cracking was more pronounced when a load of 1.35kN (tyre pressure approximately 0.6MPa) was used than with a load 2.4kN (tyre pressure approximately 1.1MPa). This indicates that when high load magnitudes are expected such as on an airfield, having a reinforced interlayer may be most appropriate.

- Furthermore, the test results showed that the performance of the SAMIs was affected by temperature. The SAMIs (sand asphalt, proprietary SAMIs A and B) were found to be mostly effective at 20^{o}C and 30^{o}C, while the performance of proprietary SAMIs C and D decreased with increasing temperature.
- It was found that the relative benefit of the SAMIs decreases as the overlay thickness increases.

REFERENCES

Barksdale R.D. (1991): Fabrics in Asphalt Overlay and Pavement Maintenance. National Cooperative Highway Research Program Synthesis of Highway Practice 171. Transportation Research Board. Washington D.C.

BSI (2003): Bituminous Mixtures-Test Method for Hot Mix Asphalt: Specimen Prepared by Roller Compactor. British Standard Institution, London, UK (BS EN 12697-33:2003).

BSI (2004): Bituminous Mixtures-Test Method for Hot Mix Asphalt: Laboratory Mixing. British Standard Institution, London, UK (BS EN 12697-35:2004).

Debondt A.H. (1999): Anti Reflective Cracking Design of (Reinforced) Asphaltic overlays. PhD Thesis submitted to Delft University of Technology, Netherlands.

Elseifi M.A. (2003): Performance Quantification of Interlayer Systems in Flexible Pavements Using Finite Element Analysis, Instrument Response and Non Destructive Testing. PhD Thesis submitted to Virginia Polytechnic Institute and State University.

Molenaar A.A.A., Heerkens J.C.P. and Verhoeven J.M.H (1986): Effects of Stress Absorbing Membrane Interlayers. Proceedings of Association of American Pavement Technologists, V 55, 453-481.

Sanders P.J. (2001): Reinforced Asphalt Overlays for Pavements. PhD Thesis submitted to University of Nottingham, Nottingham, United Kingdom.

6 FINITE ELEMENT ANALYSIS OF WHEEL TRACKING TEST

6.0 Introduction

Finite element modelling was carried out in this study to give a better understanding of the deflection and stress-strain distribution in overlaid cracked pavements with and without SAMIs. Successful modelling of a well controlled laboratory test will allow the model to be applied to other conditions. In the modelling, the propagation of the crack was not considered; therefore the modelling only gives the deflection and stress-strain distribution before crack initiation.

In mechanistic analysis, hot-mix asphalt has traditionally being considered to behave in a linear elastic manner. This has some shortcomings in that, in reality, asphalt concrete behaves more like a viscoelastic material. Hot-mix asphalt only behaves as an elastic material at low temperature and high loading frequency, while it behaves like a viscous fluid at high temperature and low loading frequency. At intermediate temperatures and loading frequencies, it behaves like a viscoelastic material that exhibits a significant level of elastic solid stiffness while dissipating energy by frictional resistance as a viscous fluid.

Although asphalt behaves more like a viscoelastic material, for simplicity it was considered appropriate to use a linear elastic model for the analysis. As observed by Sousa et al (2001), two major factors are of particular interest in the mechanical analysis of hot-mix asphalt: the material characterization method and its accuracy in reflecting the material resistance to loading; and the accuracy of mechanistic models to predict the pavement performance. For this study, the material stiffnesses were determined. The modelling was done with a commercial finite element program Abaqus 6.7-1. The Abaqus finite element system includes (Abaqus Theory Manual, 2007):

- Abaqus/Standard, a general-purpose finite element program
- Abaqus/Explicit, an explicit dynamics finite element program
- Abaqus/CAE, an interactive environment used to create finite element models, submit Abaqus analyses, monitor and diagnose jobs and evaluate results; and
- Abaqus/Viewer, a subset of Abaqus/CAE that contains only the postprocessing capabilities of the Visualization module.

For this study, Abaqus/Standard was implemented in Abaqus/CAE to generate models for the study.

6.1 Finite element formulation for the wheel tracking test

The procedure for the wheel tracking test has been described in section 5.3. The specimens were manufactured in three layers; the base layer (simulating the existing pavement) with a 10 mm notch (simulating the crack), which was made of 10 mm asphalt concrete with 10/20 penetration grade bitumen, the middle layer (where present) was SAMI, the SAMIs considered in the modelling being proprietary SAMIs A and B and sand asphalt, and the top layer (overlay) was also made of 10 mm asphalt concrete but with 40/60 penetration grade bitumen. The control specimens were made in two layers: the top layer and the base layer. The specimen was placed on a 10 mm rubber mat in a steel mould. It was loaded after clamping it at the top and side at both ends to simulate pavement continuity. The specimen arrangement for the control and test models is as shown in Figure 6.1.

As mentioned earlier, a linear elastic material model was adopted for the specimens. Therefore, each layer was assumed to behave in an elastic manner. Thus, the material properties required for the finite element modelling are the elastic modulus, E and Poisson's ratio, μ. The elastic modulus (stiffness) was determined using the indirect tensile stiffness

modulus (ITSM) test described in section 3.5.3. The stiffness was used directly because the temperatures are the same and wheel loading rate is close to the ITSM loading rate. The properties of each of the layers at 10°C, 20°C and 30°C are as shown in Table 6.1. The parameters considered in the modelling include the overlay and SAMI thicknesses, and the test temperature. The test temperature was considered by using the material properties obtained in the laboratory tests at 10°C, 20°C and 30°C for the modelling.

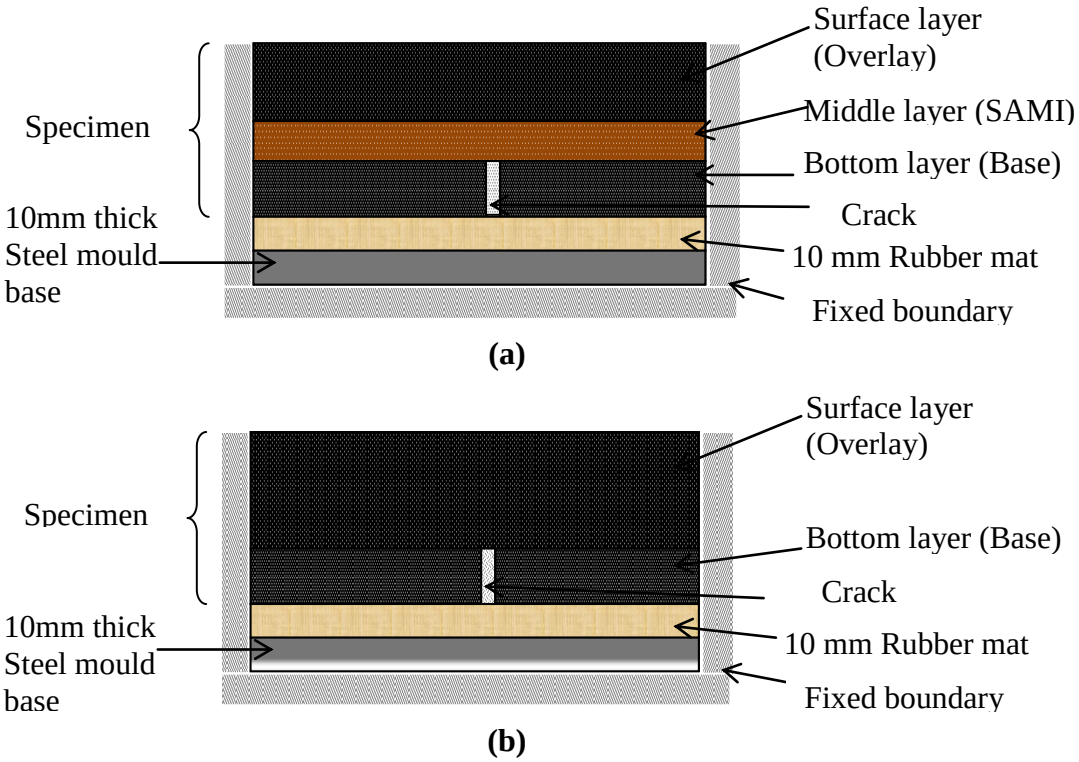

Figure 6.1: Specimen arrangement (a) with SAMI (b) without SAMI

Table 6.1: Layer properties

Materials	Properties		
	E, MPa, (μ) at 10°C	E, MPa, (μ) at 20°C	E, MPa, (μ) at 30°C
10 mm AC (40/60)	10035 (0.25)	3899 (0.35)	1098 (0.45)
10 mm AC (10/20)	15435 (0.25)	9591 (0.35)	5008 (0.45)
Proprietary SAMI A	8548 (0.25)	2725 (0.35)	635 (0.45)
Proprietary SAMI B	7564 (0.25)	2444 (0.35)	510 (0.45)
Sand asphalt	635 (0.25)	209 (0.35)	118 (0.45)
Crack	1 (0.35)		
Rubber	6.45 (0.49)		
Steel	209000 (0.3)		

6.2 Model geometry and dimension

To investigate the performance of the SAMIs, two models were developed: one incorporating SAMIs and the other without SAMIs (Control). The model length and width are 404 mm and 50 mm, respectively. The overall model thickness varies with thicknesses of the middle (SAMI) and the surface (overlay) layers. The overall thicknesses considered in the model are 110 mm, 120 mm and 130 mm. The combinations investigated are as shown in Table 6.2. Each combination was investigated at 10^{o}C, 20^{o}C and 30^{o}C for the three SAMIs: Proprietary SAMI A and B and sand asphalt.

A 3-dimensional analysis was carried out allowing the load to be placed across the entire beam width of 50 mm as was the case for the laboratory study. All the layers were simulated using an 8-node linear brick, reduced integration element (C3D8R) – a first order isoparametric element. The C3D8R elements have only one integration point, thereby reducing the computational time without any great effect on the result accuracy. Reduced integration usually means that an integration scheme one order less than the full scheme is used to integrate the element internal forces and stiffness (Abaqus Theory Manual, 2007). Typical 3-dimensional structural models for the wheel tacking test for specimens with 10 mm and 20 mm SAMIs and 60 mm overlay are shown in Figures 6.2 and 6.3, respectively. The models for specimens with 30 mm and 20 mm SAMIs and 40 mm overlay are shown in Figures 6.4 and 6.5, respectively. Typical Control models (no SAMI) with 60 mm, 70 mm and 80 mm overlay are shown in Figures 6.6, 6.7 and 6.8, respectively. Cracks in an existing pavement have been modelled using different approaches by researchers. Wu and Harvey (2008) modelled a crack with empty spaces in the underlying layer; Minhoto et al (2008) in their study of reflective cracking behaviour for traffic and temperature effects modelled cracks using elements without stiffness. Pais and Pereira (2000) modelled cracks as a void with a negligible stiffness of 1MPa. Also, Dave et al (2008) and Baek and Al-Qadi (2008)

modelled cracks using a cohesive zone model. In this study, for simplicity, the crack was modelled by assigning a low material stiffness to the elements (see Table 6.1).

The mesh density that is appropriate for the study was determined by checking different mesh densities. A density that saved time without affecting the accuracy of the results was selected. For this analysis, the specimens with 20 mm SAMI and 40 mm overlay and control specimens with 60 mm overlay are modelled with 31200 elements, while the specimens with 30 mm SAMI and 40 mm overlay, 10 mm SAMI and 60mm overlay and control specimens with 70 mm overlay are modelled with 33600 elements. Lastly, the specimens with 20 mm SAMI and 60 mm overlay and control specimens with 80 mm overlay were modelled with 37200 elements.

Table 6.2: Combinations investigated

Layer thickness (mm)	C1	C2	C3	C4	C5 (Control)	C6 (Control)	C7 (Control)
Overlay	40	40	60	60	60	70	80
SAMI	20	30	10	20	-	-	-
Base	30	30	30	30	30	30	30
Rubber	10	10	10	10	10	10	10
Steel	10	10	10	10	10	10	10
Total	110	120	120	130	110	120	130

C- Combination

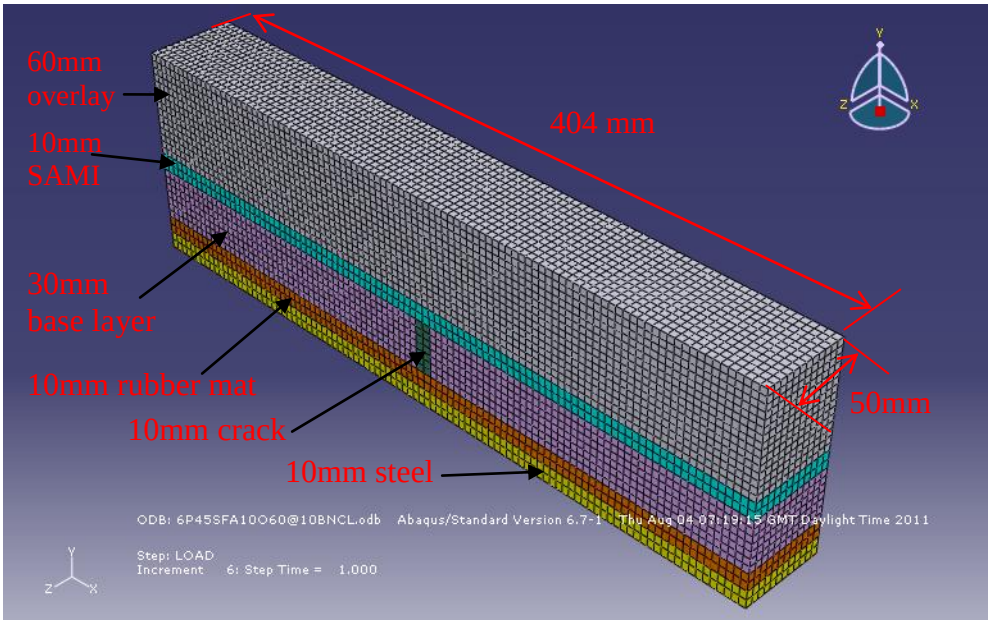

Figure 6.2: A typical model with 10 mm SAMI and 60 mm overlay

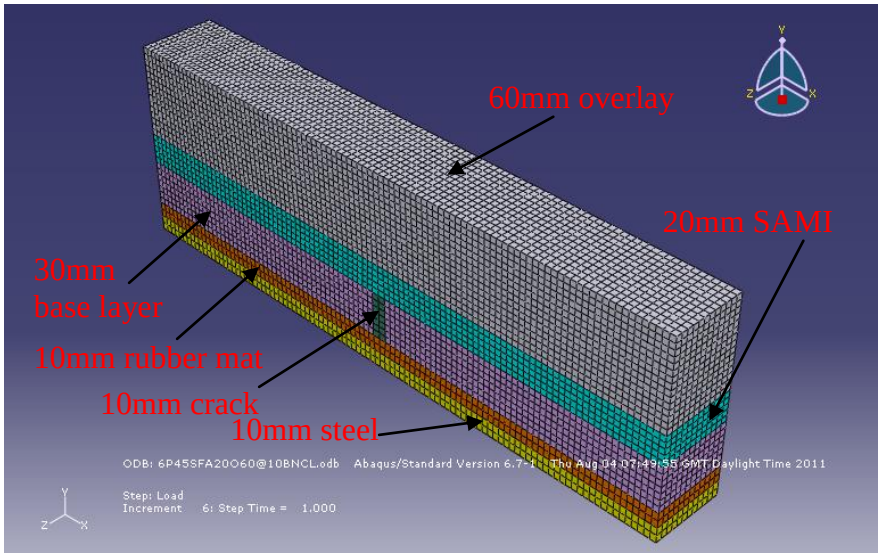

Figure 6.3: A typical model with 20 mm SAMI and 60 mm overlay

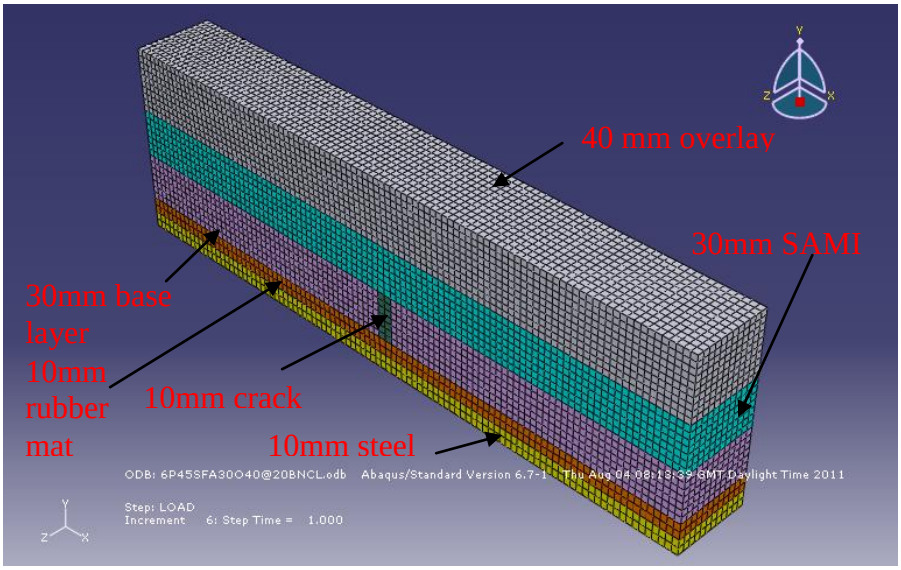

Figure 6.4: A typical model with 30 mm SAMI and 40 mm overlay

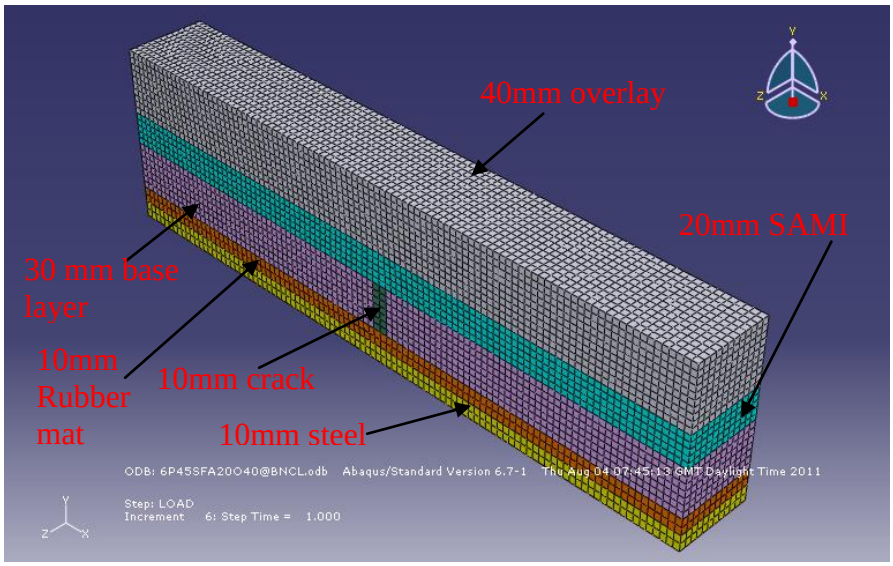

Figure 6.5: A typical model with 20 mm SAMI and 40 mm overlay

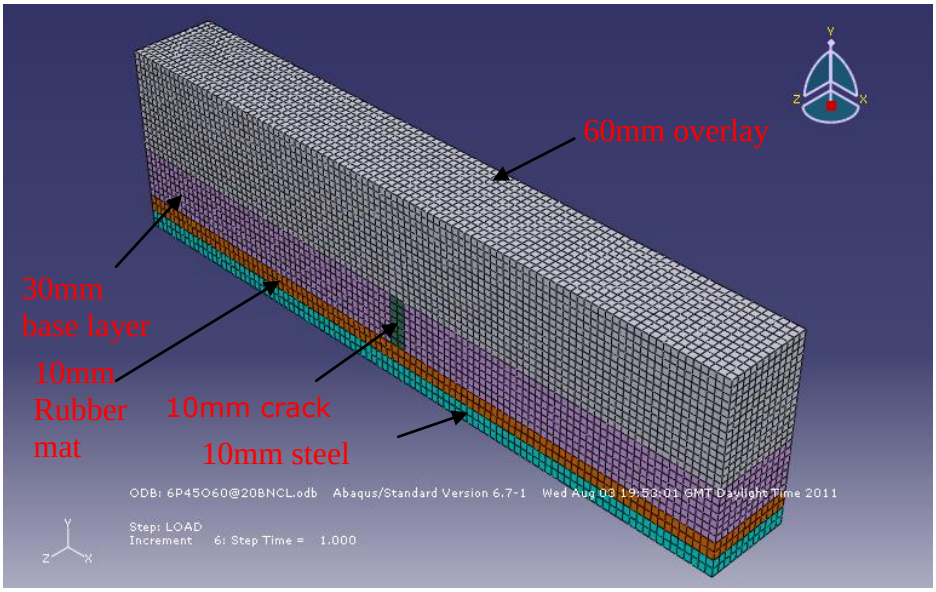

Figure 6.6: A typical model (Control) 60 mm overlay

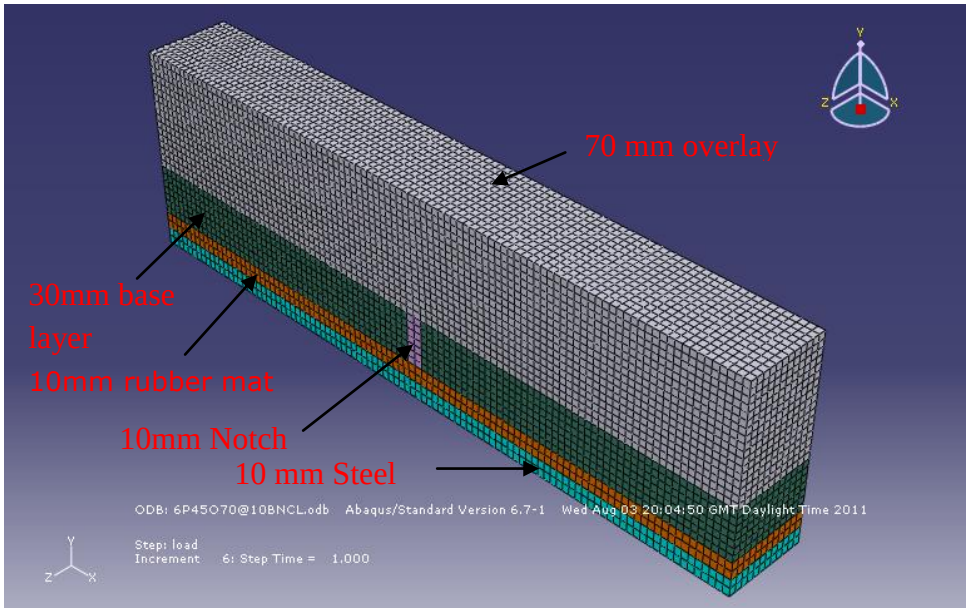

Figure 6.7: A typical model (Control) 70 mm overlay

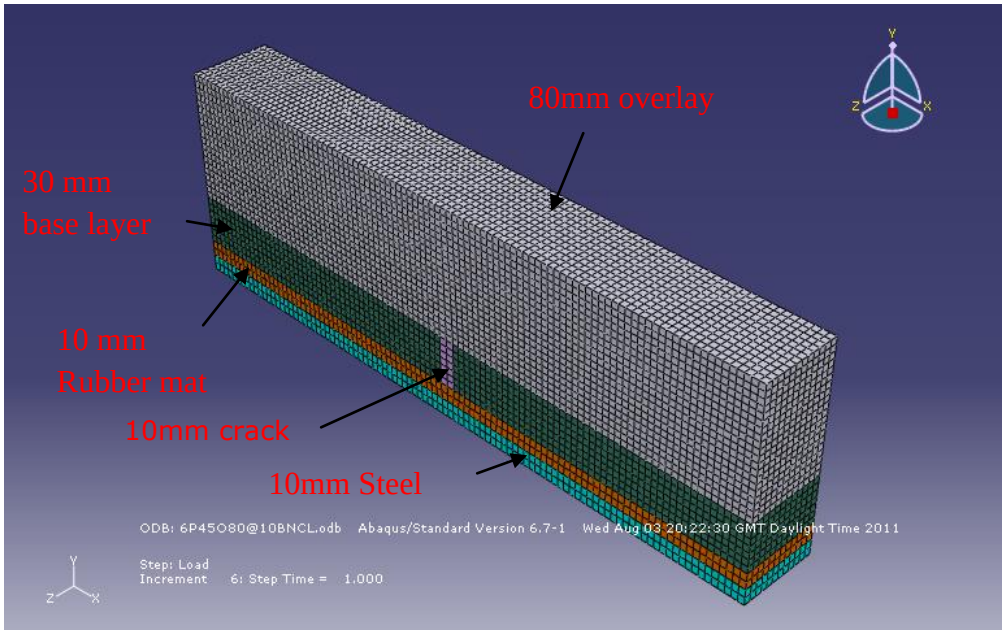

Figure 6.8: A typical model (Control) 80 mm overlay

6.3 Loading and boundary conditions

A distributed load of 2.4 kN (1.1MPa) was used in the modelling. This was placed on the whole width (50 mm) of the beam over a length of 45 mm. The load was placed at two different locations: 90 mm away from the centre of the crack, termed 'edge load', and directly above the simulated crack, termed 'centre load', as shown in Figures 6.9 and 6.10, respectively. Only one side of the model was considered because of symmetry.

The model support was simulated by applying a fixed boundary condition to the steel base. The tests simulated pavement continuity by clamping; the model simulated clamping using fixed boundaries. The fixed boundary condition (encastre) constrains the model movement, i.e., the displacement and rotation in x, y and z directions.

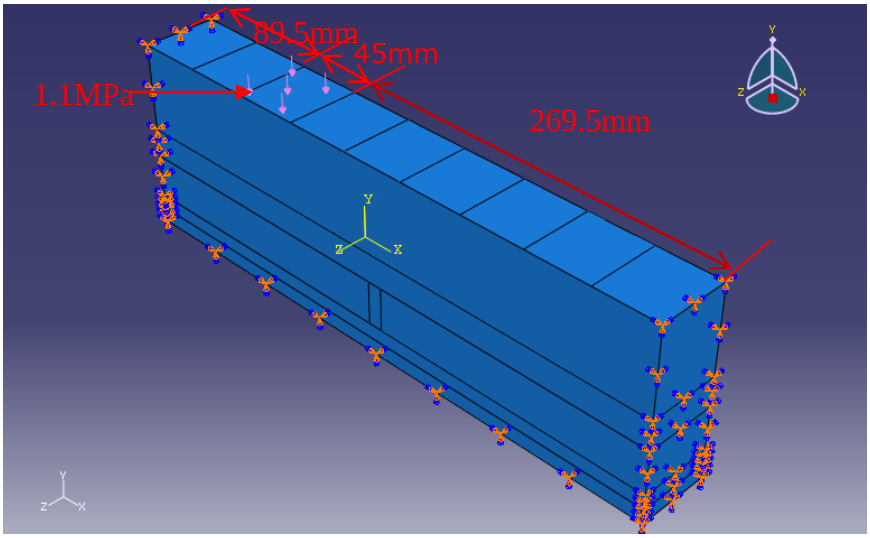

Figure 6.9: A typical model assembly with edge load and boundary conditions

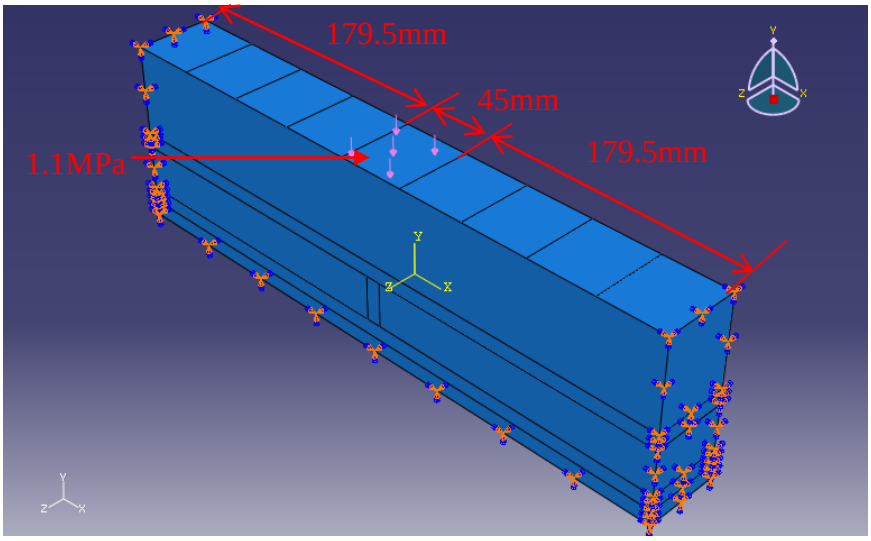

Figure 6.10: A typical model assembly with centre loading and boundary conditions

6.4 Contact modelling

Two cases were investigated for the interaction between the layers: overlay-SAMI, SAMI-base, base-rubber and rubber-steel interfaces. The first assumed a full bond condition (compatibility of stresses and strains). The second case assumed a friction-type contact (slip) between the SAMI and the base layers i.e., the layer interface was allowed to separate (debond), while other interfaces are assumed to be fully bonded. The friction-type contact

was achieved by using the penalty contact method. Finite sliding that allows arbitrary motion of the surfaces and the surface to surface discretization method were selected in Abaqus CAE. A friction coefficient of 0.7 was used and the default slip tolerance of 0.005 mm specified by Abaqus was used.

6.5 Results and analysis

For this study, 180 models were formulated and the results analysed. The results of the models were obtained at 4 mm above the crack top, the bottom of the overlay and at 20 mm from the bottom of the overlay. For the specimens with 10 mm, 20 mm and 30 mm SAMIs, 20 mm from the bottom of the overlay is equivalent to 30 mm, 40 mm and 50 mm from the bottom of the overlay in their respective control specimens. The specimen references are shown in Table 6.3

Table 6.3: Specimen references

Specimens name	Specimens references
60 mm Overlay (Control)	O60
20 mm thick sand asphalt with 40 mm overlay	SA20O40
20 mm thick Proprietary SAMI A with 40 mm overlay	PA20O40
20 mm thick Proprietary SAMI B with 40 mm overlay	PB20O40
70 mm Overlay (Control)	O70
30 mm thick sand asphalt with 40 mm overlay	SA30O40
30 mm thick Proprietary SAMI A with 40 mm overlay	PA30O40
30 mm thick Proprietary SAMI B with 40 mm overlay	PB30O40
10 mm thick sand asphalt with 60 mm overlay	SA10O60
10 mm thick Proprietary SAMI A with 60 mm overlay	PA10O60
10 mm thick Proprietary SAMI B with 60 mm overlay	PB10O60
80 mm Overlay (Control)	O80
20 mm thick sand asphalt with 60 mm overlay	SA20O60
20 mm thick Proprietary SAMI A with 60 mm overlay	PA20O60
20 mm thick Proprietary SAMI B with 60 mm overlay	PB20O60

6.5.1 Displacement

The measured and predicted absolute displacements at 10°C, 20°C and 30°C are shown in Figures 6.11, 6.12 and 6.13. It can be seen from the figures that there is more absolute displacements in the specimens with SAMIs than the control sections without SAMI. As observed in the wheel tracking test, the results show that the specimen with lower SAMI thickness has less displacement than the ones with greater thickness. Also, it can be seen that the absolute displacements of the specimens increase with temperature. The figures show that greater displacements are predicted in the debond cases than the full bond cases

The finite element analysis shows that the predicted absolute displacements are more or less the same as the measured displacements, indicating that the wheel tracking test reported in chapter five did what it was intended to do.

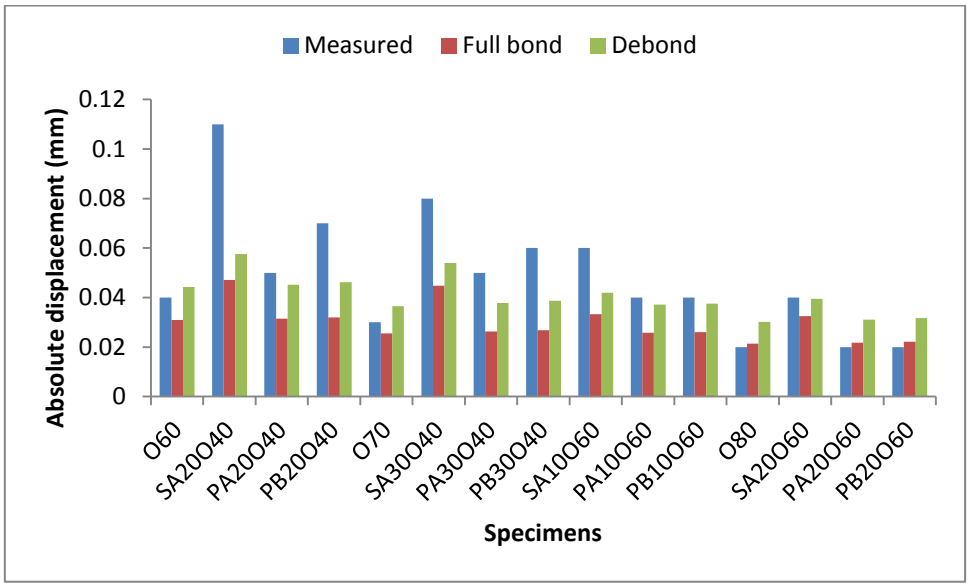

Figure 6.11: Absolute displacement at 10°C

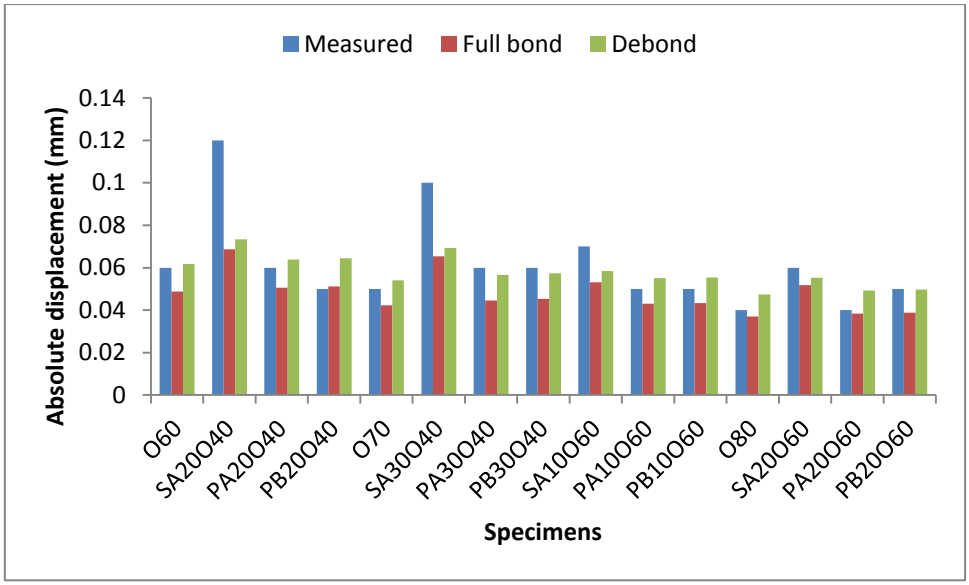

Figure 6.12: Absolute displacement at 20°C

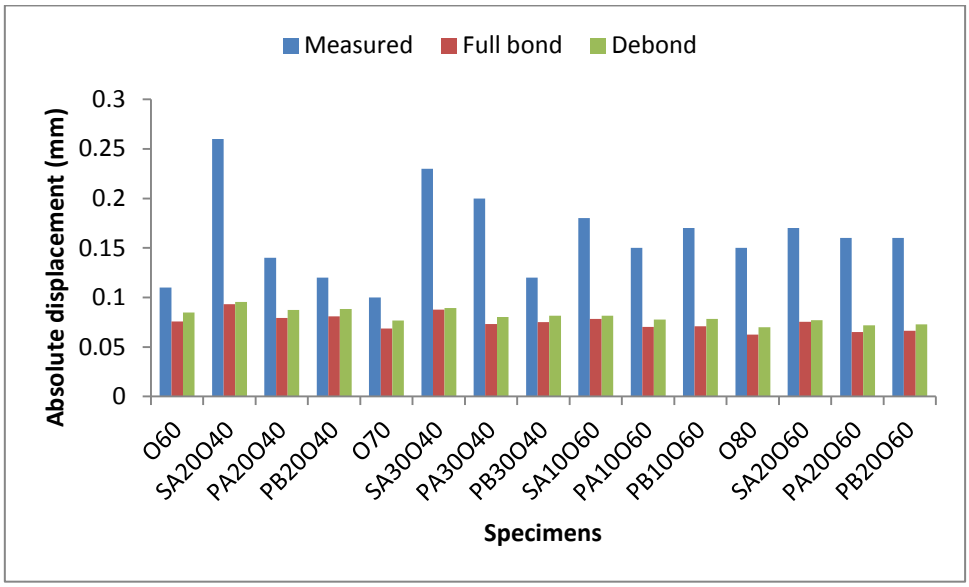

Figure 6.13: Absolute displacement at 30°C

6.5.2 Strain

The measured and predicted strain was obtained as the difference in values when the load was placed at the centre directly above the crack top and at the edge (90mm from the centre). The measured and predicted strains at 4mm above the crack top at 10°C, 20°C and 30°C are shown in Figures 6.14, 6.15 and 6.16, respectively. Figures 6.14 and 6.15 show that at 10°C and 20°C, the measured and predicted tensile strains at 4mm above the crack top in the

specimens with SAMIs are greater than strains in the control specimens with no SAMIs for both the full bond and debond conditions except for the specimens with sand asphalt as SAMI. As explained in section 6.5.1, the use of soft interlayers (SAMIs) increases deflection of the pavement. This in turn results in high strain concentration around the crack as seen in Figures 6.14 and 6.15. Figure 6.16 indicates that at 30^{o}C for the full bond cases less strain was predicted at 4 mm above the crack top in the specimens with SAMIs than the control specimens without SAMI with the exception of the specimens with sand asphalt which are in compression, while for the debond cases greater strain was predicted in the specimens with SAMIs than those without SAMI.

Figures 6.17 and 6.18 show the strain predicted at the bottom of the overlay for both control specimens and those with SAMIs (full bond and the debond cases). It can be seen from both figures that the strains at the bottom of the overlay are smaller in the specimens with SAMIs than those without SAMIs. Figures 6.19 and 6.20 show the strain measured and predicted at 20 mm from the bottom of the overlay at 10^{o}C and 20^{o}C. The figures show that for the specimens with 10 mm SAMI and 20 mm SAMI and 60 mm overlay, lower strain are measured and predicted in specimens with SAMIs than in those without SAMIs for SAMIs A and B, while the specimens with sand asphalt as SAMI have greater strain than the control.

Figure 6.21 shows that at 30^{o}C the results are mixed. This is probably due to the high load magnitude and temperature. As observed in the laboratory test, the test carried out using a reduced load of 1.35kN (0.6MPa) at 30^{o}C shows clearly, the crack resistance of SAMI against reflective cracking. Generally, it can be seen from the measured and predicted strains at 20mm from the bottom of the overlay that, although high strain concentration exists around the crack region in the specimens with SAMIs, they are able to isolate the overlay from the strain concentration. This shows the crack resistance potential of the proprietary SAMIs A

and B. Also, it can be seen from the results that greater strains are predicted in the debond cases than the full bond cases.

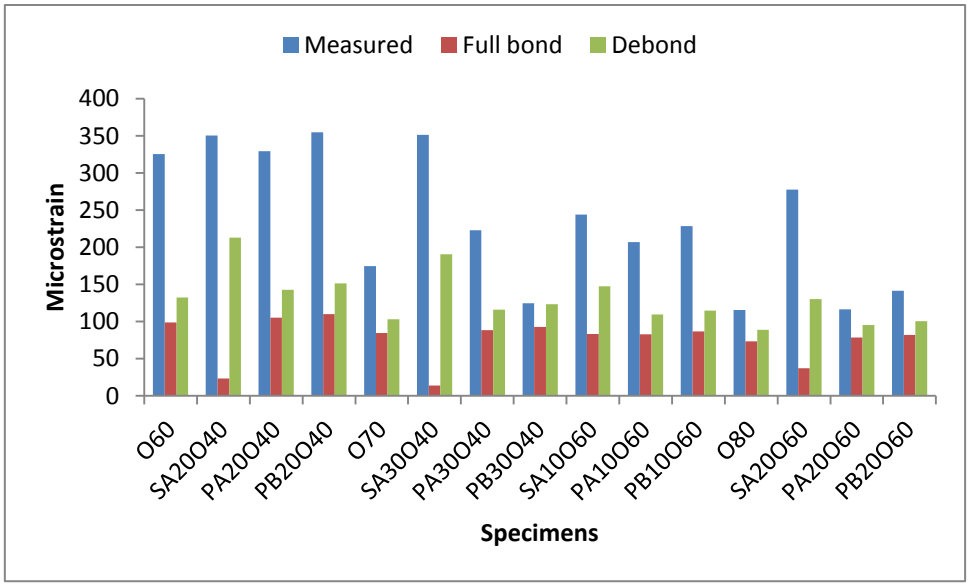

Figure 6.14: Strain at 4 mm above the crack top at 10°C

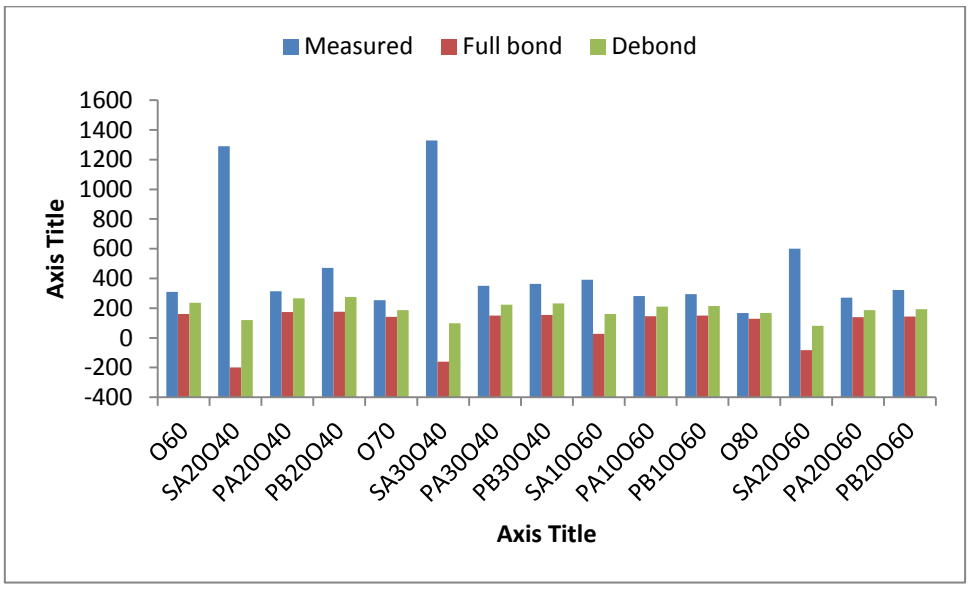

Figure 6.15: Strain at 4 mm above the crack top at 20°C

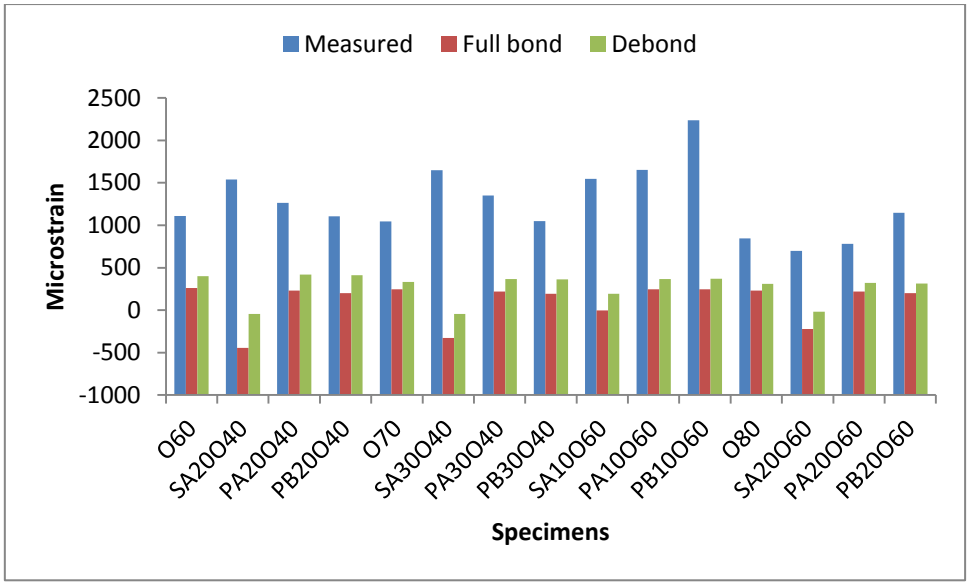

Figure 6.16: Strain at 4 mm above the crack top at 30°C

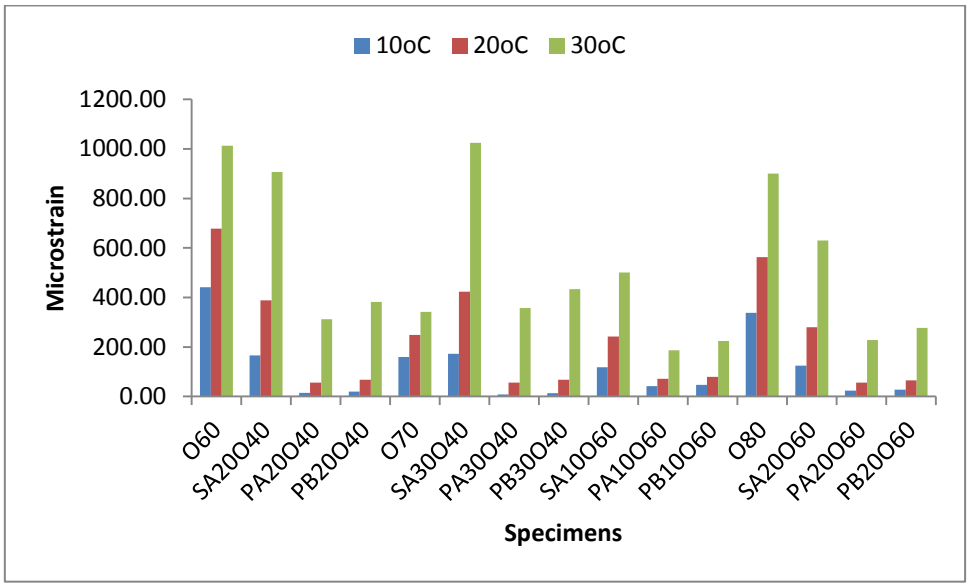

Figure 6.17: Strain at the bottom of the overlay (Full Bond)

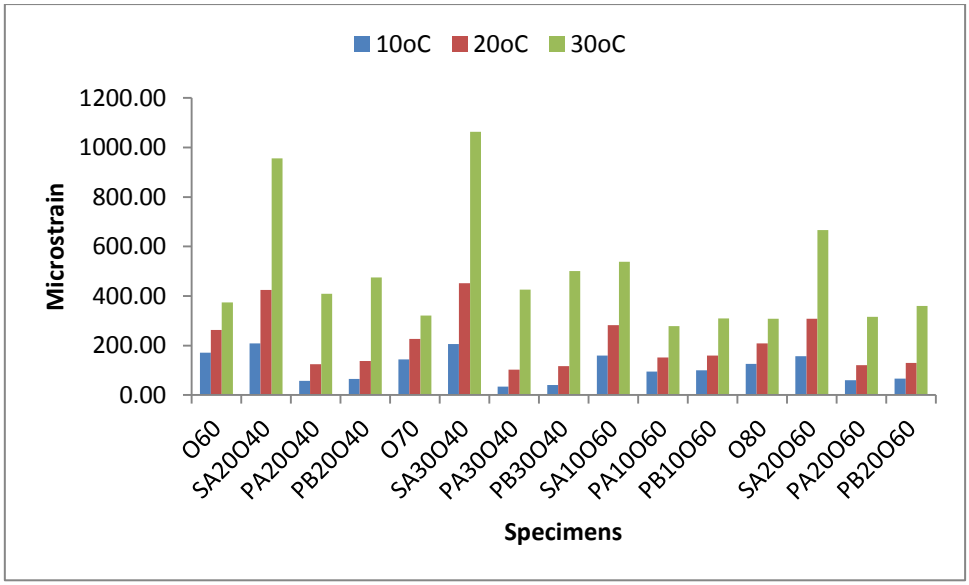

Figure 6.18: Strain at the bottom of the overlay (Debond)

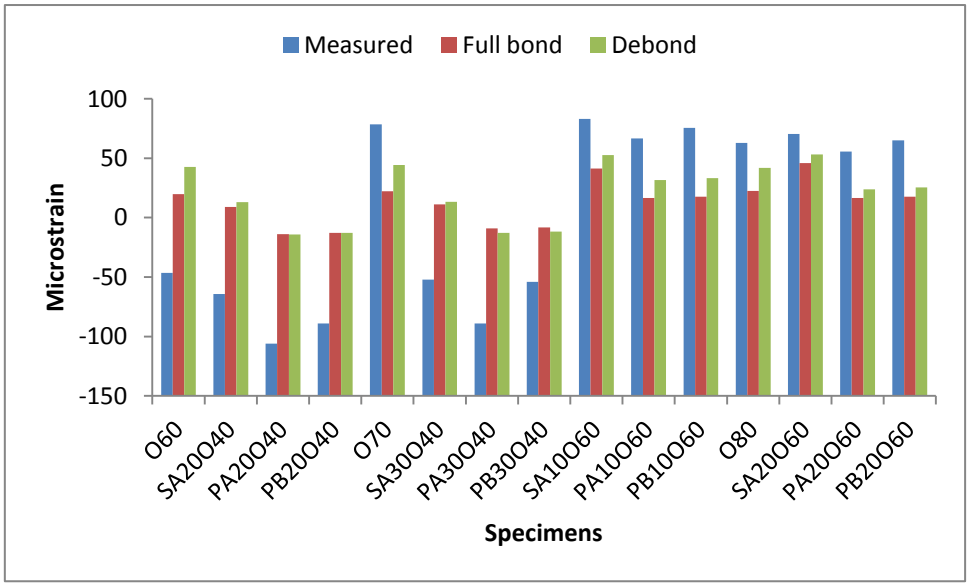

Figure 6.19: Strain at 20 mm from the bottom of the overlay at 10°C

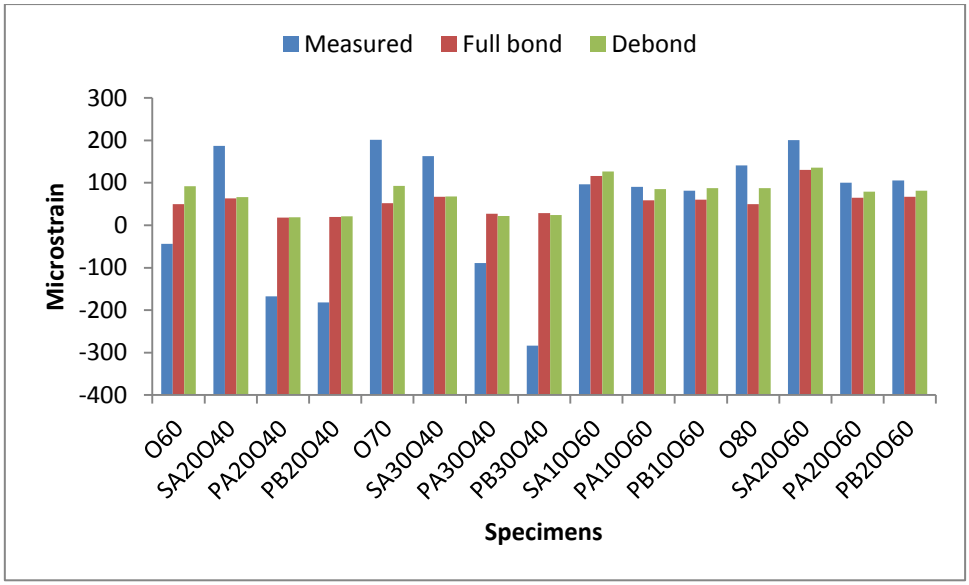

Figure 6.20: Strain at 20 mm from the bottom of the overlay at 20°C

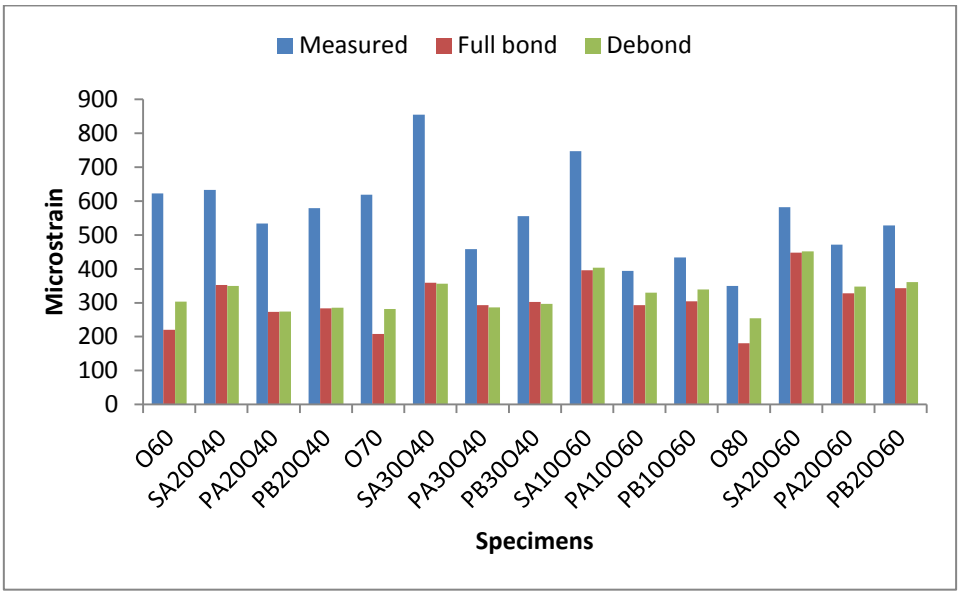

Figure 6.21: Strain at 20 mm from the bottom of the overlay at 30°C

6.5.3 Stress

6.5.3.1 Centre load

The contour plots of the longitudinal stresses for the control specimen with 80 mm thick overlay, 20 mm sand asphalt and 60 mm overlay, 20 mm SAMIs A and B and 60 mm overlay with the load placed at the centre directly above the crack tip as shown in Figure 6.9 are

shown in Figures 6.22, 6.23, 6.24 and 6.25, respectively. It can be seen from the figures the potential of SAMIs to relieve stress in the overlay.

Figure 6.26 and 6.27 show that when the load was placed at the centre, the tensile stresses predicted at 4 mm above the crack top in the specimens with SAMIs are smaller than the ones without SAMI. Also the figures show that unlike all the other specimens, the specimens with sand asphalt as SAMI are in compression. This is because of the very low stiffness of the sand asphalt, which shows the pavement might be susceptible to permanent deformation. Again, Figures 6.28 and 6.29 show that when the load was placed at the centre, the tensile stresses predicted at the bottom of the overlay of the specimens with proprietary SAMIs A and B are smaller than the tensile stresses predicted at the bottom of the overlay of their respective control specimens, while for the specimens with sand asphalt as SAMI, the tensile stresses predicted at the bottom of the overlay are greater than the ones for the specimens without SAMI. This agrees with the wheel tracking test which shows that the specimen with proprietary SAMIs A and B were able to retard reflective cracking indicating both SAMIs are able to isolate the overlay from the stress/strain concentration at the crack tip, while the extreme low stiffness of sand asphalt inhibits its crack resistance ability. As observed by Kim and Buttlar (2002), the primary benefit of a soft interlayer is to reduce the longitudinal stresses in the overlay caused by wheel load and/or thermal cycling. It is evident in this study, that the SAMIs are able to reduce the tensile stress transferred to the overlay from stress concentration generated around the crack region by traffic loading.

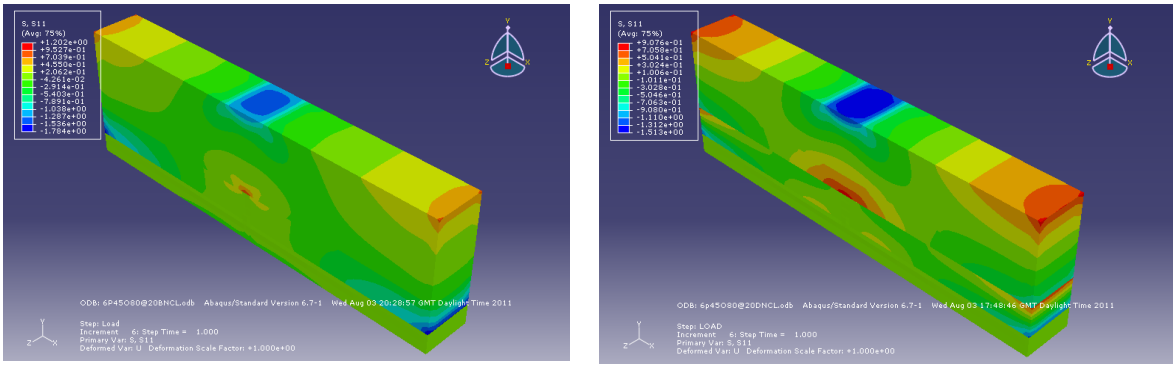

(a) **(b)**

Figure 6.22: 80 mm Overlay at 20°C with centre load (O80) (a) Full bond (b) Debond

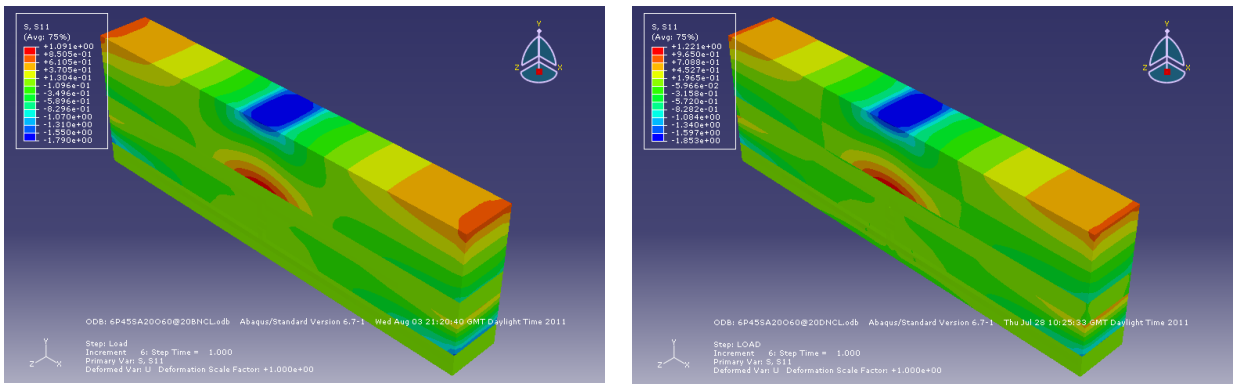

(a) **(b)**

Figure 6.23: 20 mm sand asphalt with 60 mm Overlay at 20°C with centre load (SA20O60) (a) Full bond (b) Debond

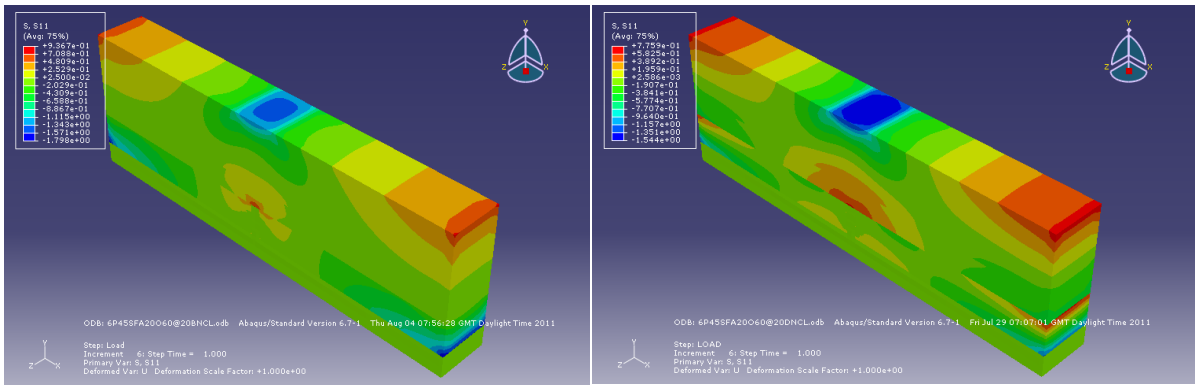

(a) **(b)**

Figure 6.24: 20 mm proprietary SAMI A with 60 mm Overlay at 20°C with centre load (PA20O60) (a) Full bond (b) Debond

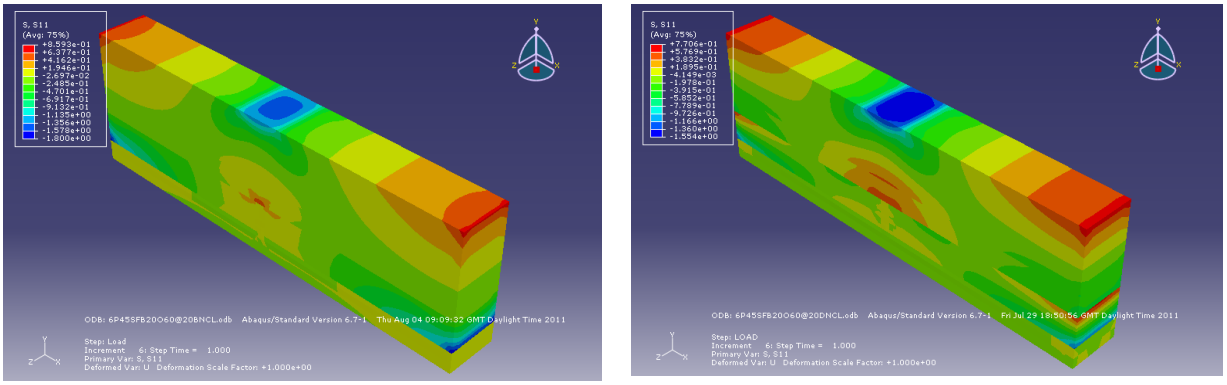

(a) **(b)**

Figure 6.25: 20 mm proprietary SAMI B with 60 mm Overlay at 20°C with centre load (PB20O60) (a) Full bond (b) Debond

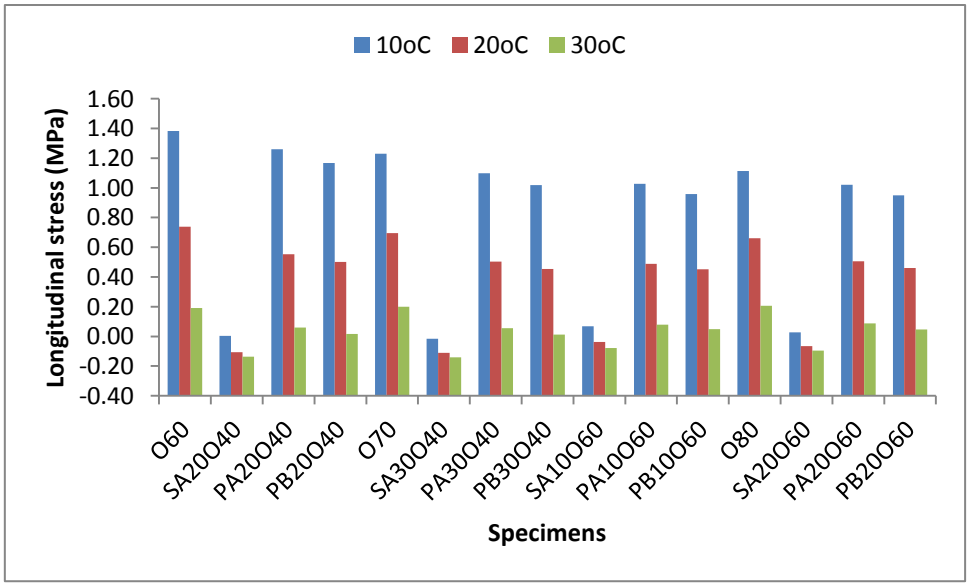

Figure 6.26: Longitudinal stress at crack tip at 10°C, 20°C and 30°C with the load placed at the centre (Full bond)

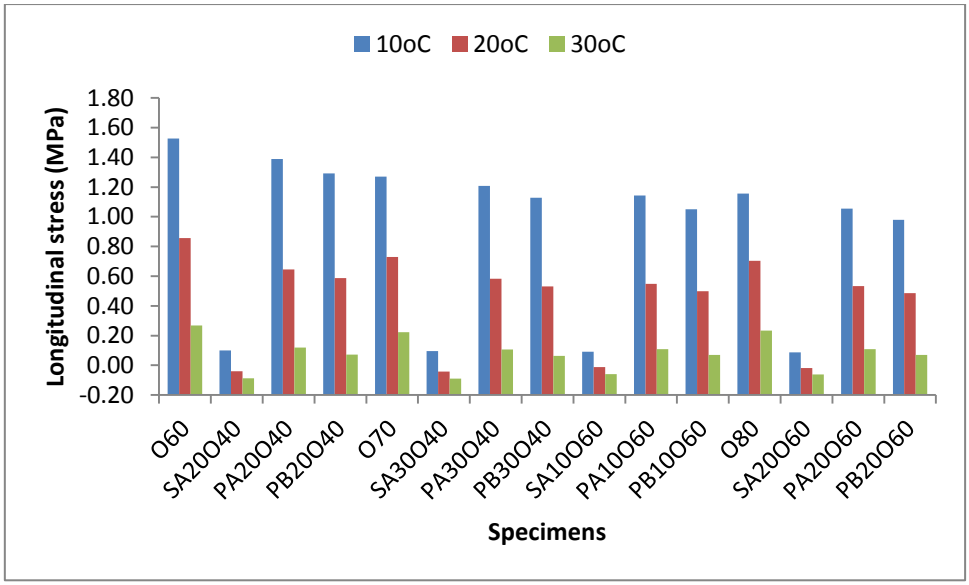

Figure 6.27: Longitudinal stress at crack tip at 10°C, 20°C and 30°C with the load placed at the centre (Debond)

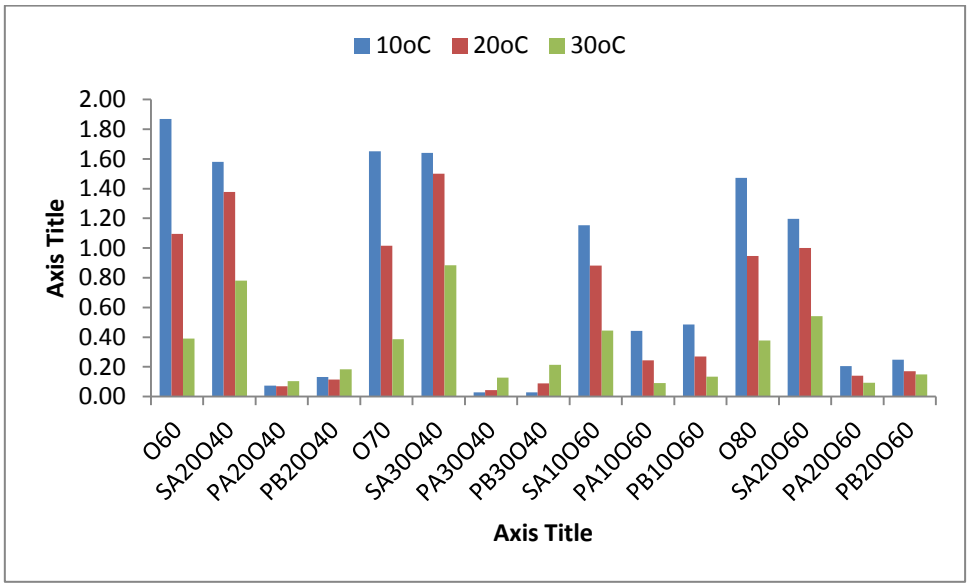

Figure 6.28: Longitudinal stress at bottom of overlay at 10°C, 20°C and 30°C with the load placed at the centre (Full bond)

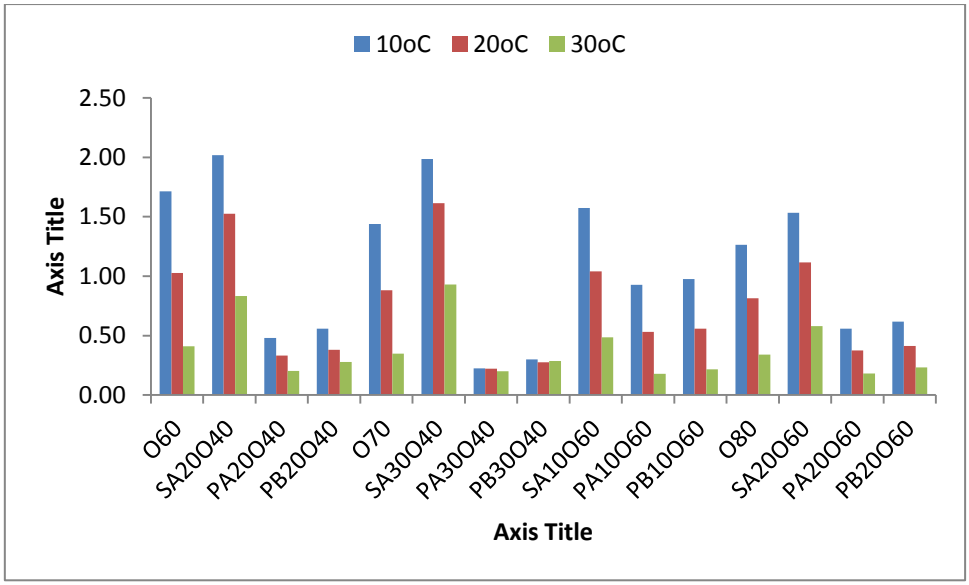

Figure 6.29: Longitudinal stress at bottom of overlay at 10°C, 20°C and 30°C with the load placed at the centre (Debond)

6.5.3.2 Edge load

The contour plots of the longitudinal stresses for the control specimen with 80 mm thick overlay, 20 mm sand asphalt and 60 mm overlay, 20 mm SAMI A and B and 60 mm overlay with the load placed at the edge (90mm from the centre) as shown in Figure 6.10 are shown in Figures 6.30, 6.31, 6.32 and 6.33, respectively. Figures 6.34 and 6.35 show the longitudinal stresses at 4mm above the crack top when the load was placed at the edge. It can be seen from Figure 6.34 that for the bonded case at 10°C and 20°C, the crack top is in compression when the SAMI is sand asphalt, while it is in tension when proprietary SAMIs A and B are used. However, for all the specimens in tension, the tensile stresses predicted at the bottom of the overlay are smaller than those predicted in the specimens with no SAMI. At 30°C, the crack top was in compression for all the specimens modelled. Figure 6.35 indicates that the predicted strains at 4 mm above the crack top are either in compression or tension.

Figures 6.36 and 6.37 show the longitudinal stresses at the bottom of the overlay when the load was placed at the edge. The mixed results observed when the load was placed at the edge

is because the major stress responsible for crack initiation and propagation in this case is the shear stress generated by the relative movement of the cracked pavement.

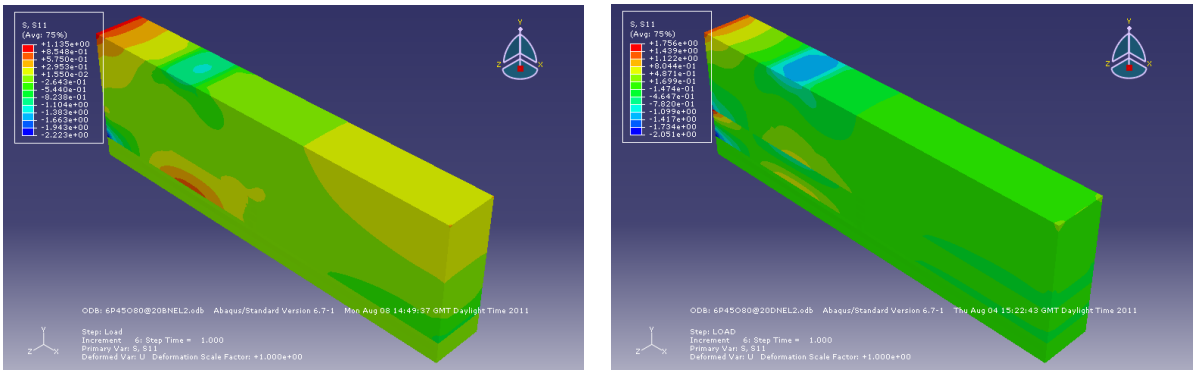

(a) **(b)**

Figure 6.30: 80 mm Overlay at 20°C with edge load (O80) (a) Full bond (b) Debond

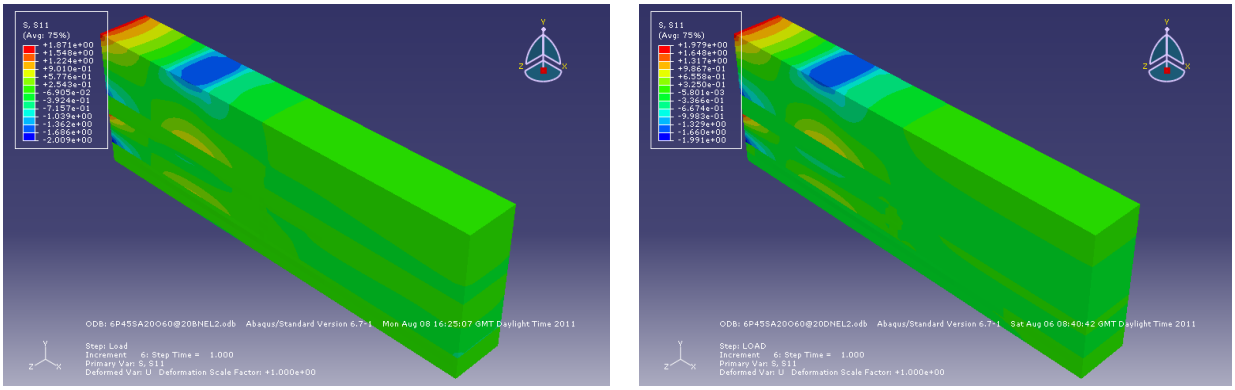

(a) **(b)**

Figure 6.31: 20 mm sand asphalt with 60 mm Overlay at 20°C with edge load (SA20O60) (a) Full bond (b) Debond

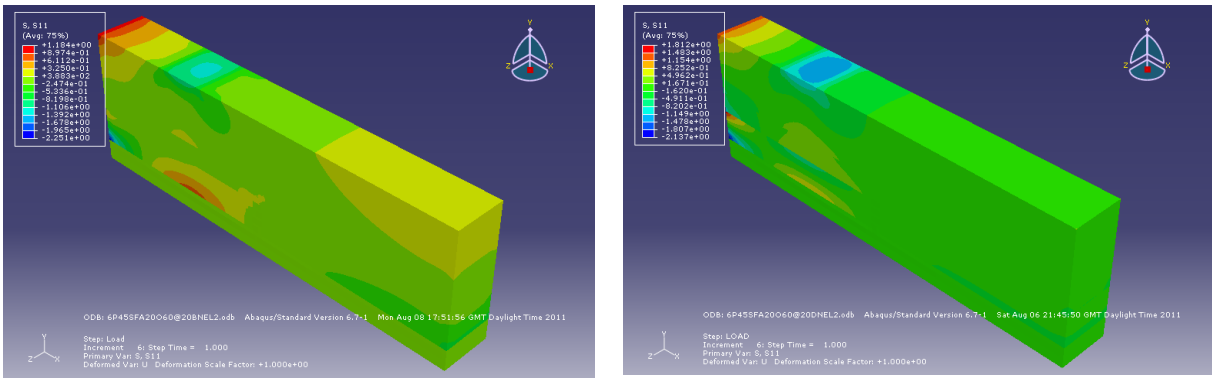

(a) **(b)**

Figure 6.32: 20 mm proprietary SAMI A with 60 mm Overlay at 20°C with edge load (SA20O60) (a) Full bond (b) Debond

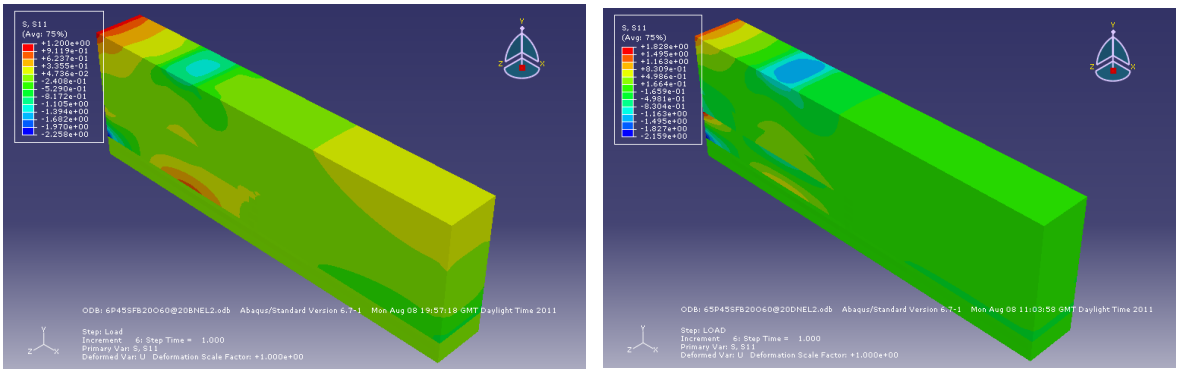

(a) (b)

Figure 6.33: 20 mm proprietary SAMI B with 60 mm Overlay at 20°C (SA20O60) (a) Full bond (b) Debond

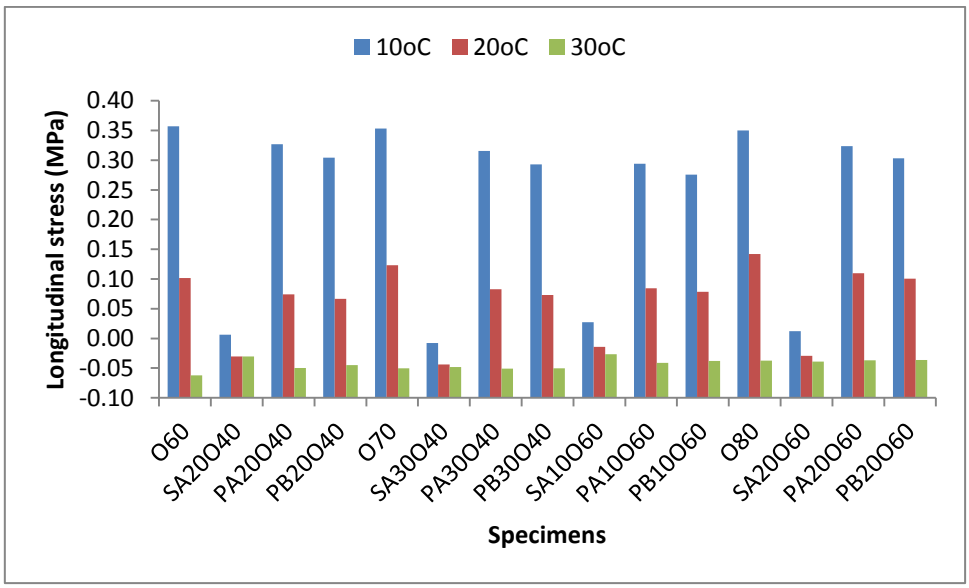

Figure 6.34: Longitudinal stress 4 mm above the crack top at 10oC, 20oC and 30°C with the load placed at the edge (Full bond)

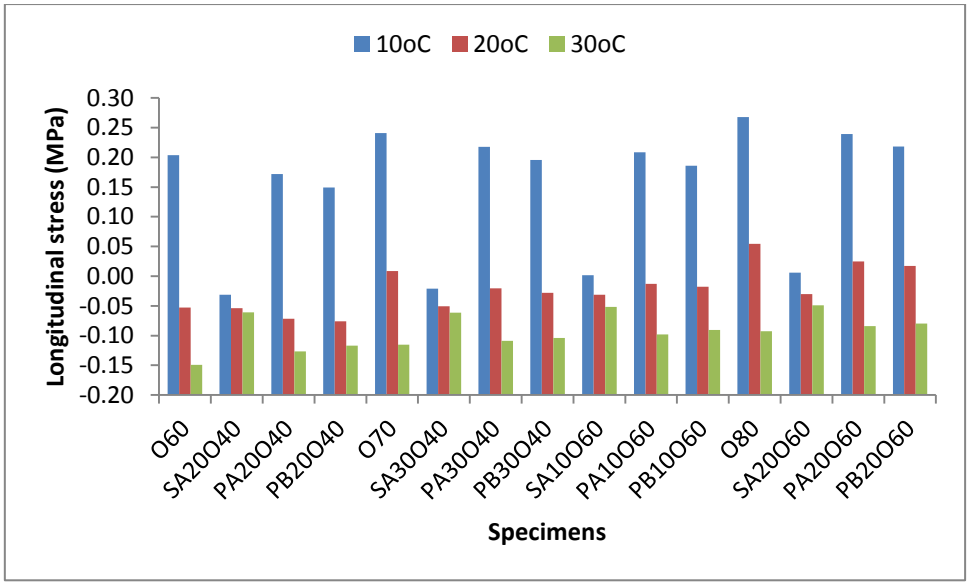

Figure 6.35: Longitudinal stress 4 mm above the crack top at 10°C, 20°C and 30°C with the load placed at the edge (Debond)

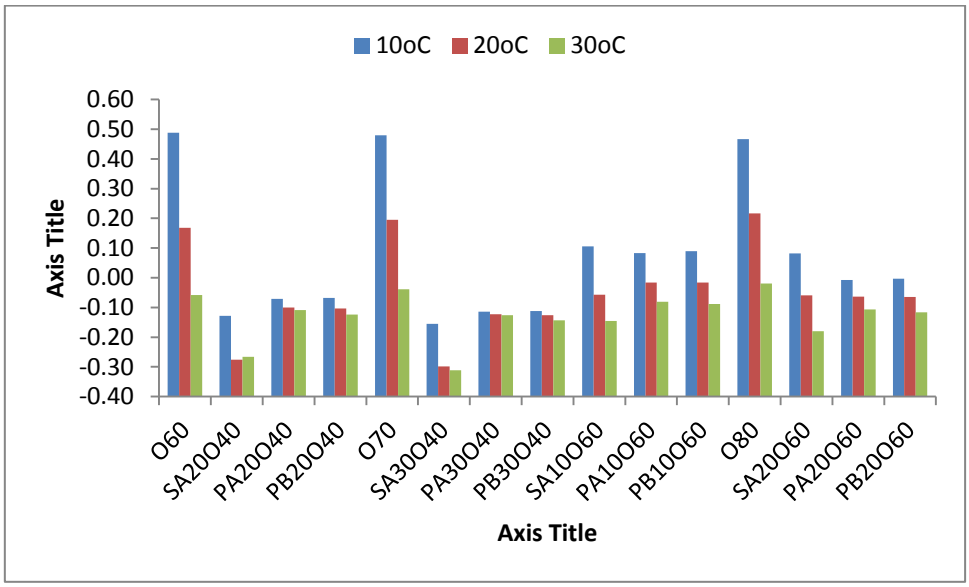

Figure 6.36: Longitudinal stress at bottom of overlay at 10°C, 20°C and 30°C with the load placed at the edge (Full bond)

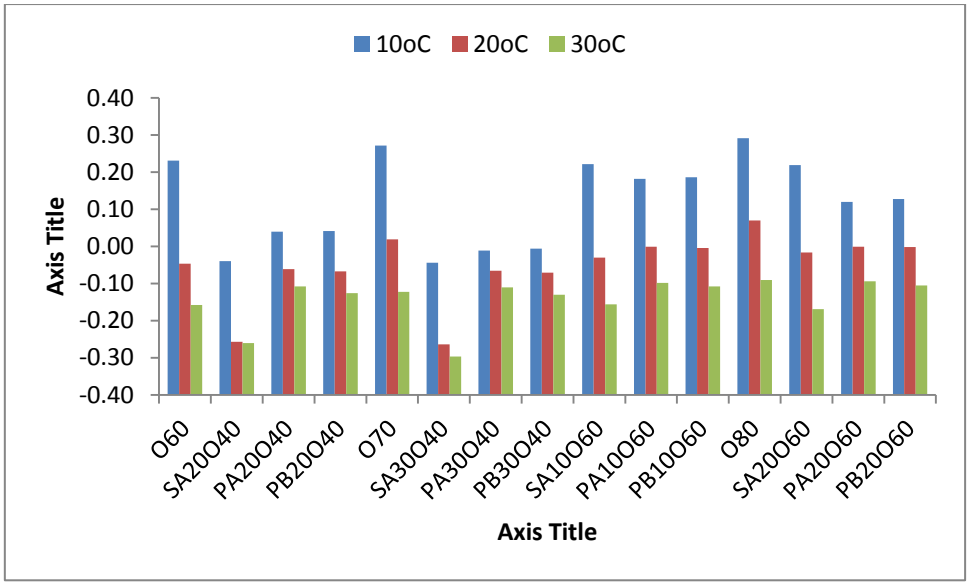

Figure 6.37: Longitudinal stress at bottom of overlay at 10°C, 20°C and 30°C with the load placed at the edge (Debond)

6.6 Conclusions

The following conclusions can be drawn from the finite element analysis:

- The results show that when SAMIs are introduced in cracked pavements to retard reflective cracking, greater deflection of the pavement occurs. This is due to the reduced axial/bending stiffness of the pavement caused by the introduction of SAMIs of lower stiffness than the overlay between the overlay and the existing pavement.
- The finite element analysis shows that the specimens (models) with greater SAMI thickness have greater deflection, which may imply less life to failure. This indicates that lower SAMI thickness gives better performance.
- The study shows that greater deflections, stresses and strains are predicted in the specimens with debond (slip between the SAMI and the base layer), which implies less crack resistance of the SAMIs in this condition, but because crack propagation was not modelled, the effect of the slip on the SAMIs' performance could not be quantified.

- The finite element analysis shows that although SAMIs are required to have lower stiffness than the overlay, an optimum stiffness exists below which the SAMIs are not able to retard reflective cracking.
- Lastly, it is clear from the finite element analysis that the predictions are good when compared with the measured results. This shows that the wheel tracking test did more or less what it was intended to do.

REFERENCES

Abaqus Theory Manual (2007): Abaqus Theory Manual, Dassault Systemes, U.S.A.

Baek J. and Al-Qadi (2008): Mechanism of Overlay Reinforcement to Retard Reflective Cracking under Vehicular Loading. Proceedings of 6th International RILEM Conference, Chicago, U.S.A. 563-573.

Dave E.V., Braham A.F., Buttlar W.G., Paulino G.H. and Zofka A. (2008): Integration of Laboratory Testing, Field Performance Data and Numerical Simulations for the Study of Low-Temperature Cracking. Proceedings of 6th International RILEM Conference, Chicago, U.S.A. 369-378.

Kim J. and Buttlar W.G. (2002): Analysis of Reflective Crack Control System Involving Reinforcing Grid over Base-Isolating Interlayer Mixture. Journal of Transportation Engineering. 375-384.

Minhoto M.J.C, Pais J.C. and Pereira P.A.A (2008): Reflective Cracking Behaviour for Traffic and Temperature Effects. Proceedings of 6th International RILEM Conference, Chicago, U.S.A. 551-561.

Pais J.C. and Pereira P.A.A. (2000): Predictions of Existing Reflective Cracking Potential of Flexible Pavements. Proceedings of 4th International RILEM Conference, Ontario, Canada. 155-164.

Sousa, J., Pais, J., Saim, R., Way, G., and Stubstad, R. (2001): Development of a Mechanistic Overlay Design Method Based on Reflective Cracking Concepts. Final Report for Rubber Pavements Association, Consulpav International.

Wu R.Z. and Harvey J.T. (2008): Evaluation of Reflective Cracking Performance of Asphalt Mixes with Asphalt Rubber Binder using HVS Tests and Non-local Continuum Damage Mechanics. Proceedings of 6th International RILEM Conference, Chicago, U.S.A. 3-12.

7 PAVEMENT TEST FACILITY

7.0 Introduction

Although, small-scale laboratory tests have been used successfully to evaluate the performance of materials and mixtures, it is not practicable to implement laboratory findings directly in the field without field or large-scale testing. This is because the field conditions cannot entirely be replicated or simulated at small scale. To bridge the gap, it is necessary to carry out field or accelerated pavement testing. Accelerated pavement testing is generally defined as the application of wheel loads to a specially constructed or in-service pavement to determine response and performance under a controlled and accelerated accumulation of damage in a short period of time (Saeed and Hall, 2003). Because of time and resources (equipment, money etc) available for this study, pavement test facility (PTF), a large scale wheel tracking test located at the Nottingham Transportation Engineering Centre, University of Nottingham laboratory was selected for this study.

This is a half scale test capable of applying a maximum wheel load of 12kN. Therefore, the pavement for the study was designed such that the failure of the pavement (appearance of crack at the surface of the overlay) would occur within a reasonable number of wheel load repetitions.

7.1 Pavement Test Facility device

The pavement test facility was developed at the University of Nottingham about three decades ago. It was developed for the purpose of assessing the performance of asphalt materials to generate data for the design of pavements. It is made up of the following: reaction beams that provide the necessary reaction for any lateral position of the loading frame and the main beam; the load carriage used to mount the guide bearings and wheel

loading assembly; the cable system which consists of an 8mm cable wound around a 150mm drum; the hydraulic system which consists of a hydraulic power pack (oil pump), hydraulic motor and a servo valve; and the feedback transducers and electronic control system used to monitor the carriage speed, carriage position and the wheel load (Brodrick, 1977). The pavement test facility is shown in Figure 7.1. The wheel movement is controlled by the hydraulic motor which pulls the cable (steel ropes) in both directions (forward and backward). It was designed to apply a load magnitude of up to 12kN and maximum speed of 14.5 km/hr. The PTF pavement has length, width and depth of 5.0 m, 2.4 m and 1.5m, respectively.

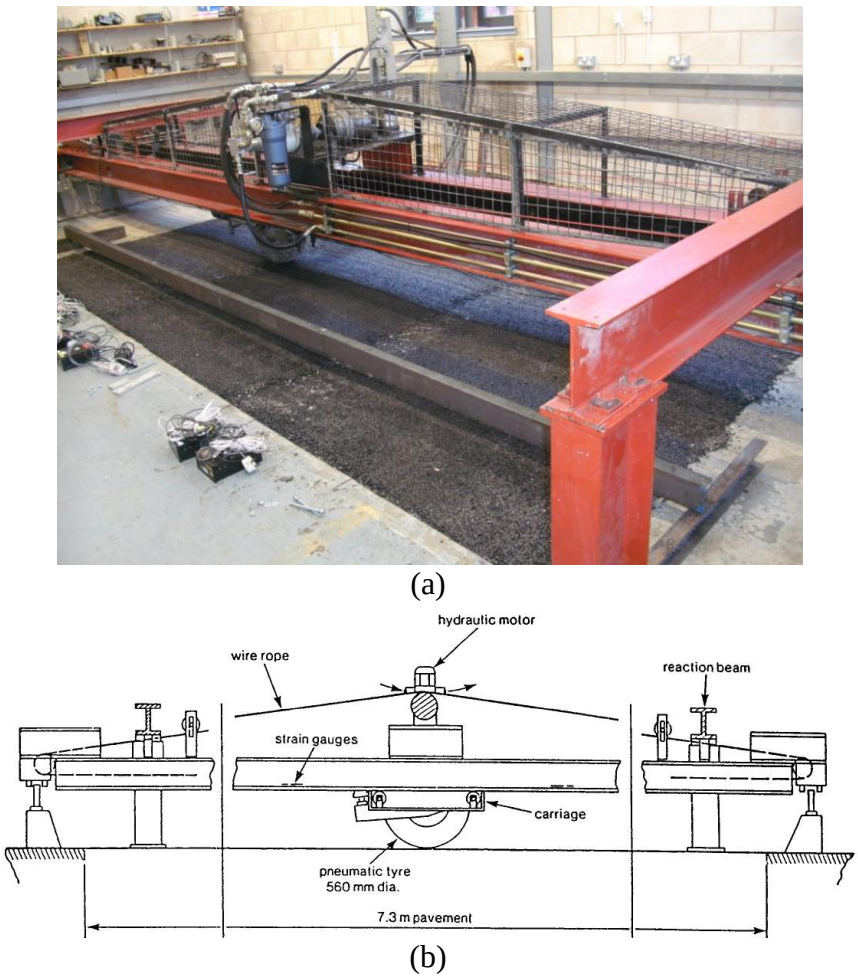

Figure 7.1: Pavement test facility (a) Photograph (b) Schematic of the PTF side view (Brown and Brodrick, 1981)

7.2 Material properties

The materials used for the construction of the pavement were clay subgrade, crushed rock subbase material, proprietary SAMIs A, C and D as SAMIs and 10 mm asphalt concrete with 40/60 penetration grade bitumen for the base and surface layers (overlay). The properties of the SAMIs have been detailed in Chapter three, while properties of the clay subgrade, subbase material and the 10mm asphalt concrete are presented here.

7.2.1 Subgrade and subbase layers

The strength of the subgrade and subbase layers was determined using the Dynamic Cone Penetrometer (DCP). The DCP has an 8kg weight dropping through a height of 575 mm and a 60^{o} cone having a diameter of 20 mm (see Figure 7.2). The result of the DCP test showing the layers is shown in Figure 7.3. The California bearing ratio (CBR) was determined from the DCP data using the software UK DCP version 3.1 described by Done and Piouslin (2006). Also, the approximate stiffness of the sections was calculated from equation 7.1 reported by Powell et al (1984). The California bearing ratio (CBR) and the stiffness values are shown in Table 7.1. The subgrade has average CBR and stiffness of 1.5% and 22.5MPa, respectively, while the subbase has average CBR and stiffness of 17% and 106MPa, respectively.

$$E = 17.6CBR^{0.64} \quad \text{..... (7.1)}$$

Figure 7.2: Dynamic cone penetrometer

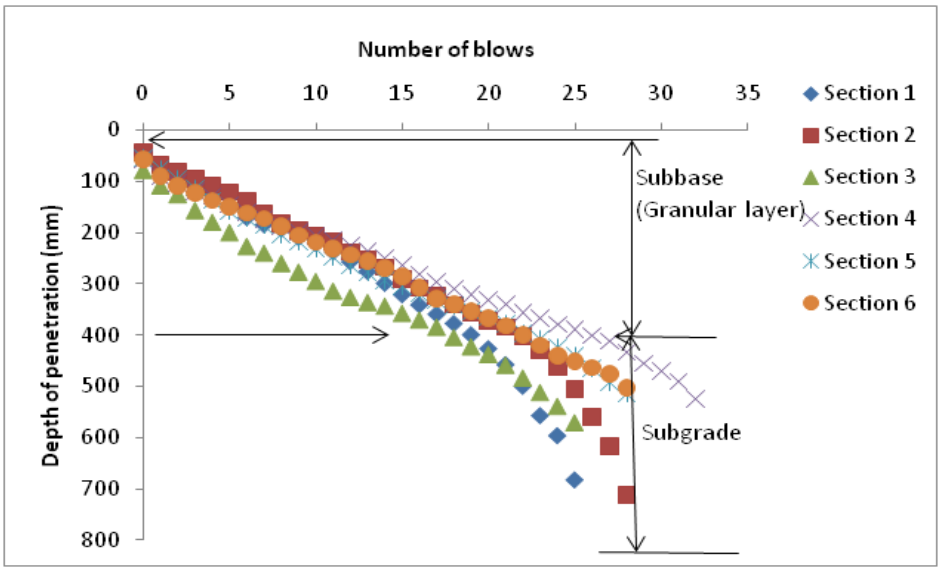

Figure 7.3: DCP test results

Table 7.1: CBR and stiffness of subgrade and subbase

Sections	Subgrade		Subbase	
	CBR (%)	Stiffness (MPa)	CBR (%)	Stiffness (MPa)
1	1	17.6	14	96.29
2	2	27.4	16	103.79
3	2	27.4	15	99.59
4	1	17.6	21	123.52
5	2	27.4	17	107.89
6	1	17.6	17	107.89
Average	1.5	22.5	17	106

7.2.2 Base and the surface (overlay) layers

The base and the surface layers as earlier stated were made of 10 mm asphalt concrete with 40/60 penetration grade bitumen. The asphalt was supplied by Cliffe Hill Quarry, Leicester. Specimens for testing were prepared by reheating some of the asphalt and compacting at 130^{o}C into a 305 mm × 305 mm × 130 mm mould to a thickness of 60 mm using a roller compactor. Five cores of diameter 100 mm and trimmed thickness 40 mm were cored from each slab. The indirect tensile stiffness modulus (ITSM) test, indirect tensile fatigue test (ITFT) and repeated load axial test (RLAT) were carried out. The procedures for the indirect tensile stiffness modulus (ITSM) test, indirect tensile fatigue test (ITFT) and repeated load axial test (RLAT) were described in sections 3.5.3, 3.5.4 and 3.5.5, respectively. The air voids and ITSM results at 10^{o}C, 20^{o}C and 30^{o}C are shown in Table 7.2. The fatigue line of the mixture and the repeated load axial test results are shown in Figures 7.4 and 7.5, respectively. These show that it has good fatigue characteristic and resistance to permanent deformation. As shown in Figure 7.5, the permanent strain at 1800 load applications was 0.9373. The results show the asphalt properties do not differ much from the mix produced in the laboratory.

Table 7.2: Indirect stiffness modulus test and air void results

Specimens	1	2	3	4	5	Average
Air voids(%)	8.00	7.79	7.97	7.50	7.54	7.76
ITSM at 10^{o}C	8106	7475	7178	7299	7661	7544
ITSM at 20^{o}C	4711	4313	3574	4261	4261	4224
ITSM at 30^{o}C	2281	2239	1923	2001	2215	2132

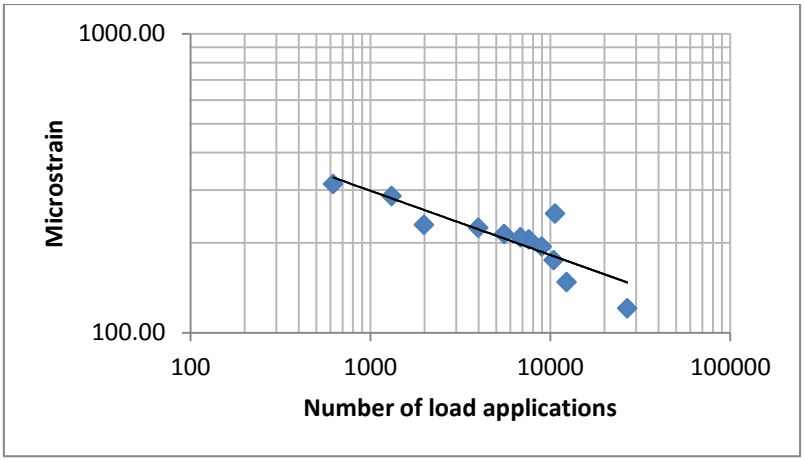

Figure 7.4: Fatigue line of the asphalt

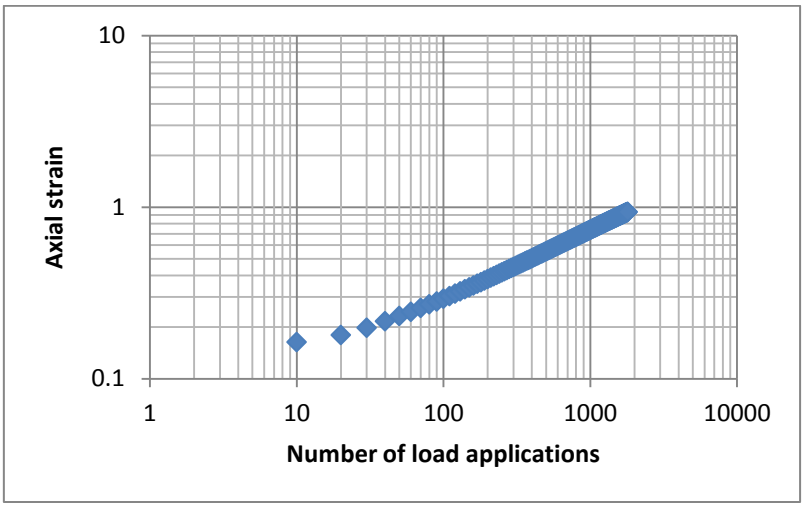

Figure 7.5: Repeated load axial test results

7.3 PTF pavement construction

The existing granular materials in the PTF were removed to the clay subgrade (with a capping of fine sand) as shown in Figure 7.6. Crushed rock subbase material supplied by Midland Quarry Products, Leicester was spread and compacted with a vibrating plate (see Figure 7.7) in three layers to a thickness of 400 mm as shown in Figure 7.8. The first and second layers of the subbase were compacted to a thickness of 130 mm, while the third layer was compacted to a thickness of 140 mm. The strength of the prepared granular layer and the subgrade was determined using a dynamic cone penetrometer (see figure 7.2). The results were reported in section 7.2.1.

Figure 7.6: PTF Subgrade and capping

Figure 7.7: Vibrating plate

Initially, the plan was to use a 40 mm thick 10 mm asphalt concrete with 10/20 penetration grade bitumen as the base, as in the small wheel tracking test reported in chapter five, but this could not be achieved because of difficulties in both supply and, potentially, compaction (because of rapid cooling of the mixture). Therefore, 10mm asphalt concrete with 40/60 penetration grade bitumen supplied by Cliffe Hill Quarry, Leicester was laid and compacted

using a pedestrian roller (See Figure 7.9) at a thickness of 60 mm instead of the 40 mm earlier planned for the base, as shown in Figure 7.10.

To create the crack, the pavement was divided into six sections as shown in Figure 7.11. Transverse cracks were created at the centre of each section by cutting the full depth of the asphalt concrete (simulating existing pavement). The cut thickness was about 5 mm (thickness of the blade). Also, to study the situation where cracks are closely-spaced in the field, cracks were created at 200 mm from the end and at the end of each section. A diagram of the cuts (cracks) and the PTF base layer with the cuts are shown in Figures 7.12 and 7.13, respectively.

The SAMI for sections 1 and 3 was proprietary SAMI A compacted to thicknesses of 10 mm and 5 mm, respectively (see Figure 7.14). The aggregates and binders for proprietary SAMI A were batched and heated at a temperature of 180^{o}C, and compacted at a temperature of 150^{o}C using a vibrating hammer (Kango) shown in Figure 7.15. The SAMI layer for sections 4 and 6 were proprietary SAMIs C and D, respectively. Proprietary SAMIs C and D were prepared by sandwiching 60 mm glass fibre strands between layers of bitumen emulsion, and 6 mm aggregates were compacted on top using a vibrating plate. Ordinary bitumen emulsion was used to prepare proprietary SAMI C, while polymer modified emulsion was used for proprietary SAMI D. Sections 2 and 5 were given no treatment (Control). The surface layer (Figure 7.16) was made of 10 mm asphalt concrete with 40/60 penetration grade bitumen. The asphalt (bagged when supplied) was reheated in the laboratory at average temperature of 130^{o}C and compacted using a pedestrian roller (Figure 7.9). The planned pavement structure of sections 1, 2 and 3 is shown in Figure 7.17, while that of sections 4, 5 and 6 is shown in Figure 7.18. However the average thickness actually achieved in the layers of each section is shown in Table 7.3.

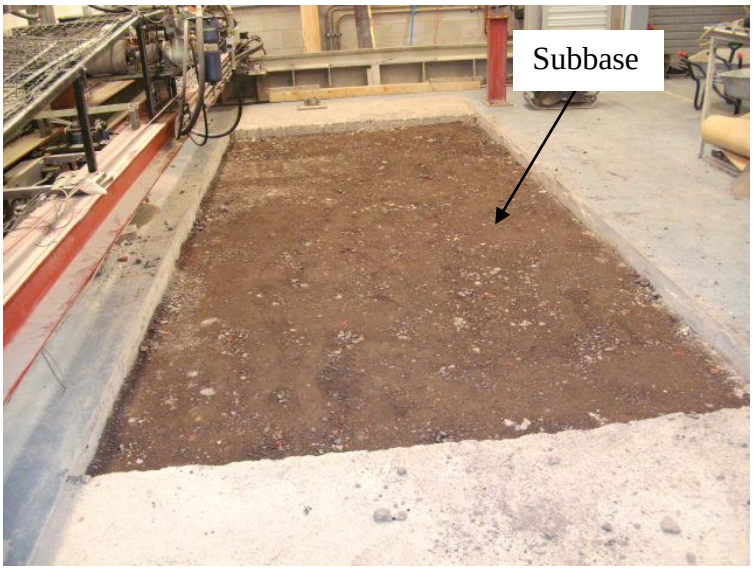

Figure 7.8: PTF granular layer

Figure 7.9: Pedestrian roller

Figure 7.10: PTF base layer

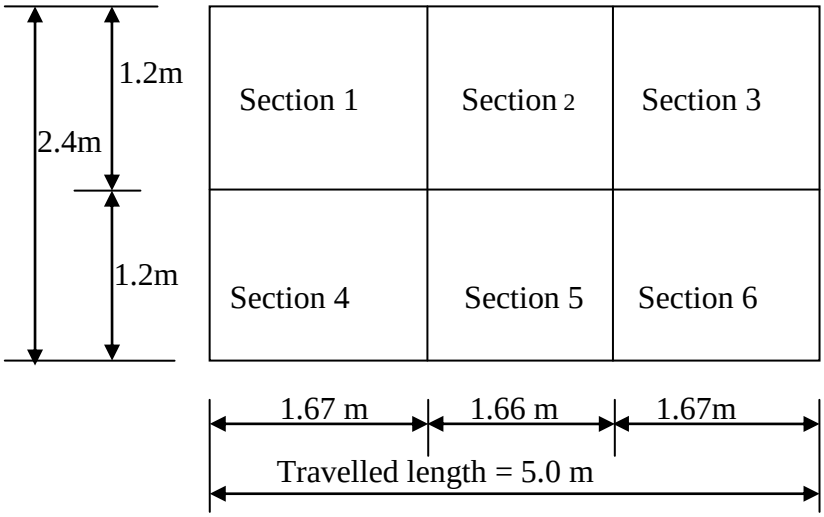

Figure 7.11: Schematic of the PTF pavement sections

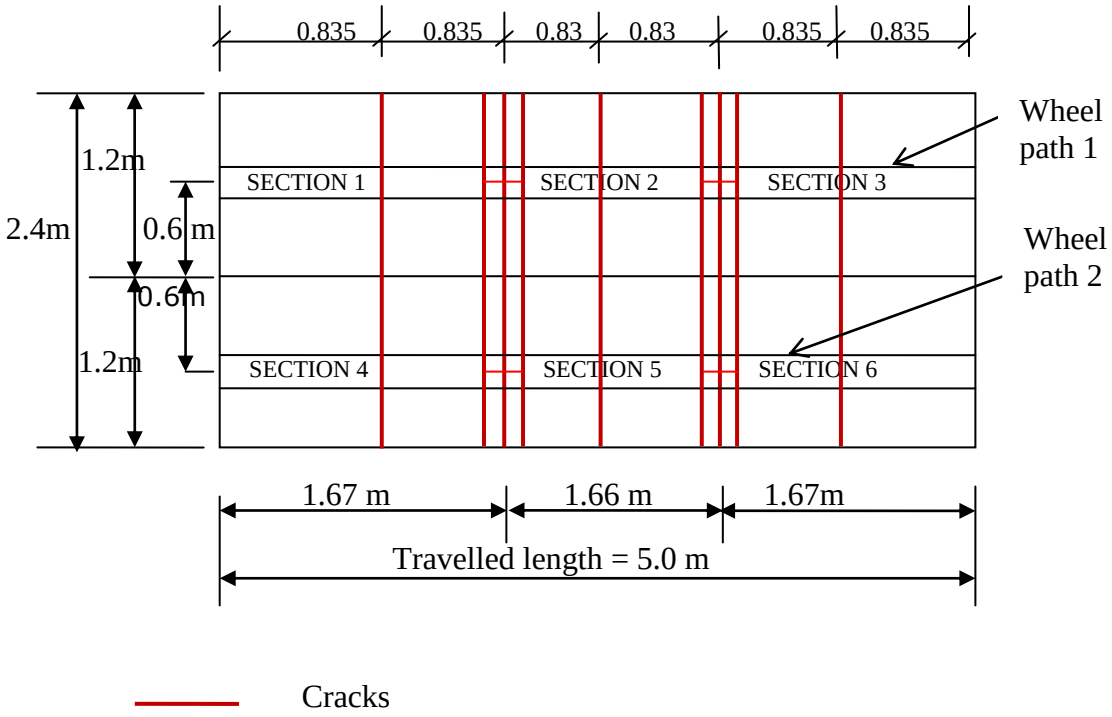

Figure 7.12: Simulated cracks in PTF sections

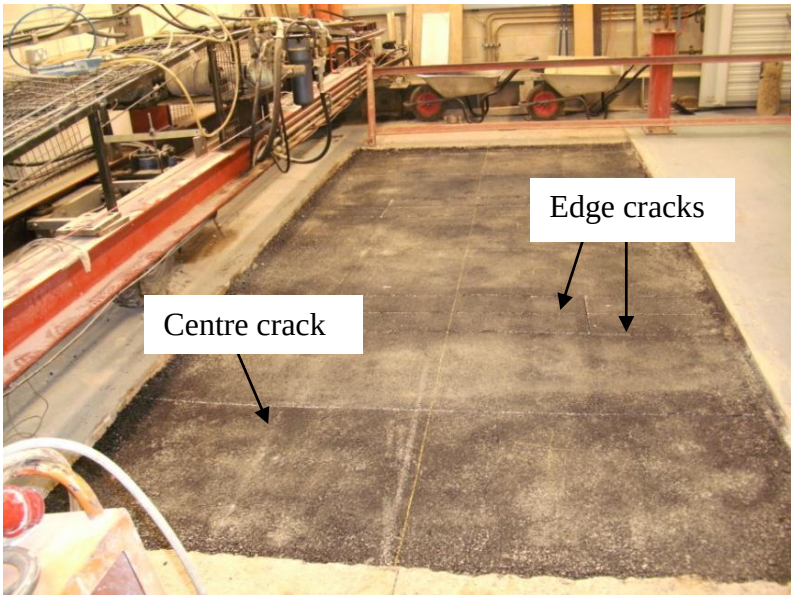

Figure 7.13: PTF base layer with cracks (cuts)

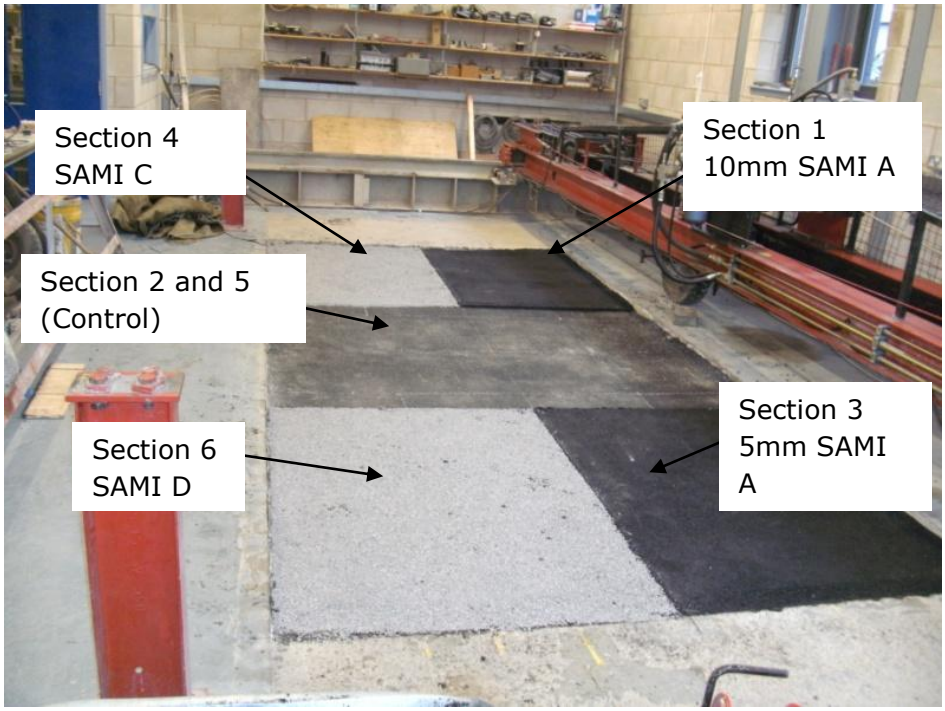

Figure 7.14: PTF SAMIs

Figure 7.15: Vibrating hammer (Kango)

Figure 7.16: PTF surface layer

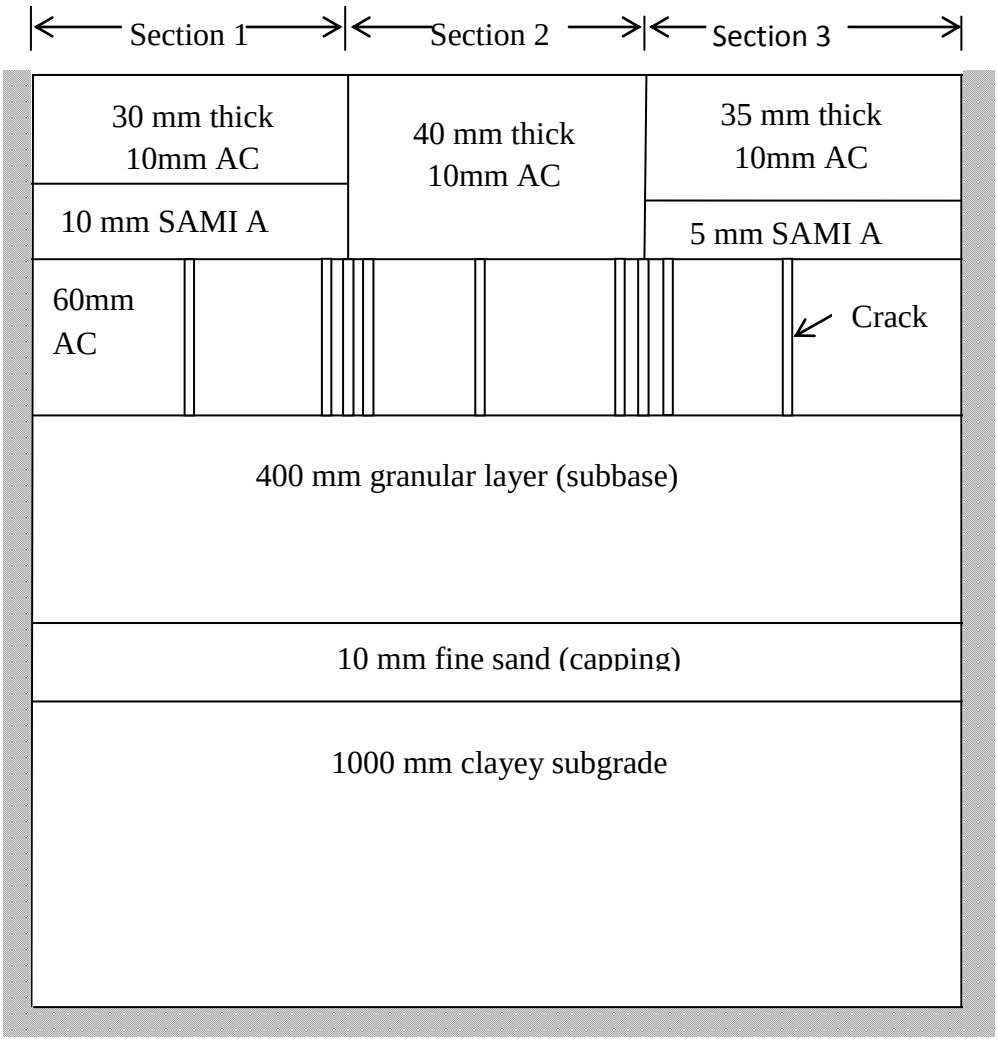

Figure 7.17: Pavement structure for sections 1, 2 and 3

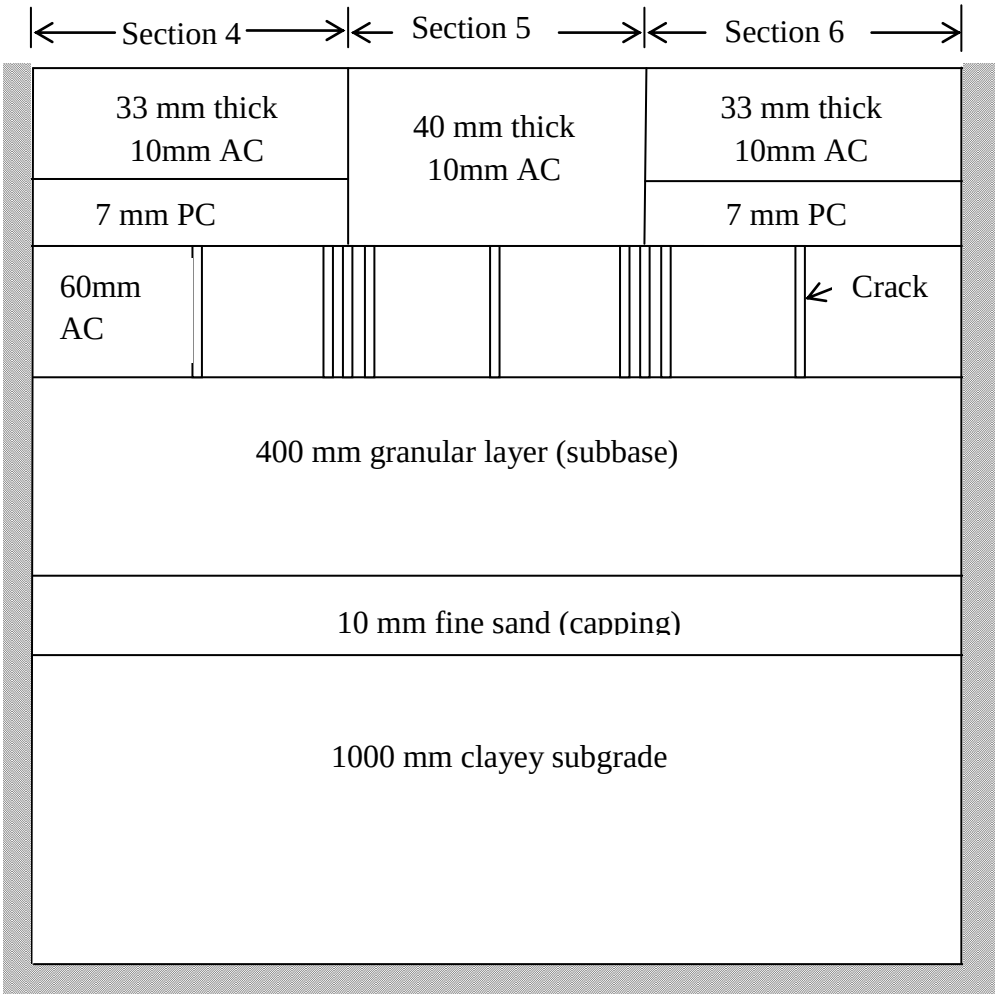

Figure 7.18: Pavement structure for sections 4, 5 and 6

Table 7.3: Layer thickness achieved in the PTF (average of two cores)

Sections	Surface layer (Overlay)	Middle layer (SAMIs)	Base layer (existing pavement)
1	36	15	53
2	53	-	57
3	44	6	55
4	47	7	55
5	57	-	62
6	45	7	51

7.4 PTF instrumentation and trafficking

The measurements taken in this study were the displacement in the crack region, the number of wheel cycles to the first appearance of cracking and to failure, and permanent deformation

of the wheel paths. A long steel channel spanning the entire length of the pavement and resting on another steel channel on the concrete part of the pavement was used to hold two linear variable differential transformers (LVDTs) placed across the crack at the centre of each section to measure the relative displacement as shown in Figure 7.19. The full opening of cracks (cracks opening and closing as the wheel passes) was chosen as the failure criterion.

The pavement was divided into two wheel paths (Figure 7.20). Wheel path one consists of sections 1, 2, and 3, while wheel path 2 consists of sections 4, 5 and 6. The wheel path was painted white to monitor the appearance of cracks on the surface layer (Figure 7.21). The pavement was trafficked using a 9.6kN wheel load at an average speed of 3 km/hr. Initial readings of the LVDTs and the transverse profiles were recorded. The number of wheel repetitions as the wheel load moves forward and backward was logged with the use of an electronic counter. A digital thermocouple was used to monitor the room temperature during the test. The two wheel paths in the pavement were trafficked and the results were analysed.

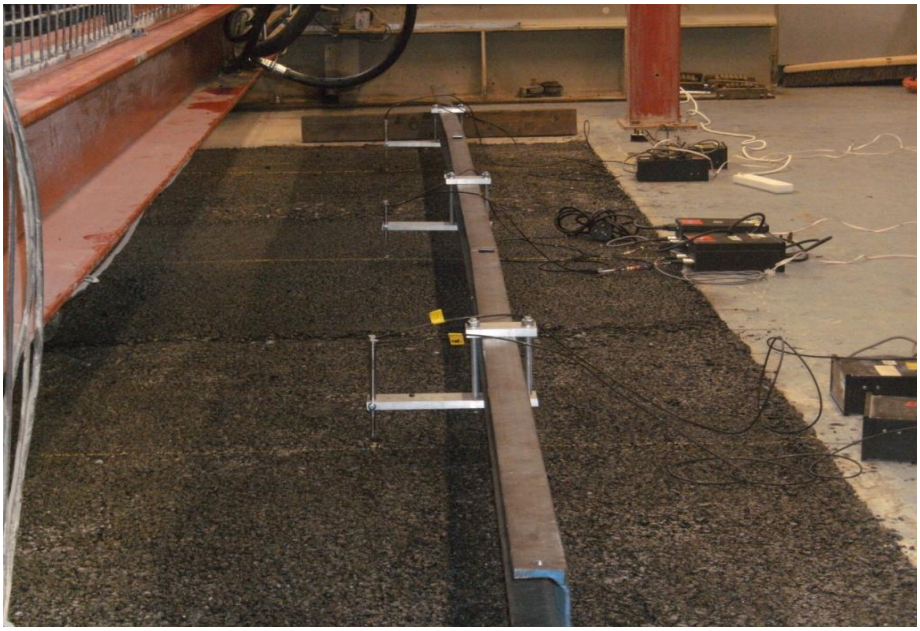

Figure 7.19: LVDTs placed across cracks

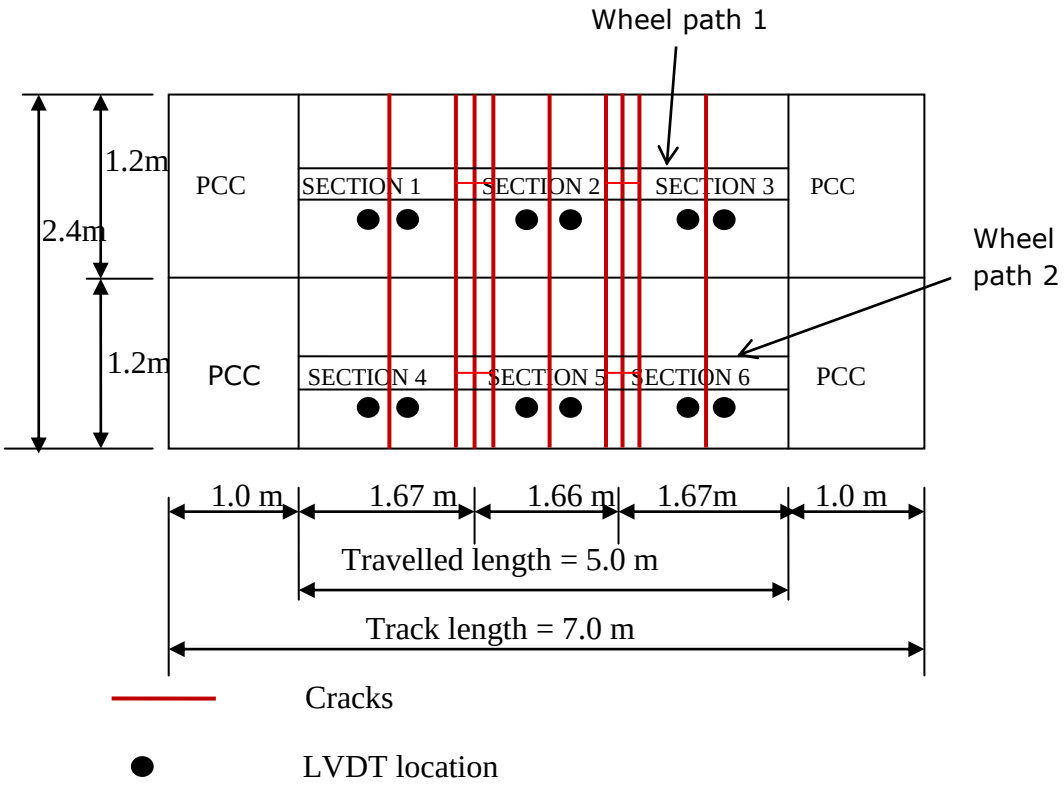

Figure 7.20: Wheel paths and LVDTs' locations

Figure 7.21: Wheel path painted white

7.5 Test results

The trafficking of the two wheel paths was carried out from May to July 2011. The average room temperature in the morning, noon and evening when wheel path one was trafficked were 24^{o}C, 27.1^{o}C and 28.2^{o}C, respectively, while for wheel path 2 the average morning, noon and evening room temperature were 22.7^{o}C, 25.9^{o}C and 26.9^{o}C, respectively. The number of wheel cycles to first appearance of cracking and to failure, relative displacement and permanent deformation results are presented here. Also, cores were taken from the pavement after the test to check the interface bond of the trafficked and non-trafficked areas and the air void and stiffness of the 10 mm asphalt concrete.

7.5.1 Number of wheel cycles to failure

The number of wheel load applications to the first appearance of cracking and to failure for wheel paths 1 and 2 are shown in Tables 7.4 and 7.5, respectively. The tables show that the crack appeared first in the control sections 2 and 5 with no SAMI. Figure 7.22 shows that section 3 with 5 mm thick proprietary SAMI A withstood 63828 wheel load applications before failure, while section 1 with 10 mm thick proprietary SAMI A withstood 31880 before failure. This indicates that section with 5 mm proprietary SAMI A has life before failure twice and 4.5 times that of the sections with 10 mm proprietary SAMI A and control (no SAMI), respectively. This finding agrees with the wheel tracking test which showed that SAMI with lower thickness was more effective. This better performance of the section with 5 mm proprietary SAMI A over the section with 10 mm proprietary SAMI A is thought to be due to reduced flexural bending of the surfacing layer that accompanies the use of lower SAMI's thickness. It can be seen in Figure 7.23 that both sections 4 and 6 with proprietary SAMIs C and D performed better than section 5 with no SAMI. Also, section 4 with proprietary SAMI C performed better than section 6 with proprietary SAMI D. This also agrees with the findings of the wheel tracking test. The lower viscosity of the bitumen

emulsion used in the proprietary SAMIs aids the SAMI's performance, therefore allowing more flexibility of the layer.

Since the two wheel paths were not trafficked simultaneously, it was considered unreasonable to compare the performance of the SAMI sections in both wheel paths directly. Therefore, to make comparison, the number of wheel cycles to failure for the SAMI sections was divided by those of their respective control sections. Figure 7.24 shows the life to failure of the SAMI sections as a ratio of the control. It can be seen from the results that life to failure as a ratio of control ranges from 1.93 to 4.53. Also, section 3 with 5 mm proprietary SAMI A gave the best performance with life to failure of 4.53 times that of the control. This was followed by section 4 having proprietary SAMI C, then section 1 having 10 mm thick proprietary SAMI A and section 6 with proprietary SAMI D, with lives to failure of 2.92, 2.26 and 1.93 times the control, respectively. The results show that the SAMIs in this study were able to retard reflective cracking.

To investigate a situation where cracks are closely spaced, cracks were simulated in the base layer by cutting three transverse cracks that were 200mm apart as shown in Figure 7.11. The number of wheel cycles to first appearance of cracking and to failure is presented in Tables 7.6 and 7.7, respectively. It was observed that cracks appeared at the surface shortly after trafficking started. This was thought to be due to the fact that the surfacing layer (overlay) was laid and compacted in three parts, thereby creating joints in the overlay close to the closely-spaced cracks in the base layer.

Figures 7.25 and 7.26 show that the results followed the same trend as the case when the cracks were located at the centre. As seen in Figure 7.25, section 3 with 5 mm thick proprietary SAMI A performed better than section 1 with 10 mm thick proprietary SAMI A. Also Figure 7.26 shows that section 4 with proprietary SAMI C performed slightly better

than section 6 with proprietary SAMI D. Again, to compare all the sections with SAMI treatment, the number of wheel cycles to failure of the SAMI section was divided by the number of wheel cycles to failure of the control section. Figure 7.27 shows that section 3 with 5mm proprietary SAMI A gave the best performance with a life to failure 1.77 times that of the control, followed by section 5 with proprietary SAMI C, then section 6 with proprietary SAMI D and section 1 with 10 mm proprietary SAMI A with lives 1.36, 1.29 and 1.27 times that of control, respectively.

For the cracks at the centre of each section in the base layer, it was observed during the test that for the SAMI sections cracks appeared first in the overlay, about 100 mm away from the simulated crack in the base. These are thought to be top-down cracks because a final crack always appeared right above the crack in the base. The crack patterns on the two wheel paths are shown in Figure 7.28. After trafficking was stopped (cracks deemed to have appeared fully on the overlay), cores were taken from the two wheel paths to show the crack propagation through the base layer to the overlay. The cores and the holes showing the cracks are shown in Appendix B.

Table 7.4: Number of wheel load applications to the first appearance of cracks

Wheel path 1				Wheel path 2			
Section	Interlayer (SAMI)	No of load application	Ratio of control	Section	Interlayer (SAMI)	No of load application	Ratio of control
1	10 mm thick SAMI A	23639	2.26	4	SAMI C	44258	4.51
2	Control (No SAMI)	10456	1	5	Control	9810	1
3	5 mm thick SAMI A	34083	3.26	6	SAMI D	26513	2.70

Table 7.5: Number of wheel load applications to failure

Wheel path 1				Wheel path 2			
Section	Interlayer (SAMI)	No of load application	Ratio of control	Section	Interlayer (SAMI)	No of load application	Ratio of control
1	10 mm thick SAMI A	31880	2.26	4	SAMI C	58995	2.92
2	Control (No SAMI)	14105	1	5	Control	20185	1
3	5 mm thick SAMI A	63828	4.53	6	SAMI D	39052	1.93

Table 7.6: Number of wheel load applications to the first appearance of cracks for the closely spaced cracked section

Wheel path 1				Wheel path 2			
Section	Interlayer (SAMI)	No of load application	Ratio of control	Section	Interlayer (SAMI)	No of load application	Ratio of control
1	10 mm thick SAMI A	1345	1.33	4	SAMI C	2380	1.24
2	Control (No SAMI)	1012/1012	1	5	Control	1805/2023	1
3	5 mm thick SAMI A	1138	1.12	6	SAMI D	2504	1.31

Table 7.7: Number of wheel load applications to failure for the closely spaced cracked section

Wheel path 1				Wheel path 2			
Section	Interlayer (SAMI)	No of load application	Ratio of control	Section	Interlayer (SAMI)	No of load application	Ratio of control
1	10 mm thick SAMI A	7185	1.27	4	SAMI C	9180	1.36
2	Control (No SAMI)	6020/5280	1	5	Control	6275/7183	1
3	5 mm thick SAMI A	10015	1.77	6	SAMI D	8673	1.29

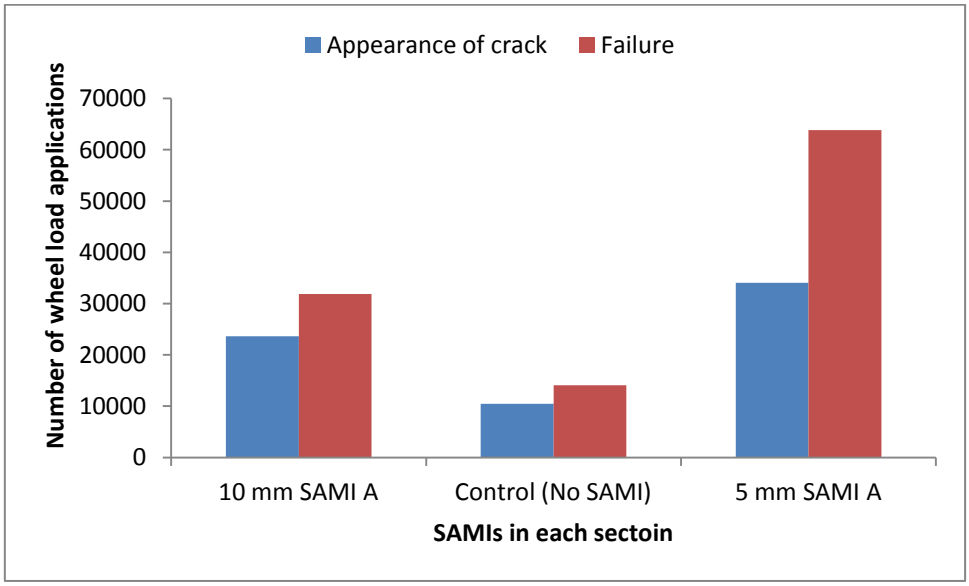

Figure 7.22: Number of load applications to the appearance of cracks and failure for wheel path 1

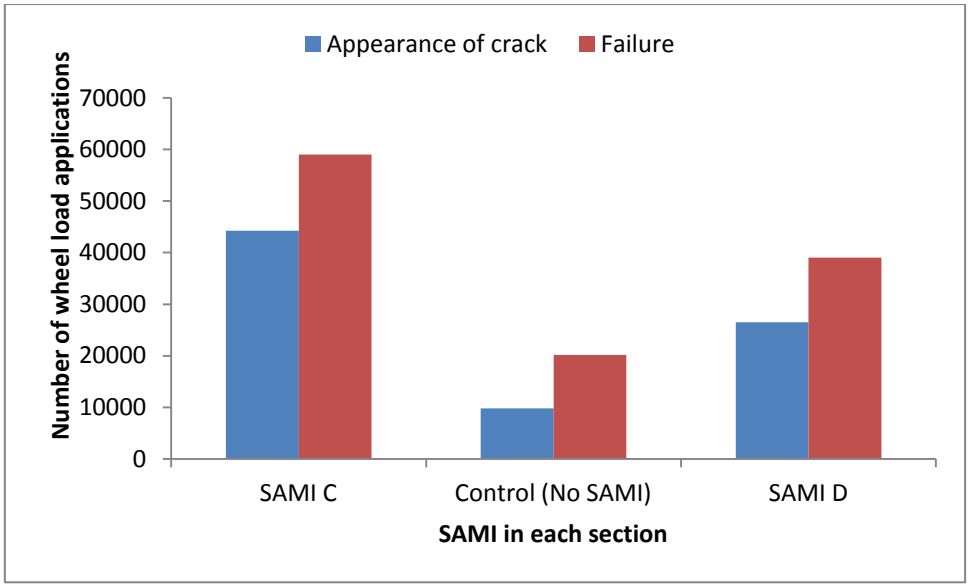

Figure 7.23: Number of load applications to the appearance of cracks and failure for wheel path 2

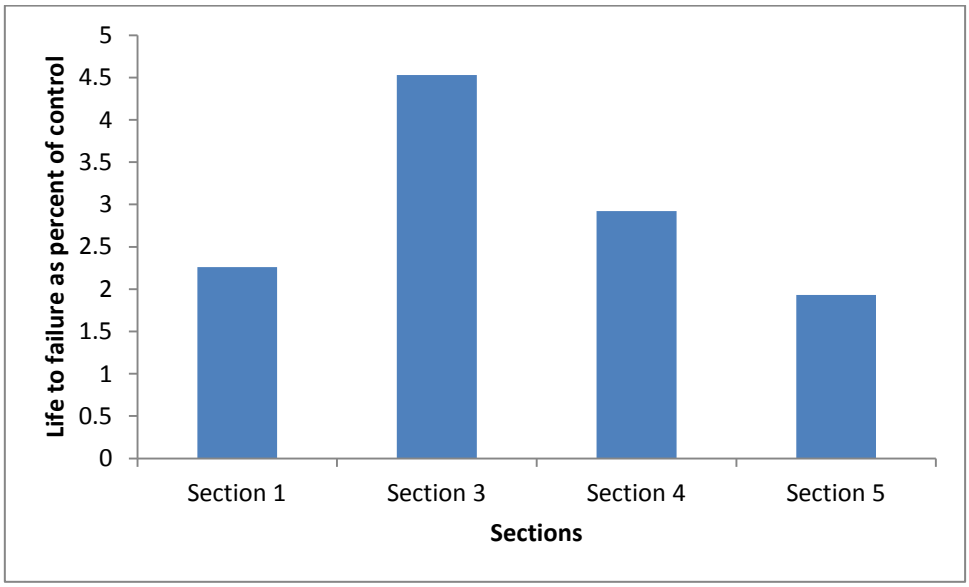

Figure 7.24: Life to failure as ratio of control

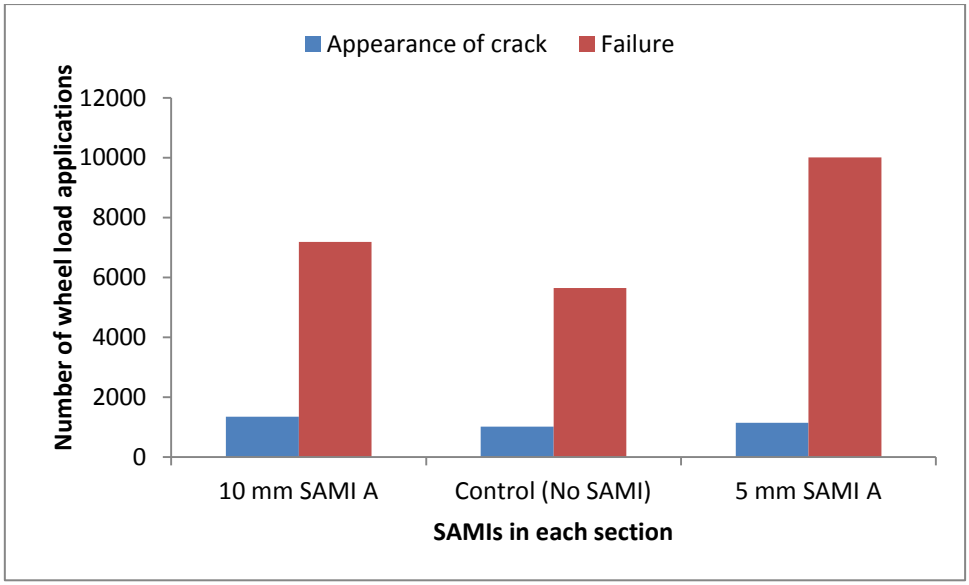

Figure 7.25: Number of load applications to the appearance of cracks and failure for wheel path 1 for closely spaced cracks

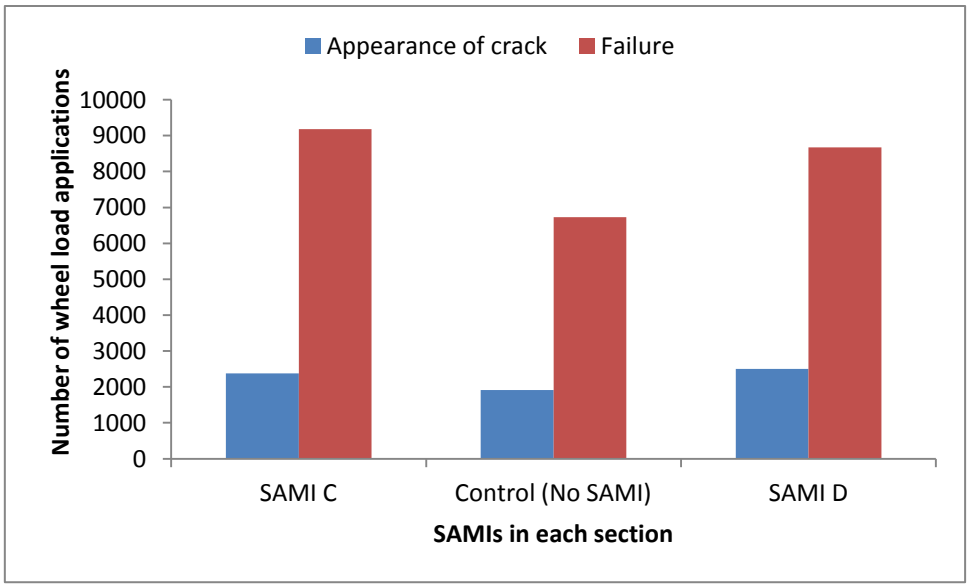

Figure 7.26: Number of load applications to the appearance of cracks and failure for wheel path 2 for closely spaced cracks

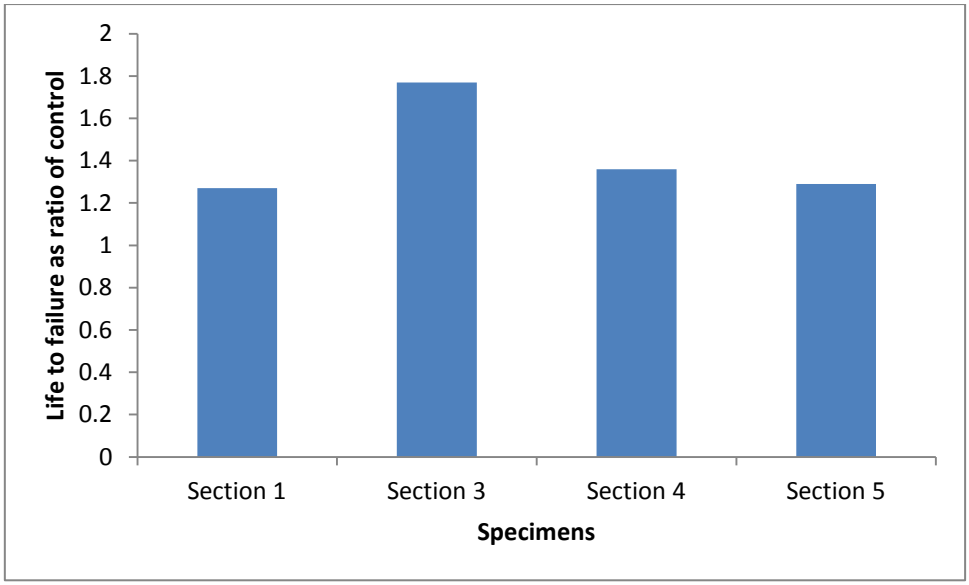

Figure 7.27: Life to failure as ratio of control for closely-spaced cracks

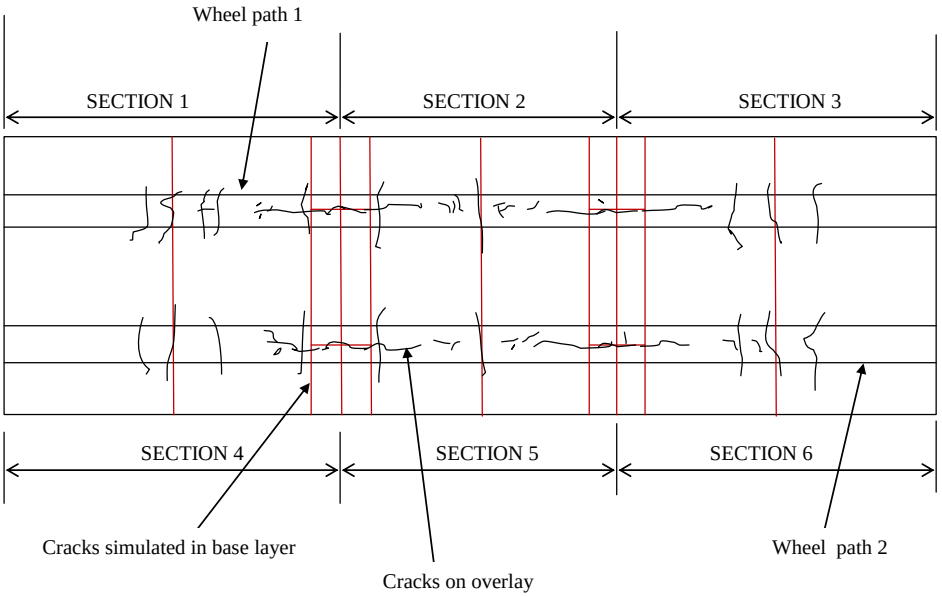

Figure 7.28: Crack patterns on wheel paths 1 and 2

7.5.2 Relative displacement

The relative displacements during trafficking for wheel paths 1 and 2 are shown in Figures 7.29 and 7.30, respectively. Both figures show that the relative displacement increases as the load application number increases, probably as the cracks start to propagate. It can be seen in Figure 7.29 that for wheel path 1, section 3 having 5 mm proprietary SAMI A has less

relative displacement than section 1 having 10 mm proprietary SAMI A, while section 2 with no SAMI has more relative displacement. The relative displacement was more in the section 1 with 10 mm proprietary SAMI A than in section 3 with 5 mm SAMI A because the additional 5 mm of the SAMI results in less bending stiffness of the section and in turn more deflection. Also Figure 7.30 show that section 4 with proprietary SAMI C has less relative deflection than section 6 with proprietary SAMI D and section 5 with no SAMI (control). In this case, section 5 with no SAMI has less displacement that section 6 with SAMI D.

This probably explains why the crack propagates faster to the surface in the control section than in those sections with a SAMI, because the SAMI was able to isolate the overlay from the relative movement of the underlying layer. The section with SAMI D has higher deflection because of the lower viscosity of the modified polymer bitumen emulsion compared to the ordinary bitumen emulsion used in proprietary SAMI C.

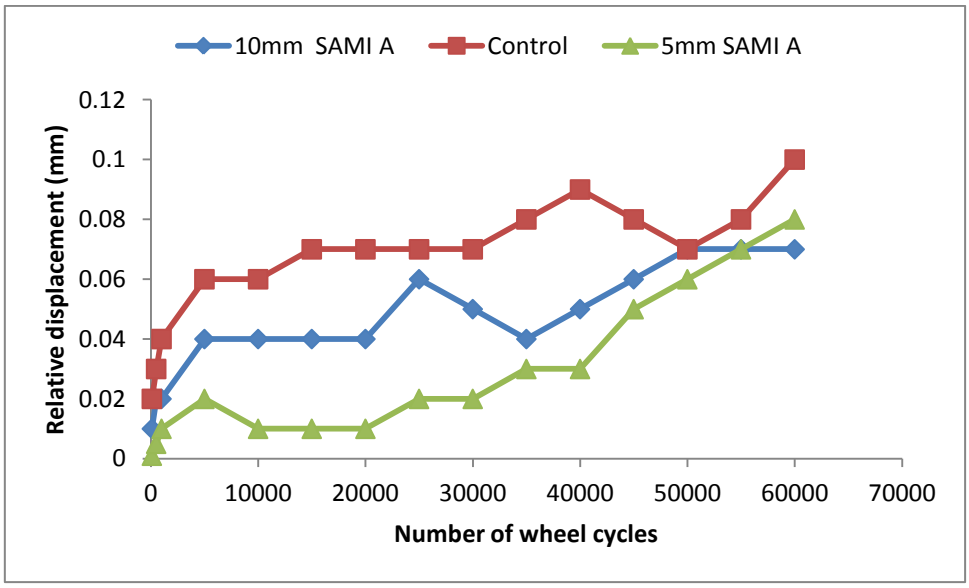

Figure 7.29: Relative displacement for wheel path 1

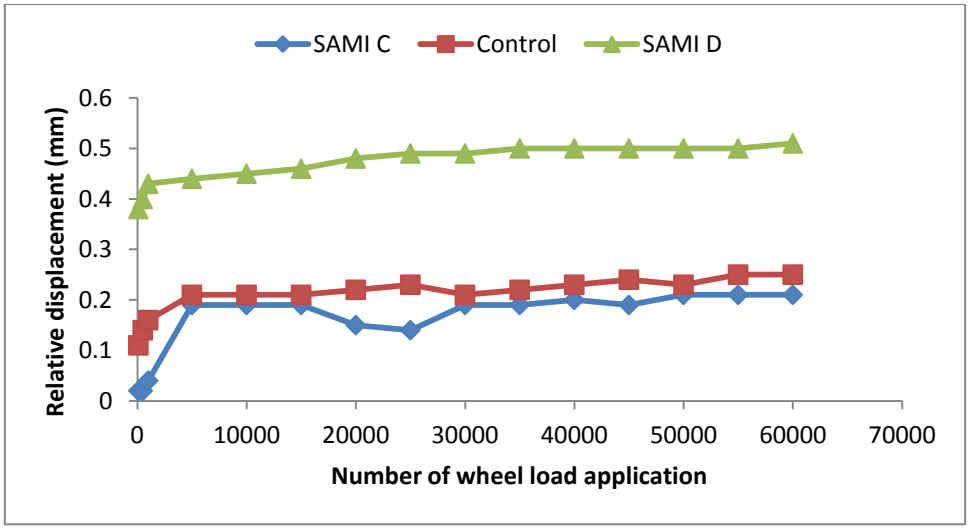

Figure 7.30: Relative displacement for wheel path 2

7.5.3 Permanent Deformation

The permanent deformation of the pavement was measured after trafficking. That of wheel path 1 which consists of sections 1, 2 and 3 having 10 mm proprietary SAMIs A, no SAMI and 5 mm proprietary SAMI A as the SAMI layers was measured after 64495 wheel load applications, while wheel path 2 consisting of sections 4, 5 and 6 having proprietary SAMI C, no SAMI and proprietary SAMI D was measured after 61662 wheel load applications. The rut depths measured at seven points along the wheel paths are shown in Tables 7.8 and 7.9. Figures 7.31 and 7.32 show that the permanent deformation of the control sections (2 and 5) of both wheel paths 1 and 2 is less than their respective test sections with SAMIs (1, 3, 4 and 6). This agrees with the findings of Elseifi (2003) that when a soft interlayer is used, more vertical and horizontal deformations are expected. However, the life of the test sections (with SAMIs) before the appearance of cracks and to failure was more than the control sections, despite more permanent deformation of the test sections.

It is not reasonable to compare the permanent deformation of the two wheel paths because the room temperatures during trafficking and the number of wheel loads applied to the wheel paths were different. As reported in section 7.5, the average room temperatures in the morning, noon and evening during trafficking of wheel path 1 were 24^{o}C, 27.1^{o}C and 28.2^{o}C,

respectively, while those of wheel path 2 were 22.7°C, 25.9°C and 26.9°C, respectively. Knowing that deformation of bituminous mixtures is greatly affected by temperature; obviously more deformation is expected in the sections in wheel path 1. This proved to be the case as the average deformation of the control (no SAMI) section for wheel path 1 was 5.36mm while that of wheel path 2 was 3.36mm. It can be seen from Figure 7.31 that the permanent deformation of section 3 having 5 mm proprietary SAMI A is less than that of section 1 having 10 mm proprietary SAMI A. This is because increasing the thickness of the SAMI results in the reduction of the flexural stiffness of the pavement. Also, as shown in Figure 7.32, the lower viscosity of the emulsion used in SAMI D reflected in the results as section 4 with proprietary SAMI C has significant less permanent deformation than proprietary SAMI D. Again, the permanent deformation of the sections may also be because of the weak subgrade (1.5% CBR) used in this study.

Table 7.8: Permanent deformation measurement for wheel path 1

Points	Permanent deformation (mm)		
	Section 1 (10 mm thick SAMI A)	Section 2 (Control)	Section 3 (5 mm thick SAMI A)
1	7.0	5.5	7.0
2	8.0	5.0	6 .5
3	7.5	6.0	6.5.
4	7.5	6.0	7.5
5	7.5	6.0	6.0
6	5.5	4.5	7.5
7	7.0	4.5	7.0
Average	7.14	5.36	6.86

Table 7.9: Permanent deformation measurement for wheel path 2

Points	Permanent deformation (mm)		
	Section 1 (SAMI C)	Control	Section 1 (SAMI D)
1	3.0	4.0	10.0
2	4.5	2.5	9.5
3	6.5	3.0	9.5
4	5.5	3.5	10.0
5	4.0	3.5	7.0
6	5.5	2.0	10.0
7	4.5	5.0	9.5
Average	4.79	3.36	9.36

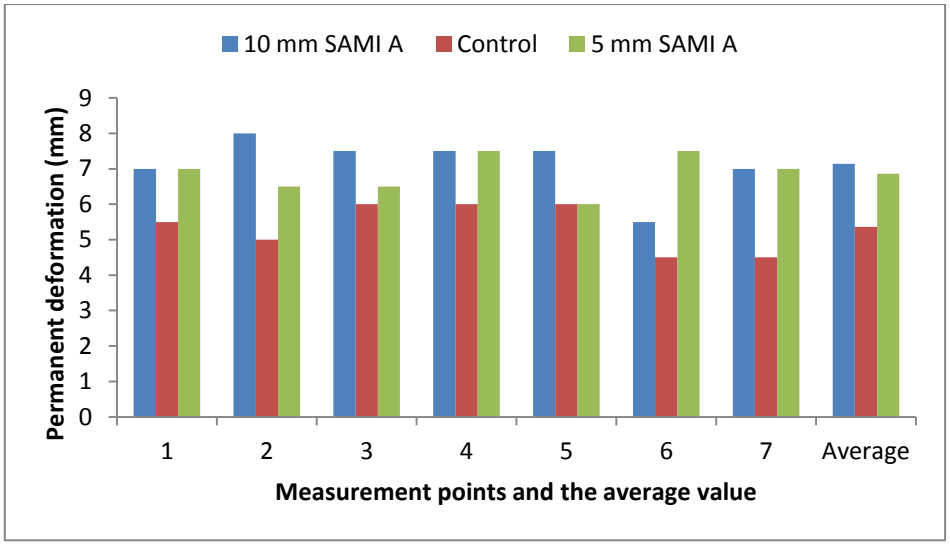

Figure 7.31: Permanent deformation for wheel path 1

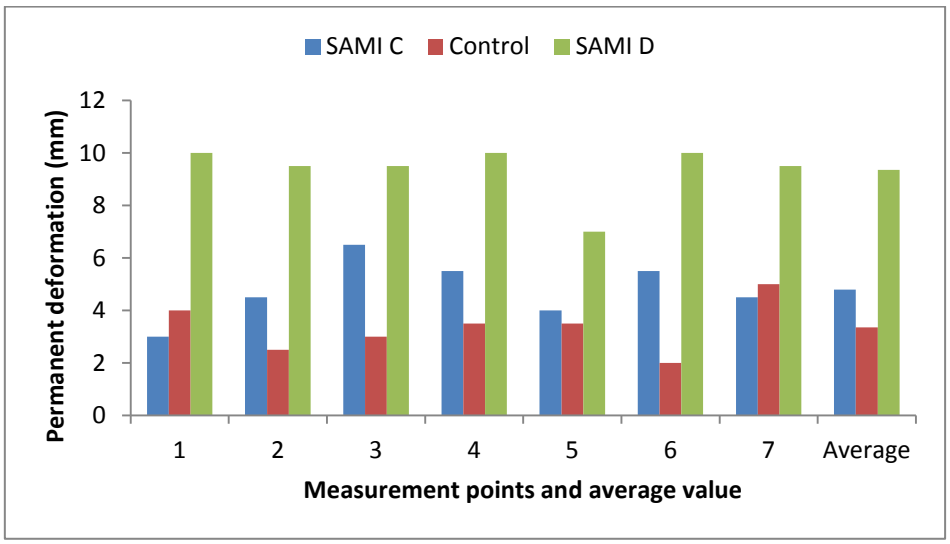

Figure 7.32: Permanent deformation for wheel path 2

7.5.4 Asphalt concrete and the pavement interface properties

After trafficking of the PTF pavement, 150 mm cores were taken from the trafficked areas while 100 mm and 150 mm cores were taken from the non-trafficked areas. The 100 mm cores were used to determine the asphalt concrete air voids and stiffness. The 150 mm cores were used to evaluate the interface bond between the surface layer (overlay) and the SAMI layer for the test sections or the base layer for the control sections before and after trafficking.

7.5.4.1 Interface test

Leutner shear tests were carried on cores at 20^{o}C. Only cores from sections 1, 2, 3 and 5 were tested. Cores from sections 4 and 6 with proprietary SAMIs C and D split into two during coring, indicating weak bond between the layers. The test procedure has been described in section 4.3. The results are presented in Table 7.10 and Figure 7.33. It can be seen from Figure 7.33 that the interface strength increased after trafficking except for section 5. This indicates that the interface bond becomes stronger under trafficking. Also, Figure 7.33 shows that the interface shear strength between the overlay and 10 mm SAMI A in section was greater than that of section 2 (control) and section 3 (5mm SAMI A), while that of 5mm SAMI A was less than the control section.

7.5.4.2 Stiffness modulus and the air voids

The air voids and the stiffness modulus of the cores were determined at 10^{o}C, 20^{o}C and 30^{o}C. The results are presented in Table 7.11. The results show there was high voids content which is thought to be due to rapid cooling of the mixture during compaction. Also as expected because of the high voids content, the mixture stiffnesses are considerably lower compared to the specimens compacted with the roller compactor. The stiffnesses for the sections at 10^{o}C, 20^{o}C and 30^{o}C as shown in Figures 7.34, 7.35 and 7.36, respectively indicate there is no appreciable difference in the stiffness of the cores from the sections, therefore this could not have an effect on the number of wheel load applications recorded for the test and control sections.

Table 7.10: Leutner shear test results at 20°C

Section	Interface	Cores condition	Mean peak shear force (kN)	Mean peak displacement (mm)	Mean peak shear stress (MPa)	Mean stiffness modulus (MPa/mm)
1	Overlay- 10 mm SAMI A	NT1	16.8	1.66	0.98	0.61
		T1	18	2.07	1.03	0.50
2	Overlay-base layer	NT2	12.8	1.52	0.74	0.49
		T2	15	1.40	0.86	0.61
3	Overlay-5mm SAMI	NT3	10.1	1.27	0.58	0.47
		T3	13.8	2.17	0.79	0.37
5	Overlay-base layer	NT5	14.3	1.29	0.82	1.29
		T5	12.7	1.48	0.73	0.49

NT: Non-trafficked T: Trafficked

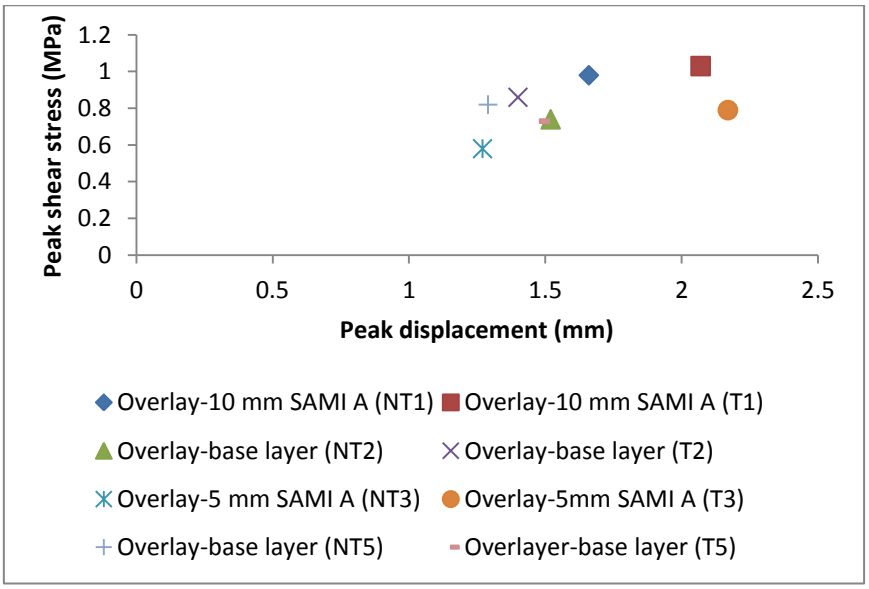

Figure 7.33: Peak shear stress versus peak displacement (mm)

Table 7.11: Indirect tensile stiffness modulus (ITSM) of the cores from the PTF pavement

Sections	Layer	SAMIs	Air void (%)	Stiffness (MPa)					
				10°C	Mean	20°C	Mean	30°C	Mean
1	10mm proprietary SAMI A	Overlay	15.62	5537	4907	3921	3231	2014	1786
			20.55	4276		2541		1558	
		Base	15.97	4383	3934	2766	2405	994	924
			18.19	3484		2044		853	
2	No SAMI (Control)	Overlay	16.40	4732	5030	3124	3045	1327	1350
			17.46	5328		2966		1373	
		Base	14.11	5562	5539	3011	2979	1222	1249
			12.42	5515		2946		1276	
3	5mm proprietary SAMI A	Overlay	15.23	5261	5292	2673	2941	1535	1451
			14.07	5322		3209		1367	
		Base	14.41	5132	5096	2588	2602	1021	1012
			14.71	5059		2615		1002	
4	Proprietary SAMI C	Overlay	15.97	5548	5160	3693	3318	1763	1556
			19.00	4771		2943		1348	
		Base	16.96	4059	4182	2444	2372	944	944
			16.29	4305		2299		943	
5	No SAMI (Control)	Overlay	15.20	5519	5283	3009	2928	1376	1377
			15.31	5047		2846		1378	
		Base	14.88	5135	4845	2649	2504	1094	1058
			16.66	4555		2359		1021	
6	Proprietary SAMI D	Overlay	16.53	4424	4679	2678	2770	995	1193
			14.93	4934		2861		1390	
		Base	19.76	3998	4723	2420	2416	855	902
			14.91	5447		2411		948	

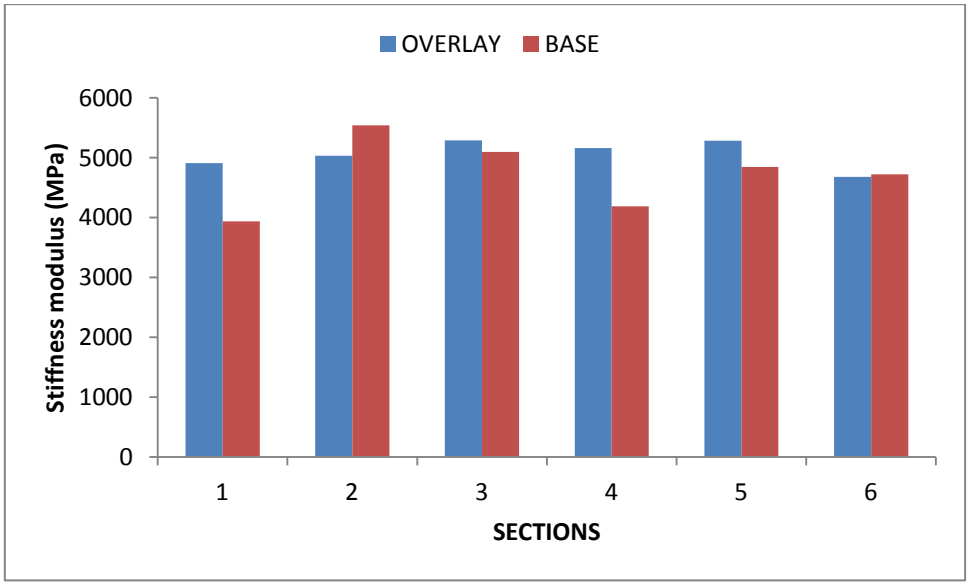

Figure 7.34: Stiffness modulus at 10°C

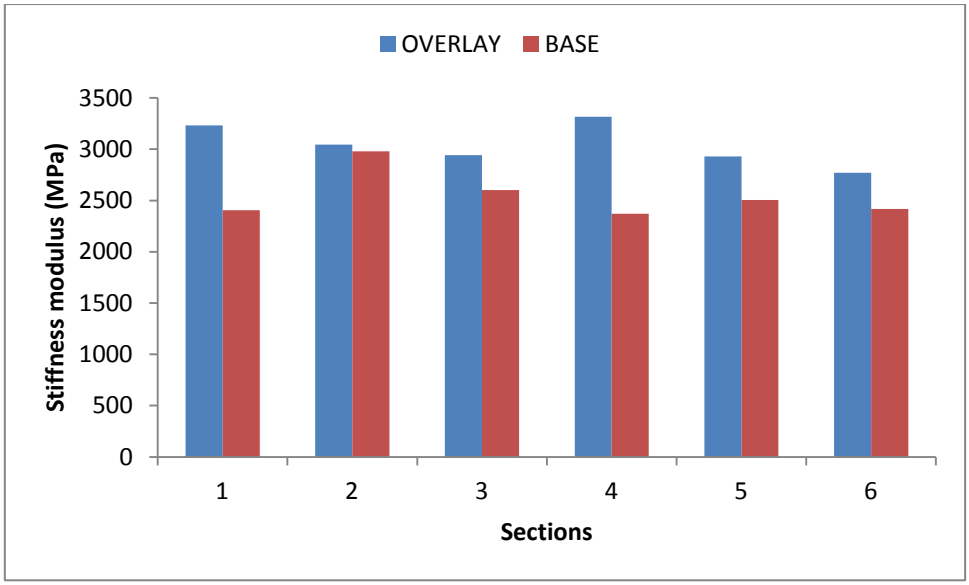

Figure 7.35: Stiffness modulus at 20°C

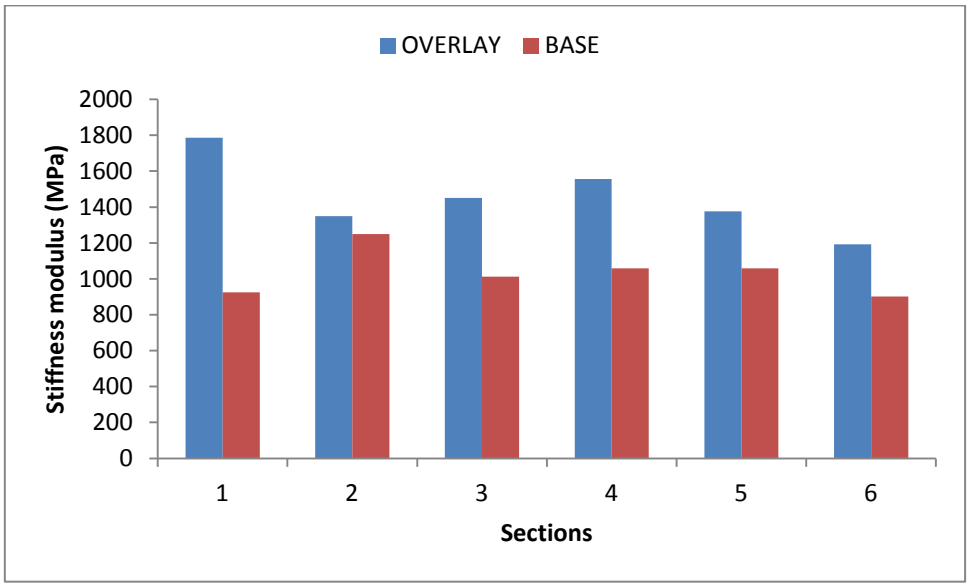

Figure 7.36: Stiffness modulus at 30°C

7.6 Conclusion

The following conclusions can be drawn from the study:

- The study shows that all the SAMIs (proprietary SAMIs A, C and D) are able to retard reflective cracking, with the 5 mm proprietary SAMI A giving the best performance.

- The results show that section with 5 mm proprietary SAMI A performed better than that with 10mm proprietary SAMI A, indicating that SAMI of lower thickness gives better results.
- The study shows that when SAMIs are used in pavement, more deflection of the pavement occurs demonstrating the importance of using an overlay with good fatigue properties.
- The study also shows that when SAMIs are introduced into a pavement to retard reflective cracking, more permanent deformation of the pavement is expected; therefore, it is important that the mixture that is used in the overlay have good resistance to permanent deformation.
- Lastly, it can be seen from this study that the crack resistance of the SAMI is influenced by a number of factors like the interface properties between the overlay and the SAMI, the SAMI stiffness and the thickness of the SAMI.

REFERENCES

Brodrick V.B. (1997): The Development of a Wheel Loading Facility and In Situ Instruments for Pavement Experiments. MPhil Thesis, University of Nottingham, Nottingham, UK.

Brown, S. F. and Brodrick, V. B. (1981): Nottingham pavement test facility. Transportation Research Record 810. 67-72.

Done P. and Piouslin S. (2006): UK DCP 3.1 User Manual: Measuring Road Pavement Strength and Designing Low Volume Sealed Road using the Dynamic Cone Penetrometer. Department for International Development (DFID), Project Record No R7783.

Elseifi M.A. (2003): Performance Quantification of Interlayer Systems in Flexible Pavements Using Finite Element Analysis, Instrument Response and Non Destructive Testing. PhD Thesis submitted to Virginia Polytechnic Institute and State University.

Powell W.D., Potter J.F., Mayhew H.C., and Nunn, M.E. (1984): The Structural Design of Bituminous Roads. Report LR1132. Transport and Road Research Laboratory, Crowthorne, UK.

Saeed A. and Hall J.W. (2003): Accelerated Pavement Testing: Data Guidelines. National Cooperative Highway Research Program. NCHRPReport512.

8 THERMAL CYCLING TEST

8.0 Introduction

It has been identified that daily and/or seasonal temperature variation is one of the causes of reflective cracking in rehabilitated pavement (overlaid with new surfacing material). This causes the cracks on the existing pavement to propagate to the surface of the overlay. The appearance of cracks on the surface paves the way for water to penetrate the pavement causing the deterioration of its structure. This study looks into the crack resistance of some stress absorbing membrane interlayers (SAMIs) used in pavement subjected to temperature variation.

Thermal cracking in pavements is common in countries with extreme winter weather and/or large daily/seasonal temperature fluctuation. Two types of thermal cracking are the low temperature cracking and the thermal fatigue cracking. The low temperature cracking is caused by a single drop in temperature below the fracture temperature of the asphalt concrete while thermal fatigue cracking is caused by a series of repeated temperature variation over a period with the temperature above the fracture temperature of the asphalt concrete (Epps, 2000). The thermal cracking mechanism is such that when the temperature drops, the asphalt concrete contracts. Thermal stresses develop in the overlay as the base contracts. Therefore cracks are initiated in the overlay and then grow through the overlay to the surface under further thermal loading.

As observed by Vinson et al (1989), the thermal stresses that develop when the temperature drops in warm weather are dissipated through stress relaxation because asphalt concrete behave more like a viscoelastic material at this temperature range. At low temperature when asphalt concrete behave more like an elastic material, the thermal stresses cannot dissipate, therefore cracks appear in the asphalt and the stress is relieved.

The factors that influence thermal cracking include: type and percentage of binder in a mix; aggregate type and gradation; air voids content; temperature; rate of cooling; pavement thickness; age of pavement; bond between the pavement layers; and the subgrade strength (Boutin and Lupien, (2000), Epps (2000), Vinson et al (1989)). Also, Debondt (1999) stated the magnitude of the tensile stress which is generated in the overlay depends on the properties of the overlay, characteristics of overlay and existing pavement interface, length of slab (PCC), roughness of the slab (existing surface)-support interface and the magnitude of temperature variation.

The thermal stress in the pavement can be calculated from a pseudo-elastic beam analysis equation (8.1) developed by Hills and Brien (1996) cited in Kanerva et al (1994).

$$\sigma(\dot{T}) = \propto \sum_{T_o}^{T_f} S(t,T).\Delta T \quad \text{---------- 8.1}$$

Where:

$\sigma(\dot{T})$ = accumulated thermal stress for a particular cooling rate

α = coefficient of thermal contraction generally assumed to be 2 to 2.5 × 10^{-5}

T_o, T_f = initial and final temperature

S (t, T) = asphalt concrete mix stiffness (modulus) time- and temperature dependent and

ΔT = temperature increment over which S (t, T) is applicable.

Vinson et al (1990) stated that low temperature cracking is more likely to develop at temperatures lower than -7^{o}C and/or rapid cooling rate, while thermal fatigue will normally occur at milder temperatures in the range of -7^{o}C to 21^{o}C. In this study, the test was carried out at a constant temperature of -3^{o}C to simulate the low temperature condition (the lowest temperature achievable in the temperature controlled room) while the contraction and

expansion of the underlying pavement due to temperature change was achieved by opening and closing the thermal cycling apparatus over for 6 hour periods.

8.1 Thermal cycling device

The thermal cracking simulation apparatus developed by Brown et al (1999) at the University of Nottingham was used for this study. The schematic and photograph of the thermal cracking testing device are shown in Figures 8.1 and 8.2, respectively. The mould and the control unit were modified for the present study. The thermal cracking device is made up of a horizontal frame 2m and 0.2m in length and width, respectively. The horizontal frame is in two halves with one half fixed and the other half connected to a DC motor through a worm drive. This is to allow it to be opened and closed at a chosen rate.

It was modified such that the motor will provide selectable, variable extension and contraction rates between 1.0mm in one hour and 1.0mm in twenty four hours. To allow the motor to rest, the delay between individual operations varies between 5 and 95 seconds. The contraction/expansion rates were read from a linear variable differential transformer (LVDT). The indicator lights on the device control unit were used to monitor the direction of movement of the movable plate, completion of selected operation and any fault encountered during the test.

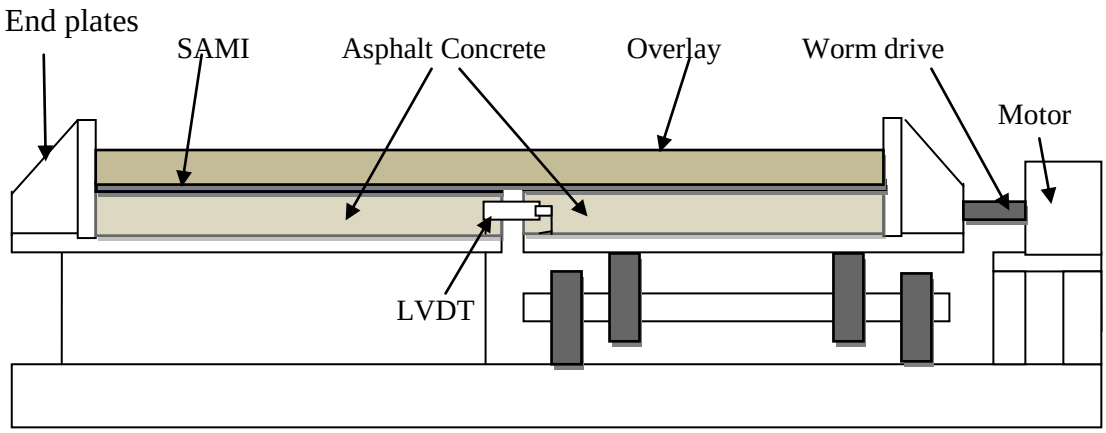

Figure 8.1: Schematic of the thermal cycling device (Baxter, 2001)

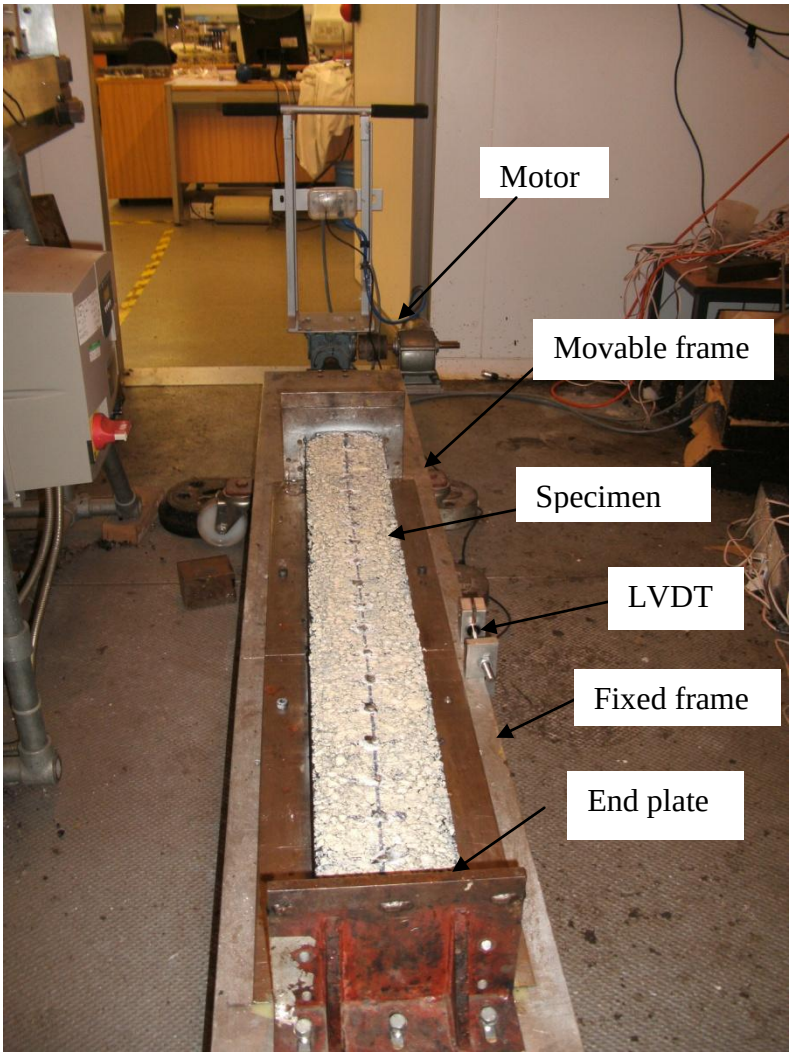

(a)

(b)

Figure 8.2: Thermal cycling device (a) rig (b) control unit

8.2 Specimen preparation and instrumentation

The test specimens were made up of 3-layer beams of length 1000mm and width 125mm. The first (base) layer was a 40mm thick 10 mm asphaltic concrete with 10/20 penetration grade bitumen, the middle layer (where present) was SAMI of 10mm thickness for sand asphalt, proprietary SAMIs A and B and about 7mm for proprietary SAMIs C and D. The top layer was a 30mm thick 10mm asphaltic concrete with 40/60 penetration grade bitumen. The control specimens were prepared in two layers without SAMI (the base and surface layers). In this case, the base and the top layers were both 40mm thick.

The beams for the first (base) layer were produced by manufacturing a slab of dimension 500mm × 500mm ×40mm. The aggregates and binder were batched as shown in Table 3.5, mixed at 185^{o}C and compacted in a mould 500mm × 500mm × 205mm with a roller compactor at a temperature of 180^{o}C just before compaction to a thickness of 40 mm. The slabs were cut into beams of 500mm and 125mm in length and width, respectively. Two steel and end plates were bolted on the frame; then the two beams were glued on the steel plates

and the sides of the mould were bolted to the end plates as shown in Figure 8.3. The SAMI material i.e. sand asphalt and proprietary SAMIs A and B were batched as shown in Tables 3.6 and 3.7. The aggregates and binders for sand asphalt were heated at 140^{o}C and compacted at 130^{o}C, while the aggregates and binder for proprietary SAMIs A and B were batched and heated to a temperature of 180^{o}C, and compacted on the bottom layer at a temperature of 150^{o}C. Proprietary SAMIs C and D were prepared by sandwiching 60mm glass fibre strands between layers of bitumen emulsion and 6 mm aggregates compacted onto them. Proprietary SAMI C was prepared with ordinary bitumen emulsion while proprietary SAMI D was prepared with polymer modified bitumen emulsion. The compaction was done with a vibrating hammer (Kango). The top layer aggregates were batched as shown in Table 3.5 and heated to 160^{o}C and compacted to the required thickness at 150^{o}C. All the mixtures were mixed in accordance with BSI, (2004). A view of the thermal testing device with a specimen in place is shown in Figure 8.4.

Demec pips were glued to the centre of the top layer 50.8mm apart to measure the surface strain. The plan for the location of the demec pips is shown in Figure 8.5, while the demec gauge and pips are shown in Figure 8.6. Also the expansion and contraction (opening and closing) of the frame was monitored using the LVDT readings. The top of the specimen was painted white to monitor the appearance of cracks.

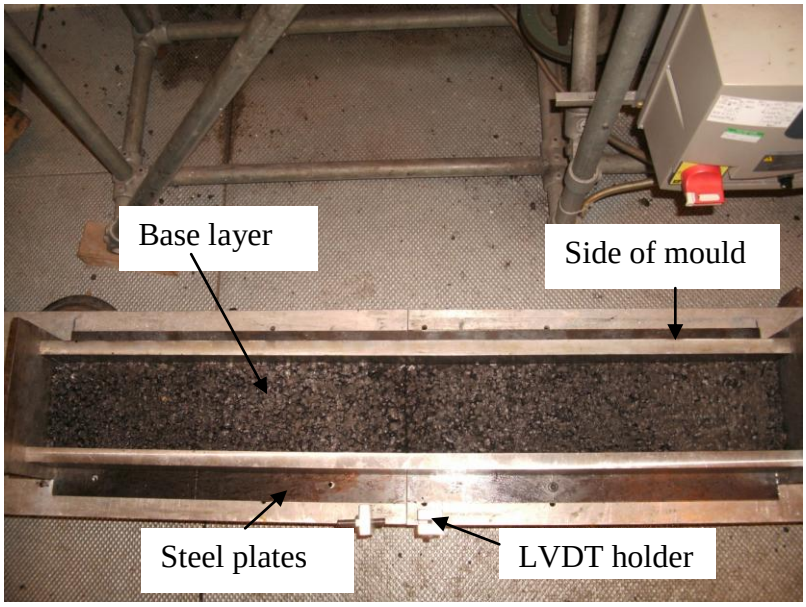

Figure 8.3: Thermal cycling testing device with the specimen's base layer, the end plates and the two side plates.

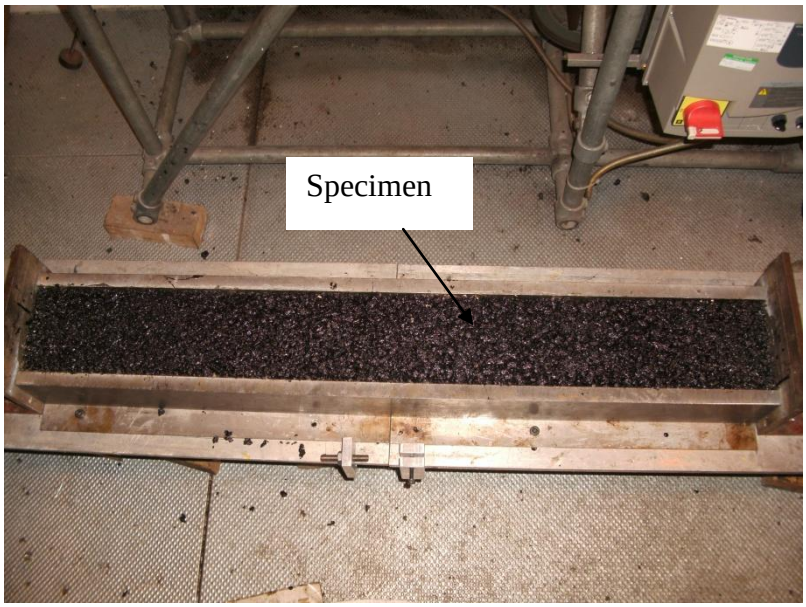

Figure 8.4: Thermal cracking testing device with the specimen in place

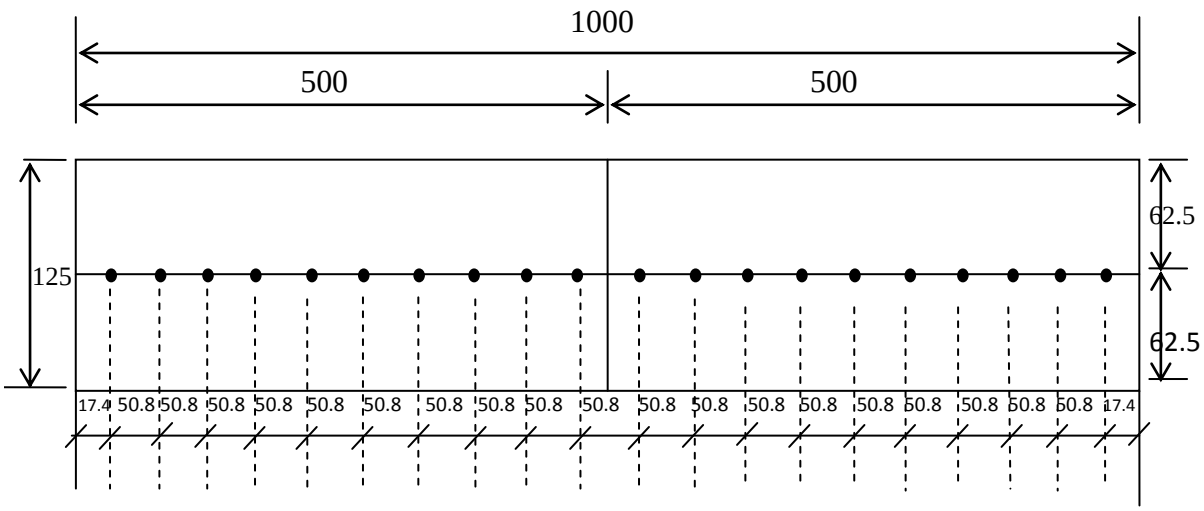

- Demec pip locations

All dimensions in mm

Figure 8.5: Plan for the location of demec pips

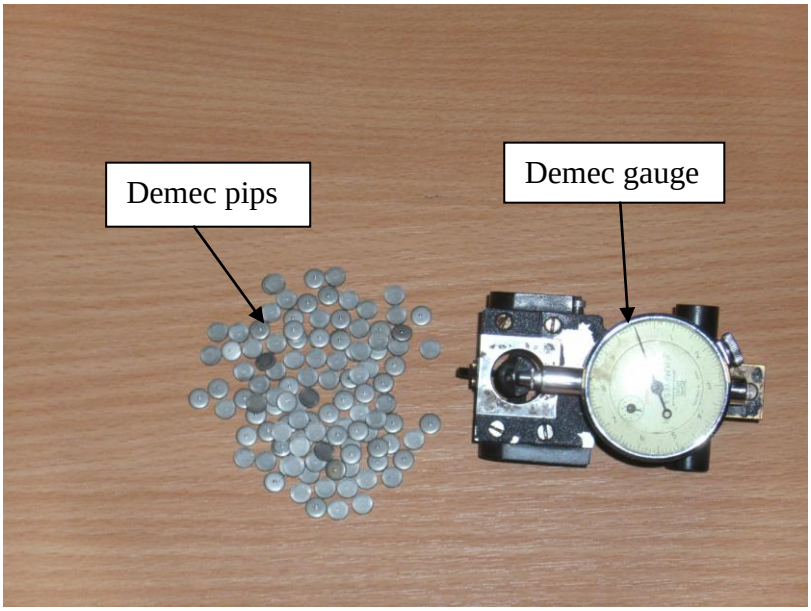

Figure 8.6: Demec gauge and pips

8.3 Test procedure

The thermal cycling testing device with the specimen in place was placed in a temperature controlled room at test temperature of -3^{o}C for a minimum of five hours. The test was conducted by opening the movable part of the rig for a period of 6 hours and closing it for

another 6 hours. This was achieved by setting the contraction (closing) or the expansion (opening) rate on the control box and the required travel distance. The travel distances used for the test were 0.5mm, 1mm, 1.5mm, 2mm, 3mm, 5mm and 7mm, applied to each specimen in sequence or until failure occurred. The appearance of a crack on the surface was monitored visually and the movement of the movable frame was read from the LVDT. The strain on the overlay (top layer) was measured and recorded every 2 hours. The test was stopped when the sample was deemed to have failed completely.

8.4 Test results

The criterion for failure was the appearance of a crack at the surface of the specimen. The surface strain was determined from the demec gauge readings.

8.4.1 Control specimen (No SAMI)

The specimen was tested by opening the movable frame for 6 hours and closing it for 6 hours at each prescribed travel distance. It failed after crack opening of 1mm. The surface strains for 0.5mm and 1mm crack openings are shown in Figures 8.7 and 8.8, respectively. Figure 8.7 shows that for 0.5mm crack opening, the strains were almost uniformly distributed with peak strain developing at -50mm (50mm to the left of the beam's centre) and at the centre, no crack was seen on the specimen at this point. Figure 8.8 shows the strain distribution for 1.0mm crack opening; at this stage, the strain concentration developed at the centre of the specimen directly above the centre of the split base and cracks appeared at the surface (centre) spanning the whole width of the specimen. The specimen before the test is shown in Figure 8.9, while the specimen after test is shown in Figure 8.10.

The reason for early appearance of a crack can be attributed to two major factors. The first is the bond between the top layer (overlay) and the base layer, subjected to tensile loading. As

can be seen in Figures 4.7 and 4.10, at low temperature, strong bond exists between the overlay and the base layer for the control specimen. The strong bond provides restraint for the horizontal movement of the base layer, therefore resulting in tensile strain concentration at the base of the overlay. The second factor is the lack of any soft interlayer (SAMI) between the overlay and the base layer. The horizontal deformation of this layer allows dissipation of energy and the slip between the layer and the overlay isolates the overlay from the tensile strain concentration because of reduced restraint to the horizontal movement of the base layer, therefore reducing the tensile strains in the overlay. In the case of a control specimen with strong bond and no SAMI, high tensile strains developed in the overlay leading to rapid propagation of a crack when the fracture strength of the overlay is exceeded. Smith (1983) pointed out that the thermal strains in the old pavement, especially Portland cement concrete (PCC) can be transmitted to the overlay if the interface bond is strong, which is the case for the control specimen in this study.

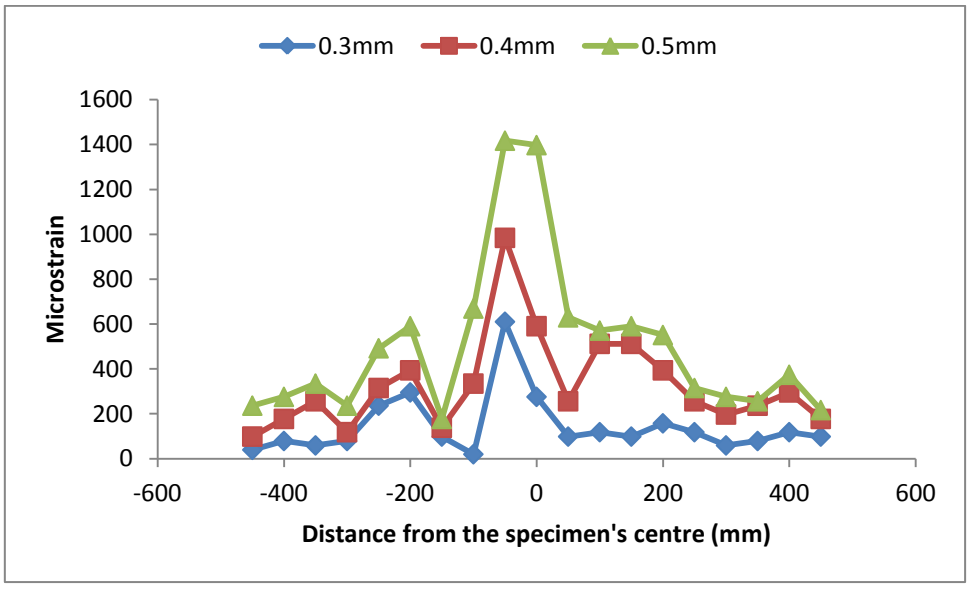

Figure 8.7: Surface strain distribution on control specimen for 0.3mm, 0.4mm and maximum of 0.5mm crack openings

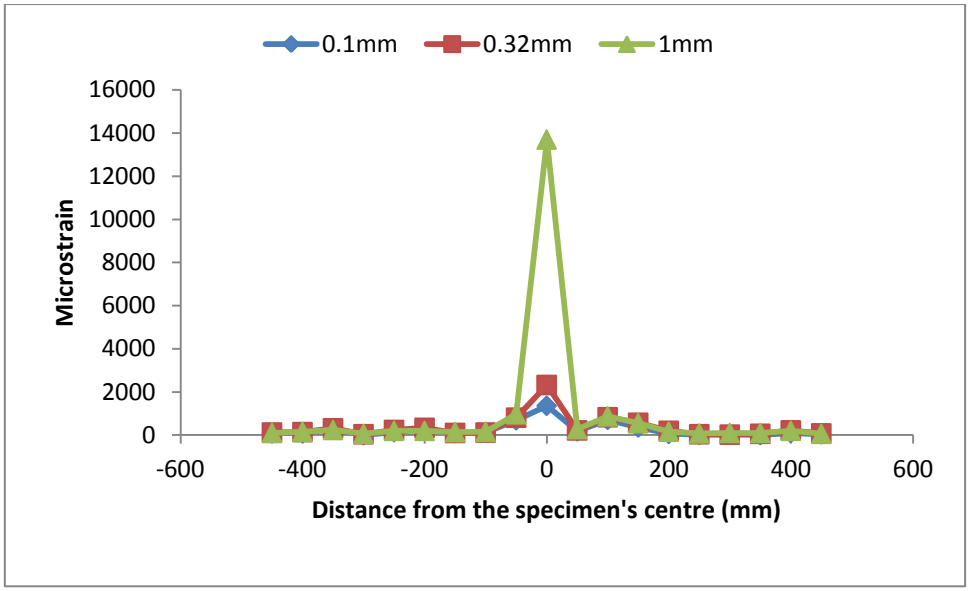

Figure 8.8: Surface strain distribution on control specimen for 0.1mm, 0.32mm and maximum of 1.0mm crack openings

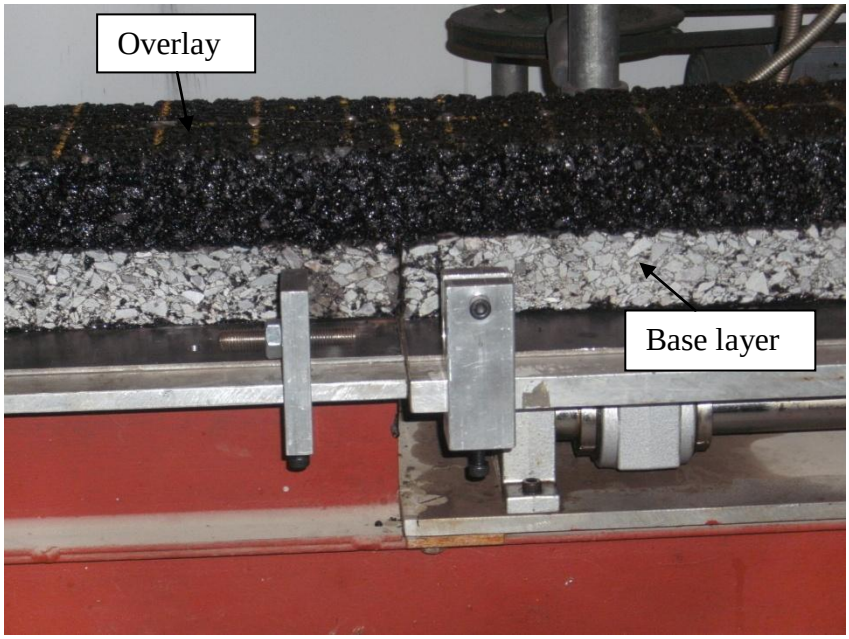

Figure 8.9: Control specimen before test

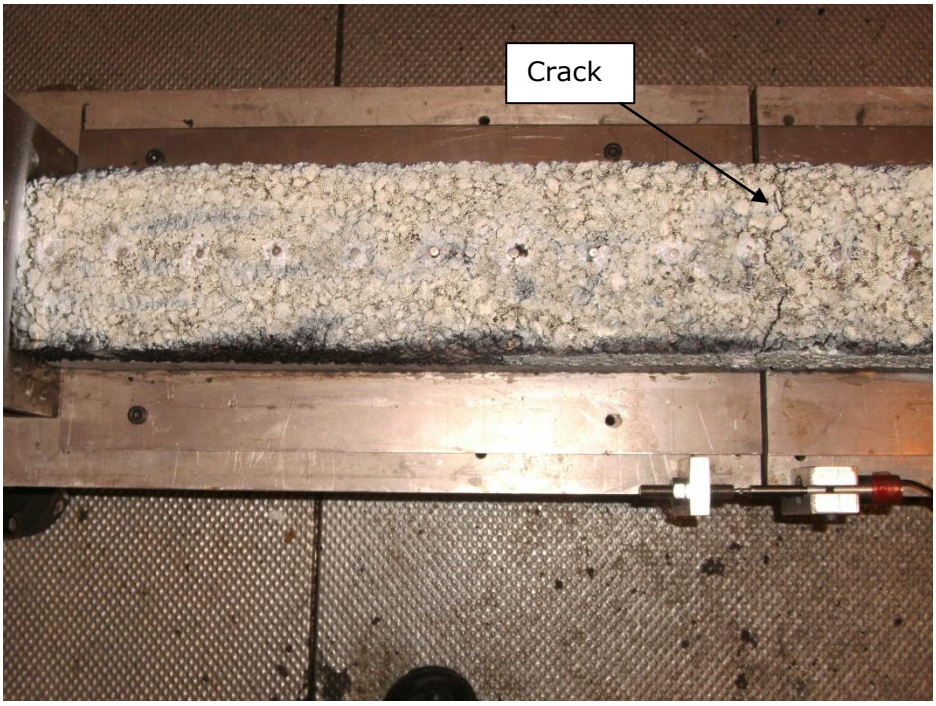

Figure 8.10: Control specimen after test

8.4.2 Specimen with proprietary SAMI A

The specimen with proprietary SAMI A was subjected to thermal cycling and cracks appeared after 2.0mm crack opening. The surface strain distribution in the specimen for crack openings of 0.5mm, 1.0mm, 1.5mm and 2.0mm are shown in Figures 8.11, 8.12, 8.13 and 8.14, respectively. The figures show that the strain distribution was uniform at -150mm to -400mm while strain concentration developed at -100mm to 450mm. Cracks were seen after the device was opened by 1.5mm at the part of the beam with high strain concentration, the test was stopped after crack opening of 2.0mm when the specimen was deemed to have failed .

The specimen before test is shown in Figure 8.15, while the specimen after test is shown in Figures 8.16, 8.17 and 8.18. It can be seen clearly from the figures that cracks developed in the area with high strain concentration (see Figures 8.16 and 8.17), while no crack was seen in the area with uniform stress concentration (see Figure 8.18).

Also, as explained for the control specimen, two factors were responsible for the performance of proprietary SAMI A, the bond between the overlay, SAMI and the base layer and the crack resistance of the SAMI because of its stiffness. Although as seen in Figure 4.7, a strong bond exists between proprietary SAMI A and asphalt concrete, the presence of a material of lower stiffness than the overlay increased the life of the overlay. The SAMI layer allows the dissipation of energy and in turn less tensile strain in the overlay. Cracks appeared after crack opening of 2.0mm compared to 1.0mm for the control specimen.

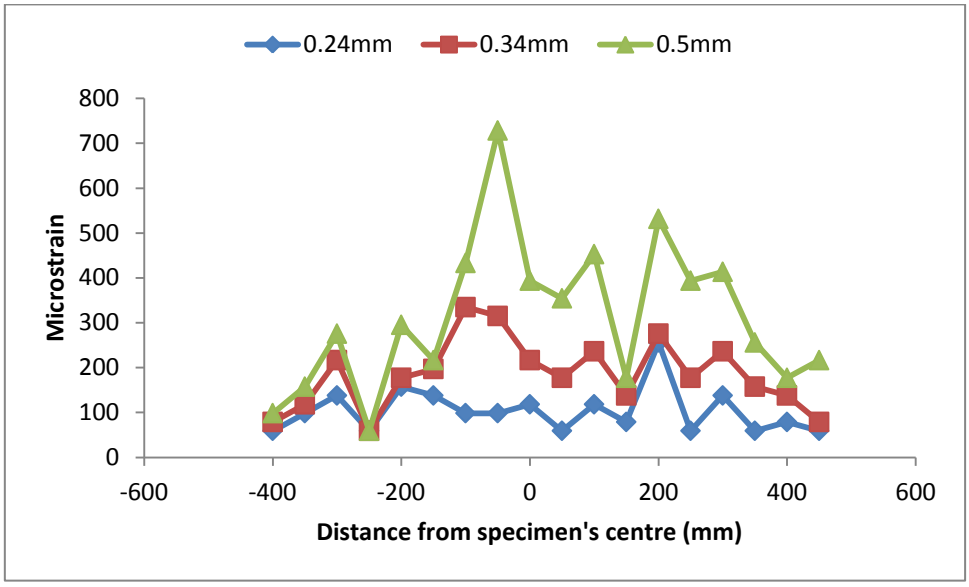

Figure 8.11: Surface strain distribution on specimen with proprietary SAMI A for 0.24mm, 0.34mm and maximum of 0.5mm crack openings

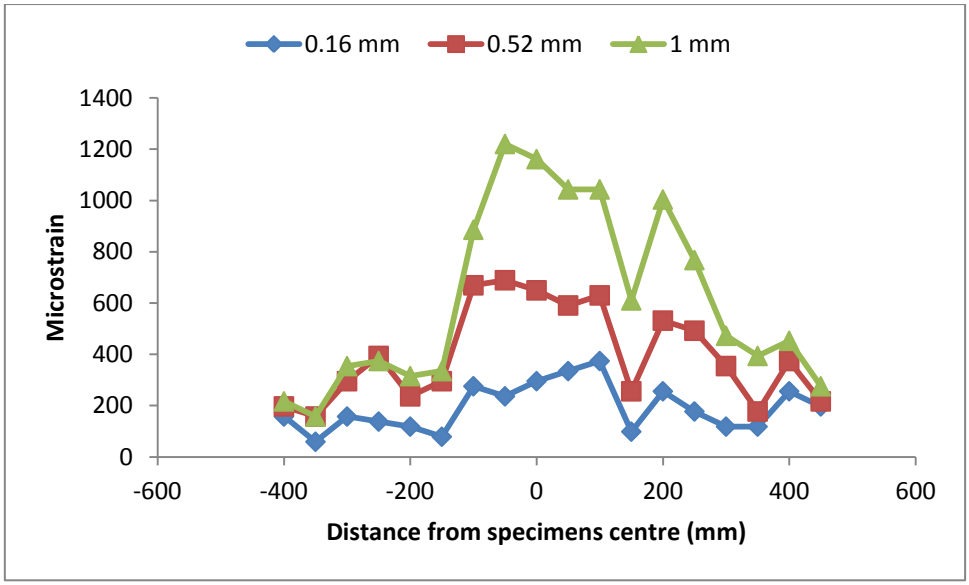

Figure 8.12: Surface strain distribution on specimen with proprietary SAMI A for 0.16mm, 0.52mm and maximum of 1.0mm crack openings

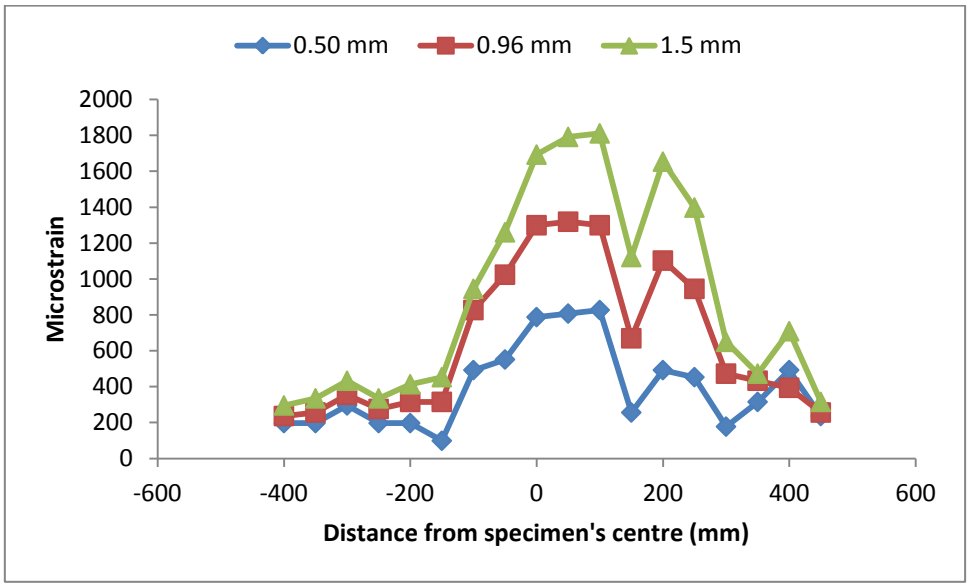

Figure 8.13: Surface strain distribution on specimen with proprietary SAMI A for 0.5mm, 0.96mm and maximum of 1.5mm crack openings

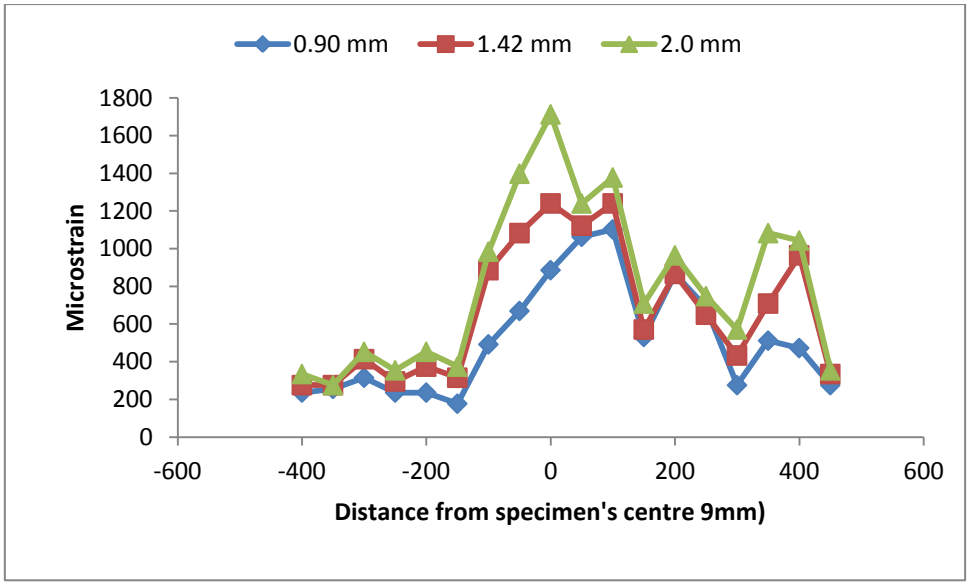

Figure 8.14: Surface strain distribution on specimen with proprietary SAMI A for 0.90mm, 1.42mm and maximum of 2.0mm crack openings

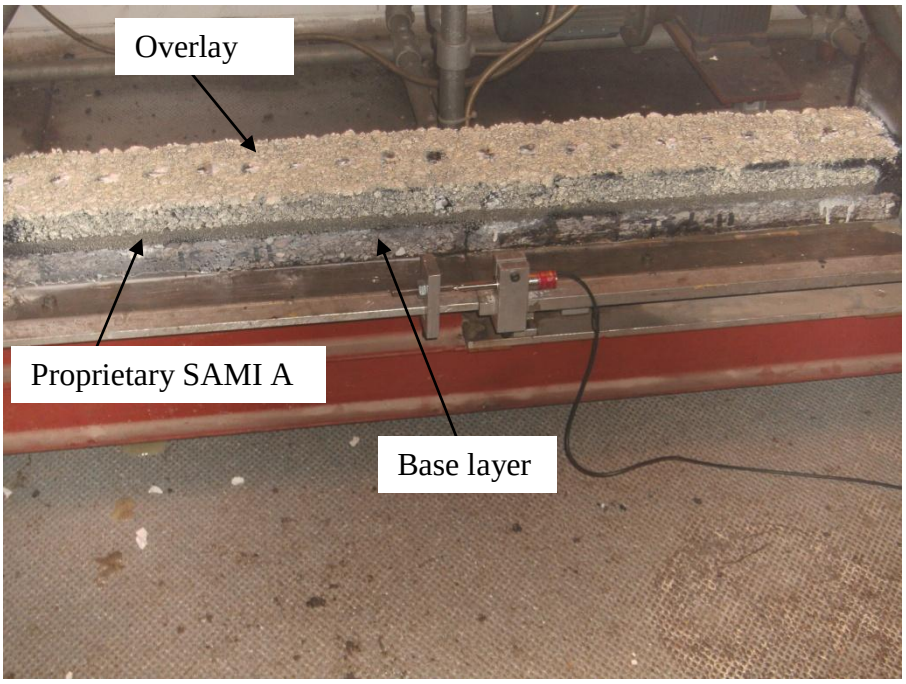

Figure 8.15: Specimen with proprietary SAMI A before test

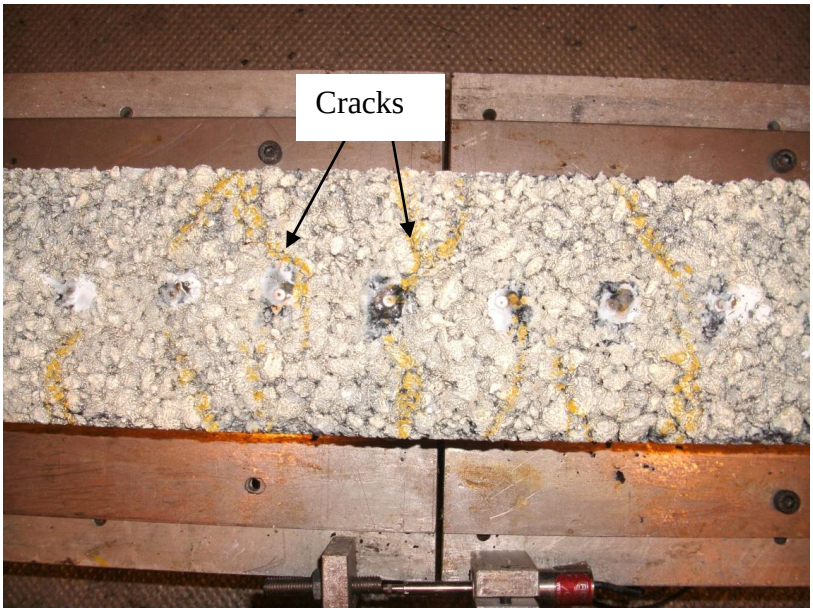

Figure 8.16: Specimen with proprietary SAMI A after test (centre)

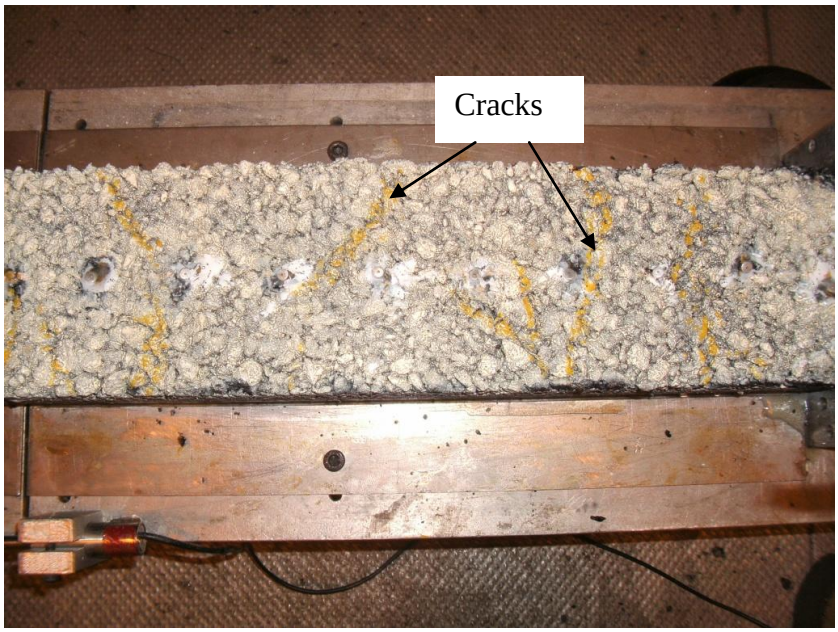

Figure 8.17: Specimen with proprietary SAMI A after test (right)

Figure 8.18: Specimen with proprietary SAMI A after test (left)

8.4.3 Specimen with proprietary SAMI B

The same test procedure was carried out for the specimen with proprietary SAMI B. The test was stopped after crack opening of 1.5mm as cracked appeared at the surface. The surface strain distributions at 0.5mm, 1.0mm and 1.5mm crack openings are shown in Figures 8.19, 8.20 and 8.21, respectively. It can be seen from the figures that strain concentration developed at the centre of the specimen, while the strain distribution was uniform at the right and left of the specimen. Cracks appeared after opening the movable frame by 1.5 mm in the region of strain concentration. The specimen before test is shown in Figure 8.22, while the specimen after test is shown in Figures 8.23.

Although the specimen with proprietary SAMI B failed at 1.5mm crack opening, the strain distribution in the overlay was more uniform than that with proprietary SAMI A. This is probably because proprietary SAMI A mixture is coarser, thus having greater stiffness and less flexibility than proprietary SAMI B as shown in Table 3.13. Also, Jung and Vinson (1994) observed that mixture fracture strength depends on the aggregate type and sizes and

the air voids of the mixture. It is clear like the specimen with proprietary SAMI A that the crack resistance is influenced by the presence of proprietary SAMI B with lower stiffness than the overlay and the base layer.

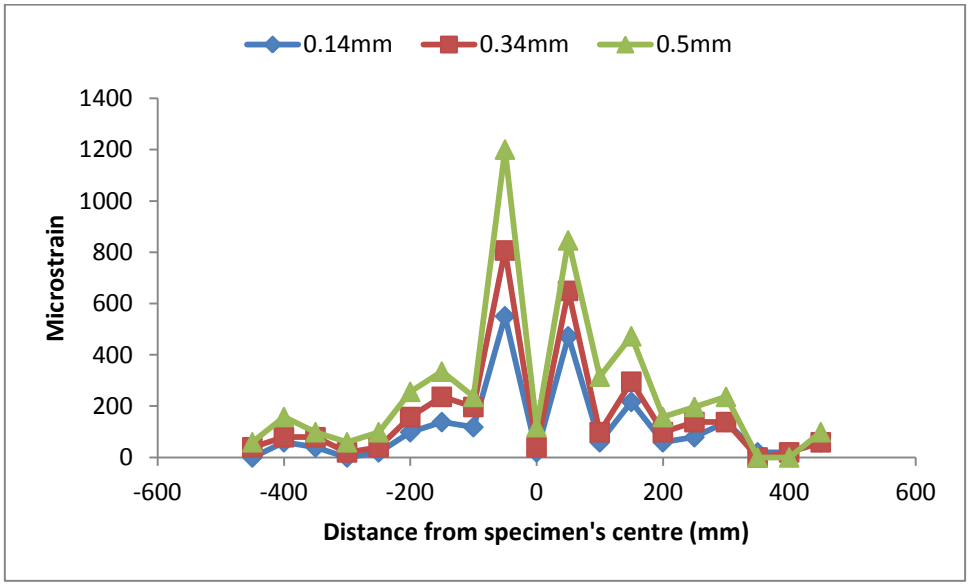

Figure 8.19: Surface strain distribution on specimen with proprietary SAMI B for 0.14mm, 0.34mm and maximum of 0.5mm crack openings

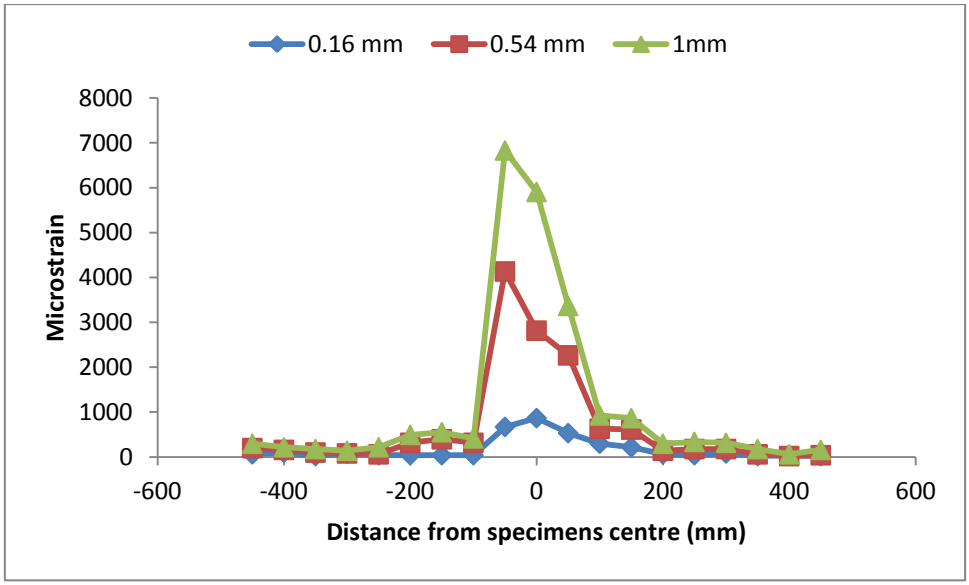

Figure 8.20: Surface strain distribution on specimen with proprietary SAMI B for 0.16mm, 0.54mm and maximum of 1.0mm crack openings

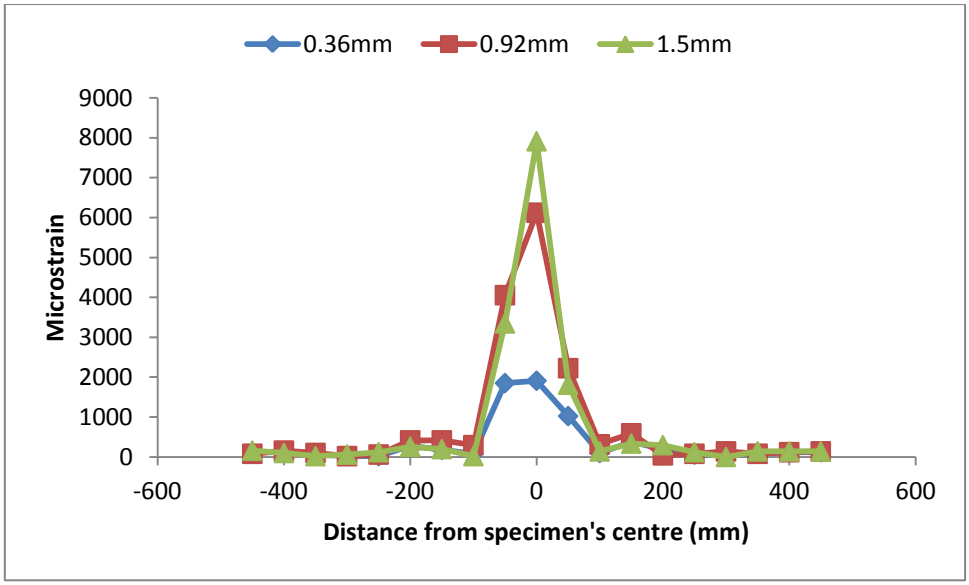

Figure 8.21: Surface strain distribution on specimen with proprietary SAMI B for 0.36mm, 0.92mm and maximum of 1.5mm crack openings

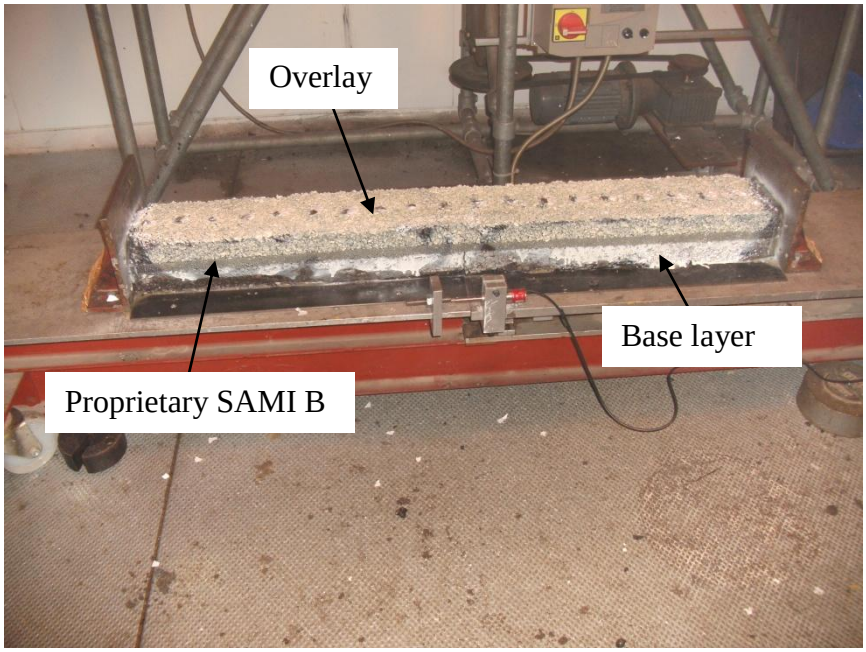

Figure 8.22: Specimen with proprietary SAMI B before test

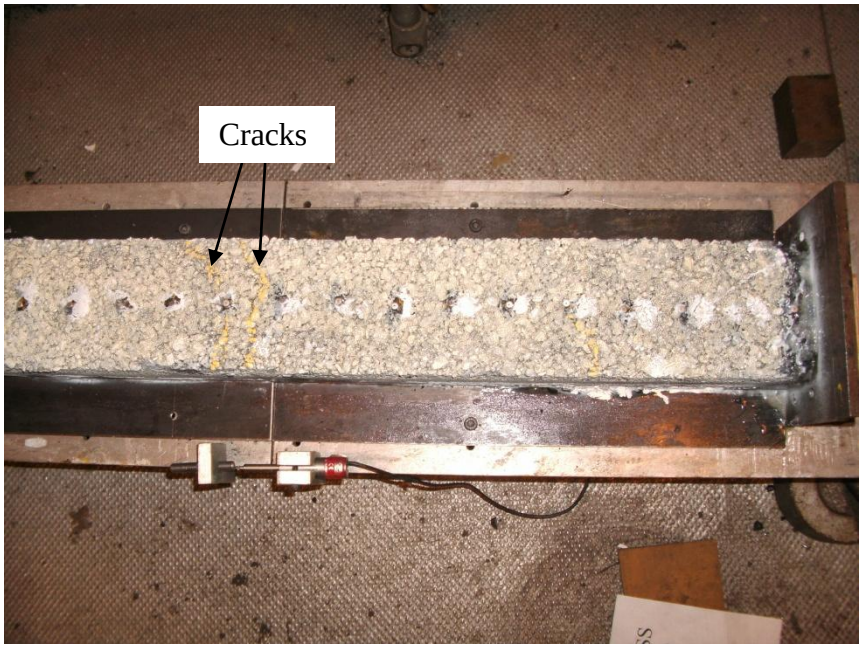

Figure 8.23: Specimen with proprietary SAMI B after test

8.4.4 Specimen with proprietary SAMI C

The specimen with proprietary SAMI C was tested as previously explained. The test was stopped after 5mm when cracks appeared at the surface. The surface strain distributions on the specimen for 0.5mm, 1.0mm, 1.5mm, 2mm, 3mm and 5mm crack openings are shown in Figures 8.24, 8.25, 8.26, 8.27, 8.28 and 8.29 respectively. It can be seen from the figures that strain distribution was uniform throughout the whole length of the specimen, with a slight peak strain concentration developing at the right of the specimen. Also, it can be seen in Figures 8.28 and 8.29 that there is small difference in the strains during crack opening, because of the failure of the bond between the end of the specimen and the end plates. The reason for the increased life of the specimen was the weak bond between the SAMI and the overlay, therefore allowing the movement of the underlying layer without strain concentration in the overlay. This phenomenon is similar to the slip plane theory reported by Smith (1981) for fabrics which states that a fabric interlayer will fail in shear (in the plane of the fabric) before transferring any significant amount of stress from the old pavement (under

layer) to the overlay. Figures 8.28 and 8.29 show that at 3mm and 5mm crack openings, respectively, a slight strain concentration developed at 150mm, 200mm and 350mm. The test was stopped after a crack opening of 5 mm as cracks appeared at the surface. The specimen before is shown in Figure 8.30, while the specimen after test is shown in Figures 8.31 and 8.32. Figure 8.31 show that the cracks appeared in the region of strain concentration.

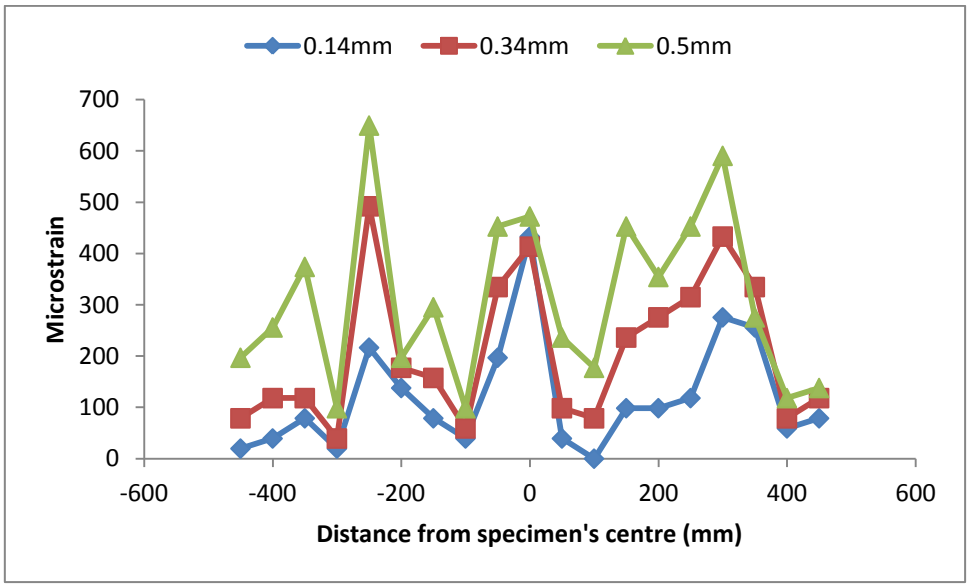

Figure 8.24: Surface strain distribution on specimen with proprietary SAMI C for 0.14mm, 0.34mm and maximum of 0.5mm crack openings

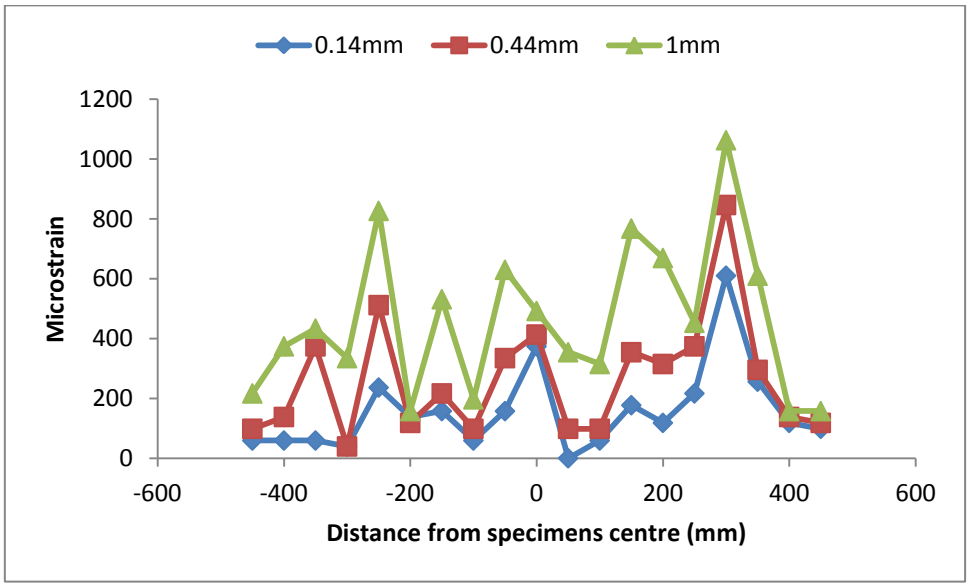

Figure 8.25: Surface strain distribution on specimen with proprietary SAMI C for 0.14mm, 0.44mm and maximum of 1.0mm crack openings

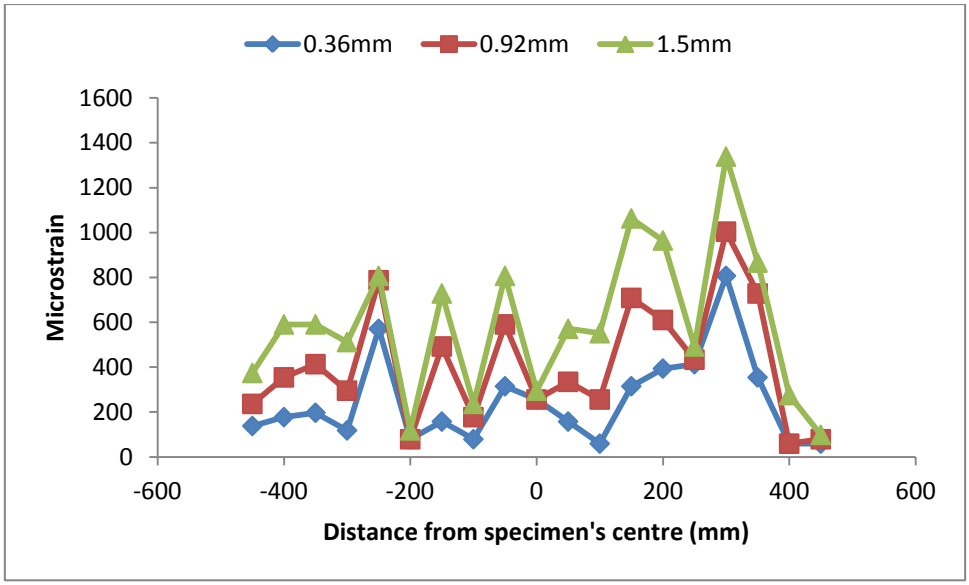

Figure 8.26: Surface strain distribution on specimen with proprietary SAMI C for 0.36mm, 0.92mm and maximum of 1.5mm crack openings

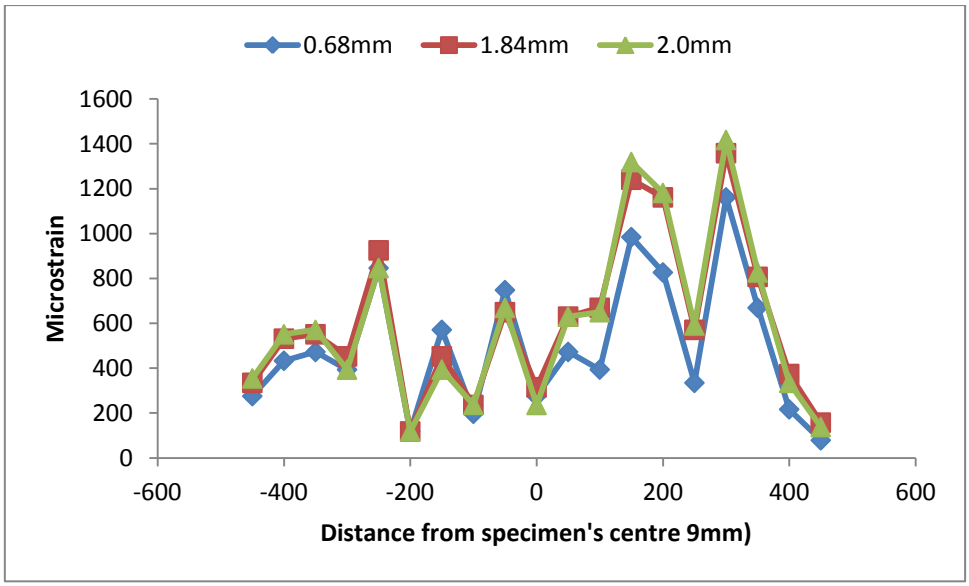

Figure 8.27: Surface strain distribution on specimen with proprietary SAMI C for 0.68mm, 1.84mm and maximum of 2.0mm crack openings

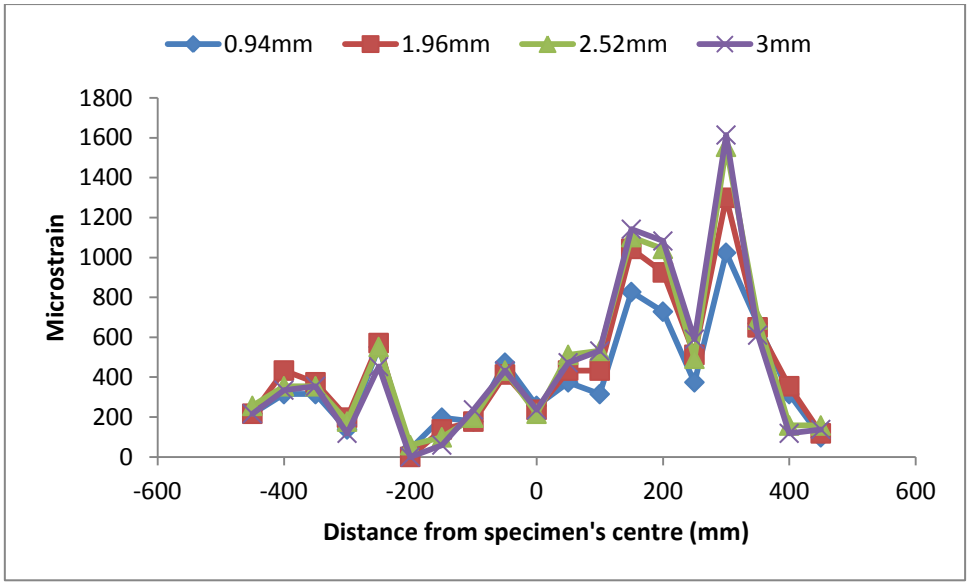

Figure 8.28: Surface strain distribution on specimen with proprietary SAMI C for 0.94mm, 1.96mm, 2.52mm and maximum of 3.0mm crack openings

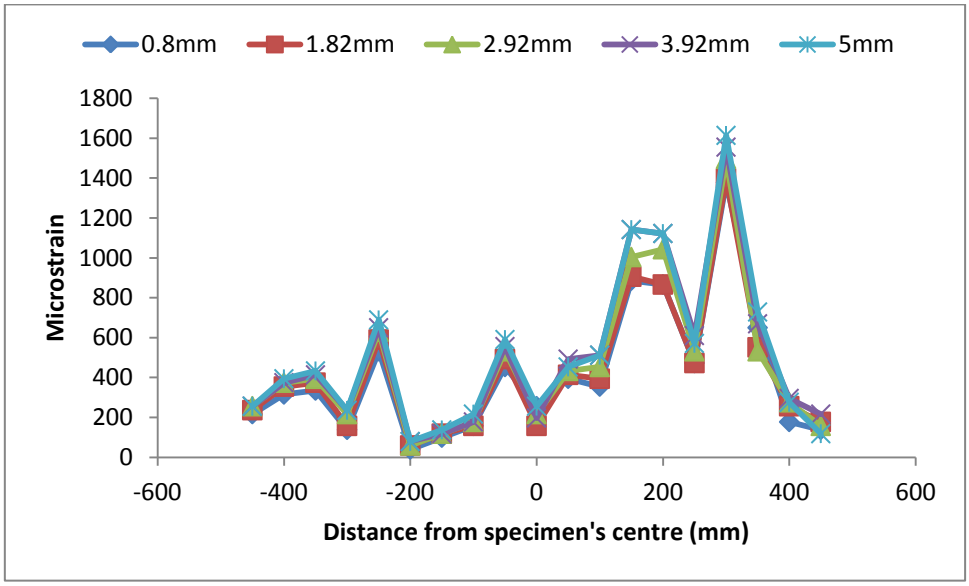

Figure 8.29: Surface strain distribution on specimen with proprietary SAMI C for 0.8mm, 1.82mm, 2.92mm, 3.92mm and maximum of 5.0mm crack openings

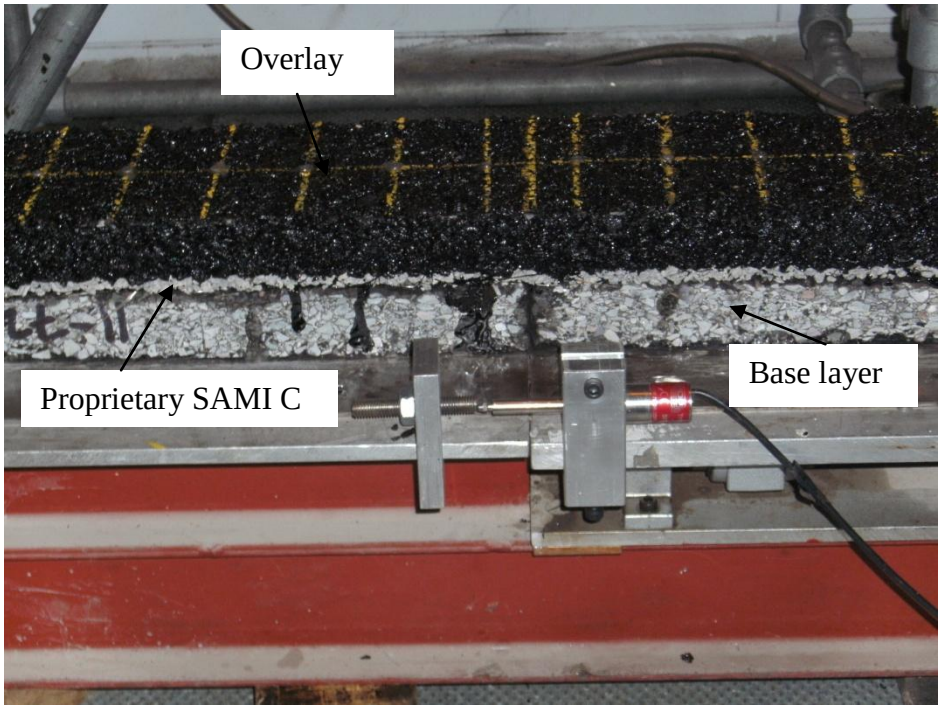

Figure 8.30: Specimen with proprietary SAMI C before test

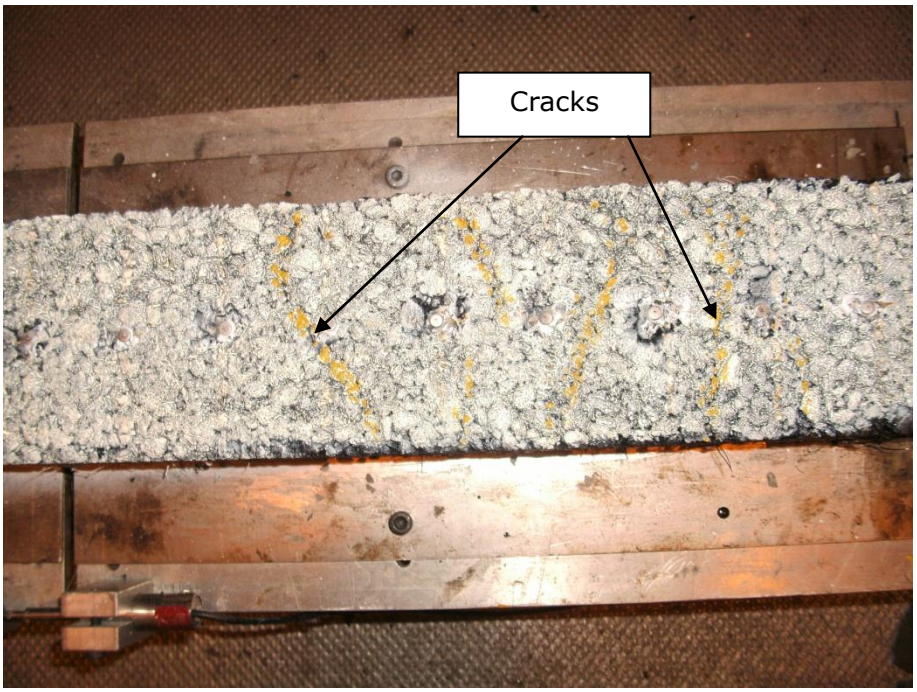

Figure 8.31: Specimen with proprietary SAMI C after test (right) t

(b)

Figure 8.32: Specimen with proprietary SAMI C after test (left)

8.4.5 Specimen with proprietary SAMI D

The specimen with proprietary SAMI D was subjected to the same test procedure. The test was concluded after 5mm crack opening when cracks appeared at the surface. The surface strain distributions at 0.5mm, 1mm, 1.5mm, 2mm, 3mm and 5mm crack openings are shown in Figures 8.33 to 8.38. The figures show that the strain distribution is uniform throughout the whole length of the specimen. Also, this demonstrates the importance of the slip between the overlay and SAMI and the introduction of SAMI when temperature variation is the principal cause of reflective cracking. The slip isolates the overlay from the horizontal movement of the underlying layer, therefore reducing the strain concentration in the overlay. Debondt (1999) observed in his study that the presence of a stress relieving layer in a pavement subjected to temperature variation enables the slip of the overlay and the old surface without creating large shear stresses. Also he pointed out that the axial force in the existing pavement increases with increasing interface stiffness, therefore generating more tensile stresses when

it tends to contract due to temperature variation. As observed from the test, the strain distribution in the specimen with proprietary SAMI D like proprietary SAMI C was more uniform than in other specimens. The specimen before test is shown in Figure 8.39, while photographs of the specimen after test are shown in Figures 8.40 and 8.41. As seen in Figures 8.40 and 8.41 cracks appeared after 5.0mm crack opening.

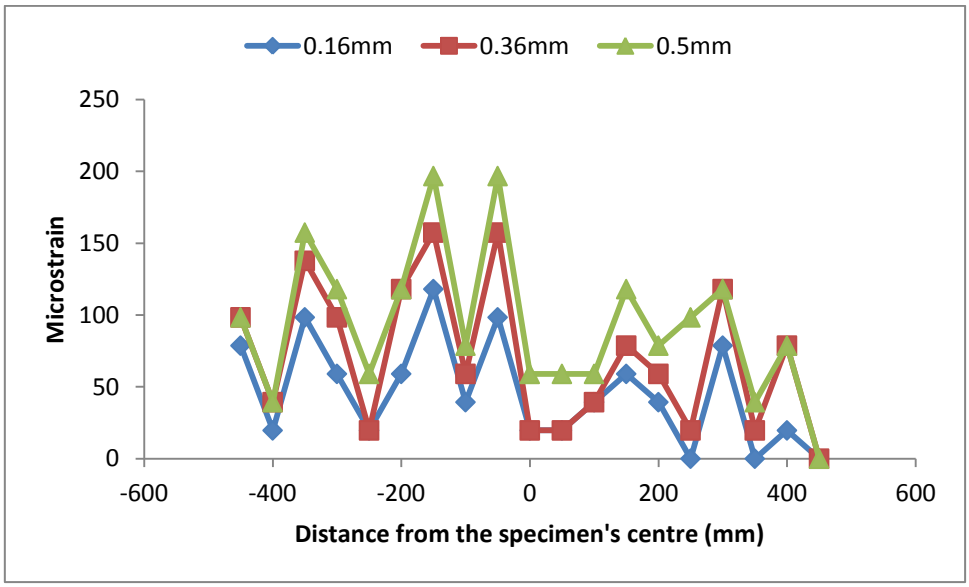

Figure 8.33: Surface strain distribution on specimen with proprietary SAMI D for 0.16mm, 0.36mm and maximum of 0.5mm crack openings

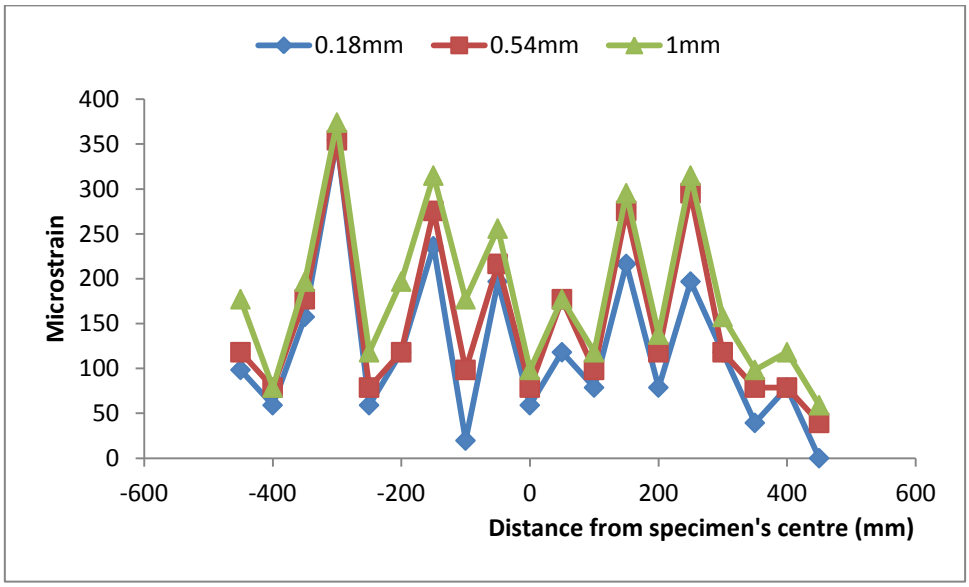

Figure 8.34: Surface strain distribution on specimen with proprietary SAMI D for 0.18mm, 0.54mm and maximum of 1mm crack openings

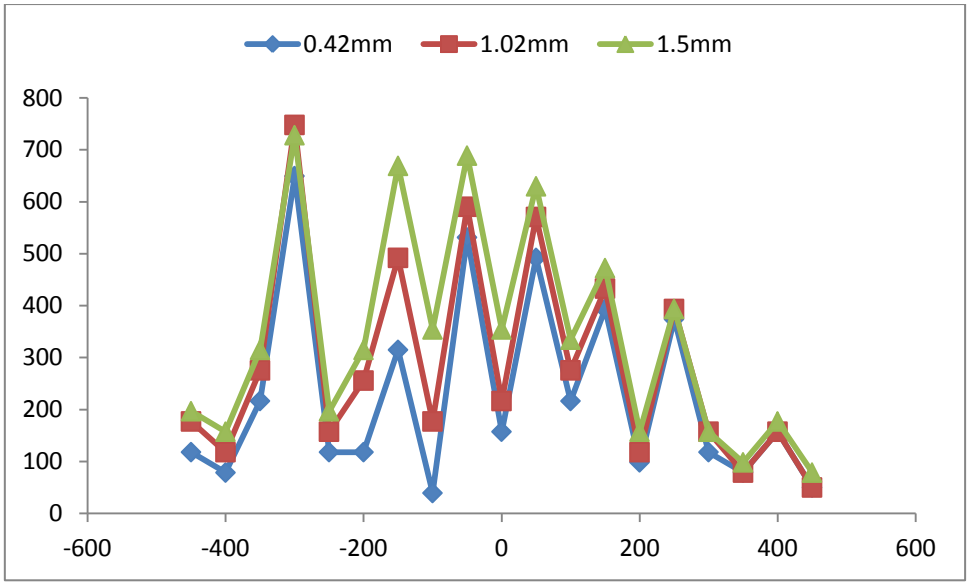

Figure 8.35: Surface strain distribution on specimen with proprietary SAMI D for 0.42mm, 1.02mm and maximum of 1.5mm crack openings

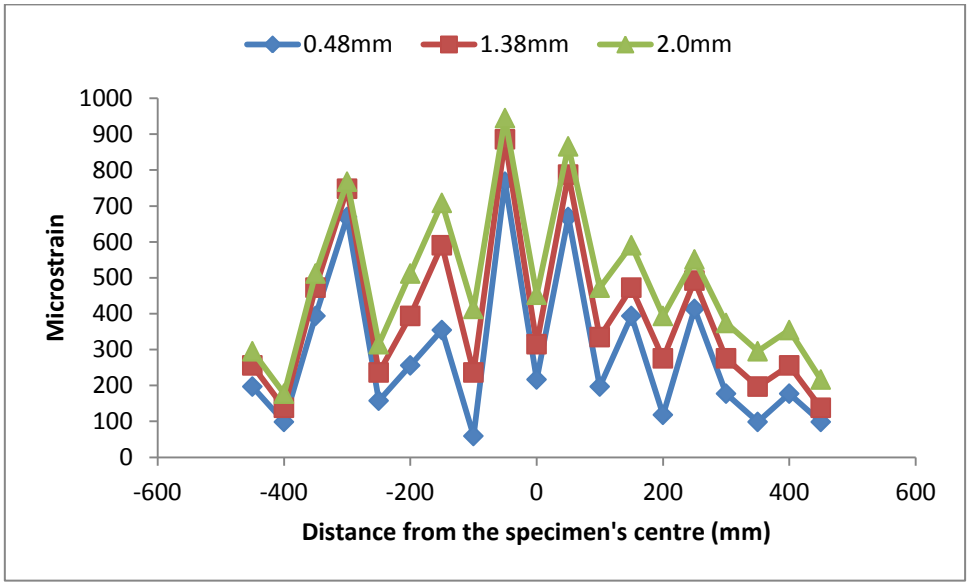

Figure 8.36: Surface strain distribution on specimen with proprietary SAMI D for 0.48mm, 1.38mm and maximum of 2mm crack openings

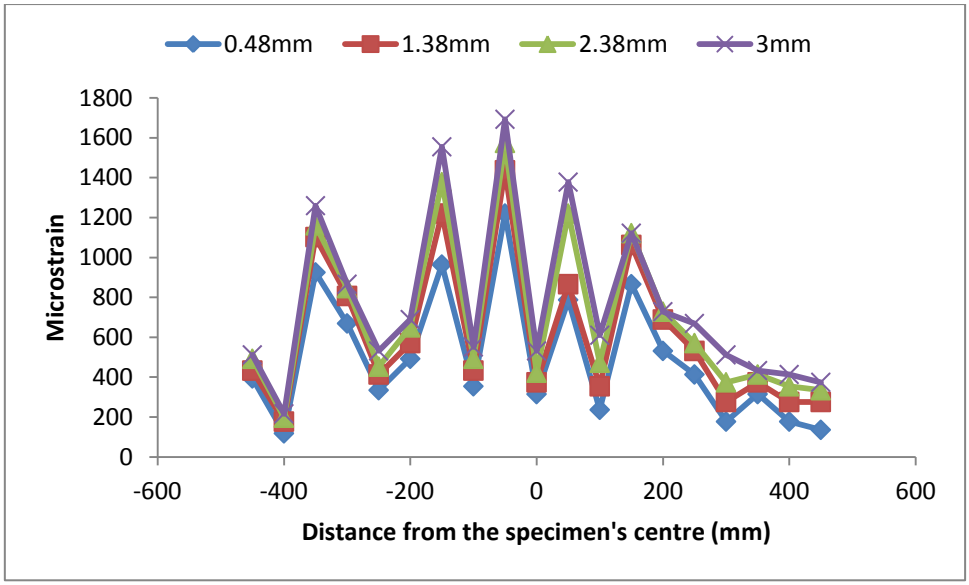

Figure 8.37: Surface strain distribution on specimen with proprietary SAMI D for 0.48mm, 1.38mm, 2.38mm, and maximum of 3mm crack openings

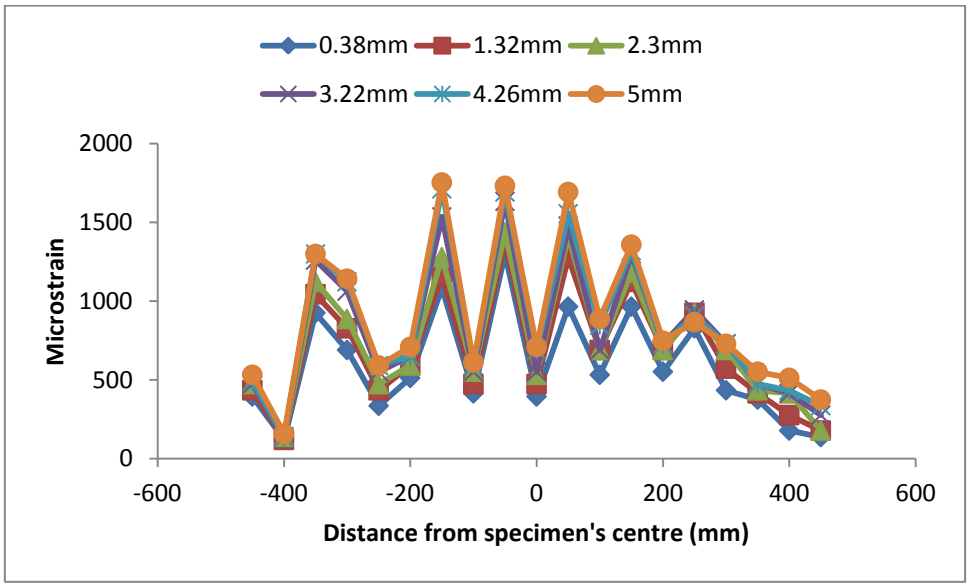

Figure 8.38: Surface strain distribution on specimen with proprietary SAMI D for 0.38mm, 1.32mm, 2.30mm, 3.22mm, 4.26mm and maximum of 5mm crack openings

Figure 8.39: Specimen with proprietary SAMI D at the start of test

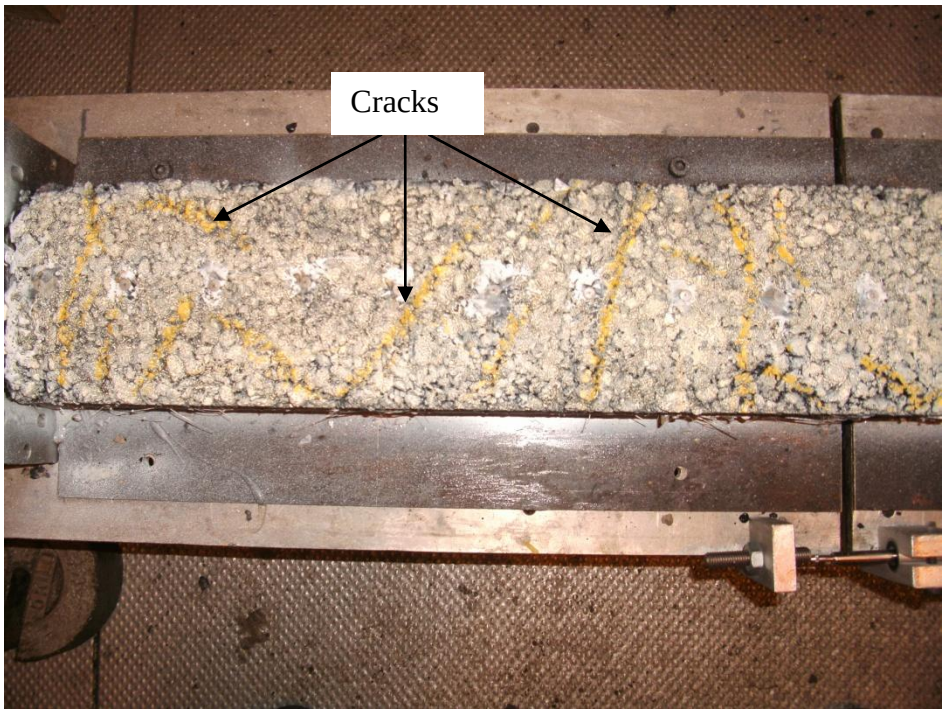

Figure 8.40: Specimen with proprietary SAMI D at the end of test (left)

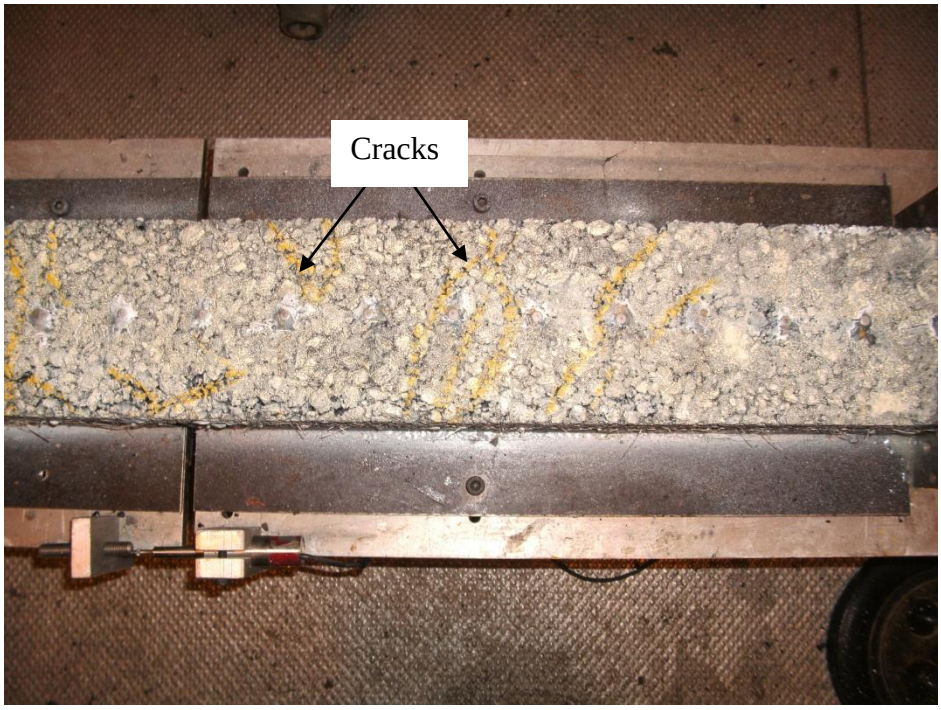

Figure 8.41: Specimen with proprietary SAMI D at the end of test (right)

8.4.6 Specimen with sand asphalt

The test for the specimen with sand asphalt as the SAMI layer was carried out like the other specimens. At 0.5mm and 1mm crack openings as shown in Figures 8.42 and 8.43, respectively, the strain distribution was uniform at the two ends with peak concentration developing around the centre of the specimen (crack region). Also, Figures 8.44 and 8.45 show that at 1.5mm and 2.0mm crack openings, the stress at this stage was concentrated at the centre and the test was concluded after 2.0mm when a full width crack developed at the centre. Dave et al (2007) found in their study that sections with highly modified sand asphalt placed under the overlay under thermo-mechanical loading cycle showed no crack, but that the bottom of the binder course (overlay-interlayer interface) was at the threshold of complete softening and separation. This shows the importance of the interface bond to the resistance of the SAMIs to crack developing at the surface of the overlay under thermal loading.

Also, in this case, the specimen benefits from the slip between the overlay and the SAMI allowing relative movement of the base layer and isolating the overlay from stress concentration in the crack region. The specimen at the start and after test is shown in Figures 8.46 and 8.47. However, the ineffectiveness of the sand asphalt against reflective cracking under traffic loading has to be taken into consideration.

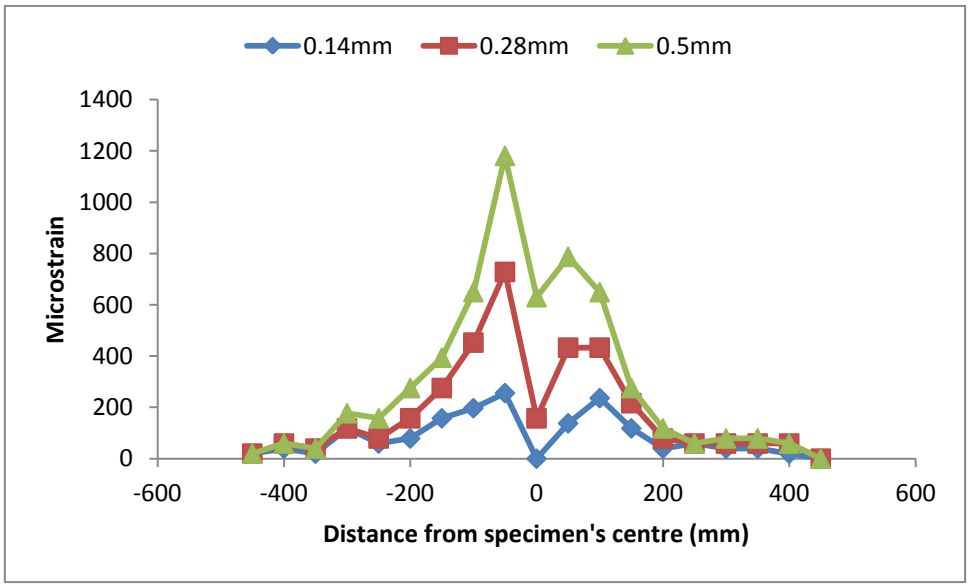

Figure 8.42: Surface strain distribution on specimen with sand asphalt for 0.14mm, 0.28mm and maximum of 0.5mm crack openings

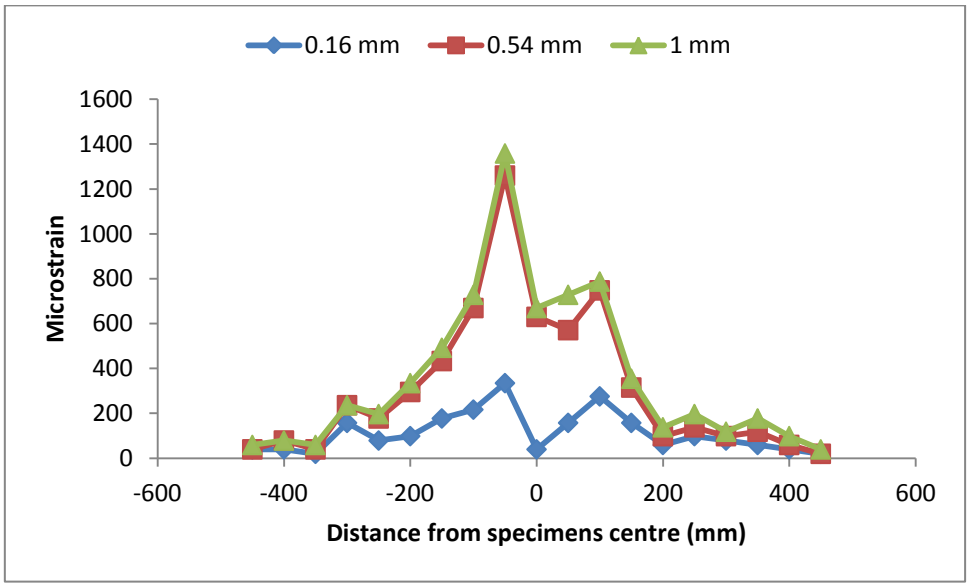

Figure 8.43: Surface strain distribution on specimen with sand asphalt for 0.16mm, 0.54mm and maximum of 1mm crack openings

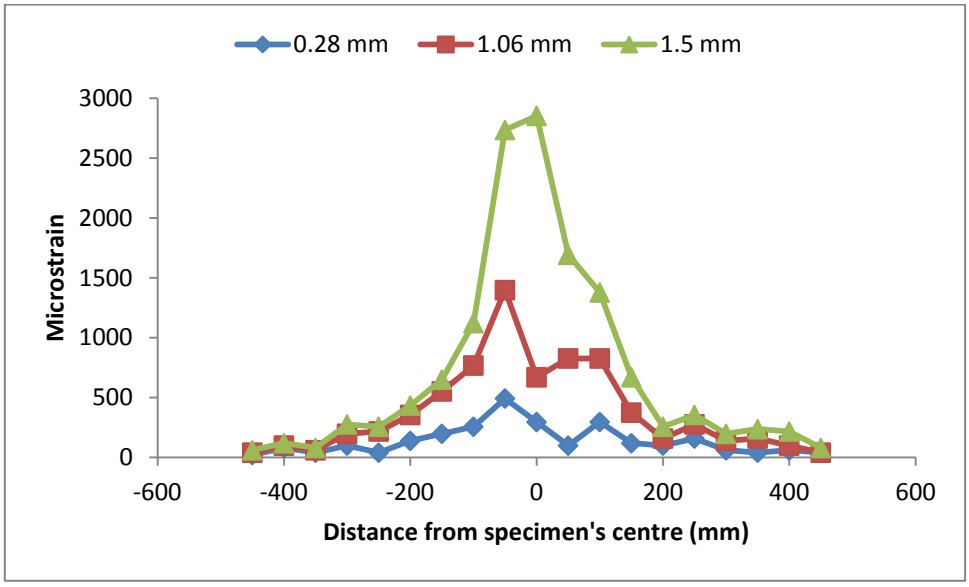

Figure 8.44: Surface strain distribution on specimen with sand asphalt for 0.28mm, 1.06mm and maximum of 1.5mm crack openings

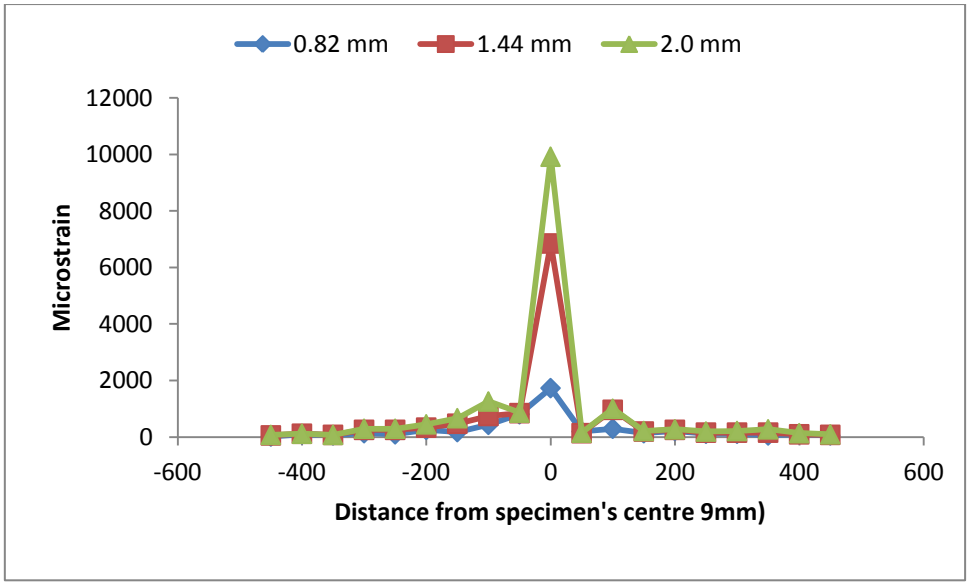

Figure 8.45: Surface strain distribution on specimen with sand asphalt for 0.82mm, 1.44mm and maximum of 2.0mm crack openings

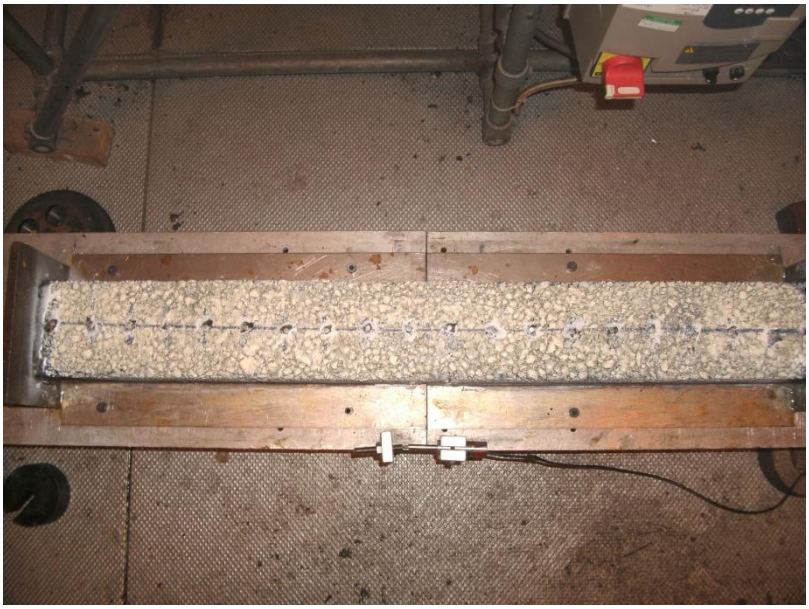

Figure 8.46: Specimen with sand asphalt at the start of test

Figure 8.47: Specimen with sand asphalt at the end of test

8.5 Conclusion

The following conclusions can be drawn from this study:

- It can be seen from the tests that all the specimens with SAMIs (proprietary SAMIs A, B, C and D and sand asphalt) performed better than the control specimen with no SAMI.

- The strain distribution was more uniform in all the specimens with SAMIs than the control specimen and they sustained greater crack opening than the control specimen.
- Also, the tests show that the performance of the specimens incorporating SAMIs varies with the SAMIs used. The specimens with proprietary SAMIs C and D gave better results than those with proprietary SAMIs A and B and sand asphalt as the crack only appeared at the surface of the overlay after 5 mm compared to 2 mm, 1.5 mm and 1.5 mm for the specimens with proprietary SAMIs A and B and sand asphalt, respectively.
- The test results established the importance of the slip between the overlay and SAMIs to the crack resistance of SAMIs used as interlayer between overlay and existing pavement.

REFERENCES

Epps A. (2000): Design and Analysis System for Thermal Cracking in Asphalt Concrete. Journal of Transportation Engineering. 300-307.

Baxter R.E. (2001): Let the Membrane Take The Strain!. MSc Dissertation, University of Nottingham, UK.

Boutin G. and Lupien C. (2000): Thermal Cracking of Asphalt Pavement. 2nd Eurasphalt and Eurobitume Congress, Barcelona. 45-59.

Brown S.F., Thom N.H., Sander P.J., Brodrick B.V. and Cooper S. (2000): Reinforced Asphalt. Report No: PGR 99025, University of Nottingham, UK.

BSI (2004): Bituminous Mixtures-Test Method for Hot Mix Asphalt: Laboratory Mixing. British Standard Institution, London, UK (BS EN 12697-35:2004).

Dave E.V., Song S.H., Buttlar W.G. and Paulino G.H (2007): Reflective and Thermal Cracking Modeling of Asphalt Concrete Overlays. Advanced Characterization of Pavement and Soil Engineering Materials. 1241-1252.

Debondt A.H. (1999): Anti Reflective Cracking Design of (Reinforced) Asphaltic overlays. PhD Thesis submitted to Delft University of Technology, Netherlands.

Hills J.F. and Drien D. (1996): The Fracture of Bitumens and Asphalt Mixes by Temperature Induced Stresses. Proceedings, Association of Asphalt Paving Technologists, Vol. 35.

Jung D.H. and Vinson T.S. (1994): Low Temperature Cracking: Test Selection. Strategic Highway Research Program, National Research Council, Washington DC. SHRP-A-400.

Kanerva H.K.; Vinson T.S. and Zeng H. (1994): Low-Temperature Cracking: Field Validation of the Thermal Stress Restrained Specimen Test. Strategic Highway Research Program, National Research Council, Washington DC. SHRP-A-401.

Smith R.G. (1983): Laboratory Testing of Fabric Interlayers for Asphalt Concrete Paving: Interim Report. Transportation Research Record 916. 6-17.

Vinson T.S., Janoo V.C and Haas R.C. G. (1989): Low Temperature Cracking and Thermal Fatigue Cracking. Summary Report SR-OSU-A-003A-89-1.

Vinson T.S., Janoo V.C and Haas R.G. (1990): Summary Report on Low Temperature Cracking and Thermal Fatigue Cracking. SHRP-A/IR-90-001, National Research Council, Washington,D.C.

9 DESIGN GUIDE

9.0 Design guidelines

This section gives guidelines for the use of SAMIs against reflective cracking. The guidelines are based on the study carried out under this project. This consists of tests to determine the interface properties of the overlay-SAMI interface, a laboratory wheel tracking test to evaluate the crack resistance potential of SAMIs, a finite element analysis to determine deflection and stress/strain distribution in a cracked pavement with and without a SAMI, a large scale wheel tracking test (pavement test facility) to evaluate the crack resistance potential of SAMIs under loading conditions close to the field situation and lastly, a thermal cycling test to determine the crack resistance of SAMIs under thermal loading.

The findings of the tests have been used to draw up the guidelines for effective use of SAMIs to retard reflective cracking. Also, the OLCRACK software developed by Thom (2000) was adopted to demonstrate the crack resistance potential of the SAMIs.

9.1 Site Investigation/survey

This involves visiting the site to evaluate the condition of the existing pavement in order to be able to select a suitable remedial measure to restore the pavement to good condition. The site investigation should involve checking the type of cracks predominant on the existing pavement, as this could help in identifying the principal cause of the cracking. Also the extent of damage of the pavement should be checked. Other data that should be collected on the site visits include: the crack width; crack spacing; and the type of existing pavement. Photographs of the pavement may also be taken for further analysis in the office.

After the field inspection and the measurements have been done, it is important to analyse the data collected to identify the principal cause of the cracks and conditions that the overlay will be subjected to. Based on this study, conclusions can be drawn on the data collected. For instance, in a situation where transverse cracks are predominant in the field, the principal cause of the cracks and the main factor that may cause reflective cracking may be temperature variation (daily/seasonal). This can be confirmed from the data available on the weather experienced at that location, from the time of construction to when cracks appeared on the surface.

Also, if the type of crack that is predominant in the field is longitudinal cracking, this may suggest that the principal cause of the cracks and the main factor that may cause reflective cracking may be the action of traffic loads. Again, when the cracks predominant in the field are alligator cracks, this may suggest a fatigue related problem. This is not to say that traffic loading does not contribute to transverse cracks or that the causes of cracks in a pavement are exclusively due to either traffic loads or temperature variations. Other factors could also be responsible for the cracks; as highlighted in section 1.3, factors such as consolidation of subgrade, moisture change in an existing pavement, frost heave, expansive soils etc could be responsible for the cracks. Also, when ruts are noticed it is important to identify the cause, which may be due to poor subgrade or low permanent deformation resistance of the asphalt.

9.2 Evaluation of the existing pavement properties

The properties of the existing pavement are important because it must be able to withstand the traffic loading that will be imposed through the design life of the overlay. Also, the existing pavement properties are required as input for the design of the overlay thickness. The properties that are required include: the thickness and stiffness of the existing asphalt layer; the thickness and stiffness of the subbase; and the stiffness of the subgrade. The properties of

the pavement indicate whether a structural rehabilitation is required or not. When structural rehabilitation is not required, appropriate measure is carried out to extend the life of the pavement.

Methods available to measure these properties include the dynamic cone penetrometer testing for the assessment of unbound foundation layer and subgrade, Benkelman beam - the oldest and simplest form of deflection test, Lacroix deflectograph - an extension of Benkelman beam with different frame that allows vehicle to travel continuously along the road and deflection measurement taken every 3-4m, and falling weight deflectometer that gives a very precise value of absolute deflection (accuracies of ±2 μm commonly quoted) and able to distinguish between two pavements with the same deflection under load but with quite different individual layer stiffnesses, etc. Also, cores can be taken from the pavement to determine the asphalt stiffness using the indirect tensile stiffness modulus method and the thickness of the pavement could be determined from the cores and ground penetrating radar survey. Cores from the cracked sections could also reveal the origin of the crack (top down or bottom up) provided it has not grown through the entire depth of the pavement. When rutting is noticed, the rut depth should be measured and the cause(s) should be identified to prevent the overlay from having similar problem.

Also, it is important to determine the remaining life of the existing pavement. The remaining life approach requires that the pavement history be looked into - the construction history, past traffic and environmental conditions. Khweir (2011) stated that the fatigue profile is the most important parameter in calculating pavement life. He stated further that the residual life of an existing pavement and the calculation of the required overlay thickness are based on the criteria of limiting the tensile strain at the underside of the lower base layer. He highlighted three approaches for calculating the life of a pavement with an existing base layer. This include calculation of the percentage of the past traffic compared to the original design,

testing of the lower layers in a laboratory and adjusting with a shift factor to take into account the difference between road traffic loading and dynamic loading of the laboratory and calculation of the fatigue life of an existing pavement by introducing a new factor to the standard fatigue formula.

9.3 selection of suitable remedial measures

Treatment options are then selected based on the observations from site investigation, evaluation of the existing pavement properties and the residual life. The treatment options might include reactive maintenance, thick overlay, introduction of stress relieving or a reinforcing interlayer or reconstruction. The focus of the present study is on the use of stress absorbing membrane interlayers.

9.3.1 Choosing an appropriate interlayer to delay reflective cracking

After the causes of the cracks and factor(s) that may cause reflective cracking have been established and the residual life of the pavement indicate that it will sustain the load the will be imposed through the design life of the overlay, then the type of interlayer that can be used to retard reflective cracking can be proposed. From this study, the factors that influence the performance of a SAMI include: the stiffness of the SAMI; the thickness of the SAMI; the interlayer bond between the SAMI and both the overlay and the existing pavement, the stiffness and fatigue characteristics of the overlay, and the temperature.

If it has been established that one factor that may cause reflective cracking is temperature variation. As observed in this study the most important property of the SAMIs that influences its crack resistance in this situation is the reduced shear stiffness of the interface achieved by introducing a SAMI. This is because the introduction of the SAMIs allows a slip (debonding) between the SAMI and the overlay, therefore giving room for the horizontal movement

(contraction/expansion) of the underlying cracked layer without causing large tensile stresses at the top of the overlay. In this respect, SAMIs with low SAMI-overlay interface stiffness will be most beneficial. It can be seen in the thermal cycling test reported in chapter eight of this thesis that the SAMIs in this category are proprietary SAMIs C and D. However, in this case, it has to be stated that the SAMIs must also have good resistance against rutting and must be able to withstand the traffic loads that will be imposed throughout the design life of the overlay. Both proprietary SAMIs C and D have been found to provide good performance against reflective cracking under traffic loading in the wheel tracking test reported in chapter five and the pavement facility test reported in chapter seven.

In cases where it has been established that the factor that may be responsible for reflective cracking is traffic loading, the factors that should be considered in choosing the SAMIs include their stiffness, the interface shear stiffness between the SAMIs and overlay and climatic factors such as temperature. As observed in the wheel tracking test reported in chapter five, an optimum stiffness exists at which SAMIs are able to delay reflective crack. The optimum stiffness may be between 1000MPa and 3000MPa, depending on test temperature. Stiffnesses below and above this range may yield undesirable results. Therefore, in the context of this study proprietary SAMIs C and D should be considered when the temperature of the location is expected to be 10^{o}C or lower. When a temperature greater than 10^{o}C is expected, then all the SAMIs tested would perform well except the sand asphalt.

Generally in this case the factors mentioned earlier must be considered in selecting the SAMIs. The thickness of the SAMI and the overlay are equally important. The OLCRACK software allows the optimization of thickness of the SAMIs and overlay to achieve the best result.

9.4 OLCRACK Software

OLCRACK was mentioned in section 2.2.3 and is adopted in this study for the design of overlays with and without SAMIs. The software gives two options - the first one considers two layers of asphalt over the existing pavement, while the second considers one layer of asphalt with grid reinforcement over existing pavement. The OLCRACK two-layer system was chosen for this study. This design method was chosen because it takes into account some of the factors that influence the crack resistance potential of SAMIs. These factors are the thickness of SAMI, stiffness, temperature, fatigue characteristics of the SAMI, stiffness of the existing asphalt pavement, crack spacing, crack width factor - which considers whether the crack is fully open or closed, crack shear modulus - which accounts for the crack activity under loading, stiffness and fatigue characteristics of the overlay, thickness and stiffness of subbase and the subgrade stiffness. The software is designed such that the designer can optimise the thickness of the layers to obtain a desirable design life for the overlay in terms of the number of load applications to failure.

The OLCRACK software was used to predict the number of load applications to failure for the SAMIs examined in the pavement test facility. The design parameters for the sections with 6mm proprietary SAMI A, 15 mm proprietary SAMI A, proprietary SAMIs C and D and control are shown in Tables 9.1, 9.2, 9.3, 9.4 and 9.5. The stiffness modulus and the fatigue parameters used in the design were obtained from the indirect tensile stiffness modulus test and indirect tensile fatigue test, respectively. It was considered appropriate to use the stiffness directly for the design because the load pulse durations in the NAT and the PTF are quite similar. The air temperature increased slightly during the test.

Plots of the crack development for sections with 6mm proprietary SAMI A, 15 mm proprietary SAMI A, proprietary SAMIs C and D and control are shown in Figure 9.1, 9.2, 9.3, 9.4 and 9.5. A summary of the PTF results and the OLCRACK predictions is shown in

Table 9.6. This shows that OLCRACK software is able to predict the life of pavement incorporating SAMIs reasonably well.

Furthermore, OLCRACK was used to predict the life of some of the other combinations studied in the wheel tracking test. The parameters considered are shown in Tables 9.7 and 9.8. The results shown in Table 9.9 indicate that the specimens with SAMIs have a larger number of load applications to failure than the specimens without SAMIs.

OLCRACK was used to predict the life to failure of pavements incorporating 20mm proprietary SAMIs A and B with 50 mm overlay and a pavement having 70 mm overlay with no SAMI under full scale loading. The loading parameters, base, subbase and subgrade properties and thicknesses considered are shown in Table 9.10. The overlay and SAMIs properties are shown in Table 9.11. The design results shown in Table 9.12 show that pavement with proprietary SAMIs A and B have lives 2.73 and 9.73 times that of the pavement with 70 mm overlay (no SAMI), respectively.

Table 9.1: Design parameters for cracked pavement with 6 mm proprietary SAMI A

Data Input		**Data Output**	
Load (kN)	9.6	**Number of Load Applications to Failure**	
Radius (mm)	65	(see sheet 'Life' for details)	
Std Dev of Wheel Track (mm)	0	**0.044577** million	
Asphalt Layer 1 Thickness (mm)	44	**SAMI Thickness (mm)**	6
Stiffness (MPa)	4224	Stiffness (MPa)	2725
Poisson's Ratio	0.35	Poisson's Ratio	0.35
Indirect Tensile Fatigue Test Data:		Indirect Tensile Fatigue Test Data:	
Strain for failure at N=1	1313.7	Strain for failure at N=1	4242.6
Slope of fatigue characteristic	0.215	Slope of fatigue characteristic	0.325
Specimen diameter (mm)	100	Specimen diameter (mm)	100
Existing Asphalt Thickness (mm)	55	**Sub-base Thickness (mm)**	400
Stiffness (MPa)	4224	Stiffness (MPa)	144.3
Crack Spacing (m)	0.835		
Crack Shear Modulus (MN/m3) (10000=excellent; 100=very poor)	100	**Subgrade Stiffness (MPa)**	10
Crack Width Factor (1 = tightly closed; 0 = fully open)	0		

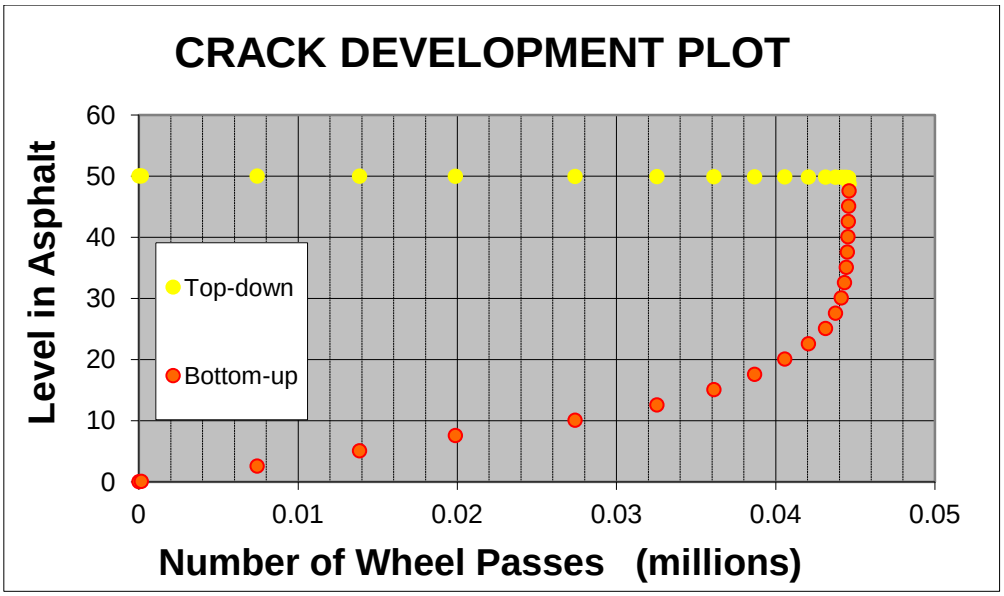

Figure 9.1: Graph of crack development for cracked pavement with 6 mm proprietary SAMI A

Table 9.2: Design parameters for cracked pavement with 15 mm proprietary SAMI A

Data Input		**Data Output**	
Load (kN)	9.6	**Number of Load Applications to Failure** (see sheet 'Life' for details) **0.031789** million	
Radius (mm)	65		
Std Dev of Wheel Track (mm)	0		
Asphalt Layer 1 Thickness (mm)	36	**SAMI Thickness (mm)**	15
Stiffness (MPa)	4224	Stiffness (MPa)	2725
Poisson's Ratio	0.35	Poisson's Ratio	0.35
Indirect Tensile Fatigue Test Data:		Indirect Tensile Fatigue Test Data:	
Strain for failure at N=1	1313.7	Strain for failure at N=1	4242.6
Slope of fatigue characteristic	0.215	Slope of fatigue characteristic	0.325
Specimen diameter (mm)	100	Specimen diameter (mm)	100
Existing Asphalt Thickness (mm)	53	**Sub-base Thickness (mm)**	400
Stiffness (MPa)	4224	Stiffness (MPa)	144.3
Crack Spacing (m)	0.835		
Crack Shear Modulus (MN/m3) (10000=excellent; 100=very poor)	100	**Subgrade Stiffness (MPa)**	10
Crack Width Factor (1 = tightly closed; 0 = fully open)	0		

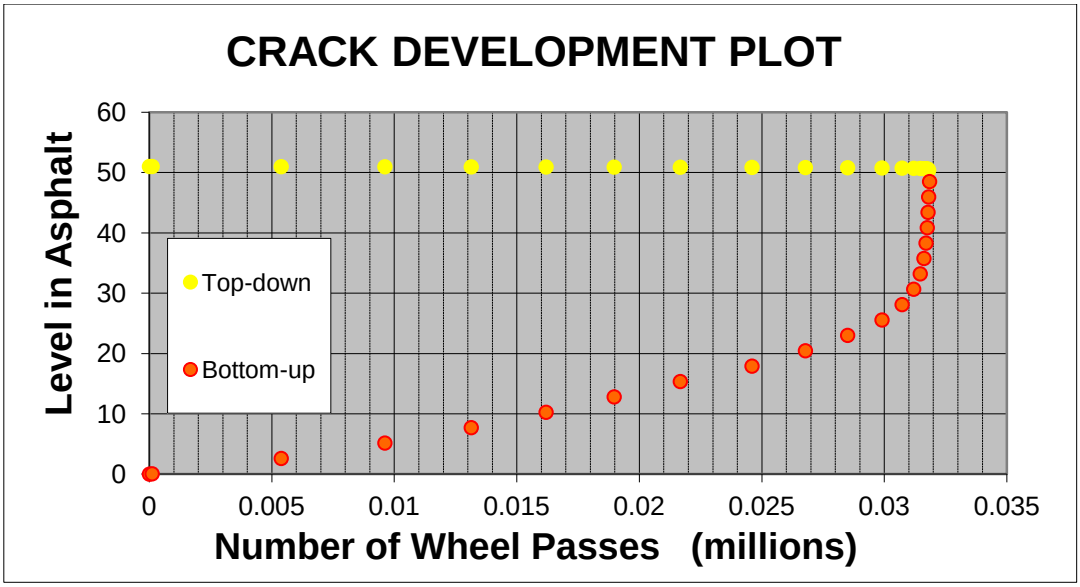

Figure 9.2: Graph of crack development for cracked pavement with 15 mm proprietary SAMI A

Table 9.3: Design parameters for cracked pavement with proprietary SAMI C

Data Input		**Data Output**	
Load (kN)	9.6	**Number of Load Applications to Failure** (see sheet 'Life' for details) **0.058944** million	
Radius (mm)	65		
Std Dev of Wheel Track (mm)	0		
Asphalt Layer 1 Thickness (mm)	47	**SAMI Thickness (mm)**	7
Stiffness (MPa)	4224	Stiffness (MPa)	1000
Poisson's Ratio	0.35	Poisson's Ratio	0.35
Indirect Tensile Fatigue Test Data:		Indirect Tensile Fatigue Test Data:	
Strain for failure at N=1	1313.7	Strain for failure at N=1	1175
Slope of fatigue characteristic	0.215	Slope of fatigue characteristic	0.215
Specimen diameter (mm)	100	Specimen diameter (mm)	100
Existing Asphalt Thickness (mm)	55	**Sub-base Thickness (mm)**	400
Stiffness (MPa)	4224	Stiffness (MPa)	144.3
Crack Spacing (m)	0.835		
Crack Shear Modulus (MN/m3) (10000=excellent; 100=very poor)	100	**Subgrade Stiffness (MPa)**	10
Crack Width Factor (1 = tightly closed; 0 = fully open)	0		

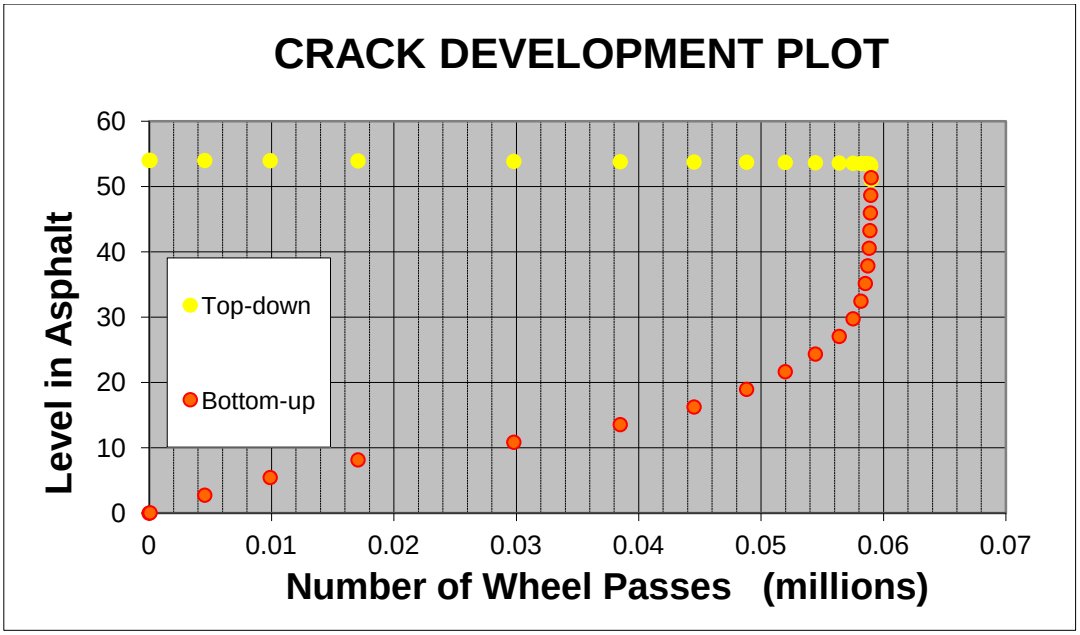

Figure 9.3: Graph of crack development for pavement with proprietary SAMI C

Table 9.4: Design parameters for cracked with pavement proprietary SAMI D

Data Input	
Load (kN)	9.6
Radius (mm)	65
Std Dev of Wheel Track (mm)	0
Asphalt Layer 1 Thickness (mm)	45
Stiffness (MPa)	4224
Poisson's Ratio	0.35
Indirect Tensile Fatigue Test Data:	
Strain for failure at N=1	1313.7
Slope of fatigue characteristic	0.215
Specimen diameter (mm)	100
Existing Asphalt Thickness (mm)	51
Stiffness (MPa)	4224
Crack Spacing (m)	0.835
Crack Shear Modulus (MN/m3)	100
(10000=excellent; 100=very poor)	
Crack Width Factor	0
(1 = tightly closed; 0 = fully open)	

Data Output	
Number of Load Applications to Failure	
(see sheet 'Life' for details)	
0.039173 million	
SAMI Thickness (mm)	7
Stiffness (MPa)	1200
Poisson's Ratio	0.35
Indirect Tensile Fatigue Test Data:	
Strain for failure at N=1	1175
Slope of fatigue characteristic	0.215
Specimen diameter (mm)	100
Sub-base Thickness (mm)	400
Stiffness (MPa)	144.3
Subgrade Stiffness (MPa)	10

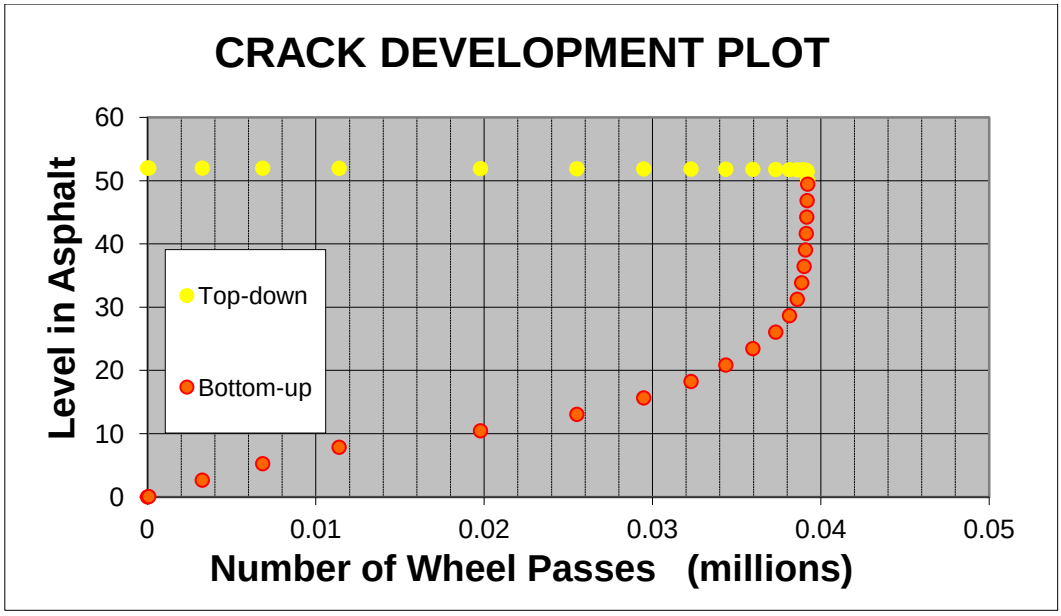

Figure 9.4: Graph of crack development for pavement with proprietary SAMI D

Table 9.5: Design parameters for cracked pavement with no SAMI (Control)

Data Input		**Data Output**	
Load (kN)	9.6	**Number of Load Applications to Failure**	
Radius (mm)	65	(see sheet 'Life' for details)	
Std Dev of Wheel Track (mm)	0	**0.020187** million	
Asphalt Layer 1 Thickness (mm)	53	**Asphalt Layer 2 Thickness (mm)**	0
Stiffness (MPa)	4224	Stiffness (MPa)	2725
Poisson's Ratio	0.35	Poisson's Ratio	0.35
Indirect Tensile Fatigue Test Data:		Indirect Tensile Fatigue Test Data:	
Strain for failure at N=1	1313.7	Strain for failure at N=1	3061.2
Slope of fatigue characteristic	0.215	Slope of fatigue characteristic	0.287
Specimen diameter (mm)	100	Specimen diameter (mm)	100
Base Thickness (mm)	57	**Sub-base Thickness (mm)**	400
Stiffness (MPa)	4224	Stiffness (MPa)	144.3
Crack Spacing (m)	0.63		
Crack Shear Modulus (MN/m3)	100	**Subgrade Stiffness (MPa)**	10
(10000=excellent; 100=very poor)			
Crack Width Factor	0		
(1 = tightly closed; 0 = fully open)			

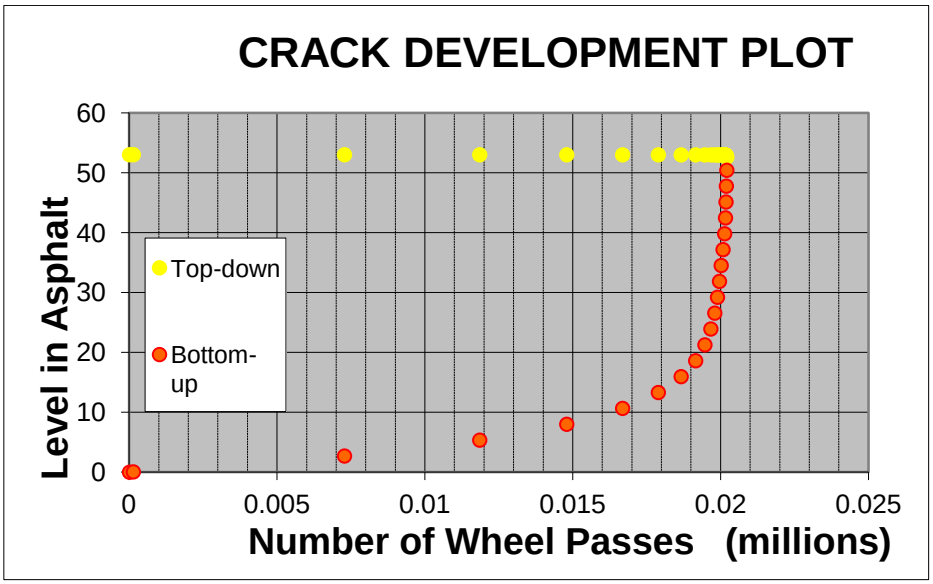

Figure 9.5: Graph of crack development for pavement with no SAMI (Control)

Table 9.6: Pavement test facility and OLCRACK number of load applications to failure in cracked section with SAMIs and without SAMIs

SAMIs	Pavement Test Facility	OLCRACK
6mm proprietary SAMI A	63828	44577
15mm proprietary SAMI A	31880	31789
proprietary SAMI C	58995	58944
proprietary SAMI D	39052	39173
Control	20185	20187

Table 9.7: Loading parameters, base, subbase and subgrade properties and thicknesses

Loading	Load	9.6kN
	Radius of tyre contact	65mm
	Standard deviation of tyre contact	0
Base	Thickness	60mm
	Stiffness	9591MPa
	Crack spacing	0.635m
	Crack width factor	0
	Crack shear modulus	100MN/m^3
Subbase	Thickness	400
	Stiffness	144.3MPa
Subgrade	Stiffness	10MPa

Table 9.8: Overlay and proprietary SAMIs A and B properties

Properties	Overlay	SAMI A	SAMI B	Sand asphalt
Stiffness (MPa)	3899	2725	2444	209
Strain at N = 1 (microstrain)	3447	4242.6	3697.2	18694
Slope of fatigue characteristics	0.345	0.325	0.284	0.527
Poisson's ratio	0.35			

Table 9.9: OLCRACK design of some combinations evaluated using wheel tracking test

Specimens	**References**	**load applications to failure**	**Life (ratio of control)**
60 mm Overlay (Control)	O60	10843	1
20 mm thick sand asphalt with 40 mm overlay	SA20O40	6751	0.62
20 mm thick SAMI A with 40 mm overlay	PA20O40	28658	2.64
20 mm thick SAMI B with 40 mm overlay	PB20O40	51759	4.77
70 mm Overlay (Control)	O70	17134	1
30 mm thick sand asphalt with 40 mm overlay	SA30O40	6477	0.39
30 mm thick SAMI A with 40 mm overlay	PA30O40	45413	2.65
30 mm thick SAMI B with 40 mm overlay	PB30O40	80231	4.68
10 mm thick sand asphalt with 60 mm overlay	SA10O60	12401	0.72
10 mm thick SAMI A with 60 mm overlay	PA10O60	48869	2.85
10 mm thick SAMI B with 60 mm overlay	PB10O60	91615	5.35
80 mm Overlay (Control)	O80	27355	1
20 mm thick sand asphalt with 60 mm overlay	SA20O60	13272	0.49
20 mm thick SAMI A with 60 mm overlay	PA20O60	83139	3.04
20 mm thick SAMI B with 60 mm overlay	PB20O60	163436	5.97

Table 9.10: Loading parameters, base, subbase and subgrade properties and thicknesses

Loading	Load	40kN
	Radius of tyre contact	150mm
	Standard deviation of tyre contact	0.15
Base	Thickness	250mm
	Stiffness	3000MPa
	Crack spacing	2m
	Crack width factor	0.5
	Crack shear modulus	1000MN/m^3
Subbase	Thickness	400
	Stiffness	150MPa
Subgrade	Stiffness	50MPa

Table 9.11: Overlay and proprietary SAMIs A and B properties

Properties	Overlay	SAMI A	SAMI B
Stiffness (MPa)	3899	2725	2444
Strain at N = 1 (microstrain)	3447	4242.6	3697.2
Slope of fatigue characteristics	0.345	0.325	0.284
Poisson's ratio	0.35		

Table 9.12: Life to failure under full scale loading

	Number of load applications to failure	Load applications to failure as ratio of control
70 mm overlay with no SAMI	154380	1
20 mm proprietary SAMI A with 50 mm overlay	434340	2.81
20 mm proprietary SAMI B with 50 mm overlay	1614570	10.46

9.5 Design against reflective cracking under thermal loading

It has been established in the thermal cycling tests that the principal factor that aids the crack resistance of a SAMI under thermal loading (temperature variation) is the slip between the overlay and the SAMI. An attempt has been made in this section to predict the life of a cracked pavement incorporating SAMIs compared to those without SAMIs.

In the thermal cycling tests, it was found that the specimen without SAMI (control) failed at crack opening of 1.0 mm, while the specimens with proprietary SAMIs A, B, C, and D and sand asphalt failed at crack openings of 2.0mm, 1.5mm, 5.0mm, 5.0mm, and 2.0mm, respectively. This showed the specimens with proprietary SAMIs A, B, C, and D and sand asphalt withstood crack openings twice, 1.5 times, 5 times, 5 times and twice that of the control, respectively. It is reasoned that the tensile strains within the overlay for the specimens with proprietary SAMIs A, B, C, and D and sand asphalt at the same crack opening as the control might have been 0.5 times, 0.7 times, 0.2 times, 0.2 times and 0.5 times that of the control, respectively.

Therefore, knowing that the slope of the fatigue characteristic of the overlay is 0.345, the lives to failure of the specimens with proprietary SAMIs A and sand asphalt might be approximately 7.46 times that of the control, while that of the specimen with proprietary SAMI B might be around 3.2 times that of control. Lastly, the lives to failure of the specimens with proprietary SAMIs C and D might be around 106 times that of the control. This suggests that proprietary SAMIs C and D are much the best of the tested when an overlay over a cracked pavement is expected to be subjected to daily/seasonal temperature variations.

9.6 Conclusions

The following conclusions can be drawn from this study:

- Guidelines for the successful use of SAMIs against reflective cracking have been prepared from the results of tests and modelling.
- It has been pointed out that it is important that the factors responsible for the existing cracks on the pavement and those that may cause reflective cracking of the overlay be established in order to propose a suitable SAMI that may help reduce reflective cracking.
- It was also mentioned that the type of cracks predominant on site and the information about the site/region may help in establishing the cause(s) of the cracking on the existing pavement and the factor(s) that may cause reflective cracking of the overlay.
- Also, it was stated that when temperature variation is responsible for the crack on the existing pavement, that the most important factor of the SAMIs that should be considered is the reduced shear stiffness provided by the introduction of SAMIs.

- It was reported that when traffic loading is expected to be the principal cause of reflective cracking, the most important factor among others to be considered is the stiffness and thickness of the SAMIs.
- OLCRACK software has been used to demonstrate the crack resistance of SAMIs under laboratory and full scale loading.

REFERENCE

Thom N.H. (2000): A Simplified Computer Model for Grid Reinforced Asphalt Overlays. Proceedings of 4th International RILEM Conference on Reflective Cracking in Pavements, Otawa, Ontario, Canada, Pp 37-46.

Khweir K.A. (2011): UK Overlay Design of Flexible Pavement, Determination of the Important Parameters. Journal of Transportation Engineering, American Society of Civil Engineers (ASCE). doi10.1061/ (ASCE)TE.1943-5436.0000340.

10 CONCLUSIONS AND RECOMMENDATIONS

10.1 Conclusions

This study has investigated the crack resistance potential of some selected stress absorbing membrane interlayers (SAMIs). It was achieved by carrying out laboratory tests which include Leutner shear tests, pull off tests, wheel tracking tests (supported by finite element analysis), a large scale pavement test facility test, and thermal cycling tests. The following conclusions can be drawn from the study:

Leutner shear test and the pull off test

- It was found that there is reduced stiffness at the overlay-SAMI interface compared to the control interface (no SAMI).
- The test showed that, of the SAMIs investigated; proprietary SAMIs C and D have the lowest stiffness at the overlay-SAMI interface followed by sand asphalt and proprietary SAMIs A and B.

Wheel tracking test

- It was discovered that proprietary SAMIs A and B are not effective at 10^{o}C due to increased stiffness of the SAMIs and increased interface stiffness, while they have good resistance to reflective cracking at 20^{o}C and 30^{o}C. They had lives in the range of 1.10-4.64 and 1.12-2.64 times those of the control (no SAMI) at 20^{o}C and 30^{o}C, respectively under a load 2.4kN (1.1MPa) and 1.58-4.03 times those of the control under a load 1.35kN (0.6MPa).

- The test showed that proprietary SAMIs C and D were able to retard reflective cracking at 10^{o}C, 20^{o}C and 30^{o}C with lives to failure in the range 3.65-5.50 times those of control (no SAMI) at 20^{o}C.
- The study showed that sand asphalt is not able to retard reflective cracking. This indicated that while SAMIs are required to have lower stiffness than the overlay, a SAMI of extreme low stiffness is not beneficial for crack resistance.
- The test showed that lower SAMI thickness is more effective against reflective cracking. It indicates that a thickness of between 10 and 20 mm would probably be most appropriate when SAMIs are considered for rehabilitation of a cracked pavement.
- The test showed that SAMIs performed better against reflective cracking at the lower load level of 1.35kN (0.6MPa) than at the greater load level of 2.4kN (1.1MPa), thus making them probably more suitable for highways than, for example, airfields.
- It can be seen from the study that using SAMIs with a thin overlay (40mm) is more beneficial in relative terms than with a thicker overlay (60mm).
- It was demonstrated that when SAMIs are introduced beneath an overlay to a cracked pavement, increased deflections are expected; therefore the overlay must be well designed against fatigue related problems.

Finite element modelling

- The finite element modelling, like the wheel tracking test, shows that when SAMIs are introduced into a pavement, increased deflection is expected because of the lower stiffness of the SAMIs.

- The lower strains/stresses predicted in the overlay of the specimens with SAMIs imply increased life of the overlay. This showed that SAMIs are able to isolate the overlay from strain/stress concentration at the crack region.
- Also, it can be seen from the finite element modelling that increasing the SAMI's thickness leads to increased deflection of the pavement. This is reflected by the results of the wheel tracking test, in that lower SAMI thickness gives better performance against reflective cracking.
- It was discovered that when slip was introduced at the SAMI-existing pavement interface, predicted deflections, strains and stresses were relatively closer to those measured in the tests. They were also increased relative to the no-slip case, which may imply less life to failure. However, this cannot be said to be the case with confidence because crack propagation was not modelled, so the effect of the slip on a SAMI's crack resistance could not be fully quantified.

Pavement test facility

- The pavement test facility test, like the wheel tracking test and finite element analysis, showed that the use of SAMIs results in greater deflection in the pavement.
- It showed that all the sections with SAMIs had greater life to failure in the range 1.93-4.53 times those of the control sections (no SAMI).
- The test showed that the thickness of the SAMI influences its performance with better performance observed when lower thickness is used. It was observed that a section with 5 mm (10 mm in full-scale) proprietary SAMI A had life to failure twice that of the section with 10 mm (20 mm in full-scale) thickness of same SAMI.

- The test demonstrated that when SAMIs are introduced into a cracked pavement, more permanent deformation occurs, hence the need for an overlay with good resistance to permanent deformation.
- Lastly the test showed that the SAMI's composition, stiffness and the interface shear stiffness influence its performance.

Thermal cycling test

- The test showed that the introduction of the SAMIs allows more uniform strain distribution on the overlay.
- It can be seen from the test that the main factor that influences the performance of SAMIs introduced into a cracked pavement subjected to thermal loading is the slip between the overlay and SAMI, which is achieved by the reduced stiffness of the overlay-SAMI interface.
- The test showed that all the specimens with the SAMIs performed better than the control specimen (no SAMI).
- The test indicated that the specimens with proprietary SAMIs C and D are the most appropriate under thermal loading. They withstood a crack opening 5 times that of the control (no SAMI).

Design Guidelines

- The findings from all the tests have been used to prepare guidelines for effective use of SAMIs against reflective cracking.
- OLCRACK software has been used to demonstrate the benefits of SAMIs in a cracked pavement under laboratory and full-scale loadings.

10.2 Recommendations

The following recommendations are made for further studies:

- Further combinations of different overlay materials with maximum nominal aggregate size greater than 10 mm, SAMI compositions and thicknesses should be studied in the pavement test facility or in the field to evaluate further the better performance of the SAMIs at large scale.
- Crack propagation should be modelled in the finite element model to evaluate the effect of debonding on the crack resistance of the SAMIs.
- In the study, only asphalt concrete was considered; further study should be carried out using cement concrete as the existing pavement.
- The thermal cracking test should be carried out at other temperatures as this study only considered a temperature of -3^{o}C. This is because temperature has a great effect on the interface stiffness – the main factor that influences the performance of SAMIs under thermal loading.
- The SAMI and the overlay layers were compacted on the thermal cycling rig. Thus poor compaction was achieved which resulted in high voids in the SAMIs and overlay. The equipment should be further designed such that the specimen can be compacted in the laboratory and transferred to the thermal cycling rig.
- More combinations should be tested to evaluate the effects of different factors such as SAMI thickness, overlay thickness and cycling rate on crack resistance of SAMIs under thermal loading (temperature variation).
- The OLCRACK design software should be upgraded to account for the effect of interface shear stiffness on a SAMI's crack resistance potential.

APPENDIX A

A.1 Leutner shear test at 10°C

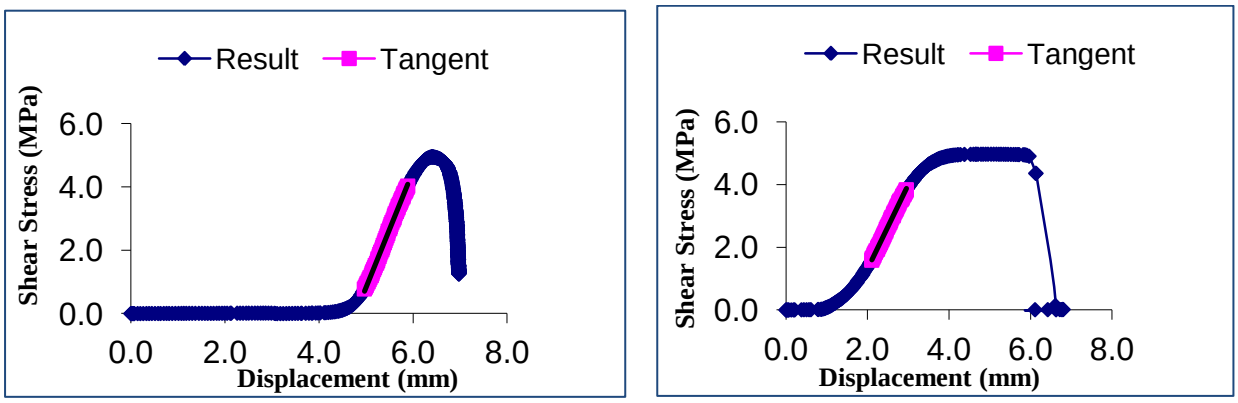

Figure A.1: Stress versus displacement graph for overlay-proprietary SAMI A interface at 10°C

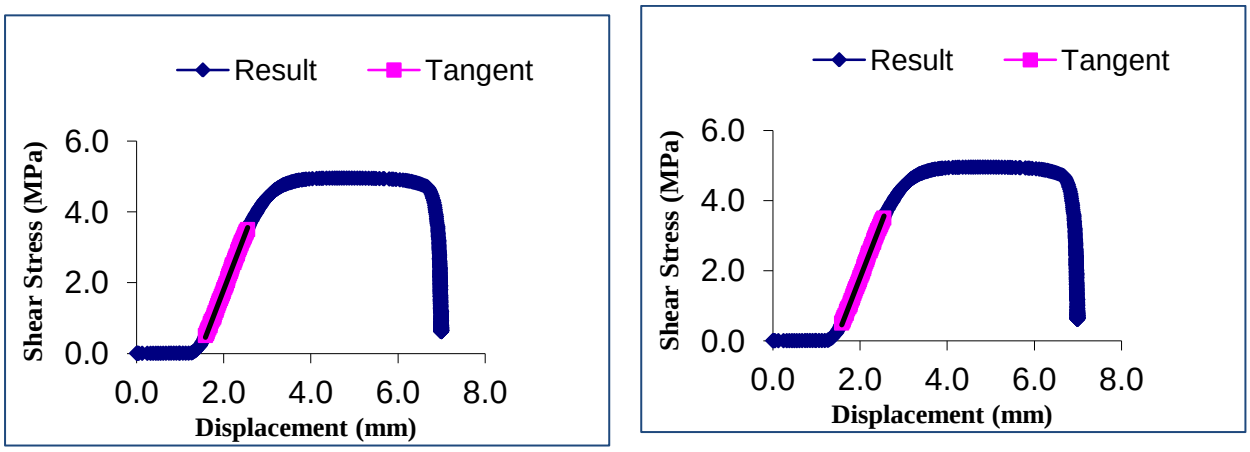

Figure A.2: Stress versus displacement graph for overlay-proprietary SAMI B interface at 10°C

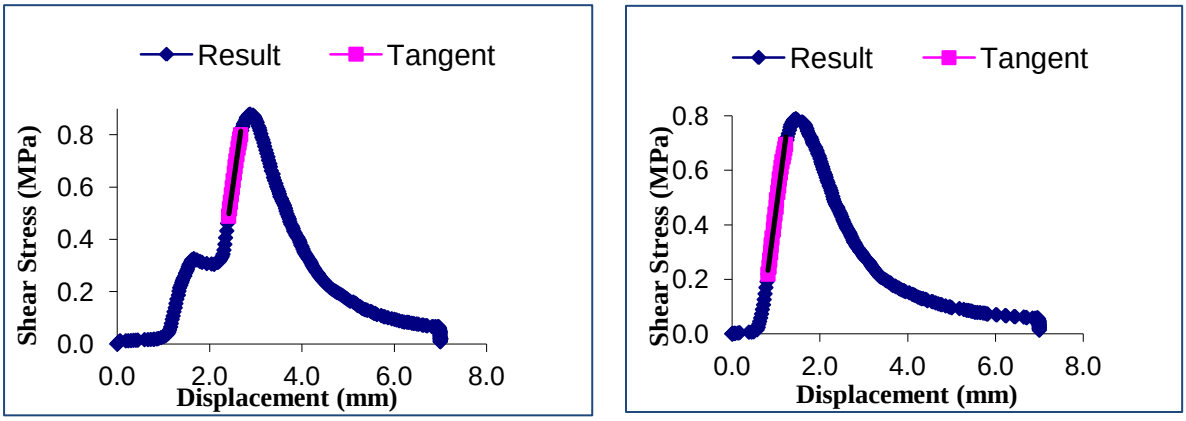

Figure A.3: Stress versus displacement graph for overlay-proprietary SAMI C interface at 10°C

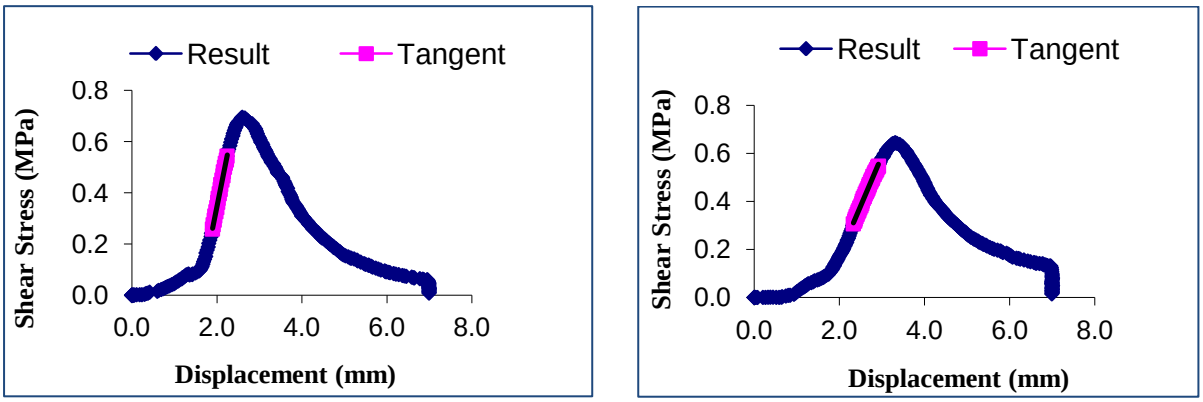

Figure A.4: Stress versus displacement graph for overlay-proprietary SAMI D interface at 10°C

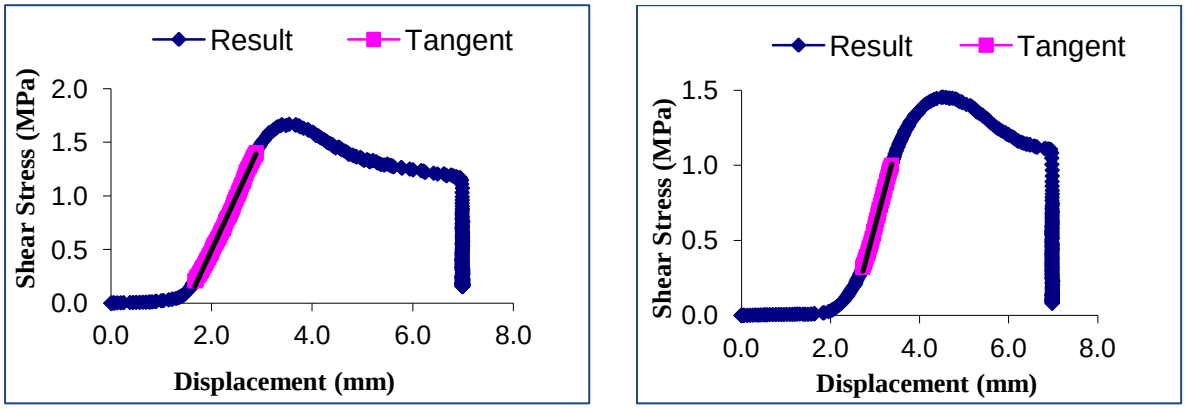

Figure A.5: Stress versus displacement graph for overlay-proprietary sand asphalt interface at 10°C

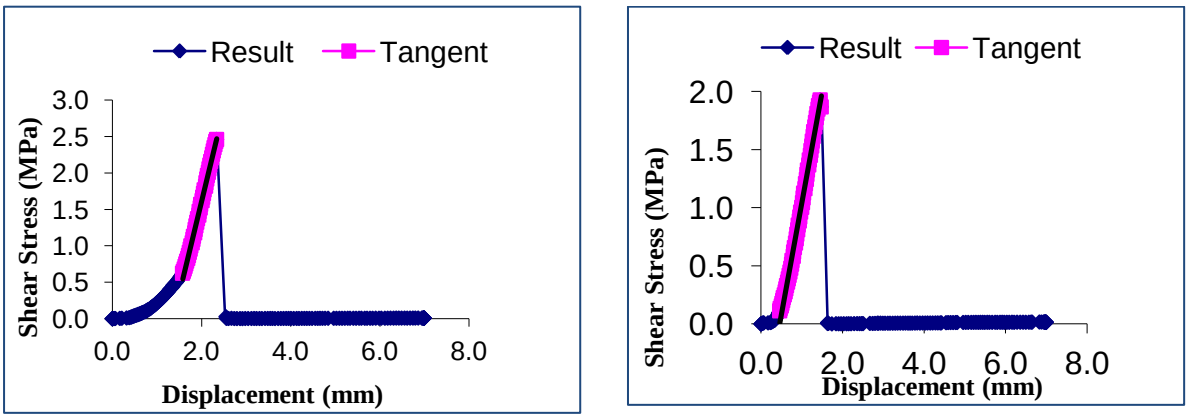

Figure A.6: Stress versus displacement graph for control (10 AC 40/60-10AC 10/20) interface at 10°C

A.2 Leutner shear test at 20°C

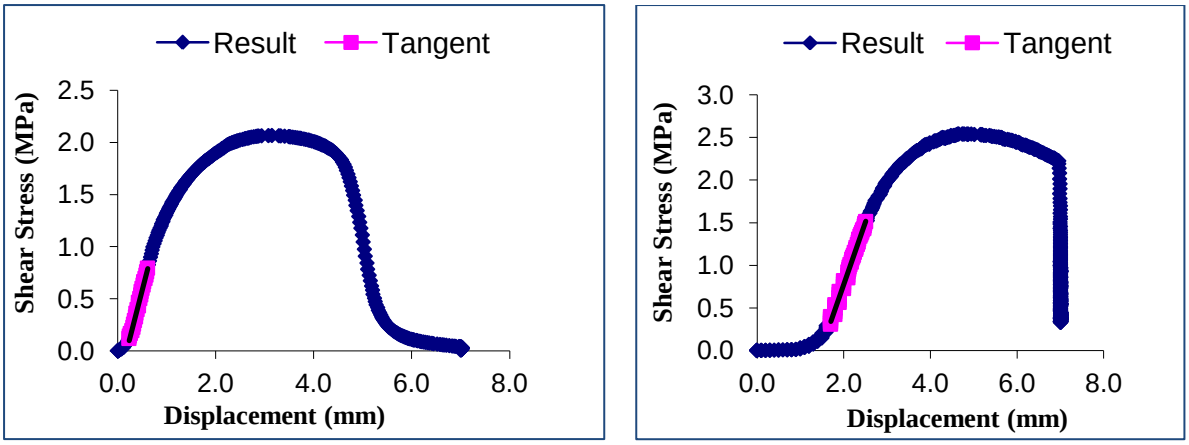

Figure A.7: Stress versus displacement graph for overlay-proprietary SAMI A interface at 20°C

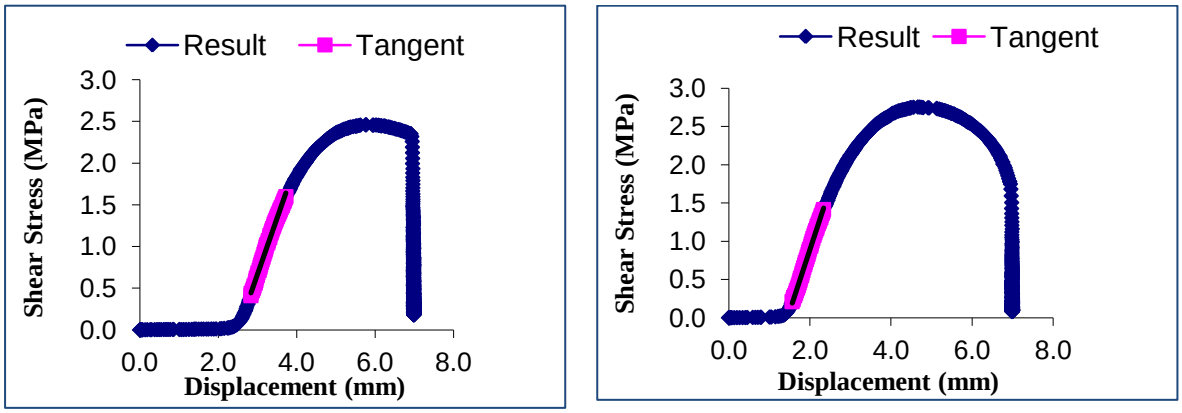

Figure A.8: Stress versus displacement graph for overlay-proprietary SAMI B interface at 20°C

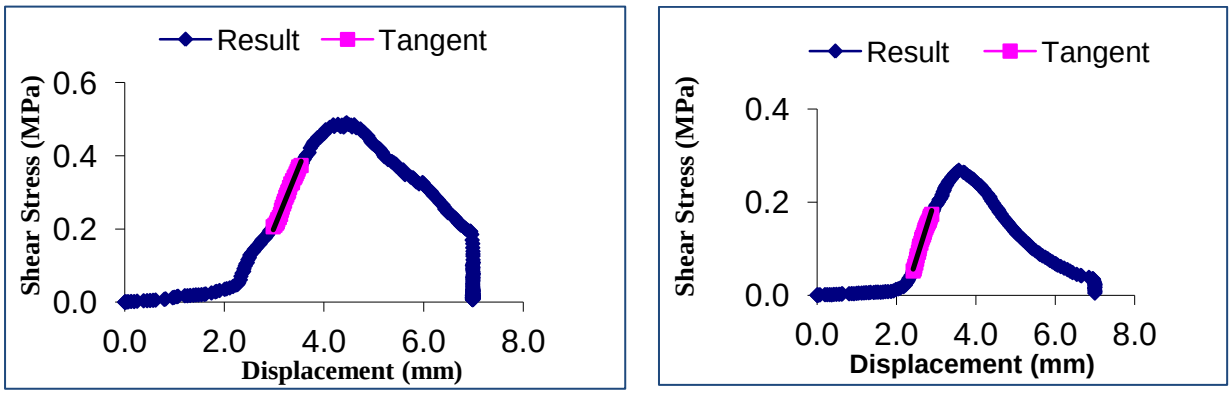

Figure A.9: Stress versus displacement graph for overlay- proprietary SAMI C interface at 20°C

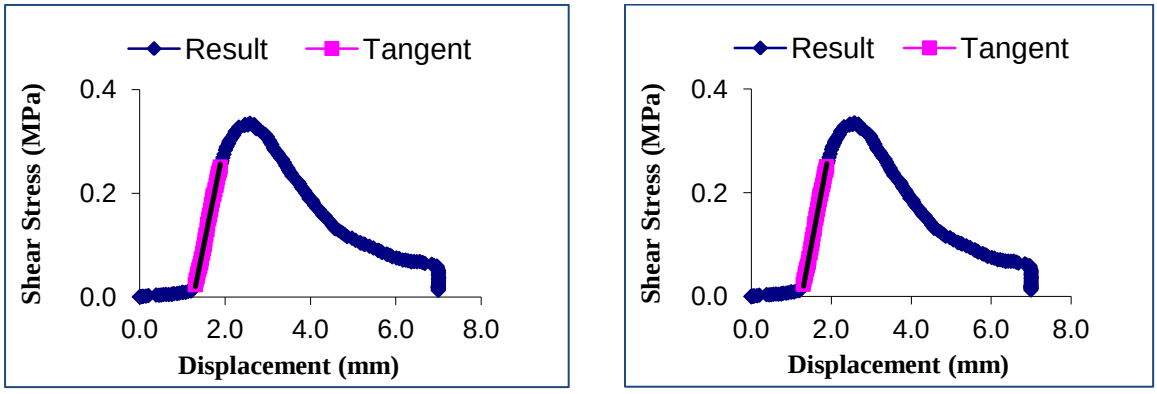

Figure A.10: Stress versus displacement graph for overlay-proprietary SAMI D interface at 20°C

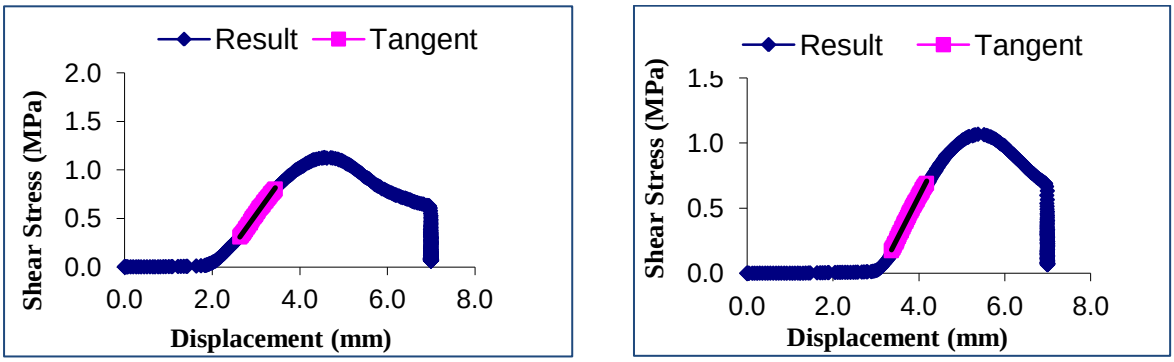

Figure A.11: Stress versus displacement graph for overlay-proprietary sand asphalt interface at 20°C

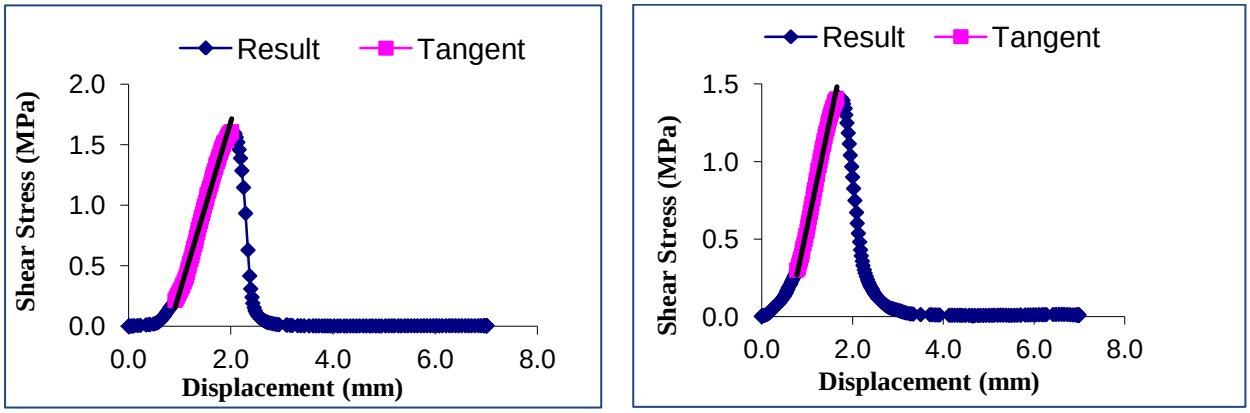

Figure A.12: Stress versus displacement graph for control (10 AC 40/60 -10AC 10/20) interface at 20°C

A.3 Leutner shear test at 30°C

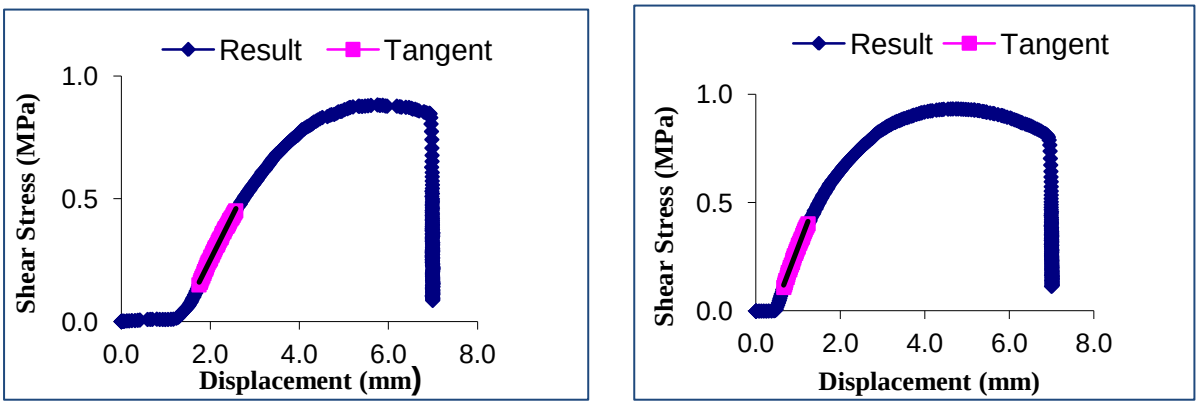

Figure A.13: Stress versus displacement graph for overlay-proprietary SAMI A interface at 30°C

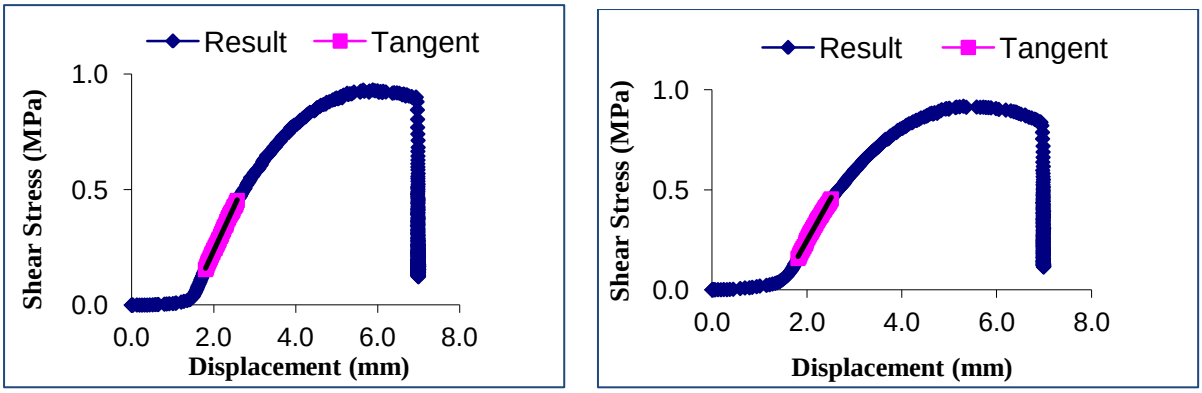

Figure A.14: Stress versus displacement graph for overlay-proprietary SAMI B interface at 30°C

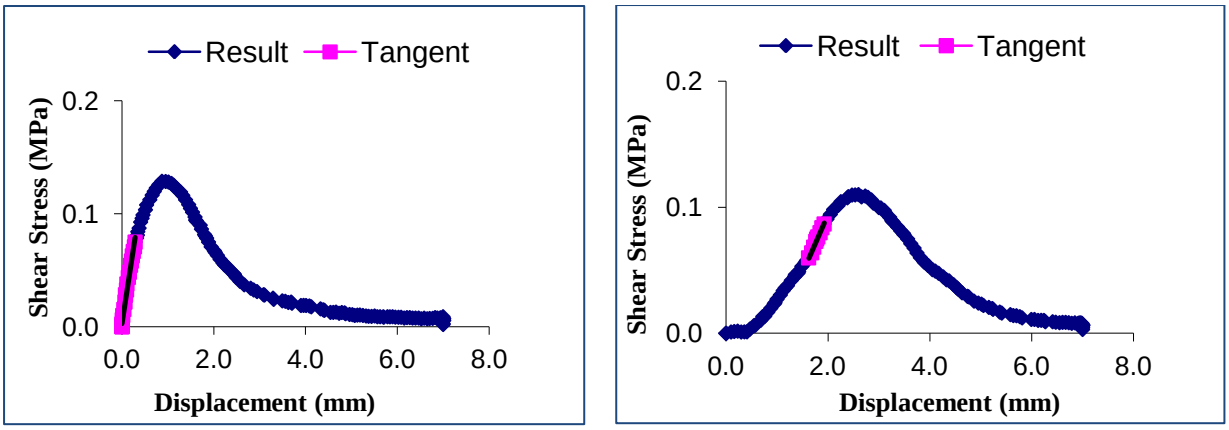

Figure A.15: Stress versus displacement graph for overlay-proprietary SAMI C interface at 30°C

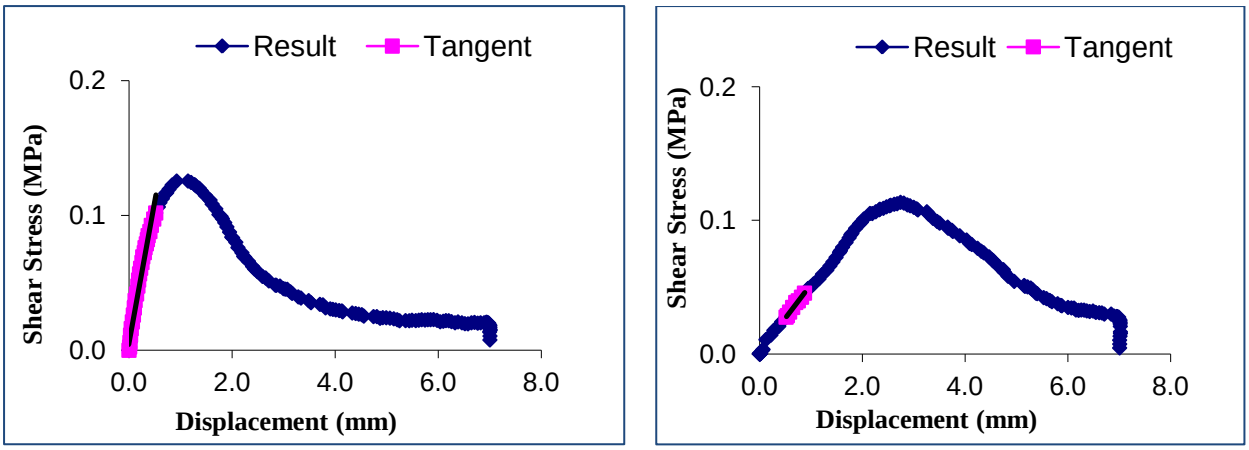

Figure A.16: Stress versus displacement graph for overlay-proprietary SAMI D interface at 30°C

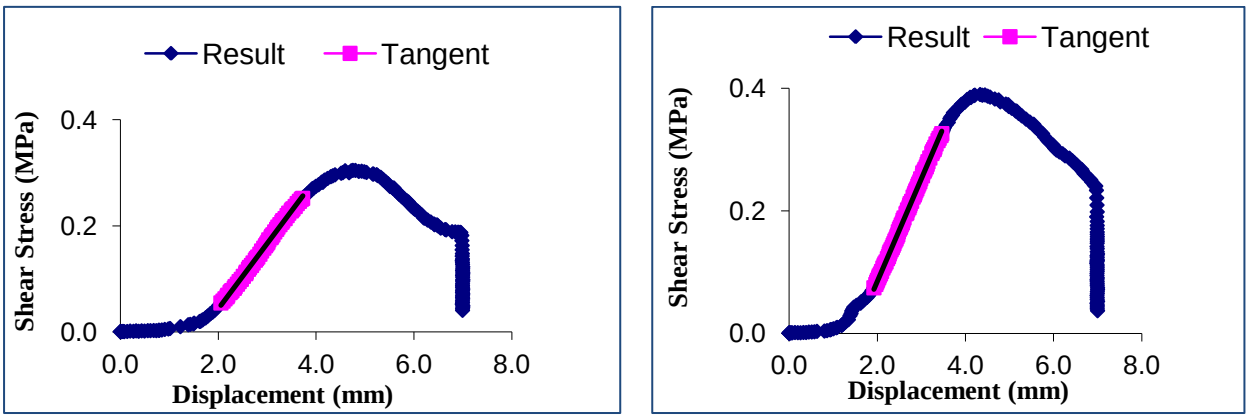

Figure A.17: Stress versus displacement graph for overlay-proprietary sand asphalt interface at 30°C

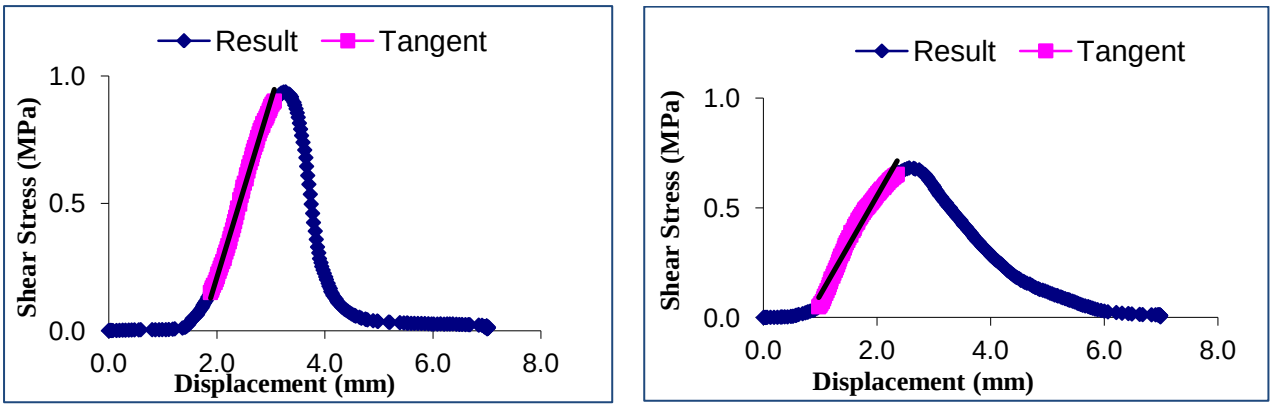

Figure A.18: Stress versus displacement graph for control (10 AC 40/60 -10AC 10/20) interface at 30°C

APPENDIX B

B.1 Cores and holes to show crack paths

Figure B-1: Section 1 (10 mm SAMI A)

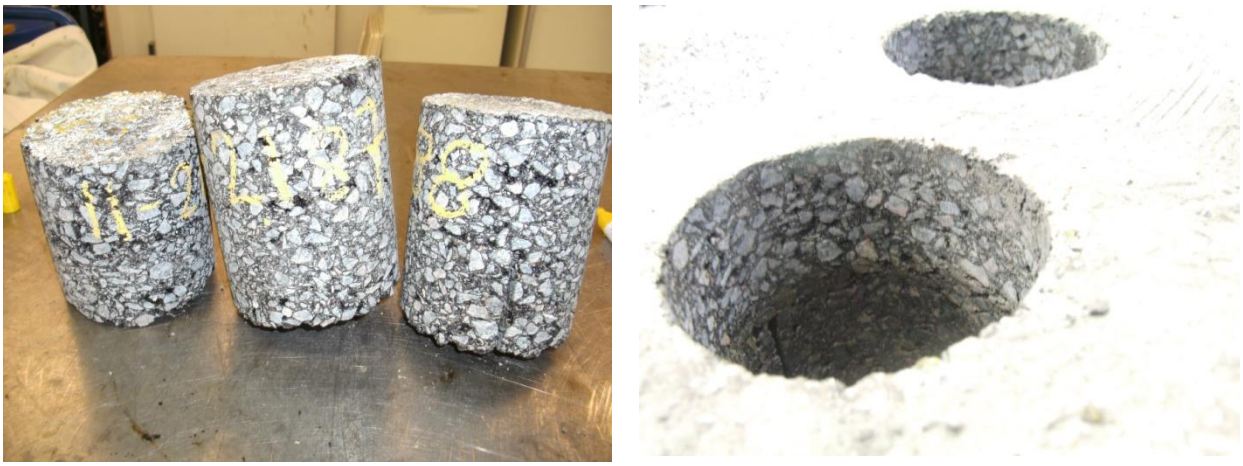

Figure B-2: Section 2 (Control)

Figure B-3: Section 3 (5 mm SAMI A)

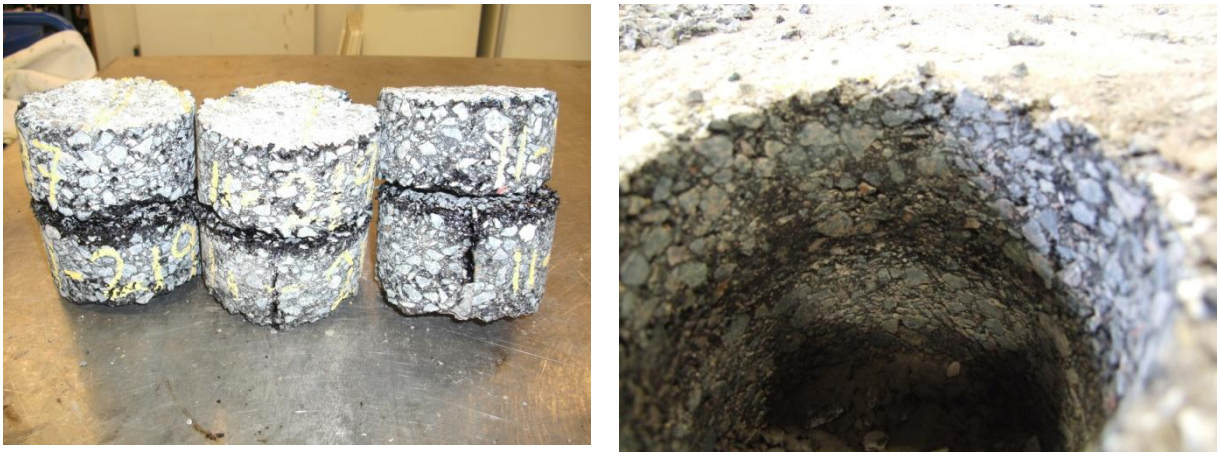

Figure B-4: Section 4 (SAMI C)

Figure B-5: Section 5 (Control)

Figure B-6: Section 6 (SAMI D)

B.2 Leutner shear test results on PTF cores

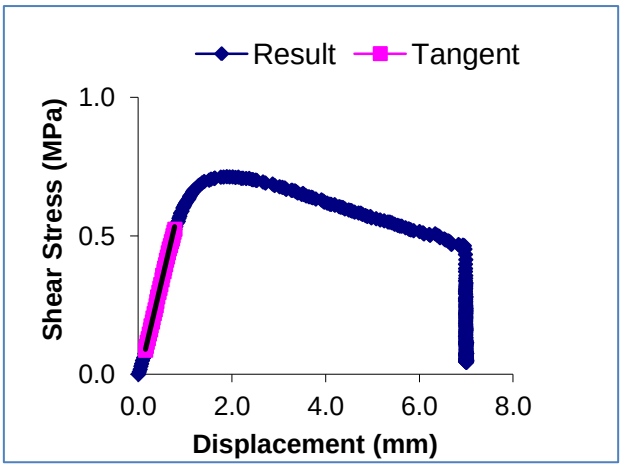

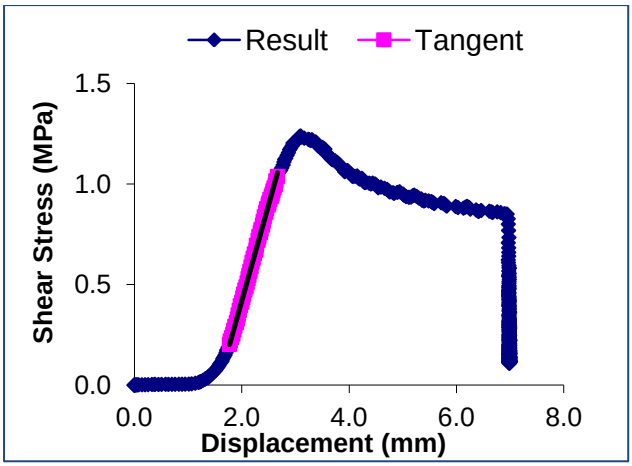

Figure B-7: Shear stress versus displacement for section 1 with 10 mm proprietary SAMI A before trafficking at 20°C

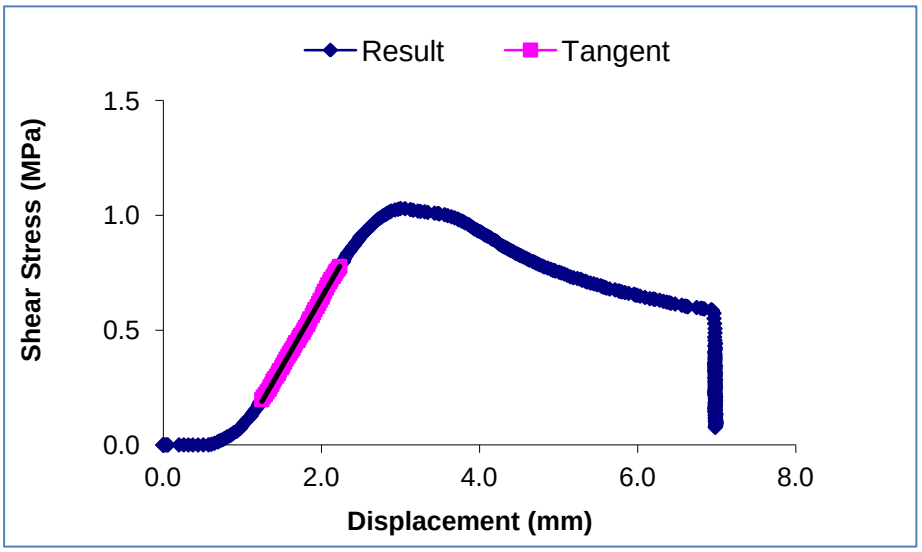

Figure B-8: Shear stress versus displacement for section 1 with 10 mm proprietary SAMI A after trafficking at 20°C

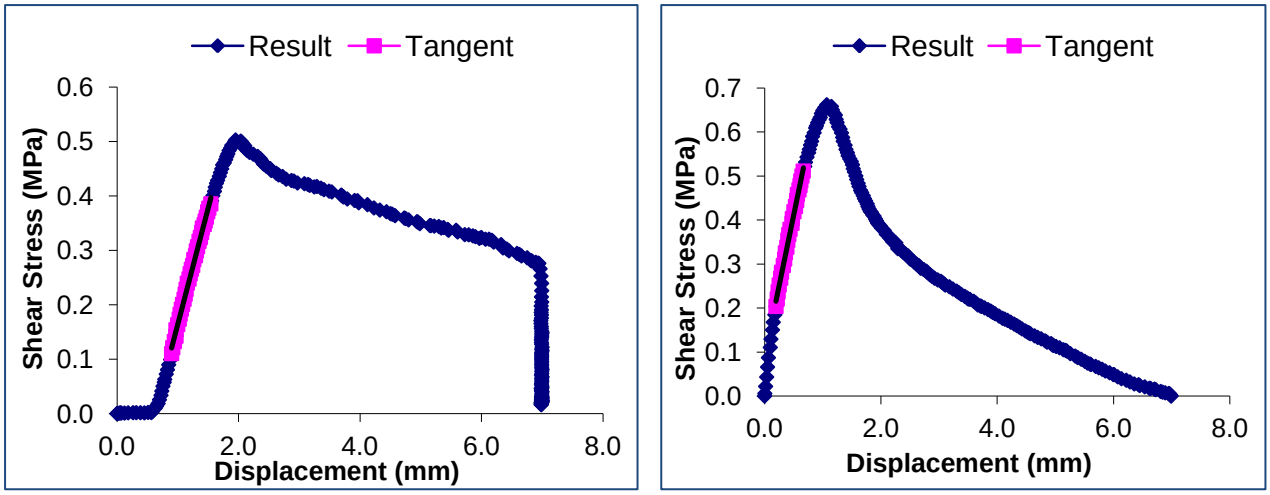

Figure B-9: Shear stress versus displacement for section 3 with 5 mm proprietary SAMI A before trafficking at 20°C

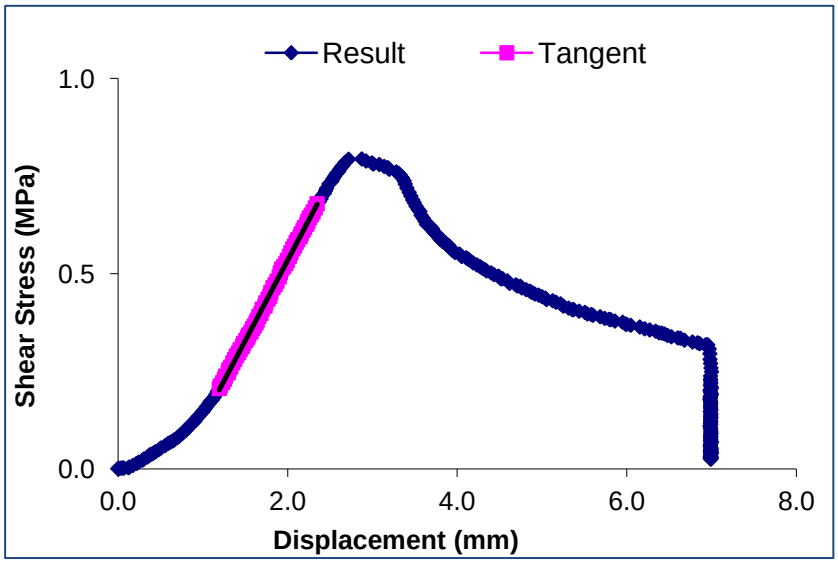

Figure B-10: Shear stress against displacement for section 3 with 5 mm proprietary SAMI A after trafficking at 20°C

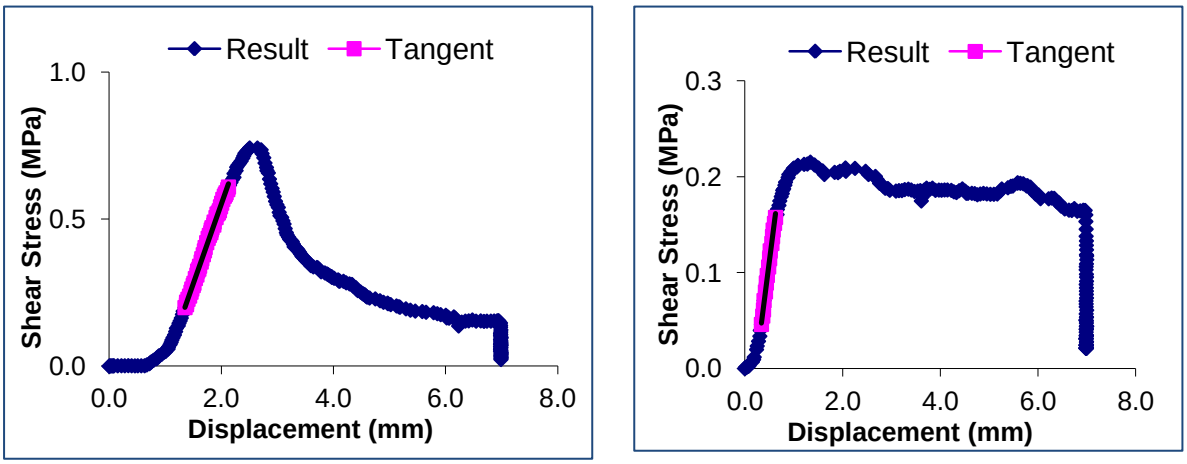

Figure B-11: Shear stress against displacement for section 2 with no SAMI (Control) before trafficking at 20°C

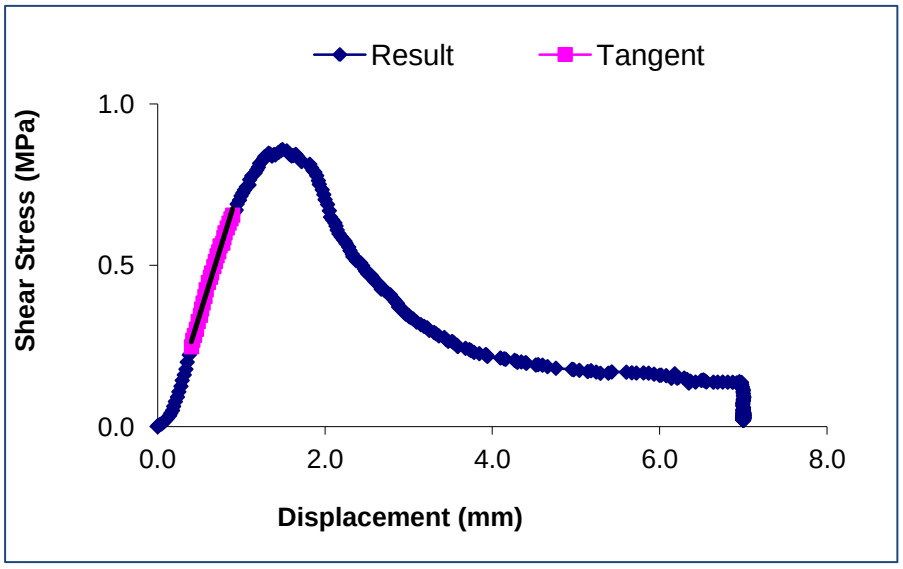

Figure B-12: Shear stress against displacement for section 2 with no SAMI (Control) after trafficking at 20°C

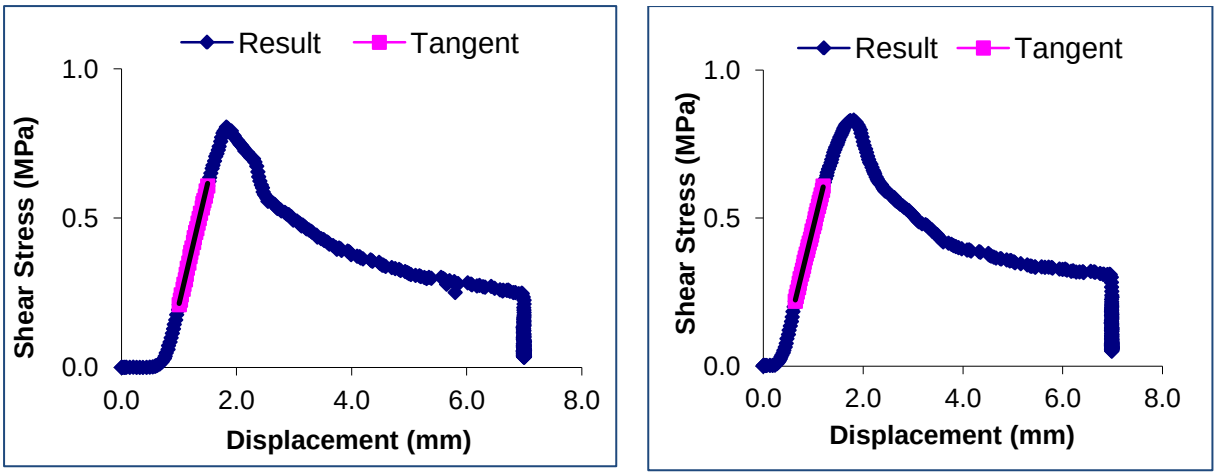

Figure B-13: Shear stress versus displacement for section 5 with no SAMI (Control) before trafficking at 20°C

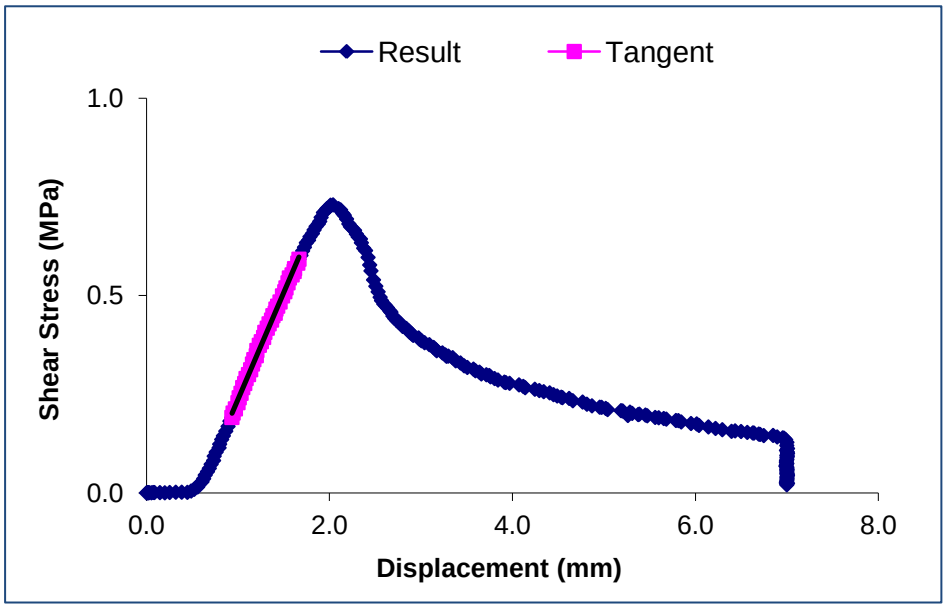

Figure B-14: Shear stress against displacement for section 5 with no SAMI (Control) after trafficking at 20°C